

OSTEOARTHRITIS: PATHOGENESIS AND THERAPEUTIC INTERVENTIONS FOR A WHOLE JOINT DISEASE

Michiel Siebelt

OSTEOARTHRITIS: PATHOGENESIS AND THERAPEUTIC INTERVENTIONS FOR A WHOLE JOINT DISEASE

Michiel Siebelt



ChipSoft

Erasmus MC
Universitair Medisch Centrum Rotterdam
Erasmus

 **LINK** Best of both worlds
 Lima Corporate

 **NEDERLANDSE
ORTHOPAEDISCHE
VERENIGING | NOV**


Anna
Fonds

The printing of this thesis was financially supported by:

Erasmus MC, department of Orthopaedics

Nederlandse Orthopedische Vereniging

Anna Fonds

Link & Lima Nederland

ABN Amro Bank

Chipsoft

The research leading to the results described in this thesis was financially supported by the Dutch Arthritis Association, and the BMM/TerM P2.02 Program of the Netherlands Ministry of Economic Affairs and the Netherlands Ministry of Education, culture and Science.

© M. Siebelt. All rights reserved. No parts of this publication may be reproduced, stored in a retrieval system or transmitted in any form or by any means, without prior written permission of the author.

ISBN: 978-94-91487-22-4

Lay out: Sinds 1961 | Grafisch Ontwerp

Printed by: Print Service Ede

Publisher: Medix Publishers BV, Keizersgracht 317A, 1016 EE Amsterdam, the Netherlands

De digitale versie van dit proefschrift is te vinden in de YourThesis-app en kan gelezen worden op een tablet of smartphone. De app kan gedownload worden in de App Store en de Google Play store of middels het scannen van de onderstaande QR-code.

YourThesis
Spreading the word



OSTEOARTHRITIS: PATHOGENESIS AND THERAPEUTIC INTERVENTIONS FOR A WHOLE JOINT DISEASE

Artrose: pathogenese en therapeutische interventies voor een ziekte
van het hele gewricht

Proefschrift

ter verkrijging van de graad van doctor aan de Erasmus Universiteit Rotterdam op
gezag van de rector magnificus

Prof.Dr. H.A.P. Pols

en volgens besluit van het College voor Promoties.

De openbare verdediging zal plaatsvinden op

Woensdag 3 juni 2015 om 09:30 uur

door

Michiel Siebelt

geboren te Nuenen



PROMOTIECOMMISSIE:

Promotoren:

Prof.Dr.Ir. H.H. Weinans

Prof.Dr.Ir. M. Hendriks-de Jong

Prof.Dr. J.A.N. Verhaar

Leescommissie:

Prof.Dr. S.E.R. Hovius

Prof.Dr. J.F. Verzijlbergen

Dr. J.B.J. van Meurs

TABLE OF CONTENTS

Chapter 1:	Introduction	9
Chapter 2:	Quantifying osteoarthritic changes accurately using in vivo μ CT-arthrography in three etiologically distinct rat models	25
Chapter 3:	Increased physical activity severely induces osteoarthritic changes in knee joints with sulfated-glycosaminoglycan depleted cartilage	41
Chapter 4:	Inhibition of Gsk3 β in cartilage induces osteoarthritic features through activation of the canonical Wnt signalling pathway	59
Chapter 5:	Hsp90 inhibition protect against biomechanically induced osteoarthritis	77
Chapter 6:	FK506 protects against articular cartilage extra-cellular matrix degradation	93
Chapter 7:	Alendronate treatment protect against cartilage matrix degradation during severe osteoarthritis progression	111
Chapter 8:	Triamcinolone acetonide activates an anti-inflammatory and folate receptor positive macrophage that prevents osteophytosis in vivo	127
Chapter 9:	Mesenchymal stem cells reduce pain but not degenerative changes in a mono-iodoacetate rat model of osteoarthritis	145
Chapter 10:	Clinically applied CT arthrography to measure the sulfated glycosaminoglycan content of cartilage	159
Chapter 11:	CT arthrography of the human knee to measure cartilage quality with low radiation dose	173
Chapter 12:	General discussion	187
	Summary	203
	Samenvatting	209
	References	215
Appendices:	List of abbreviations	245
	Curriculum Vitae	
	Phd portfolio	
	List of publications	
	Dankwoord	

CHAPTER 1

INTRODUCTION

Part of this chapter is based on the following publications:

PATHOPHYSIOLOGY OF PERI-ARTICULAR BONE

CHANGES IN OSTEOARTHRITIS

H. Weinans, M. Siebelt, R. Agricola, S.M. Botter, T.M. Pijpers, J.H. Waarsing

Bone, 2012 (Aug);51(2): 190-6

THE ROLE OF IMAGING IN EARLY HIP OA

M. Siebelt, R. Agricola, H. Weinans, Y.J. Kim

Osteoarthritis Cartilage, 2014 (Oct);22(10): 1470-80

OSTEOARTHRITIS: A WHOLE JOINT DISEASE

Osteoarthritis (OA) is an invalidating disease characterized by progressive cartilage degradation¹. OA is the most prevalent arthritic disease and leading cause of disability that affects approximately 34% of the population in the United States over age 65^{2,3}. Also in the Netherlands, approximately 30% of persons aged 65 and older are affected in either the hip or knee joint by this severely disabling disease⁴. Due to the obvious cartilage pathology, research has much focused on articular cartilage and chondrocyte pathobiology. Over the years more knowledge has been gained on complex biochemical and biomechanical influences of chondrocyte behavior. During the past decade, however, pathologic cellular and structural changes in subchondral and trabecular bone, ligaments, synovium, supporting musculature, fibrocartilagenous structures such as the meniscus, and intra-articular fat tissue support the idea that osteoarthritis is not just a cartilage problem. In the current dogma, OA is explained as 'a whole joint disease' that involves a degenerative continuum between multiple joint tissues and cell types⁵.

Cartilage in distress

Cartilage is evolutionary designed to facilitate motion in joints where two bones meet. Its specific composition of extra-cellular matrix (ECM) allows a frictionless movement and functions as a biological shock absorber of mechanical forces that are distributed via the underlying subchondral bone (**Figure 1A**). Articular cartilage ECM is composed of a highly organized collagen network, predominantly made up of collagen type II. From the deep calcified cartilage to the superficial zone of cartilage, collagen molecules are oriented differently which allows to withstand stresses from different directions⁶. Within this collagen network, embedded in lacunae, reside chondrocytes. Chondrocytes in the deep zone are larger with a hypertrophic appearance, where in the superficial zone chondrocytes have a more flattened or fibroblastic appearance (**Figure 1A**). The chondrocyte is the only cell type responsible for cartilage ECM maintenance through high production of sulfated-glycosaminoglycans (sGAG)⁷. sGAG contain negatively charged sulphate groups that give cartilage a fixed charge density. Due to this fixed charge density, large amounts of positive ions and water enter the cartilage creating a high hydrostatic pressure within the collagen network. This water is squeezed out during every load build-up during joint movement. Since sGAG remain in the ECM, cartilage has a sponge-like function and water is immediately attracted back into ECM when compressive forces are reduced. It is due to this preservation of hydrostatic pressure that cartilage is continuously able to absorb forces up to 10-20MPa⁸, and facilitate dissipation of these forces to the underlying bone. In relation to the number of compressive forces, chondrocytes tightly regulate cartilage sGAG content in order to equalize its shock absorbing property that meets the demand of daily use⁹⁻¹¹.

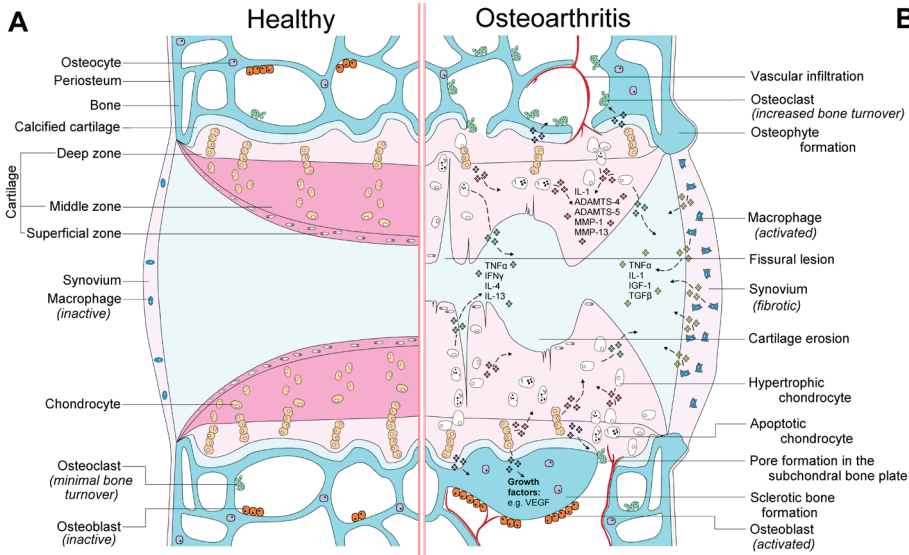


Figure 1: Schematic representation of the differences between a healthy joint and an osteoarthritic joint. In the healthy situation, chondrocytes within the cartilage synthesize sulphated-glycosaminoglycans (sGAG; pink intensity represents sGAG content). A high sGAG content attracts large amounts of positive ions into the cartilage and water diffuses passively into the extra-cellular matrix (ECM). This generates a high hydrostatic pressure, which enables cartilage to dissipate high loads during joint loading. When cartilage is compressed, the underlying intact subchondral bone plate provides support and stability for the cartilage. Superficial chondrocytes and cells within the synovial membrane produce substances like lubricin and hyaluronic acid, both compounds provide lubrication and therefore reduce friction during joint articulation. In osteoarthritis (OA) the joint becomes pathologically changed due to alterations of multiple cell types. Chondrocytes become hypertrophic or in the case of severe OA progression become apoptotic, lacking sGAG synthesis to sustain proper hydrostatic pressure. The cartilage ECM becomes vulnerable, wear-and-tear forces may induce fissural lesions and cartilage erosions. Osteoclasts within the subchondral bone become activated and start to resorb bone, tunneling their way through the subchondral bone plate, and reduces its supportive function. Vascular ingrowth is promoted and osteoblasts start to deposit large amounts of bone, generating a sclerotic bone phenotype. Synovial macrophages are activated and they produce large quantities of cytokines that promotes osteophyte formation, synovial fibrosis and enhances cartilage degradation. This figure was published as part of an article by Glyn-Jones et al, 'Osteoarthritis', Lancet 2015

Normal chondrocyte functioning depends on their ability to cope with stress¹². Reduced coping mechanisms induce important changes like abnormal cell activation, terminal differentiation and adaptation of a hypertrophic state. Hypertrophic chondrocytes synthesize more cytokines that promote cartilage ECM remodeling, for example, like interleukin (IL)-1, A Disintegrin And Metalloproteinase with Thrombospondin Motifs (ADAMTS)-4, ADAMTS-5, and Matrix Metalloproteinase (MMP)-1, MMP-13 (**Figure 1B**). Additionally, hypertrophic chondrocytes produce less sGAG. As a result, the hydrostatic pressure within the ECM is reduced which

increases cartilage vulnerability for wear-and-tear-induced lesions to the collagen network. Regrettably, functional collagen type II turnover is known to be limited during a human life span. Any damage to the collagen network is beyond the repair mechanism of articular chondrocytes, and once ECM integrity is compromised OA will ultimately manifest in the joint (Figure 1B)¹³.

As mentioned before, healthy chondrocytes adopt a hypertrophic state during OA progression. Chondrocyte hypertrophy is a known feature of endochondral ossification. Endochondral ossification is the biological process that dictates longitudinal bone growth during mammalian skeletal development until adult length (i.e. of the bone) is achieved¹⁴. During this process they proliferate and severely increase their production of ECM. Eventually they adopt a hypertrophic state and when terminally differentiated, they will die through programmed cell death (apoptosis)¹⁵. Gene expression pattern of chondrocytes during endochondral ossification is closely resembled in differentiating chondrocytes present in OA¹⁶. Both in physiological endochondral ossification and pathological OA processes, hypertrophic chondrocytes stimulate invasion of cells from the subchondral bone¹⁷. This recruitment of osteoblasts and osteoclasts will collectively start to replace cartilage tissue with bone tissue. As a result, it is not surprising that OA is also characterized by prominent periarticular bone changes.

Peri-articular bone changes in osteoarthritis

The anatomy of subchondral bone in a healthy joint is nicely built with a thin dome-like subchondral plate supported by vertical oriented trabeculae (Figure 1A). The subchondral bone has an important role in evenly distributing forces from weight bearing and impact during physical activity, which protects the cartilage from high peak stresses and ECM damage. Normally, healthy cartilage is avascular and aneural¹⁸, so there is no need for perforations through the subchondral bone plate that otherwise would compromise its biomechanical function. However, this steady state is completely disturbed during OA progression (Figure 1B).

Although OA can be triggered by different initiating events (e.g. ligament¹⁹/meniscal trauma²⁰ or shape incongruity²¹⁻²³), eventually changes will develop within the subchondral bone. These early OA related bone changes are widely investigated in numerous animal models²⁴⁻²⁶. During early OA progression, subchondral bone first shows a reduction in thickness²⁷⁻²⁹ with increased numbers of subchondral pores³⁰⁻³⁴. On TRAP-stained histology sections, osteoclastic resorption was found to form these pores that extend up into the noncalcified cartilage region²⁹. In a longitudinal follow-up study, Botter et al investigated collagenase injected C57Bl/6 mice, within two weeks after OA induction there was a significant increase in bone perforations in diseased knee joints related to increased osteoclast activity³⁵.

Many hypotheses concerning the pathophysiology of OA concentrate on the cartilage-bone interface and its interaction. As mentioned before, OA shows many aspects of endochondral

ossification which involves the subchondral bone³⁶. Physiological endochondral ossification is highly dependent on vascularization, and angiogenesis plays an essential role in this process³⁷. Similar events are seen during OA progression. When chondrocytes within the deep cartilage zone become hypertrophic, they release angiogenic factors such as vascular endothelial growth factor (VEGF)³⁸. VEGF stimulates growth of new blood vessels from the perichondrial vascular network and subchondral bone spaces³⁹. Osteoclast infiltration is stimulated in order to make room for the neovascularisation from the bone up to the deep cartilage zone⁴⁰⁻⁴², and explains why vascular infiltration into subchondral bone is increased in human OA patients⁴³. As a consequence of osteoclast induced bone resorption, there is a loss of integrity and plasticity at the osteochondral junction. This compromises its biomechanical function and might promote further cartilage damage (**Figure 1B**).

After this initial phase of OA related bone resorption, studies have demonstrated a subsequent marked increase in osteoblast activity leading to thickening of the subchondral plate (**Figure 1B**). Other studies with larger animals showed similar results and reported thinning of the subchondral bone plate as well⁴⁴⁻⁴⁶ followed by a recovery and subsequent thickening of bone^{44, 46, 47}. During this increased bone turnover in OA joints, there is an altered phenotypic expression of osteoblasts that start to produce increasing amounts of collagen type I homotrimer (an increasing ratio of collagen type I $\alpha 1/\alpha 2$ chains of 4-17:1, compared to the healthy ratio of 2.4:1) instead of the normal collagen type I heterodimer^{48, 49}. This changed collagen ratio is typical for a sclerotic bone phenotype. When sclerotic bone is analyzed more closely, it shows an increased bone volume density and a reduction of its mineralization content^{50, 51}. When tested biomechanically, the material properties show a decreased energy absorbing capacity and increased stiffness^{52, 53}, but a stiffness that is lower than expected based on its higher volume fraction^{51, 54-57}. It is suggested that the larger bone volume fraction compensates for reduced bone tissue stiffness of OA subchondral bone⁵⁸. Eventually, the pathological high bone turnover may also induce possible cyst and osteophyte development, characteristic for late phase OA (**Figure 1B**)¹⁷. Interestingly, osteophyte formation has been linked to activation of macrophages that reside in the synovial membrane^{59, 60}.

Synovitis and osteophyte formation

The healthy synovial lining is composed of a thin layer synoviocytes and fibroblasts, which is inhabited by macrophages (**Figure 1A**)⁶¹. In contrast to cartilage, synovium is innervated with sensory neurons and highly vascularized enabling small molecules to diffuse through the synovium into the synovial fluid. All except the deepest chondrocytes in articular cartilage are supplied with necessary nutrients and oxygen through the synovial fluid. Synovial lining cells actively produce large amounts of hyaluronic acid (HA) and lubricin⁶². Both compounds provide lubrication and reduce friction between cartilage surfaces in an articular joint. High molecular weight molecules like HA and lubricin are not able to diffuse through the synovium and cannot

enter the bloodstream. Large molecules within the bloodstream are also not able to diffuse into the synovial fluid. In this way, the synovium function as a membrane preserving synovial fluid composition and viscosity.

During OA progression (**Figure 1B**), chondrocytes produce large amounts of cytokines that activate synovial macrophages (e.g. Tumor Necrosis Factor (TNF) α , Interferon (IFN) γ , IL-4, IL-13). When macrophages become activated, they also start to secrete cytokines and growth factors. These molecules are small and able to diffuse through the entire joint, even into the cartilage ECM. This inflammatory response induces synovial hyperplasia, stimulates macrophage infiltration, neoangiogenesis and fibrosis⁵³. As a result, the synovium becomes a source of proinflammatory and catabolic products, including metalloproteinases and aggrecanases that contribute to articular matrix turnover and degradation. As a result of macrophage TGF β production, synoviocytes produce bone morphogenetic protein (BMP)-2 and BMP-4 that stimulates osteophyte formation^{59, 60}. Additionally, synoviocytes produce less HA and lubricin and due to enhanced synovial permeability both molecules now diffuse readily out of the joint. As a result, the synovial fluid viscosity is reduced and its lubrication property diminished, which increases the friction and mechanical forces upon the cartilage and further contributes to cartilage degradation.

ANIMAL MODELS FOR OSTEOARTHRITIS

Most of the findings discussed in the previous sections, were investigated in animal models for OA. There are numerous models available and can roughly be divided into five different categories: (1) spontaneous, (2) surgical, (3) enzymatic, (4) chemical, and (5) biomechanical. Although each animal model has a completely distinct approach to induce OA, these differences help us to unravel specific cellular or molecular changes related to the OA pathogenesis. However, before starting with animal experiments, one has to carefully evaluate which model is best suited to answer the research question at hand (**Table 1**).

Spontaneous OA does not develop in all available laboratory animals. There are various strains of mice⁸⁷, guinea pigs⁶⁴, and even nonhuman primates that develop OA⁸⁸. Rats, however, hardly develop OA spontaneously⁸⁹. In spontaneous models, morphological joint changes closely resemble features of different stages seen in human OA. Due to this similar pathophysiological developmental pattern, there are equally large variations regarding speed of OA progression in each animal and extent of damage. Consequently, large study groups are needed in order to obtain significant differences between control and intervention groups, the period for drug testing or studies of pathogenesis is long, and experiments are costly⁸⁹.

	Ref	Induction	Pro	Contra
Spontaneous	64, 65	Aging Time	<ul style="list-style-type: none"> - Pathological similar to human knee OA progression - Bilateral similar progression - Progressive development of OA - Interaction with bodyweight 	<ul style="list-style-type: none"> - Variable and inhomogenous disease progression - Long follow up, time consuming and costly - Limited to several species, not in rats
	66-70	ACLT Surgical transection of the anterior cruciate ligament, medial or lateral collateral ligament	<ul style="list-style-type: none"> - Described in several species - Induction resembles traumatic lesion in humans - Homogenous cartilage lesions develop in short time span - Ideal for chondroprotective drug testing 	<ul style="list-style-type: none"> - Invasive surgical procedure - Risk of coinduction due to cartilage dehydration while operating, or infection. - Possible direct damage to cartilage during micro-surgery - The induced stability is permanent, which counteracts possible treatment effect.
	67, 71, 72	MMT Surgical destabilization or complete revoval of the medial meniscus	<ul style="list-style-type: none"> - Combination of surgical techniques possible - The greater the instability, the greater the lesions 	<ul style="list-style-type: none"> - Therefore not favorable for regenerative therapies
Surgical	25, 26, 73	Groove Chondral grooves in articular cartilage, without damage to the subchondral bone	<ul style="list-style-type: none"> - Primarily cartilage-driven disease - Spontaneous progression to other anatomical parts in the joint 	<ul style="list-style-type: none"> - Complex microsurgery, especially in rodents - Standarized application of grooves is hard to achieve
	74-78	MIA Inhibitor of glyceraldehydes-3-phosphate dehydrogenase activity, induces chondrocyte death	<ul style="list-style-type: none"> - Possible in nearly all animals - Very quick induction, lesions develop within 1 week - Reproducible lesions - Functional impairment as in humans - Dose response relation - Well described in literature 	<ul style="list-style-type: none"> - Due to specific chondrocyte cell death, loss of target cell for chondroprotective drug testing - Aggressive dysregulation of MMP production - Targetting pathways in MIA could lead to false positive or false negative results in human disease
Enzymatic / chemical	29, 78-80	Collagenase Digestive enzyme for collagen	<ul style="list-style-type: none"> - Homogenous lesions - Short time span - Can be achieved using one single injection intra articular injection in mice - Well described in literature 	<ul style="list-style-type: none"> - Collagenase injections degrades ligament within articular joints, and represents a enzymatic instability model - As for the ACLT model, therefore less suitable for regenerative therapies
	74, 81, 82	Papain Digestive enzyme that degrades the bond of proteoglycans	<ul style="list-style-type: none"> - sGAG loss without direct damage to collagen - No direct toxicity for chondrocytes 	<ul style="list-style-type: none"> - Overdosing leads to complete loss of articular surface - Damage of low dose can be restored - Multiple injections needed
Biomechanical	83, 84	Exercise Forced running on a motorized treadmill	<ul style="list-style-type: none"> - No surgery/injection needed - No direct toxic effect on chondrocytes or articular structures - Microscopic features similar to human disease progression 	<ul style="list-style-type: none"> - Only mild disease progression - A 30km running protocol is exhaustive for animals to complete - Bilateral model
	85, 86	Varus loading Surgical stance correction	<ul style="list-style-type: none"> - Severity of lesions can be controlled through applied load - Allows for thorough investigation of biomechanics and OA onset - Unilateral application 	<ul style="list-style-type: none"> - Risk for infection through external fixation - Complex application of varus loading devise

Table 1: Overview of different animal models for OA divided over different categories: spontaneous, surgical, enzymatic/chemical, and biomechanical models.

Surgical models are most commonly used in OA research. In general, during surgery a ligament is transected in the animal's knee joint that induces some form of instability. Transection of the anterior cruciate ligament⁶⁶, medial or lateral collateral ligament⁷², and destabilization of medial or lateral menisci⁹⁰ induce OA. It is possible to combine several transections to create larger instabilities in the knee joint, and it is assumed that with a greater instability OA will progress more severely⁶⁷. These models are considered to develop OA quite similar to patients that suffered traumatic knee injuries. The major disadvantage of these models is that the induced instability is irreversible and during tests with disease modifying drugs, the persisting instability will continuously counteract any potential beneficial therapeutic effect.

Enzymatic injections also induce OA, with the advantage of rapid OA development with consistent severity of joint degradation. One of them is the enzymatic model using collagenase injections, which has some similarity to surgical instability models^{78, 80}. When mice are injected with type VII collagenase, all ligaments in the knee joint will be damaged. Due to this ligament damage, knee joint instability develops which subsequently leads to cartilage degradation³⁴. Another enzyme used for OA induction is papain. Papain selectively degrades the bond of cartilage ECM proteoglycans (PG) with their core protein⁷⁴. Papain directly induces a loss of sGAG from cartilage and does not interfere with collagen. Therefore, papain is thought to induce an early feature of OA (sGAG loss) without induction of ligament instability. Although this is an advantage of the model, one has to be careful with the injected dose, because high doses of papain will result in complete loss of articular cartilage within days⁷⁴. Low doses of papain on the other hand induce minor sGAG loss that can be restored by chondrocytes without induction of an ongoing OA process⁷⁷, an effect that can be mistaken for a therapeutic effect.

Cartilage sGAG loss can also be induced via intra-articular injection of mono-iodoacetate (MIA), a chemical compound that is an inhibitor of glyceraldehydes-3-phosphate dehydrogenase activity and therefore an inhibitor of glycolysis shown to induce chondrocyte death⁹¹. Following MIA injection, cartilage lesions will develop characterized by chondrocyte necrosis, cell cloning (chondrones), fibrillation, loss of stainable proteoglycan matrix, and erosion with exposure of subchondral bone. Subchondral bone shows enhanced bone turnover with sclerosis and osteophyte formation⁷⁵. The combined involvement of subchondral bone together with articular cartilage degradation makes this model perfectly suited to investigate mechanisms that promote OA progression within the osteochondral subunit. Since MIA kills chondrocytes within a short time span⁷⁵, this model is not suited to investigate therapeutic interventions targeted at chondrocytes.

Finally, there are also several biomechanical models for OA. Strenuous running on a motorized rodent treadmill is known to induce OA in mice⁹² and Wistar rats⁸⁴ (**Video 1**). A 30 kilometers running protocol in six weeks time, will result in minor to moderate OA related

cartilage lesions, decreased sGAG content, uneven collagen type II distribution and increased MMP-13 expression. Gait analysis showed a unique change in gait pattern with stride lengths that reduce with ongoing OA⁹³. Exercise as induction method for OA is interesting, since it uses a physiological functioning of the joint in order to expose chondrocytes to supraphysiological compressive loads. Another approach to induce chronic loads on cartilage is to apply a varus loading device⁸⁵. This device can be placed as a external fixative and the increase of compressive load on the medial side of the knee joint can be tightly regulated. This compression results in diminished cellularity and increased histological degeneration which may replicate slow development of non-traumatic OA in which mechanical loads play a primary etiological role⁸⁶.

IMAGING TECHNIQUES FOR OSTEOARTHRITIS

Nowadays there are multiple imaging techniques available in for clinical diagnostics and for (pre-)clinical studies (Table 2). In the following paragraphs, all imaging techniques used in this thesis are presented.

Radiography

OA of hip and knee is usually assessed with weight-bearing made radiographs of the affected joint. X-ray radiographs allow for excellent imaging of dense tissues, like bone. Cartilage is not a dense tissue and therefore cannot be visualized directly using plain radiographs. However, cartilage thickness can be seen indirectly as the joint space width between the bony parts of an articular joint (Figure 2A). With progressing OA cartilage ECM is lost and the joint space becomes smaller (Figure 2A). The most commonly used grading scheme for the detection of OA on radiographs is the Kellgren-Lawrence score⁹⁴. This technique evaluates joint space narrowing (JSN) and bone related changes that are associated with the disease (like osteophyte formation, cysts and sclerosis).

Magnetic resonance imaging

Nowadays, clinical OA measurements (mainly pain scores) remain important, but due to subjectivity they poorly correlate with severity of OA^{95, 96}. Therefore, semi-quantitative MRI scoring systems for OA (Whole-Organ MRI Score (WORMS) and MRI Osteoarthritis Knee Score (MOAKS)) have been developed⁹⁷. In 1996, delayed gadolinium enhanced magnetic resonance imaging of cartilage (dGEMRIC) was first described⁹⁸. This technique was a breakthrough for OA research, since this technique enabled quantitative measurement of cartilage sGAG loss. dGEMRIC visualizes cartilage sGAG distribution after intravenous or intra-articular injection of a negatively charged contrast agent called gadolinium⁹⁸⁻¹⁰². Healthy cartilage ECM contains high amounts of sGAG and its content is an indicator of cartilage health¹⁰³. Due to sGAG negatively charged sulphate groups, negatively charged gadolinium is repelled from the cartilage. Due to sGAG loss in OA, less negatively charged sulphated groups are present in cartilage ECM. As a

result, more gadolinium penetrates the cartilage, which can be imaged and quantified using MRI. After first publications on this topic, MRI based imaging techniques have seen a rapid improvement during the last years. Several newly developed techniques have been developed to measure articular cartilage quality (e.g. Na²³ mapping, T2 mapping, and T1rho^{104, 105}). Due to more commonly available 3.0 Tesla MR systems and other novel MRI sequences (e.g., Ultrashort TE¹⁰⁶, SSFP¹⁰⁷, UTE T2*¹⁰⁸, and DENSE-FSE¹⁰⁹), fast MR scans with high in plane resolution for quantitative cartilage can now be acquired.

Imaging Technique	Abbreviation	Basic Principle	Pro	Contra
Radiographs	X-ray	Electromagnetic radiation is forced through an object and attenuation patterns are captured on a detector	<ul style="list-style-type: none"> - Simple - Low costs - Widely available - Well described in literature 	<ul style="list-style-type: none"> - Radiation exposure - 2D - Not every Xray is recorded in the exact same orientation
Computed Tomography	CT	X-ray projections are made over 180 degrees and reconstructed to 3D images using back projections	<ul style="list-style-type: none"> - 3D datasets - High resolution - Fast - Low costs - Widely available - Well described in literature - Allows contrast enhancement - Quantitative outcome 	<ul style="list-style-type: none"> - Radiation exposure - Less suited for soft-tissue imaging
Magnetic Resonance Imaging*	MRI	A strong magnetic field is used to align hydrogen nuclei, using radiowaves these nuclei are rotated. While returning to equilibrium in the magnetic field they emit a radio signal that can be detected using antennas (coils)	<ul style="list-style-type: none"> - Perfectly suited for soft-tissue imaging - Without radiation - Multiple sequences available for specific purposes - Quantitative outcome 	<ul style="list-style-type: none"> - Relative low resolution - Long scanning time - Absolute contra-indications: metal items, like pacemakers - Relative contra-indications: e.g. claustrophobia - Costs
Single Photon Emission Computed Tomography	SPECT	Delivery of a gamma-radiation emitting radionuclide. During the scan multiple gamma cameras acquire multiple 2D projections of recorded gamma radiation, which are reconstructed to a 3D dataset	<ul style="list-style-type: none"> - Coupling of radionuclides to specific receptors allows for imaging of molecular processes - Coregistration using plain CT (SPECT/CT) allows for anatomical localization of the SPECT signal - Quantitative outcome 	<ul style="list-style-type: none"> - Radiation exposure - Technically more challenging - More logistical limitations when applied for in vivo imaging

Table 2: Overview of different imaging techniques used for OA research in this thesis. *: MRI was not used for the experiments in this thesis, but frequently discussed when compared with CT based techniques.

Computed tomography

Computed tomography (CT) scanning is an X-ray based imaging technique that allows for three dimensional imaging of patients or objects, and predominantly used for bone analysis in musculoskeletal imaging. One of the main advantages of CT, is its ability for accurate imaging of (subchondral) bone. Müller-Gerbl et al showed already in the 90s that CT can provide a surface representation of the 3D density distribution in joints of living subjects¹¹⁰. The distribution of Hounsfield density within subchondral bone represents the distribution of bone mineralization. Using CT, age-related changes in bone mineralization of hip, wrist and ankle joints have already been reported. CT showed qualitative bone adaptation related to different levels of physical activity with increased mineralization in gymnasts or reduced mineralization due to postoperative immobilization¹¹¹. CT also proved a suitable technique for noninvasive investigation of subchondral bone changes within (OA) patients^{111, 112}.

Regular clinical CT systems have pixel dimensions of approximately 0.5 mm × 0.5 mm with a slice thickness of ~0.5 – 1.0 mm. As mentioned before, OA changes do not only imply changes of gross bone morphology, but also involve small changes of the subchondral bone plate and the underlying trabecular bone. This resolution therefore poses a problem for small animal imaging, since the average healthy subchondral plate thickness of mice is ~200µm, and ~250µm for rats. Nowadays, high-resolution µCT scanners are able to scan samples with spatial resolutions within the range of 5-30µm and are ideal for accurate imaging of early OA changes within subchondral bone and trabecular bone in small animals (**Figure 2B**)²⁸. This technique can be performed in a longitudinal fashion, measuring subchondral changes over time within a single animal. Longitudinal follow up for *in vivo* experiments will seriously reducing the need for large amounts of laboratory animals.

Through the addition of a contrast agent, µCT can be used to image cartilage and soft tissue as well. Similar to the technique used for dGEMRIC, the cartilage fixed charge density can be quantified using a negatively charged contrast agent (Hexabrix), which represents the sGAG-distribution within cartilage (Figure 2C). Loss of sGAG from the ECM reduces the overall fixed charged density of cartilage, more contrast penetrates the cartilage, which results in increased cartilage X-ray attenuation values^{113, 114}. Contrast enhanced µCT (CECT) has the resolution to (quantitatively) measure changes in sGAG content of rat^{114, 115} and mice⁹² cartilage. CECT is sensitive enough to measure sGAG loss from cartilage well before the ECM degrades. Equilibrium partitioning of ionic contrast agent (EPIC) using µCT is the designated technique to image cartilage *ex vivo* ^{114, 116, 117}, whereas intra-articular injected contrast allows for cartilage imaging *in vivo*¹¹⁵ (**Figure 2C**).

Single photon emission computed tomography

Molecular imaging techniques like single photon emission computed tomography (SPECT) or positron emission tomography (PET) allow for evaluation of OA changes on a molecular and functional level. Nowadays, multi-pinhole SPECT (mph-SPECT)¹¹⁸ and micro-PET (μ PET)¹¹⁹ are both optimized for preclinical research and these higher resolution techniques are suitable for small animal imaging. A broad application of these imaging techniques will divert the scientific discussion away from tissue level, but towards a model that will explain cellular mechanisms on a molecular level. Use of these molecular imaging techniques in preclinical studies allows for immediate studying of early disease changes directly after OA induction. More comprehensive patient studies using these techniques, seem a prerequisite in order to gain more knowledge regarding the complex OA pathogenesis.

Imaging of subchondral bone remodeling using ^{99m}Tc-MDP SPECT/CT

(μ)CT only visualizes the amount and location of (ectopic) bone formation resulting from enhanced bone remodeling. However, SPECT/CT is able to capture the actual ongoing activity that leads to bone formation, which can be seen only afterwards using CT. After intravenously injection of ^{99m}Technetium-methylene diphosphonate (^{99m}Tc-MDP), ^{99m}Tc-MDP will be incorporated into the hydroxyapatite of exposed osteoid at sites of bone formation and destruction. Using single photon emission computed tomography (SPECT) scanning, it is possible to visualize the amount of ^{99m}Tc-MDP at sites of increased bone turnover. When applied in a patient with an osteochondral lesion, SPECT/CT clearly detects enhanced bone remodeling within the lateral femoral condyle (**Figure 2D**). SPECT scanning using radioactive labeled polyphosphonates already proved to be highly sensitive for detecting and monitoring osteoarthritis¹²⁰⁻¹²². It correlates with clinical pain, osteophytes on radiographs¹²³, meniscus injury^{124, 125}, osteochondral lesions¹²⁶ and arthroscopic findings¹²⁷. Also, MRI findings of bone marrow lesions (BML) showed a nice agreement with increased radioactive uptake in bone scintigraphy^{128, 129}. In one of our studies using the mono-iodoacetate OA model⁷⁶, as early as 48 hours after injection OA induction, SPECT/CT found significant alterations in the subchondral bone (**Figure 2D**). This finding suggests early OA changes happen within the osteochondral subunit, which can be measured accurately with SPECT/CT.

Imaging of synovial macrophage activation using ¹¹¹In-DTPA-folate SPECT/CT

Another interesting technique using mph-SPECT measures macrophage activation within the synovium (**Figure 2E**). It is only after activation that macrophages express the functional form of folate receptor β (FR β)¹³⁰. This receptor is absent in quiescent macrophages and other immune cells, rendering FR β a very suitable target for molecular imaging. The vitamin folic acid binds with high affinity to FR β . After injection of a diagnostic radionuclide coupled to a folic acid analogue, the presence of FR β can be traced with high sensitivity using SPECT. This technique has demonstrated elevated levels of activated macrophages in both rheumatoid arthritis as well as osteoarthritis animal models¹³¹.

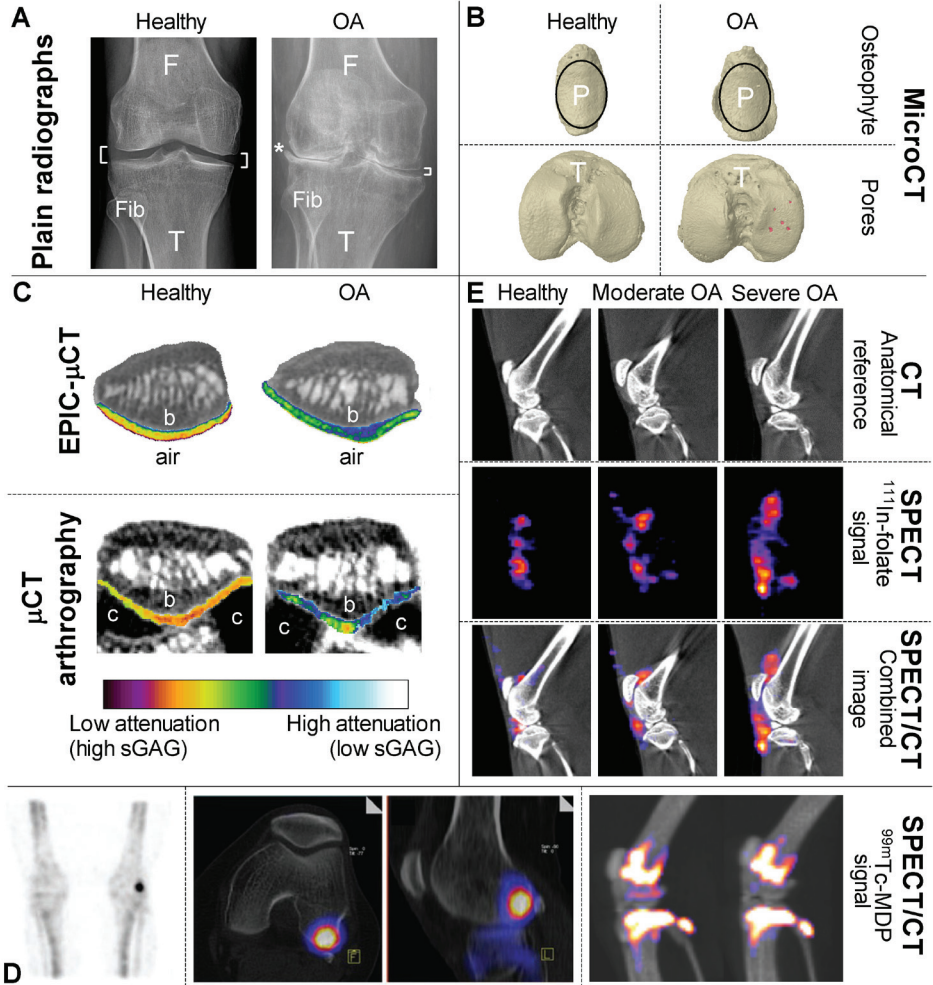


Figure 2: Different imaging techniques available for osteoarthritis research. **A:** conventional plain radiographs, in this case of the knee joint. The healthy example of a knee joint shows a wide joint space (indicated with white bars) between femur (F) and tibia (T), on both medial and lateral (side of the fibula, Fib) side of the knee. The OA knee joint shows clear joint space narrowing (JSN) and at the margins of the tibial plateau osteophyte formation can be seen (indicated with *). **B:** Three-dimensional frontal views of the patella (P) and top views of the tibial (T) plateau for healthy joints and OA made from plain microCT scans. Both circles drawn over the patella mark the physiological articular surface and is of exact equal size. This visualizes that at patellar margins in the OA joint, more bone is formed, which is in fact osteophyte formation. Top views of the tibial plateau show subchondral pore (red color) development in the OA knee joint, where the subchondral bone in the healthy joint remains intact. **C:** Contrast enhanced microCT techniques for analysis of cartilage quality (sGAG distribution) and quantity (volumetric measurements). Equilibrium partitioning of an ionic contrast agent

using microCT (EPIC- μ CT) is an ex vivo method, with this technique the articular cartilage saturated with ioxaglate and scanned at equilibrium. These measurements are highly accurate, since cartilage can be segmented using subchondral bone (b) and air as cartilage boundaries. MicroCT Arthrography is similar technique for in vivo cartilage analysis, using intra-articular ioxaglate injections. Only in this case, cartilage is segmented between subchondral bone (b) and intra-articular contrast agent (c). For both techniques, attenuation values are inversely related to the sGAG content, meaning that a high attenuation corresponds to low sGAG content. D: Macrophage activation determined after injection of ^{111}In -DOTA-Bz-folate using SPECT/CT. A plain microCT is made for anatomical reference, sagittal images are shown in black and white. Followed by single-photon emission computed tomography (SPECT), sagittal SPECT images are shown in colour. Both datasets are combined and allows the SPECT signal to be analyzed in a specific region of interest.

AIM AND OUTLINE OF THIS THESIS

Nowadays, we have no clue what drives OA progression in some patients, while in others it remains quiet for many years or even decades. As described in previous sections, OA is 'a whole joint disease' with early involvement of different tissues, including bone, cartilage and the synovium well before the cartilage ECM is degraded. A loss of joint space width on radiographs as a measure for OA is therefore not sensitive enough to detect early OA changes. When patients are diagnosed with OA they suffer from pain and severe limited range of motion in the effected joint; in other words the disease has already progressed significantly. In this phase of the disease, costly and invasive joint replacement surgery is currently the only treatment option that effectively treats OA patients' pain and limited functioning.

It is the aim of this thesis to study OA pathology in different animal models with multi-modality imaging techniques in order to clarify early pathological changes in OA, and test whether different therapeutic strategies might be beneficial for OA management.

In **Chapter 2** and **Chapter 3**, we present data of five animal models that were longitudinally monitored using different imaging techniques dedicated for small laboratory animals. This work enabled us to accurately monitor early OA related changes in cartilage, bone and synovium simultaneously and provided us with suitable reference data to further investigate specific aspects of OA pathogenesis.

As mentioned before, articular cartilage is evolutionary designed to facilitate joint mobilization. Cartilage is daily exposed to high-peak forces during physical activity⁸. Chondrocytes within the cartilage are sensitive to mechanical stimuli, which can compromise homeostasis^{8, 132}. The canonical Wnt/ β -catenin signaling pathway is recently suggested as a regulator of cartilage development and homeostasis¹³³⁻¹³⁵. In **Chapter 4** this signaling pathway was investigated *in vitro*, as well as *in vivo* using μ CT-arthrography. In respect to chondrocyte homeostasis and cellular stress responses, we investigated the role of Heat Shock Protein (Hsp) 90 and Hsp70

during biomechanically induced OA in rats subjected to strenuous running and present this data in **Chapter 5**.

Since OA is a ‘whole joint disease’ with involvement of cartilage, bone and synovium, we tested different therapeutic approaches thought to influence specific cell types in these tissues. First of all, tacrolimus (or FK506) is an immunosuppressive drug known to inhibit calcineurin activity and exerts positive effects on ECM marker expression on *in vitro* cultured chondrocytes. In **Chapter 6** FK506 is tested as a therapeutic agent for OA *in vitro* as well as *in vivo*. Secondly, alendronate (ALN) is a potent inhibitor of bone resorption and used widely as therapeutic for osteoporosis treatment. In **Chapter 7** alendronate was tested *in vivo* to see whether an inhibited osteoclastic bone resorption may prevent sclerotic bone formation. In the third place, we investigated intra-articular triamcinolone injections for OA management. Triamcinolon is widely used as a corticosteroid therapy for clinical patient care that predominantly acts as functional pain management. **Chapter 8** describes the effect of triamcinolon on macrophage activation *in vivo*. Finally, also mesenchymal stem cells (MSCs) and bone marrow mononuclear cells (BMMNCs) might be able to influence OA progression. These pluripotent cells are thought to stimulate anabolic processes and reduce catabolic events that promote cartilage health. The effects of intra-articular treatment of OA with these cell types is presented in **Chapter 9**.

All experiments in **Chapters 2-9** were conducted in animal models for OA using multi-modality imaging techniques. These techniques give insights to disease development with regard to OA as a ‘whole joint disease’. The current standard to diagnose OA in human patients remains plain radiography, but this technique is not sensitive enough to detect early OA. CT-arthrography (CTa) is an established clinical technique for imaging knee abnormalities, but it has not yet been investigated in humans as an indicator for cartilage sGAG content. In **Chapter 10** and **Chapter 11**, we describe the use of clinical CTa as a measure for cartilage quality.

Finally, a general discussion on the results of our presented work in this thesis is provided in **Chapter 12**. Here, we discuss how this thesis work might contribute to new therapeutic management strategies for OA and how it may provide a basis for further studies.

CHAPTER 2

QUANTIFYING OSTEOARTHRITIC CARTILAGE CHANGES ACCURATELY
USING IN VIVO μ CT ARTHROGRAPHY IN THREE ETIOLOGICALLY
DISTINCT RAT MODELS

M. Siebelt, J.H. Waarsing, N. Kops, T.M. Pijssens, J.A.N. Verhaar, E.H.G. Oei, H. Weinans

Osteoarthritis Cartilage, 2014 (Oct);22(10): 1470-80

ABSTRACT

Introduction

In vivo μ CT arthrography (μ CTa) can be used to measure both quantity (volumetric) and quality (glycosaminoglycan content) of cartilage. This study investigated the accuracy of four segmentation techniques to isolate cartilage from μ CTa datasets and then used the most accurate one to investigate if the μ CTa method could show osteoarthritic changes in rat models during longitudinal follow-up.

Methods

Volumetric measurements and glycosaminoglycan contents of patellar cartilage from *in vivo* μ CTa-scans were compared with an *ex vivo* gold standard μ CT-scan. Cartilage was segmented with three global thresholds and one local threshold algorithm. Comparisons were made for healthy and osteoarthritic cartilage. Next, three rat models were investigated for 24 weeks using μ CTa. Osteoarthritis was induced by injection with a chemical (mono-iodoacetate), a surgical intervention (grooves applied in articular cartilage), and via exercise (strenuous running). After euthanasia all knee joints were isolated for histology.

Results

Local thresholds accurately segmented cartilage from *in vivo* μ CTa scans and best measured cartilage quantity and glycosaminoglycan content. Each of the three osteoarthritic rat models showed a specific pattern of osteoarthritis progression. All μ CTa results were comparable to histology.

Conclusion

In vivo μ CTa is a sensitive technique for imaging cartilage degradation. Local thresholds enhanced the sensitivity of this method and will probably more accurately detect disease-modulating effects from interventional strategies. The data from rat models presented in this paper may serve as a reference for the time sequence of cartilage degeneration during *in vivo* testing of new strategies in osteoarthritis treatment.

INTRODUCTION

Current treatment strategies for osteoarthritis (OA) are limited and end-stage OA is treated with costly, invasive joint replacement surgery. Disease-modifying osteoarthritic drugs (DMOADs) that may target early disease progression are unavailable for clinical use. Therefore, a large need exists for testing the potential of DMOADs in animal OA models.

OA research in small animals using *in vivo* μ CT has mainly been limited to subchondral bone changes²⁹, since μ CT is not suited for soft tissue imaging. However, μ CT-arthrography (μ CTa) can accurately measure changes within cartilage tissue. Similar to delayed gadolinium enhanced magnetic resonance imaging (dGEMRIC)^{98, 101}, cartilage can be imaged and its sulfated glycosaminoglycan (sGAG) determined using a suitable X-ray contrast agent^{113, 136}. As sGAG forms the main component of the negative fixed charge density (FCD) in cartilage, the influx of a negative charged contrast agent is inversely related to the sGAG content. With OA progression, the FCD diminishes due to sGAG depletion and consequently more contrast agent will penetrate, which can be measured as a surrogate for cartilage quality.

Previous publications described an *in vitro* technique where cartilage samples were saturated in ioxaglate until an equilibrium between both the negative charge of the sGAG and the contrast was reached^{113, 114, 116}. This resulted in an excellent correlation between sGAG content and contrast inside the cartilage, which could be accurately quantified from μ CT-images. Further characterization of contrast-enhanced μ CT showed that before equilibrium, contrast diffusion strongly correlated with the inverse of the sGAG content^{137, 138}. A similar relationship between OA progression and contrast diffusion into cartilage was reported *in vivo*¹¹⁵.

Ideally, μ CTa can be used to measure both volume (quantity) and sGAG content (quality) of cartilage. However, severely sGAG depleted cartilage will contain high amounts of contrast, making it difficult to distinguish from free contrast in the joint. Therefore, accurate segmentation is necessary to obtain a correct structural representation of the tissue¹³⁹. We present methods to optimally represent both quantity and quality in one micro-CT scan. We gathered 24 week longitudinal reference data for three models each representing a different etiology¹⁴⁰: the intra-articular mono-iodoacetate (MIA) injection model that induces chondrocyte apoptosis⁹¹, the groove model that simulates OA after local trauma²⁶, and the running model that mimics physical overloading⁸⁴.

METHODS

Animal care

The Animal Ethic Committee of Erasmus Medical Center approved all conducted procedures. Eighteen 16-week-old male Wistar rats (Harlan Netherlands BV, Horst, the Netherlands) were housed in the Center's animal facility, with a 12-h light-dark regimen, at 21°C. Animals received standard food pellets and water ad libitum.

μCTa-procedure

The same μCTa technique as described by Piscaer et al¹¹⁵ was used. Briefly, under isoflurane anesthesia, the rat knee was shaved and injected with 70μl non-diluted Hexabrix320 (Mallinckrodt, Hazelwood, MO, USA) using a 27G needle (Sherwood-Davis & Geck, Gosport, UK). Epinephrine (Centrafarm, Etten-Leur, the Netherlands) (10μg/ml) was mixed with the contrast agent and to prevent loss of ioxaglate from the joint cavity.

After transfer to a holder with the rat in supine position and the hind leg fixed in extension, a μCTa was made using the Skyscan 1076 *in vivo* μCT scanner (Skyscan, Kontich, Belgium). Fifteen minutes of scan time was required at an isotropic voxel size of 35μm, at a voltage of 55kV, a current of 181mA, field of view of 35mm, and a 0.5mm aluminum filter, over 198° with a 1 degree rotation step. All scans were performed using these same settings, and all scan data was reconstructed in an identical way.

Optimal segmentation of cartilage

Six male Wistar rats received a single injection with 1 milligram MIA (Sigma-Aldrich, St. Louis, MO) dissolved in 50 μl saline under isoflurane anesthesia. MIA inhibits glyceraldehydes-3-phosphate dehydrogenase activity and directly acts on cartilage metabolism resulting in OA-like pathology⁹¹. All contralateral knee joints were injected with a similar volume of saline and served as a control.

Three weeks after OA induction⁷⁶, both knee joints of each rat were scanned with μCTa¹¹⁵. After euthanasia, all patellas were isolated for *ex vivo* analysis. All soft tissue were removed without damaging the cartilage. All patellas were incubated in saline diluted 40% Hexabrix320 for 30 minutes and all contrast saturated patellas were re-scanned *ex vivo* (Figure 1A₁). This protocol (exclusive of epinephrine) accurately measures both sGAG content¹¹³ and volumetric parameters¹¹⁶ of cartilage samples.

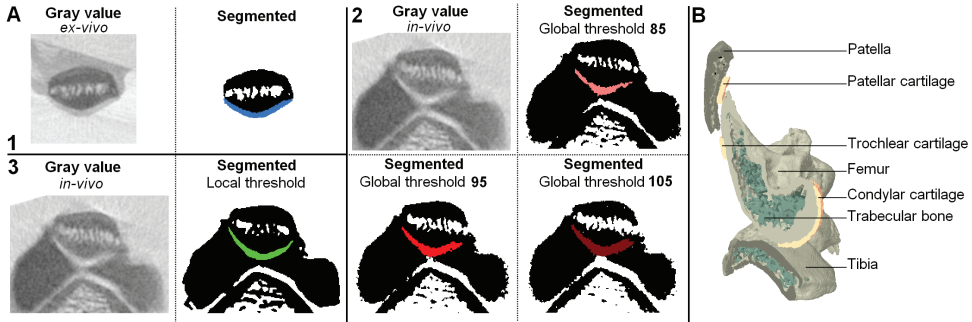


Figure 1: A: CT scan segmentation for four different techniques. Original gray value and segmented images are shown, coloured fields represent studied regions of interest. A1: Gold standard ex vivo CT scan of cartilage that is fully saturated with contrast. Accurate segmentation is possible due to the sharp transition of attenuation values between cartilage and (background) air. A2: Structural appearance of three different global thresholds. A3: Segmentation of in vivo CT scans via a local threshold. B: Anatomical regions of cartilage analyzed with microCT arthrography.

All generated *in vivo* datasets were stored as images with pixels of different gray-values that resemble X-ray attenuation of the material density, ranging from zero to 255 (from black to white). To segment cartilage, 3 fixed (global) threshold were used, 85, 95 and 105 (**Figure 1A₂**), set below bone and intra-cavitary contrast but well above soft tissue attenuation. All μ CT-datasets were also segmented using a local thresholds algorithm (3D Calculator software can be requested via: <http://www.erasmusmc.nl/orthopaedie/research/labor/downloads>) introduced by Waarsing et al¹⁴¹. This segmentation method maximized the structural representation of trabecular bone in original μ CT datasets. In summary, to find transitions between either bone and cartilage or contrast and cartilage, this local segmentation algorithm uses a standard edge-detection algorithm that is extended to 3D. μ CTa datasets are segmented into binary images, which serve as a mask that is laid over the original gray value images (**Figure 1A₃**) using freeware software (ImageJ software, National Institutes of Health, Bethesda, MD). Cartilage attenuation could be measured from the resulting images. Using Skyscan software, regions of interest (ROI) were drawn and in these ROIs, mean cartilage thickness, cartilage volumes and mean attenuation were calculated. Healthy cartilage has a high sGAG content, and little ionic contrast agent diffuses into the tissue, resulting in low CT attenuation numbers, and vice versa¹¹⁵. All measures were compared with the outcome from ex vivo μ CT^{113, 116}.

μ CTa characterization of three in vivo OA models

Numerous OA models exist for small animals⁸⁹. Three different OA-models were selected for monitoring cartilage changes during a 24 week follow-up using μ CTa. As a chemical model, we selected the MIA model. Previous work with 1mg of MIA demonstrated severe cartilage lesions after 3 weeks⁹¹. Due to the longer follow-up time, the amount of MIA in this group of six Wistar rats was reduced to a single 300 μ gr dose^{76, 91}. All contralateral knee joints received a saline

control injection. In our second model, OA develops from surgically applied chondral defects (grooves) in the cartilage^{25, 26, 73}. Surgery was conducted on six rats under isoflurane anesthesia. A small medial incision was made through the patellar tendon. With an average thickness of trochlear cartilage being ~200-250 μ m, the tip of our surgical tool generated grooves with a depth of 100-150 μ m leaving the subchondral bone unharmed (**Figure 2**). All contralateral knee joints were sham operated and served as a control. After surgery, all animals were allowed to move freely in their cages on all limbs. Thirdly, we selected an exercise model in which rats develop OA during strenuous running using a treadmill. After 30 kilometers of running during a 6 week protocol (**Figure 3**), moderate to severe OA lesions develop⁸⁴. Six rats were trained for one week on a treadmill (LE-8700; Panlab Harvard Apparatus, Barcelona, Spain) as follows: day 1, 10 minutes at 16.7 cm/sec; day 2, 15 minutes at 20 cm/sec; day 3, 20 minutes at 25 cm/sec; day 4, 30 minutes at 30 cm/sec and day 5, 35 minutes at 33.3 cm/sec. The following 5 weeks, the rats ran for 5 days/week, the first 10 minutes at 20 cm/sec to warm-up and the following 50 minutes at 33,3 cm/sec¹⁴².

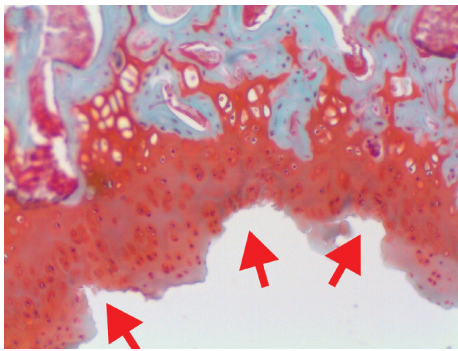


Figure 2: Histology after groove-surgery. Arrows point out to three grooves, note that the subchondral bone is not impaired. (Safranin-O stain; magnification = 100 \times)

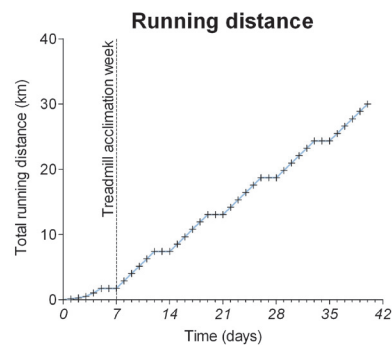


Figure 3: Distance covered in the strenuous running protocol.

All animals ($n = 18$) from the three OA models were μ CTa scanned before OA induction ($t = 0$) and after 1, 3, 6, 12, 18 and 24 weeks of follow-up. Mean attenuation and cartilage volume were calculated for three anatomical locations: condylar, patellar and trochlear cartilage (Figure 1B). However, with OA progression, sGAG loss was extensive, and contrast influx increased severely; thus severely degraded cartilage regions were excluded by the segmentation algorithm. As a result, severe sGAG depleted cartilage did not contribute to the mean attenuation. Instead, the cartilage volume was reduced. Therefore, we provided an additional measure that combines the volume loss and the mean attenuation increase to one single score that expressing the total change in attenuation in the cartilage ROI. This measure can be considered a surrogate measure for cartilage degradation:

$$\text{Cartilage degradation} = -1 \times \left(1 - \frac{(A_x \times V_x) + A_m(V_0 - V_x)}{(A_0 \times V_0)} \right)$$

in which $(A_x \times V_x)$ represents the contribution of the visible, segmented cartilage and $A_m(V_0 - V_x)$ represents the contribution of the lost volume of cartilage. The summed contributions were normalized using the average attenuation at baseline $(A_0 \times V_0)$.

Histology assessment

Animals were euthanized directly after the last μ CTa scan at 24 weeks; hind legs were harvested and fixed in paraformaldehyde for 1 week. Knees were decalcified with formic acid for 3 weeks and embedded in paraffin. Coronal sections were made at 300 μ m intervals and stained with Safranin-O to image the amount and distribution of sGAG. Sections were stained all at once, to minimize measurement artifacts. OA severity was graded using a modified Mankin scoring system for sGAG staining (0=normal cartilage; 1=slight reduction; 2=moderate reduction; 3=severe reduction; 4=no dye noted)¹ combined with a modified Pritzker score for structure composition (0=surface intact; 1=surface discontinuity; 2=vertical fissures; 3=erosions; 4=denudation; 5=deformation)¹⁴³. Decolourization and structure grading were multiplied with a separately assigned score, indicating the extent of decolourization or structural damage. The stage score was defined as follows: 1 = >0-25%; 2 = 25-50%; 3 = 50-75%; 4 = 75-100% of cartilage surface affected. When grading and staging scores were multiplied a maximum decolourization score of 16 and a maximum score for structural damage of 20 could be obtained. Scoring was applied for condylar, patellar and trochlear cartilage.

Statistical analysis

Differences between means of OA induced knees and sham treated contra-lateral knee from μ CTa data were evaluated for all parameters using unpaired t-tests. Histology averages were compared using non-parametric Mann-Whitney-tests (GraphPad Software, San Diego, CA). For all tests, p values < 0.05 were considered significant.

RESULTS

Optimal segmentation of cartilage

Our first goal was to investigate which method of cartilage segmentation method is most accurate in quantifying cartilage quantity (thickness, volume) and quality (sGAG content). We selected three global thresholds and the local threshold technique (**Figure 1A_{2,3}**). Higher global thresholds resulted in larger differences for thickness and volume measurements compared to ex vivo reference data (**Figure 4A-B**). Segmentation by local thresholds resulted in slightly more cartilage tissue for both control and MIA knee joints, but compared to using global thresholds this method showed less error in quantified thickness and volume.

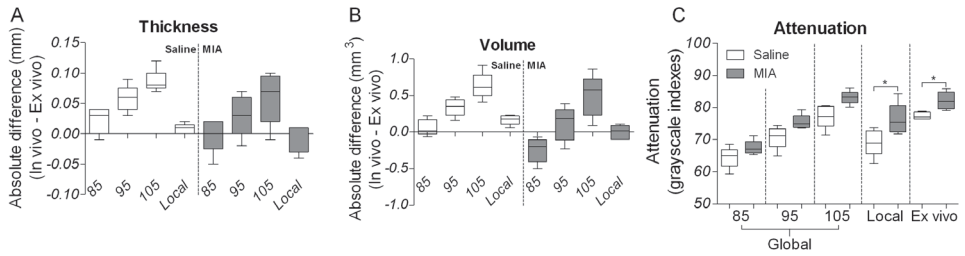


Figure 4: Cartilage quantity (thickness, volume) and quality (attenuation related to sGAG content) representation: in vivo versus ex vivo (gold standard) comparison of four microCT arthrography segmentation methods: three global segmentations at thresholds 85, 95 and 105 and the local threshold algorithm. A-B: Higher global thresholds resulted in larger differences with the gold standard, local thresholds showed less error in quantified thickness and volume. C: Average of mean patellar cartilage attenuation which is a representative measure for the sGAG content. In all cases the osteoarthritis induced knee joints (by MIA) had higher attenuation (less sGAG) compared to controls. Similar to the ex vivo gold standard, local thresholds detected the most significant difference between osteoarthritic and healthy cartilage *: $p < 0.05$.

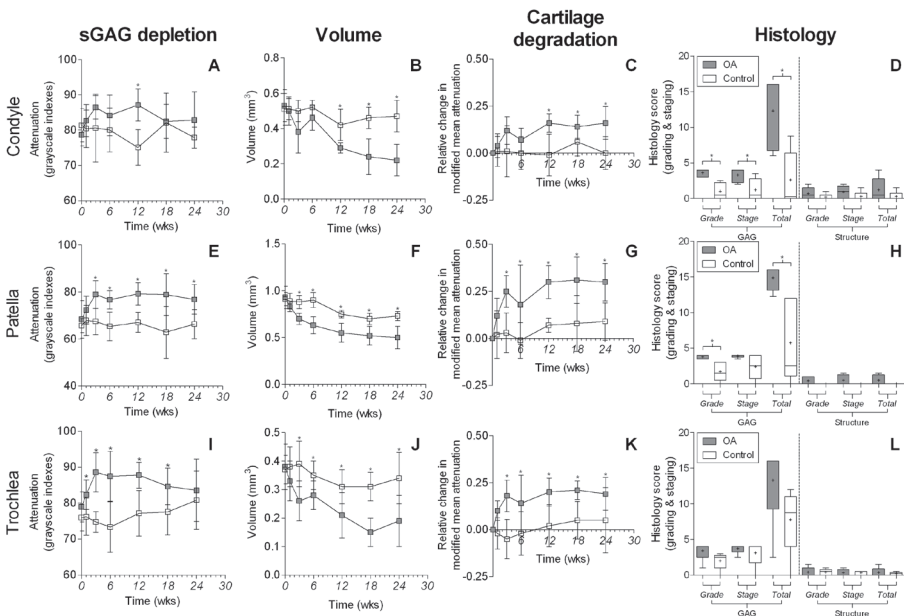


Figure 5: In vivo microCT-arthrography results showing osteoarthritic progression for all animals injected with MIA: attenuation (A,E,I), cartilage volume (B,F,J) and total GAG-loss (C,G,K); results of specific histology scores for GAG (reduced safraninO-staining) and structural architecture (D,H,L) for condylar cartilage (A-D), patellar cartilage (E-H) and trochlear cartilage (I-L). All asterisks indicate a difference between control and OA knee joints. *: $p < 0.05$

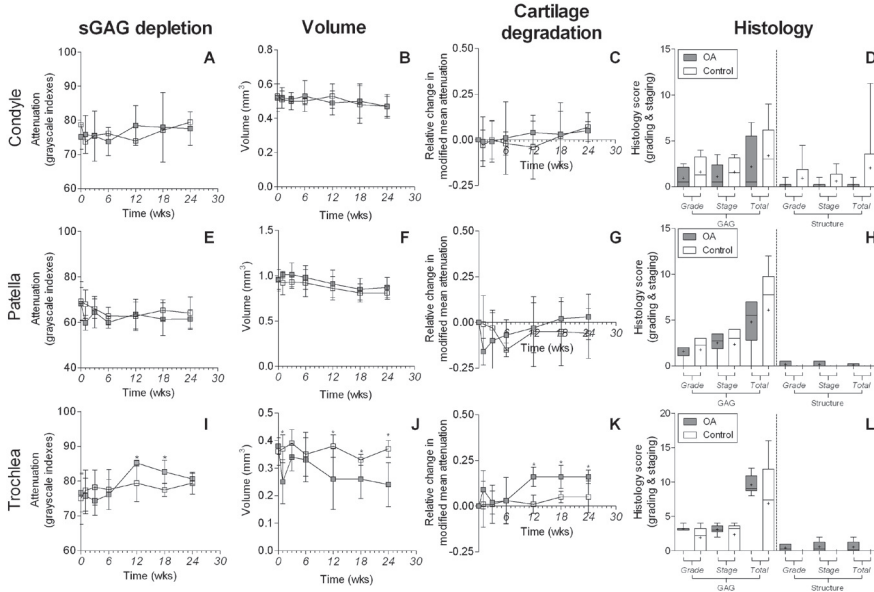


Figure 6: In vivo microCT-artrography results showing osteoarthritic progression after surgically applied chondral defects (groove) in the trochlear cartilage: attenuation (A,E,I), cartilage volume (B,F,J) and total GAG-loss (C,G,K); results of specific histology scores for GAG (reduced safraninO-staining) and structural architecture (D,H,L) for condylar cartilage (A-D), patellar cartilage (E-H) and trochlear cartilage (I-L). All asterisks indicate a difference between control and OA knee joints. *: $p < 0.05$

Quality measurements also showed a strong relationship between the degree of attenuation and the selected global threshold (Figure 4C). The pattern between healthy and OA cartilage was the same for each threshold method, but was significant only in both the local threshold analyzed *in vivo* datasets ($p = 0.02$; $mean_{saline} = 69.14$ 95%CI_{saline} 63.93 to 74.36 ; $mean_{MIA} = 76.47$ 95%CI_{MIA} 71.60 to 81.34) and the *ex vivo* reference-test ($p = 0.008$; $mean_{saline} = 77.47$ 95%CI_{saline} 76.09 to 78.84 ; $mean_{MIA} = 82.15$ 95%CI_{MIA} 78.76 to 85.54). As the local threshold algorithm performed better, we used this method to sequentially image the three OA rat models.

μ CTa characterization of three *in vivo* OA models

Three weeks after MIA injections, a significant loss of sGAG from the cartilage was seen at all locations between MIA and control knees (Figure 5). Although cartilage volume was reduced in the MIA model throughout the study, histology showed only a clear loss of sGAG from the cartilage by reduced safranin-O staining. Structural changes in cartilage composition (fissures, erosion or denudation) were minor (Figure 5D,H,L, Figure 8E-H and Figure 9).

In the second model, the trochlear cartilage was grooved (**Figure 2**), resulting in mild changes in mean attenuation and volume. With histology a homogeneous discoloration was seen in sections of all grooved knee joints (**Figure 6** and **Figure 8I-L**). Condylar and trochlear compartments showed no signs of OA compared to the sham operated control knees (**Figure 6** and **Figure 9**).

In the running model, signs of OA were detected throughout the study (**Figure 7**). The most severe μ CTa-based change in mean attenuation and loss of volume was found in trochlear cartilage (**Figure 7I-L**, **Figure 8I-L** and **Figure 9**), while in patellar cartilage only the volume reduced significantly (**Figure 7E-H**). In the weight-bearing condylar cartilage only minor and very local changes were seen with both μ CTa and histology (**Figure 7A-D**).

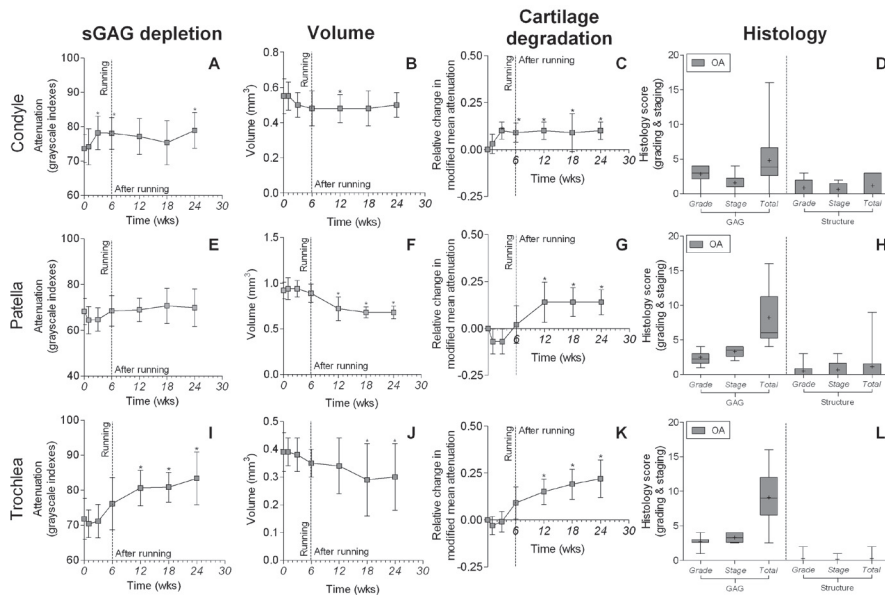


Figure 7: In vivo microCT-arthrography results showing osteoarthritic progression for rats during the running protocol and when exercise was stopped: attenuation (A,E,I), cartilage volume (B,F,J) and total GAG-loss (C,G,K); results of specific histology scores for GAG (reduced safraninO-staining) and structural architecture (D,H,L) for condylar cartilage (A-D), patellar cartilage (E-H) and trochlear cartilage (I-L) The running model is a bilateral model, all knees are included in the calculations and compared with baseline measurement. *: p < 0.05

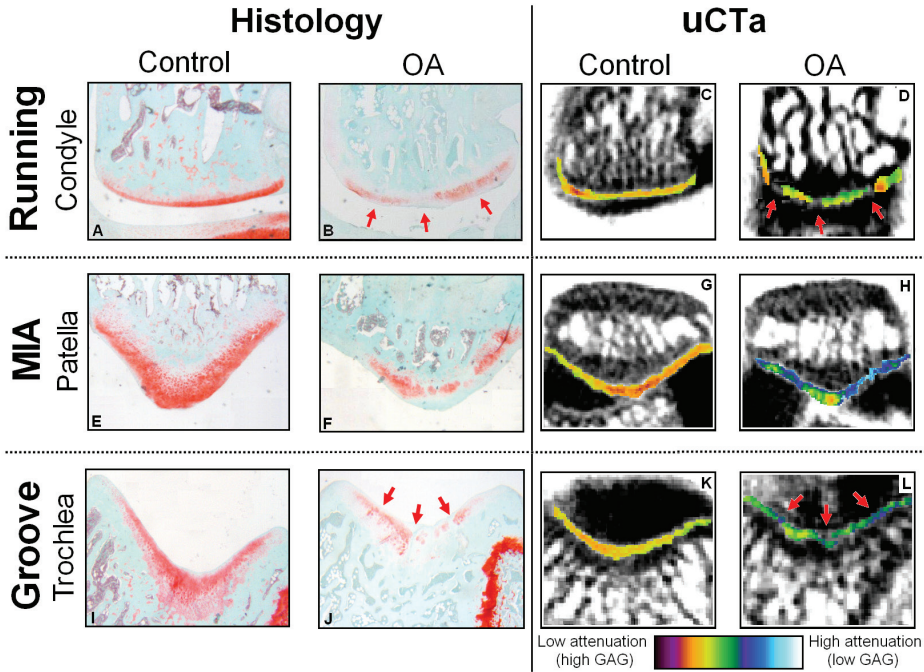


Figure 8: Histology stained with safranin-O (A-B,E-F,I-J) showing sGAG distribution and μ CT arthrography images (C-D,G-H,K-L) for condylar cartilage in running animals (A-D), patellar cartilage in MIA injected animals (E-H) and in animals with grooved trochlear cartilage (I-L). The red arrows point towards the small and focal osteoarthritic lesions in the running model seen on histology and detected with μ CT arthrography. Also the surgically grooved cartilage is pointed out with arrows. The tipped point of the surgical tool made focal lesions and comparable osteoarthritic changes were seen on μ CT scans.

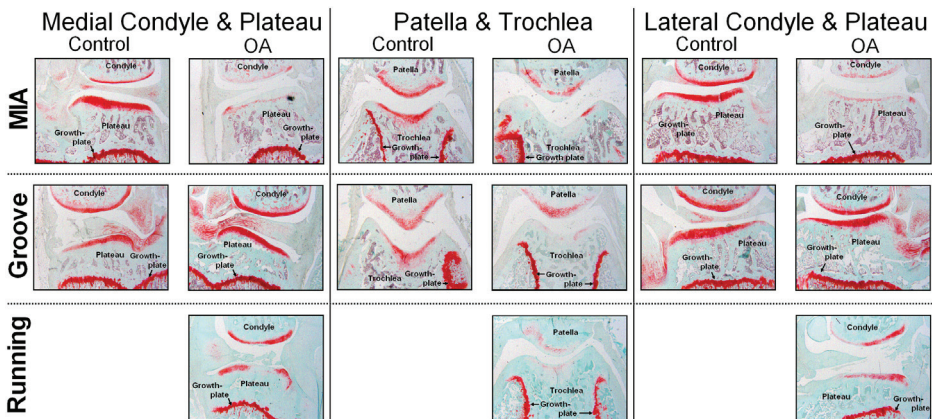


Figure 9: Histology for the running, MIA and groove-model (Safranin-O stain; magnification = 40x).

DISCUSSION

Optimal segmentation is important for assessment of quantifiable parameters using CT¹³⁹. Previously, the use of local thresholds improved the quantified outcome of bone parameters¹⁴¹. The current study demonstrates this for cartilage measurements using μ CTa (**Figure 4A-B**). Global thresholds elicit large segmentation errors and will include non-cartilage regions. Mean attenuation values determined with these segmentation techniques, therefore, do not accurately represent the sGAG content of cartilage. Besides accurate volumetric representation, the local threshold method also showed a significant increase of attenuation (less sGAG) in MIA injected knees (**Figure 4C**). We used this methodology to characterize (early) OA progression in three animal models over 24 weeks (**Figures 5-7**).

Injection with MIA quickly leads to sGAG depletion⁹¹. Patellar cartilage degenerated directly after treatment and OA developed throughout the joint (**Figure 5**). Therefore, the MIA model is suitable as a quick, homogenous model to screen whether DMOADs could benefit cartilage metabolism. It has been reported that the MIA model has little similarity with human OA gene expression and therefore discrepancies might occur between effects in animals and humans¹⁴⁴. However, for other (surgical) OA models that are widely used for testing DMOADs, these transcriptional differences also occur¹⁴⁵.

In the groove model, surgically applied grooves disrupt the collagen network, and sGAG depletion occurs, showing a close histological and biochemical resemblance with human OA⁷³. In comparison with other surgical models as ACL transection⁶⁶, the groove model does not have persistent knee instability that will counteract possible positive effects of studied treatments²⁵.

We showed that sGAG were severely depleted in grooved trochlear cartilage (**Figure 8I-L**), but OA did not progress throughout the entire joint (**Figure 6**). Our findings indicate that OA progression is slow and local, which makes the groove model suitable to test treatment strategies designed to repair cartilage lesions from local trauma. However, extensive training is needed to perform the complex microsurgery. Also factors such as inflammation or cartilage dehydration could influence the outcome. More research is required to validate the groove model.

Strenuously running rats showed signs of OA onset already after three weeks. Trochlear cartilage showed most pronounced signs of OA progression on both μ CTa and histology (**Figures 7-9**). OA progressed even though rats did not continue to run, indicating an ongoing cascade of OA processes exceeding the ability for spontaneous cartilage repair. This model does not rely on any chemical or surgical manipulation, making it suitable for use in OA research. Further characterization on a molecular level is needed to confirm its similarity with human OA.

μ CTa proves to be an excellent tool to monitor cartilage changes *in vivo*. However, a limitation of μ CTa is the ionizing radiation load and injection of contrast agent into the joint, both of which could potentially impact cartilage tissue and cause degeneration. Other longitudinal studies using μ CT did not show effects of radiation and contrast agent leading to OA¹⁴⁶. The scanning regiment used in our study resulted in a radiation dose of similar magnitude, ~ 0.5 Gy per μ CT scan¹⁴⁷, and a similar contrast dose¹¹⁵. Therefore, we assume neither factor affected cartilage metabolism.

Another limitation is the interpretation of the μ CTa data. Ioxaglate diffusion into cartilage tissue is negatively related to the amount of sGAG (Figures 5-7)^{113, 115}. With severe sGAG loss, however, attenuation increases to values close to the free contrast agent in the joint. Hence, in the severely diseased situation, complete loss of volume or severe sGAG loss only, cannot be differentiated, as demonstrated in our study by the large volume of sGAG depleted cartilage lost through segmentation. Also, when our μ CTa data are compared to histology scores, a large volume of cartilage was measured even though the cartilage was severely depleted of sGAG (Figure 7L).

μ CTa scans lack equilibrium between GAGs and contrast-agent, and diffusion properties of the cartilage matrix influence the quantified volume measures^{147, 148} as well. This likely led to the plateau seen in the degradation score (~ 0.25 - 0.30 for all severe sGAG depleted cartilage regions). With OA progression, more matrix degradation will occur, likely further increasing sGAG scores. Therefore, the cartilage degradation score represents sGAG loss (early OA onset) and matrix degradation (severe OA progression).

Previous work with μ CT in *in vivo* OA animal models demonstrated bone²⁹ and cartilage changes¹¹⁵ independently. We believe cartilage and bone parameters can be analyzed in one single *in vivo* μ CT scan, but further research is needed to develop accurate scanning protocols. Recent *in vitro* studies indicated that X-ray attenuation of tissue can predict its biomechanical properties (e.g. like compressive stiffness or dynamic modulus)^{149, 150}. More work could enhance knowledge about bone and cartilage interaction and their relation to biomechanical properties of healthy and OA knee joint.

In conclusion, we showed that μ CTa is a sensitive tool to detect early OA progression in small animal experimental models. Cartilage segmented from μ CTa scans with a local threshold resulted in more accurate sequential measurements for cartilage quality (sGAG) and quantity (thickness/volume). Use of μ CTa seriously enhances the ability to detect small changes that result from potential intervention techniques, even with a small number of animals. The models tested (MIA, groove and running) have specific advantages and disadvantages. The OA progression demonstrated by these models may serve as a reference for testing new treatment strategies.

ACKNOWLEDGEMENTS

We acknowledge the Dutch Arthritis Association and the Smart Mix Program of the Netherlands Ministry of Economic Affairs and the Netherlands Ministry of Education, culture and Science for their financial support.

CHAPTER 3

INCREASED PHYSICAL ACTIVITY SEVERELY INDUCES OSTEOARTHRITIC
CHANGES IN KNEE JOINTS WITH SULPHATE-GLYCOSAMINOGLYCAN
DEPLETED CARTILAGE

*M. Siebelt, H.C. Groen, S.J. Koelewijn, E. de Blois, M. Sandker, J.H. Waarsing,
C. Müller, G.J.V.M. van Osch, M. de Jong, H. Weinans
Arthritis Res Ther. 2014Jan;16(1):R32*

ABSTRACT

Introduction

Articular cartilage needs sulfated-glycosaminoglycans (sGAG) to withstand high pressures while mechanically loaded. Chondrocyte sGAG synthesis is regulated by exposure to compressive forces. Moderate physical exercise is known to improve cartilage sGAG content and might protect for osteoarthritis. This study investigated whether rat knee joints with sGAG depleted articular through papain injections might benefit from moderate exercise, or whether this increases the susceptibility for cartilage degeneration.

Methods

sGAG were depleted from cartilage through intra-articular papain injections in left knee joints of 40 Wistar rats, their contralateral joints served as healthy controls. Twenty rats remained sedentary, another twenty rats were subjected to a moderately intense running protocol. Animals were longitudinally monitored for 12 weeks with *in vivo* μ CT to measure subchondral bone changes and SPECT/CT to determine synovial macrophage activation. Articular cartilage was analyzed at 6 and 12 weeks with *ex vivo* contrast enhanced μ CT and histology to measure sGAG content and cartilage thickness.

Results

All outcome measures were unaffected by moderate exercise in healthy control joints of running animals compared to healthy control joints of sedentary animals. Papain injections in sedentary animals resulted in severe sGAG depleted cartilage, slight loss of subchondral cortical bone, increased macrophage activation and osteophyte formation. In running animals, papain induced sGAG depleted cartilage showed increased cartilage matrix degradation, sclerotic bone formation, increased macrophage activation and more osteophytes formation.

Conclusion

Moderate exercise enhanced OA progression in papain injected joints and did not protect against development of the disease. This was not restricted to more extensive cartilage damage, but also resulted in pronounced subchondral sclerosis, synovial macrophage activation and osteophyte formation.

INTRODUCTION

Articular cartilage is evolutionary designed to facilitate joint motion. Cartilage extra-cellular matrix (ECM) is composed of a collagen matrix in which chondrocytes reside. These cells produce high concentrations of sulfated-glycosaminoglycans (sGAG), which contain negatively charged sulphate groups that sets the cartilage fixed charged density. Due to this fixed charged density large amounts of cations and water enter the cartilage ECM, expanding the collagen network and creating a high hydrostatic pressure. Cartilage daily endures high-peak mechanical loading including shear, compression and tension (contact) stresses. During physical activity, it is estimated that compressive stresses can rise up to 10-20MPa⁸. The high internal hydrostatic pressure allows articular cartilage to absorb these stresses and facilitates the dissipation and distribution of external forces during joint mobilization⁹⁻¹¹.

The amount and type of external mechanical loading are important factors that regulates development and long-term maintenance of cartilage. This is because chondrocytes closely regulate sGAG levels dependent on the level of physical activity¹³². For example, in hamsters a sedentary lifestyle is known to reduce cartilage sGAG content, whereas daily exercise prevents this loss¹⁵¹. Galois et al investigated whether different running intensities influenced osteoarthritis (OA) progression and found that moderate running protected against OA development in anterior cruciate ligament transected knee joints¹⁵². In another experiment with mono-iodoacetate (MIA) induced OA, exercise also prevented cartilage damage. MIA inhibits glyceraldehydes-3-phosphate dehydrogenase activity, resulting in chondrocyte apoptosis and sGAG loss⁹¹. When MIA injected rats were subjected to treadmill running, the superficial and intermediate areas of the joint showed a better preservation of sGAG content⁸³. These studies support the idea that a mild biomechanical stressor on cartilage enhances chondrocytes ability to sustain sGAG levels and protect cartilage against OA onset.

Kiviranta et al also showed that moderate running augments sGAG in articular cartilage of Beagle dogs¹⁵³. However, later on they found that a strenuous exercise protocol induced marked sGAG depletion from superficial cartilage zones¹⁵⁴. Since then, strenuous exercise has been shown to reduce chondrocyte metabolism and sGAG synthesis¹⁵⁵. Besides inhibited sGAG production during strenuous exercise, chondrocytes also start to actively deplete sGAG from cartilage which is facilitated through increased matrix metalloproteinase-13 (MMP-13) production⁹³. So, cartilage loading through strenuous running seems to elicit an imbalanced ratio of sGAG synthesis and sGAG depletion. Reduced sGAG content eventually results in reduced hydrostatic pressure, compromising cartilage's ability to absorb compressive forces. This could be the reason why acute or chronic high-intensity loads are described to cause cartilage ECM damage¹⁵⁶, and may explain why healthy rats subjected to strenuous running protocols develop cartilage damage that is closely related to OA onset^{84, 157}.

In summary, moderate biomechanical loads on cartilage can stimulate chondrocyte sGAG synthesis, improve cartilage quality and can protect against OA^{152, 158}, whereas cartilage loading through strenuous running induces OA. In early OA sGAG levels in cartilage are reduced, making the tissue more vulnerable for damage by mechanical loading. This study investigated whether rat knee joints with sGAG depleted articular through papain injections might benefit from moderate exercise, or whether this increases the susceptibility for cartilage degeneration. OA is a disease not limited to articular cartilage. OA is considered a ‘whole joint disease’ with involvement of subchondral bone, synovium and articular cartilage changes^{17, 159} (Figure 1). All of these changes are most likely to play an important role in the complex cascade of pathological changes during OA development. Therefore besides measurements on articular cartilage degradation, we also measured subchondral bone changes with μ CT and macrophage activation with SPECT/CT. Our results demonstrate that moderate exercise, that does not have an effect on healthy joints, exerts detrimental effects on sGAG depleted cartilage and also on subchondral bone and synovial macrophage activation.

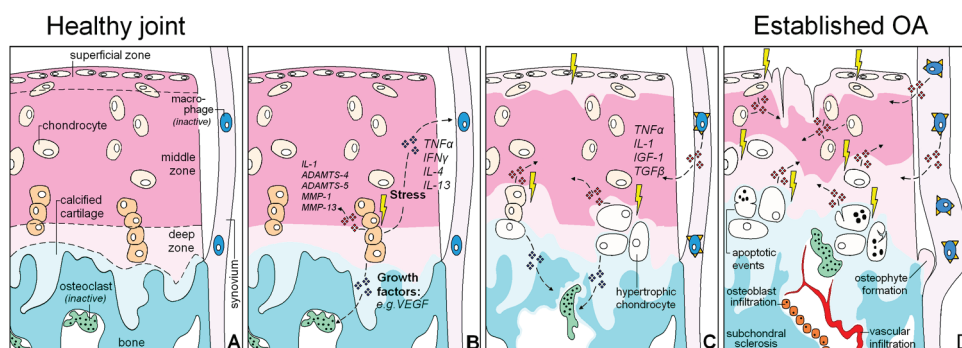


Figure 1: Hypothetical model that shows in what manner changes of cartilage, subchondral bone and synovial macrophages all contribute to osteoarthritis development. A: schematically depicted healthy joint with chondrocytes in cartilage extra-cellular matrix, bone and inactive osteoclasts, and resting synovial macrophages. B: chondrocytes suffering from a pathological strain produce cytokines and growth factors that diffuse towards the underlying bone marrow and synovium. There these products stimulate osteoclastogenesis and can activate macrophages. C: progressive phase of OA. Chondrocytes become hypertrophic and produce less sulphated-glycosaminoglycans (sGAG) to sustain the cartilage, making the ECM more susceptible for compressive forces. Osteoclasts start tunneling through the subchondral bone which compromises plate stability and changing its supportive function for the overlying cartilage. Activated synovial macrophages produce growth-factors of their own that promote synovial fibrosis, osteophyte formation and may stimulate ECM degradation. D: Eventually, cartilage is severely sGAG depleted and becomes structurally deprived. Activated macrophages stimulate fibrotic remodeling of the synovium and induce osteophyte growth. Osteoclast activity extends into the calcified cartilage, up to the border with the deep zone of the cartilage. Through subchondral pores there is vascular ingrowth into the cartilage. Later on, osteoblasts infiltrate and start to deposit bone that results in end-stage sclerosis.

METHODS

Study design

Forty 16-week-old male Wistar rats (Charles River Netherlands BV, Maastricht, the Netherlands) were housed in the animal facility of the Erasmus Medical Centre, with a 12-h light-dark regimen, at 21°C during the experimental period. Animals received standard food pellets and water ad libitum.

Intra-articular papain injections were used to reduce cartilage sGAG content in Wistar rat knee joints *in vivo*^{74, 81, 82}. Previous studies reported three intra-articular injections to induce OA on day 1, 4 and 7^{81, 160}. However, after one single papain injection, weight bearing of the injected joint restores to normal one week after the injection⁷⁷. Therefore, we injected our animals on day 8, 15, and 22. After they were adapted to the treadmill, with intervals of 1 week in order to have the rats restore their gait. All animals were injected intra-articular in their left knee joint with 30µl papain/L-cystein solution. This solution consisted of 2% w/v papain solution (type IV, double crystallized, 15 units/mg, Sigma-Aldrich, St. Louis, MO, USA) and 0.015M L-cystein (Sigma-Aldrich) in saline⁸¹. Epinephrine (10µg/ml, Centrafarm, Etten-Leur, the Netherlands) was added to induce vasoconstriction and prevent fast leakage from the knee joint^{115, 157, 161}. All right knee joints were not injected and served as healthy controls. Rats were divided over two groups: twenty rats remained sedentary, and twenty rats were forced to run on a motorized treadmill. All running rats were trained to run on a motorized rodent treadmill during the first week (LE-8700; Panlab Harvard Apparatus, Barcelona, Spain)¹⁵⁷. The following 5 weeks, rats were forced to run for five days a week, the first 5 minutes at 20 cm/sec in order to warm-up and the following 25 minutes at 35 cm/sec. The pace and duration of this protocol are equal to about 25% of a total exhaustion protocol for rats¹⁶². In total, running rats covered a total distance of 15 km over the total six week period, which is a protocol known to protect from cartilage degradation in both MIA and surgical models for OA^{83, 152}.

During the study all animals were longitudinally monitored with µCT to measure subchondral bone changes. At six and twelve weeks, ten rats in both groups were randomly selected for a full analysis sequence. This sequence consisted of SPECT/CT to quantify macrophage activation *in vivo*, and *ex vivo* EPIC-µCT and histology to measure cartilage quality. A detailed planning scheme of all groups and conducted tests is given in **Figure 2**. The Animal Ethic Committee of the Erasmus Medical Center, Rotterdam, the Netherlands, approved all conducted procedures.

In vivo µCT to measure subchondral bone changes and osteophyte growth

All animals were µCT scanned before start of the running protocol ($t = 0$) and after six and twelve weeks of follow-up. In short, under isoflurane anesthesia, after transfer to a holder with the rat in supine position and the hind leg fixed in extension, µCT scans were made using a Skyscan

1176 in vivo μ CT scanner (Skyscan, Kontich, Belgium). 10 minutes of scan time were required per knee at an isotropic voxel size of $18\mu\text{m}$, at a voltage of 65kV, a current of 385mA, field of view of 35mm, using a 1.0mm aluminum filter, over 198° with a 0.5 degree rotation step, and a 270 msec exposure time. All scans were performed using these same settings, all scan data was reconstructed in an identical way, and post-processing was done as described previously^{28, 29, 35}. Shortly, all datasets were segmented with a local threshold algorithm. This algorithm is ideal for accurate bone analysis (3D Calculator software can be requested via email)¹⁴¹. Using Skyscan analysis software, the tibial epiphysis was selected in the CT scans and analyzed for changes in cortical and trabecular bone. Cortical and trabecular bone were automatically separated using in-house software²⁸. Both subchondral plate thickness (Sb. Pl. Th. in μm) and subchondral plate porosity (Sb. Pl. Por. in mm^3) of the medial and lateral compartment of the tibial plateau were measured³⁵. In the tibial epiphysis, the trabecular thickness (Tb. Th. in μm) and trabecular bone volume fraction (BV/TV), representing the ratio of trabecular bone volume (BV, in mm^3) to endocortical tissue volume (TV, in mm^3). Ectopic bone formation (mm^3) on both lateral borders of the patella was also quantified as a measure for osteophyte growth in these longitudinal μ CT scans.

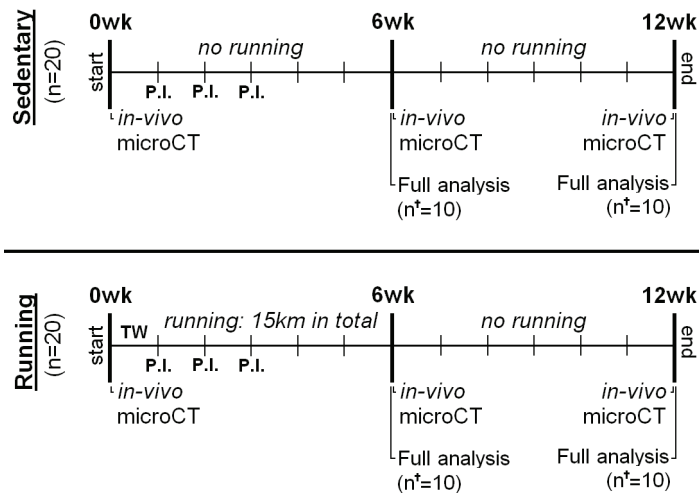


Figure 2: Experiment design indicating analytical time points and methods for each experimental group. Forty 16-week-old male Wistar rats received three intra-articular papain injections (P.I.) and divided over two different groups: a sedentary group (n=20) and a running group (n=20). All running rats were subjected to a six week moderate running protocol earlier reported to protect against OA. During the experiment three μ CT scans were made to measure longitudinal subchondral bone changes. At six and twelve weeks a full analysis sequence was done in ten animals per group (n_t), consisting of: determination of activated macrophages using SPECT/CT in vivo; and cartilage analysis with equilibrium partitioning of an ionic contrast agent using (EPIC-) μ CT and histology ex vivo.

Determination of activated macrophages by SPECT/CT using ^{111}In -EC0800

Activated macrophages express the folate-receptor- β ¹⁶³. Targeting this folate receptor with folate radioconjugates can be used to monitor activated macrophages *in vivo* by non-invasive nuclear imaging^{130, 164}. This technique was previously introduced for OA research in a rat model¹³¹. Briefly, phosphate saline-buffered (PBS, pH 6.5) DOTA-Bz-folate (DOTA-Bz-Folate, EC0800, kindly provided by Endocyte Inc., West Lafayette, USA) was incubated with $^{111}\text{InCl}_3$ (Covedien, Petten, The Netherlands) in mixture of quenchers and sodium acetate (final pH 3.5-4) for 15 minutes at 80°C as described earlier¹⁶⁵. Quality control was performed with instant thin layer chromatography medium-using a silica gel (ITLC-SG)^{166, 167} and revealed a radiochemical yield of ~93% at a specific activity of 50 MBq/ μg . After radiolabelling, Diethylenetriamine-pentaacetic acid (DTPA) was added for complexation of non-incorporated ^{111}In . The solution was further diluted in phosphate buffered saline (PBS) and administered via the tail vein twenty hours prior to scanning. Each animal received ~55MBq of ^{111}In -DOTA-Bz-folate under isoflurane anesthesia. SPECT/CT scans were performed with a 4-head multiplex multi-pinhole small animal SPECT/CT camera (NanoSPECT/CT™, Bioscan Inc., Washington DC, USA). Each detector head was fitted with a tungsten-based collimator of nine 2.5mm diameter pinholes, the field of view was 24mm in width and energy peaks were set at 170keV and 240keV ($\pm 10\%$). All knee joints were scanned with both helical μCT (acquisition time 5min) and SPECT (acquisition time 30min). After scanning, all datasets were reconstructed at an isotropic CT voxel size of 200 μm and an isotropic SPECT voxel size 600 μm using HiSPECT software (Scivis, Göttingen, Germany). All scans were analyzed using InVivoScope processing software (Bioscan Inc.). A cylindrical region of interest (ROI), based on the CT scan but blinded for the radioactivity, was manually determined for quantification of the radioactivity around and in the knee joint. In order to correct for the size of the drawn ROI, all data is presented as measured activity (kBq) per mm^3 . To reduce inter-individual variation, the absolute difference in measured radioactivity (kBq/ mm^3) of the OA knee joint compared to their internal control joint was calculated. This absolute difference was used when comparing means of papain only and papain combined with running animals.

Cartilage measurements with EPIC- μCT

Equilibrium partitioning of an ionic contrast agent using μCT (EPIC- μCT) has a strong correlation with cartilage sulfated-glycosaminoglycan (sGAG) content¹¹³. sGAG is a key-molecule of cartilage and its content is an indicator of cartilage health¹⁰³. In EPIC- μCT an equilibrium-state exists between sGAG and contrast agent after an 24 hours incubation period. Resulting cartilage X-ray attenuation in these scans are inversely related to sGAG content and thereby represent cartilage quality. This technique is suited for quantitative analysis of cartilage degradation for preclinical evaluation of OA¹¹⁷.

Animals were euthanized directly after the last SPECT/CT scan and both knee joints were harvested for EPIC- μCT analysis. The proximal tibial bone was isolated and soft tissue was

removed to a maximal extent, without harming cartilage integrity. Next, all specimens were incubated in 40% solution of ioxaglate (Hexabrix320, Mallinckrodt, Hazelwood, MO, USA) which was diluted in 60% phosphate buffered saline for 24 hours at room temperature, together with inhibitors of proteolytic enzymes (5 mM of ethylenediamine tetraacetic acid disodium salt, VWR International, Fontenay, France; and 5 mM of benzamidine

hydrochloride hydrate, Sigma-Aldrich Inc., St. Louis, MO, USA)¹³⁸. EPIC- μ CT was performed on the 1176 in vivo μ CT scanner (Skyscan), using the following scan settings: isotropic voxel size of 18 μ m, a voltage of 65kV, a current of 385mA, field of view 35mm, a 0.5 mm aluminum filter, 198° with a 0.5 degree rotation step, and a 235 msec exposure time. All scans were performed using the same settings and all data were reconstructed identically.

Using Skyscan analysis software, these datasets were segmented using a fixed attenuation threshold between air (30) and subchondral bone (120), that was selected visually for the best segmentation result in all datasets. In all segmented μ CT datasets, ROIs were drawn manually around the cartilage of the medial and lateral plateau of the tibia separately. From these ROIs, the X-ray attenuation (gray values related to sGAG content ranging from 0 to 255) and cartilage thickness (μ m) was calculated.

Histopathological examination of the knee joint

After EPIC- μ CT, the separated parts of the knee joints were fixed in 3.7% phosphate buffered formaldehyde, decalcified with formic acid and embedded in paraffin. Sagittal sections of 6 μ m thickness were made at 300 μ m intervals and stained with Safranin-O with a fast green counterstain to image the amount and distribution of the GAGs. Sections were stained all at once, to minimize artifacts in between different samples.

Statistical analysis

Differences between means of papain injected and healthy knee joints within the same animal were tested using paired t-tests at each time point for all outcome parameters, except when testing differences for osteophyte formation (GraphPad Software, San Diego, California, USA). Osteophytes did not develop in non-papain injected control joints in both experimental groups, therefore we used a one-sample t-test and tested whether the outcome of the papain injected joints differed from zero (GraphPad Software). When comparing differences between means of sedentary animals and running animals, unpaired t-tests were used at each time point for all outcome parameters (GraphPad Software). For all tests, p values < 0.05 were considered statistically significant.

RESULTS

All sedentary rats increased in weight from 404.3g (398.8 – 409.6g) to 454.0g (445.6 – 462.4g) after six weeks, and further increased to 488.0g (475.2 – 500.8g) after twelve weeks. Bodyweight of all running rats at baseline was 416.4g (411.3 – 421.5g), during the six weeks of treadmill running this did not increase (mean weight 408.3g; 398.2 – 418.3g) and was significantly lower compared to sedentary rats ($p < 0.0001$). However during the subsequent six weeks of rest, all running rats increased in bodyweight (mean weight 485.5; 473.0 – 498.0g) to levels similar to sedentary rats (Figure 3).

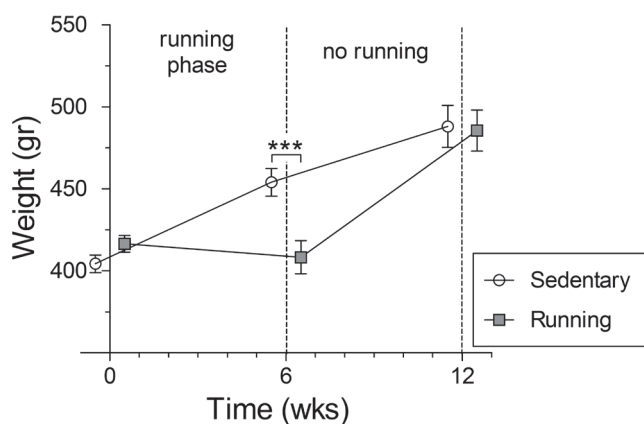


Figure 3: Increase in rat bodyweight (gram) during the experiment of sedentary (white circles) and running (gray squares) animals. **: $p < 0.01$, error bars indicate 95% confidence intervals.

Osteoarthritic changes of articular cartilage

As measured with EPIC- μ CT, intra-articular injections with papain resulted in sGAG loss from medial and lateral cartilage compartments of the tibia plateau in sedentary animals compared to their control joints ($p < 0.0001$) (Figure 4A,E). Running increased sGAG depletion from cartilage of the medial compartment of papain injected joints at six weeks compared to sedentary papain joints ($p < 0.0001$). At twelve weeks of follow-up, this difference slightly reduced but attenuation values were still significantly higher in running animals ($p = 0.03$). Running had no effect on sGAG content in healthy joints. After six weeks of running, the thickness of the medial cartilage was slightly lower in the papain injected compared to their contralateral joint ($p = 0.007$), and compared to sedentary papain joints ($p = 0.008$). Only after twelve weeks, the cartilage in sedentary papain joints slightly degraded and became thinner compared to the contralateral control joint ($p = 0.004$) (Figure 4C,E). The running papain joints, however, showed clear progression of cartilage degradation and at 12 weeks remained thinner compared to sedentary papain joints ($p < 0.0001$).

Attenuation values of lateral compartment cartilage were lower in running papain joints compared to papain joints of sedentary animals, indicating a higher sGAG content ($p = 0.03$) (Figure 4B). The lateral cartilage, however, was thinner in running animals (Figure 4D) and showed pronounced denudation of subchondral bone (Figure 4E).

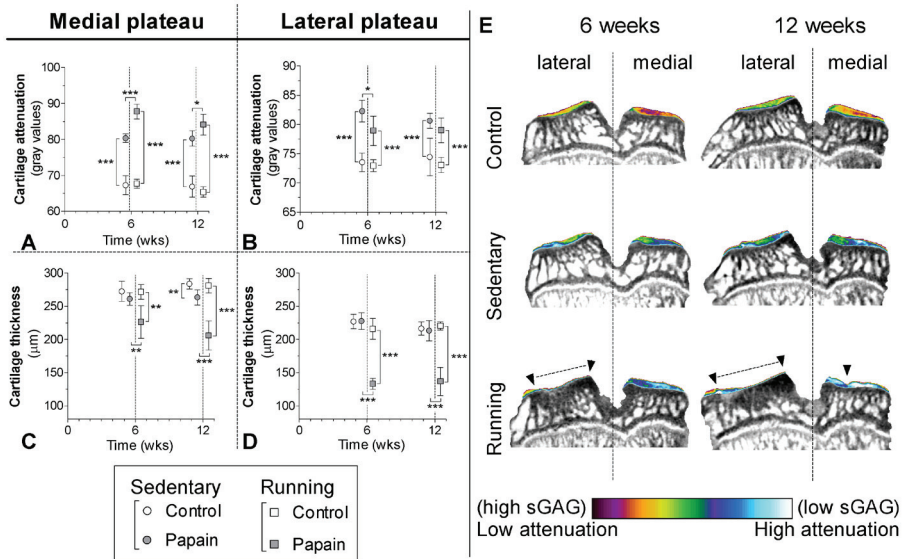


Figure 4: Cartilage quality and quantity was determined from samples of sedentary (round boxes) and running (square boxes) rats with equilibrium partitioning of a ionic contrast agent using EPIC- μ CT (A-D). The amount of sulphated-glycosaminoglycans (sGAG) (arbitrary gray values; A,B) and cartilage thickness (μm ; C,D) were measured of medial (A,C) and lateral (B,D) cartilage compartments of the tibia plateau harvested from control (blank boxes) and sGAG depleted joints (gray boxes). Attenuation values from EPIC- μ CT scans are inversely related to the sGAG content, meaning that a high attenuation corresponds to low sGAG content. Coronal images from representative EPIC- μ CT scans of the tibia plateau show the amount of cartilage (erosions indicated with \blacktriangle and dashed lines) and sGAG content (displayed in color). *: $p < 0.05$, **: $p < 0.01$, ***: $p < 0.001$, error bars indicate 95% confidence intervals.

A similar result was seen on histology sections (Figure 5). These images show that only calcified cartilage remained intact in the lateral compartment of papain injected joints subjected to running.

Subchondral bone changes

In vivo μ CT showed that subchondral bone of the medial tibia plateau increased in thickness during the experiment in all rats. Subchondral bone thickness in sedentary papain joints ($p = 0.01$) and running papain joints ($p = 0.01$) was slightly lower after six weeks of follow-up compared to sedentary control joints (Figure 6A). At six weeks, subchondral bone plate pores were only detected in sedentary papain joints ($p = 0.003$ compared to its contralateral joint, $p =$

0.02 compared to running papain joints). In some animals these pores became larger, but there was no significant difference between sedentary and running animals at twelve weeks (Figure 6B,G-H).

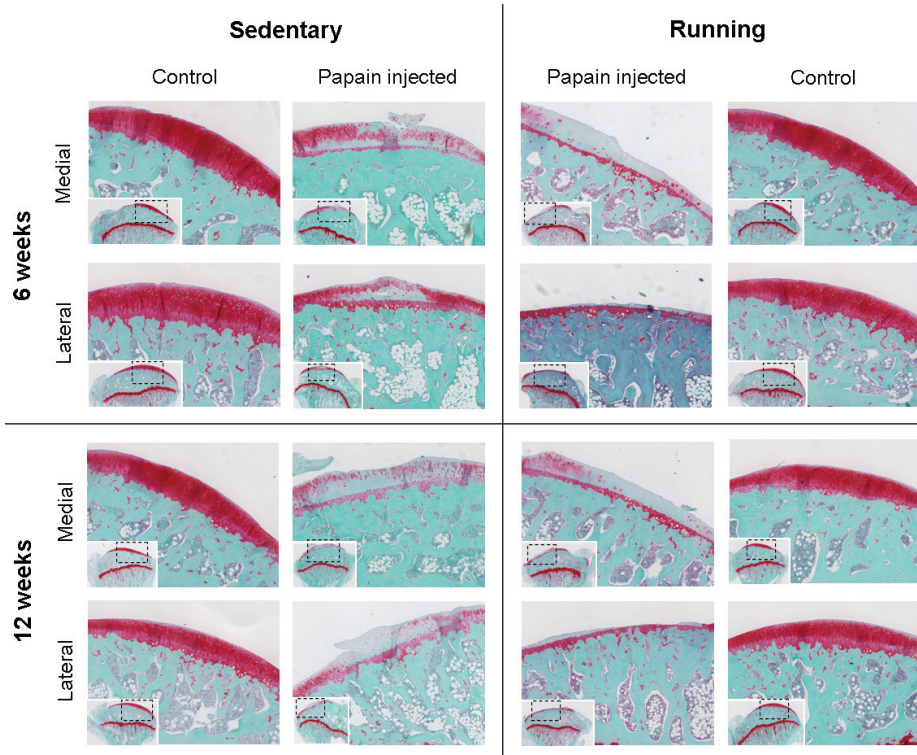


Figure 5: Histology of safranin-O stained sagittal sections of medial and lateral tibia plateau cartilage after six weeks and twelve weeks of follow up. Both in sedentary as in running animals, cartilage of papain injected joints was severely sulphated-glycosaminoglycan depleted at six weeks and twelve weeks. But in running animals the extra-cellular matrix showed clear signs of erosion in the medial compartment and even denudation of bone in the lateral compartment.

In sedentary animals lateral subchondral bone thickness showed a response similar to the medial compartment: subchondral bone of sedentary papain joints was thinner compared to its contralateral knee joint ($p = 0.004$ at six weeks, and $p = 0.003$ at twelve weeks). However, in papain injected and running joints, lateral subchondral bone showed a completely different response compared to its medial component. Here severe subchondral sclerosis developed after six weeks compared to its contralateral knee joint ($p < 0.0001$) and this sclerotic appearance persisted after subsequent six weeks of rest ($p < 0.0001$) (Figure 6C,G-H). In running animals there was a clear increase in subchondral plate porosity at six weeks compared to their healthy knee joint ($p = 0.02$) and compared to sedentary papain joints ($p = 0.02$). Plate porosity seemed

to further increase at twelve weeks but this was not significant anymore. Which is probably due to the loss of power, since our group size was reduced to 10 animals at 12 weeks compared to 20 at six weeks.

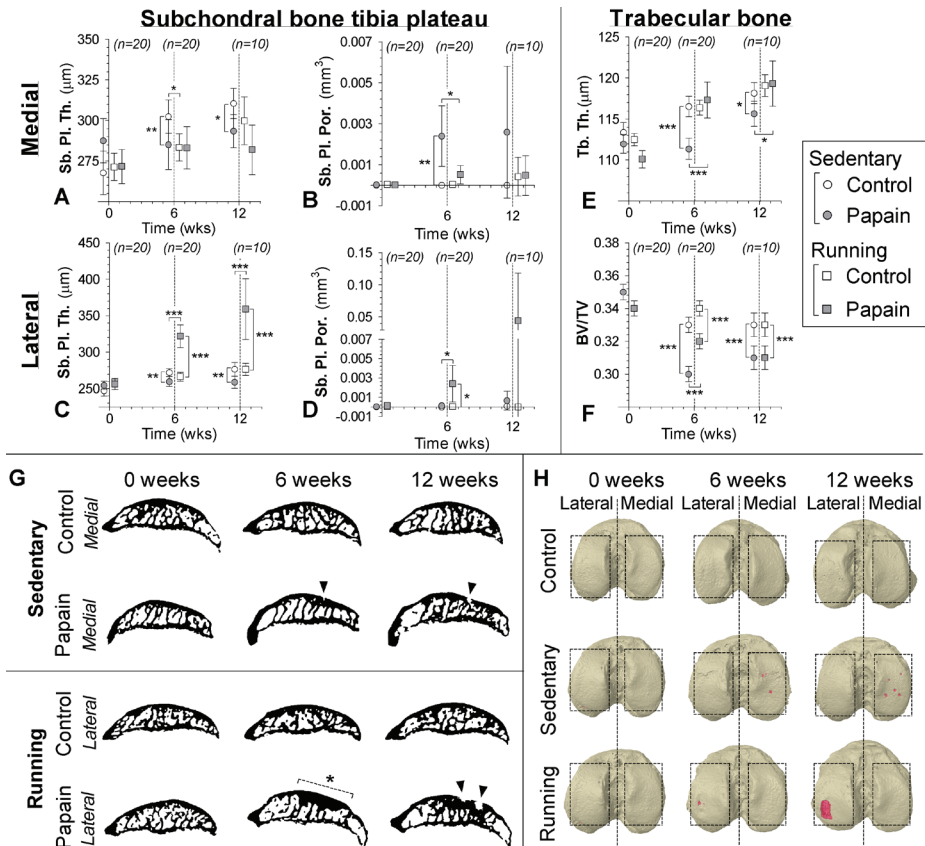


Figure 6: Subchondral bone changes analyzed with longitudinal in vivo μCT in control (white circles) and papain injected (gray squares) knee joints. Data points were nudged from analyzed time points 0, 6 and 12 weeks for clearer representation of results. Subchondral plate thickness (Sb. Pl. Th.; A, C) and porosity (Sb. Pl. Por.; B, D) were measured in the medial (A, B) and lateral (C, D) compartment of the tibial epiphysis. Changes in trabecular thickness (Tb. Th.; E) and trabecular bone volume fraction (BV/TV; F) were measured in tibial epiphysis bone marrow. G: shows representative sagittal images from binary μCT scans to show most prominent subchondral bone changes, which is pore development in medial subchondral bone of papain injected animals (indicated with \blacktriangle), and development of subchondral sclerosis (indicated with dashed line and $*$) in lateral subchondral bone of papain injected and running animals. Three-dimensional top views of the tibial plateau at different time points (H) show subchondral pore (red color) development in papain animals and papain plus running animals. $*$: $p < 0.05$, $**$: $p < 0.01$, $***$: $p < 0.001$, error bars indicate 95% confidence intervals.

Trabecular bone underlying the subchondral bone plate was thinner in sedentary papain joints compared to its contralateral joint at six weeks ($p < 0.0001$), and was still thinner at the end of the experiment ($p = 0.01$). The BV/TV in papain joints of sedentary and running animals showed a clear loss of bone mass throughout the experiment.

Control joints of all animals in both experimental groups showed no sign of patellar osteophyte formation. In sedentary papain joints and running papain joints there was evident patellar ectopic bone formation at six ($p < 0.0001$) and twelve weeks ($p < 0.0001$). We also measured a larger volume of ectopic bone formation in papain running joints compared to the sedentary papain joints at both six ($p < 0.0001$) and twelve weeks ($p = 0.03$) (Figure 7B,C).

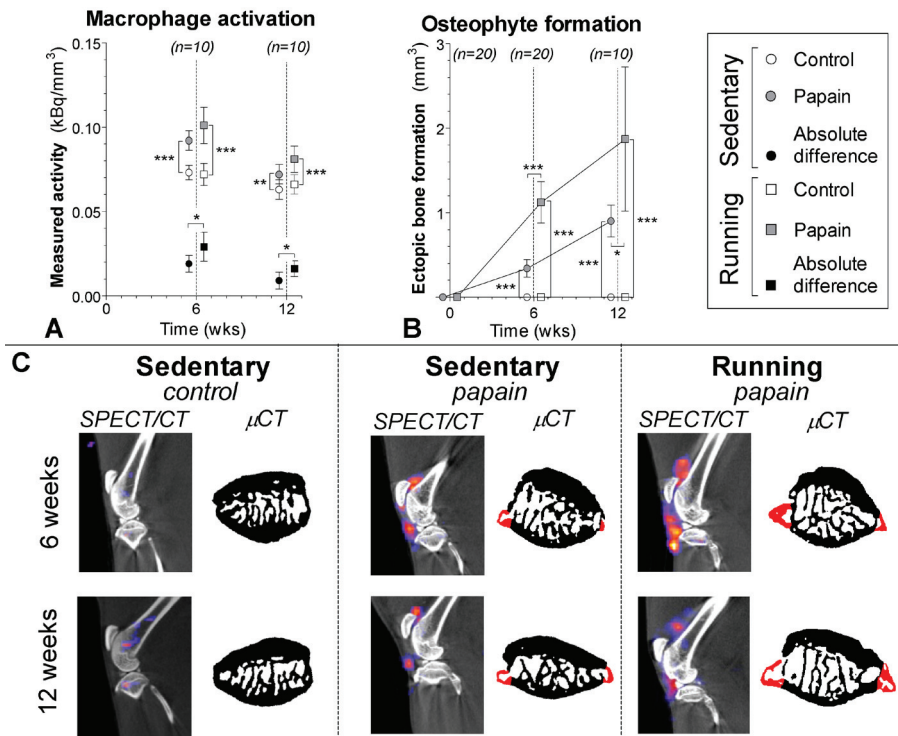


Figure 7: Macrophage activation determined in sedentary (round boxes) and running (square boxes) rats by injection of ^{111}In -DOTA-Bz-folate using SPECT/CT. A: Quantitative outcome of measured radioactivity in the control (blank boxes) and papain injected (gray boxes) knee joints normalized to the size of the cylindrical region of interest (kBq/mm^3). Absolute differences per animal were calculated (kBq/mm^3) to reduce inter-individual variation (black boxes). A high radioactivity is related to more macrophage activation. B: Ectopic bone formation (mm^3) as a measure for osteophyte development was quantified on longitudinal bone μCT scans. C: Sagittal SPECT/CT images of knee joints from representative animals. CT images shown in black and white were used for anatomical reference, the SPECT images are shown in color. Transaxial images from patellar bone extracted from binary μCT images show ectopic bone formation (red color). *: $p < 0.05$, **: $p < 0.01$, ***: $p < 0.001$, error bars indicate 95% confidence intervals.

Macrophage activation

Animals in both groups received 55 ± 2 MBq (mean \pm SD) of ^{111}In -DOTA-Bz-folate, there was no significant difference between both experimental groups. Papain joints of sedentary rats showed more macrophage activation measured with DOTA-Bz-Folate SPECT/CT compared to their control knees at six weeks ($p < 0.0001$). There was still increased macrophage activation at twelve weeks of follow-up ($p = 0.02$), but the effect was less pronounced. In running animals, macrophage activation was also higher in their papain injected joints at six ($p < 0.0001$) and twelve weeks ($p = 0.004$), but running did not increase macrophage activation in healthy knee joints. We calculated absolute differences between non-papain injected and papain injected joints and compared these values between both experimental groups. Both at six ($p = 0.03$) and twelve weeks ($p = 0.03$) macrophage activation was higher in papain injected joints of running than in joints of sedentary animals (**Figure 7A,C**).

DISCUSSION

Papain is a proteolytic enzyme that causes chondroitin sulphate release from the cartilage¹⁶⁸. We confirmed the known effect of intra-articular injections that papain injections in knee joints of sedentary animals induced sGAG depletion (**Figure 4 and 5**)⁷⁴. Besides these known changes in cartilage, *in vivo* μCT showed that papain injections induced a loss of medial subchondral plate thickness, formation of subchondral plate pores, and loss of trabecular bone (**Figure 6**). These aspects were previously related to early OA development^{28, 35}. Additionally, with *in vivo* folate-receptor- α targeted SPECT/CT, we found an increased level of activated synovial macrophages in papain injected joints of sedentary animals (**Figure 7**). Cytokine producing activated synovial macrophages are thought to play a prominent role in osteophyte development^{59, 60}. Papain injected joints of sedentary animals also showed clear increased osteophyte formation. In conclusion, papain injections induced prominent sGAG loss from cartilage and showed development of pathological features in bone and synovium related to early OA progression. However, more tissues in the joint besides articular cartilage might have suffered damage due to repetitive papain injections. Meniscal cartilage is composed of collagen matrix as well as chondroitin sulfate as its dominant sGAG⁷⁰. And synovium also has sGAG present within its extracellular matrix of the synovial intima and within the interfibrous matrix¹⁶⁹. Papain injections might also have compromised these structures, but we did not investigate this any further.

In line with other published data, our current study found no negative effects of exercise on healthy joints of running animals compared to healthy joints of sedentary animals (**Figure 4**)^{83, 152}. Thus, this exercise protocol can be considered a physiological exposure for healthy sGAG-rich cartilage. Earlier studies reported beneficial effects of moderate physical exercise on healthy cartilage and prevention of osteoarthritis^{83, 152, 153, 158}. However, sGAG depleted cartilage appears highly susceptible for OA progression when exposed to moderate exercise. In running animals

sGAG depletion and cartilage thinning was extensive compared to sedentary controls and no protective effect of moderate exercise was found. As mentioned before, articular cartilage is likely not the only tissue that suffered a loss of sGAG due to papain injections. It can be expected that papain induced degradation of meniscal cartilage, ligaments and synovium as well. Possibly, papain induced changes in several joint tissues and may explain why moderate exercise did not protect against articular cartilage degradation and OA progressed severely in those joints. Strikingly, there was a big difference in response between medial and lateral cartilage. Medial cartilage showed a clear loss of sGAG and approximate ~25% loss of medial cartilage thickness. Whereas within the lateral compartment, subchondral bone was completely denuded of articular cartilage. Healthy cartilage though, also shows a difference between medial and lateral cartilage and attenuation values of medial cartilage was ~10% lower compared to lateral cartilage for both sedentary and running animals. This means that medial cartilage is likely to have more sGAG in the medial tibia compartment, which we also have found in another study described previously¹⁷⁰. Rats are known to put more weight on their medial compartment⁸⁶. In order to withstand these enhanced loads, Chondrocytes within the medial compartment might produce higher levels of sGAG. This might be the reason, that after papain injections more sGAG remained within this compartment compared to lateral tibia cartilage. As a consequence, lateral cartilage was more susceptible for ECM damage, which might have been the reason that lateral cartilage totally eroded.

The enhanced effects of OA in running animals was not limited to cartilage. OA related pathology in bone and macrophage activation was also enhanced in those joints. Moderate running induce marked changes within the subchondral bone. In the lateral compartment, the subchondral bone plate increased in thickness and led to a sclerotic bone phenotype (**Figure 6**). We believe that the complete loss of cartilage in this compartment changed the force propagation through the subchondral bone. The sclerosis formation might be an attempt to restore subchondral biomechanical stress levels during the physically active phase, with activation of osteoblasts that increase the subchondral bone mass in order to adapt to increased physical load exposure^{171, 172}. Intriguingly, compared to sedentary animals, moderate exercise protected against a loss of trabecular subchondral bone (**Figure 6**). It is suggested that loss of trabecular bone might be due to unloading of the OA induced joint because of pain and discomfort for the animals, since gait alterations have been reported in animals with experimentally induced OA^{173, 174}. Exercise plays an important role in the development and maintenance of bone mass and strength and is known to prevent against bone loss in human patients suffering from osteoporosis^{175, 176}. We believe that exercise was able to exert a similar effect on trabecular subchondral bone maintenance in our experiments.

As mentioned before, during OA development the macrophages within the synovium become activated¹³¹ and can produce cytokines that enhance osteophyte growth⁶⁰ and mediate cartilage

destruction¹⁷⁷. In contrast to joints in sedentary animals, papain injected joints of running animals had more pronounced macrophage activation and also larger osteophytes (**Figure 7**). These results imply that macrophage activation and osteophyte formation are associated. This was previously suggested to be mediated by TGF- β and BMP-2 produced by activated synovial macrophages^{59, 60}. Depending on stimuli in the environment macrophages can be activated in different ways. Grossly they can be subdivided into a pro-inflammatory (M1), wound-healing (M2a) and regulatory (M2b) phenotype, with each subtype characterized by secretion of different cytokines and growth factors¹⁷⁸. The folate-receptor- β is highly associated with activated macrophages^{163, 164}. Although this receptor has a slightly higher predisposition on M2 macrophages, both M1 and M2 subtypes do express folate-receptor- β ¹⁷⁹. As a consequence, DOTA-Bz-Folate SPECT/CT cannot address specific subtype macrophage activation. Further *in vivo* studies that modulate macrophage activation and potentially influence folate targeted SPECT signal are required to provide more insight in the role of macrophage activation and their cytokine production related to OA development.

There are numerous animal models for OA. Instability models like the anterior cruciate ligament transection (ACLT) model⁶⁶, groove model^{25, 157}, the destabilized meniscus model⁶⁷, or meniscectomy model⁷¹) are currently most popular. In our opinion, these models represent an OA etiology related to joint trauma and allows for investigation of early changes during OA development. The results from papain injected and running animals in our study closely resembles end-stage OA-like pathology with pronounced cartilage degradation and subchondral sclerosis. This aspect of severe OA progression in papain injected joints of running animals might be suited to investigate new treatment strategies designated for regeneration of cartilage in OA joints. This type of OA induction proved to be simple and in combination with exercise induced OA in a very reproducible manner with involvement of cartilage, subchondral bone and synovial macrophages. Additionally, previous reports show that exposure of rat knee joints to low-dose papain induce a reversible sGAG loss from the cartilage¹⁶⁸ and a transient pain response after injection⁷⁷. This suggests that papain does not directly impair chondrocyte viability compared to other chemical induced OA models, like the mono-iodoacetate model that can lead to chondrocyte death shortly after injection⁷⁵. Unimpaired cell viability allows future intervention studies to therapeutically target chondrocytes in an attempt to repair damaged articular cartilage. Although this study did not investigated chondrocytes viability and more research is necessary to elucidate this feature, experimental induced OA via papain injections might be a worthwhile contributing model for OA research.

Using animal models for OA research does not allow for direct translation towards human patients. It is known that skeletal growth in rats is related to changing cartilage matrix biology and phenotypic characteristics of chondrocytes^{180, 181}. Therefore, many choices (for example species, strain, age) related to the study design might have a distinct influence on experimental

outcome. With this in mind, our results might still be interesting from a clinical perspective. sGAG is a key-molecule for proper cartilage functioning and the amount of sGAG content is an indicator of cartilage health¹⁰³. Loss of sGAG from articular cartilage is a hallmark of early OA and it was hypothesized that this occurs well before OA is detected radiographically¹⁸². For unknown reasons until now, there is a subgroup of OA patients that show signs of rapid OA progression. With radiologic evaluation such as e.g. dGEMRIC to determine cartilage sGAG content, we can investigate whether sGAG depletion and physical exercise may co-induce severe progression in human patients as well. More knowledge about cartilage sGAG content and patient activity level might guide or improve therapeutic interventions as well. Although physical exercise can be beneficial for OA patients^{183, 184}, it might prove to be important that the amount of physical exercise exposure and the intensity level of their activities are carefully balanced in light of their cartilage sGAG status.

Conclusion

Severe sGAG depleted cartilage through papain injections is vulnerable for cartilage damage. Moderate physical exercise induced not only rapid OA progression in articular cartilage of papain injected joints, but involved the whole joint with pronounced subchondral bone adaptation and activation of synovial macrophages.

ACKNOWLEDGEMENTS

We acknowledge the Dutch Arthritis Association and the Smart Mix Program of the Netherlands Ministry of Economic Affairs and the Netherlands Ministry of Education, culture and Science for their financial support.

CHAPTER 4

INHIBITION OF GSK3 β IN CARTILAGE INDUCES OSTEOARTHRITIC
FEATURES THROUGH ACTIVATION OF THE CANONICAL WNT
SIGNALING PATHWAY

*R.L. Miclea, M. Siebelt, L. Finos, J.J. Goeman, C.W. Löwik, W. Oostdijk, H. Weinans, J.M. Wit,
E.C. Robanus-Maandag, M. Karperien
Osteoarthritis Cartilage. 2011Nov;19(11):1363-72*

ABSTRACT

Introduction

In the past years, the canonical Wnt/ β -catenin signaling pathway has emerged as a critical regulator of cartilage development and homeostasis. In this pathway, glycogen synthase kinase-3 β (GSK3 β) down-regulates transduction of the canonical Wnt signal by promoting degradation of β -catenin. In this study we wanted to further investigate the role of Gsk3 β in cartilage maintenance.

Methods

Therefore, we have treated chondrocytes ex vivo and in vivo with GIN, a selective GSK3 β inhibitor.

Results

In E17.5 fetal mouse metatarsals, GIN treatment resulted in loss of expression of cartilage markers and decreased chondrocyte proliferation from day 1 onward. Late (3 days) effects of GIN included cartilage matrix degradation and increased apoptosis. Prolonged (7 days) GIN treatment resulted in resorption of the metatarsal. These changes were confirmed by microarray analysis showing a decrease in expression of typical chondrocyte markers and induction of expression of proteinases involved in cartilage matrix degradation. An intra-articular injection of GIN in rat knee joints induced nuclear accumulation of β -catenin in chondrocytes 72 h later. Three intra-articular GIN injections with a 2 days interval were associated with surface fibrillation, a decrease in glycosaminoglycan expression and chondrocyte hypocellularity 6 weeks later.

Conclusion

These results suggest that, by down-regulating β -catenin, Gsk3 β preserves the chondrocytic phenotype, and is involved in maintenance of the cartilage extracellular matrix. Short term β -catenin up-regulation in cartilage secondary to Gsk3 β inhibition may be sufficient to induce osteoarthritis-like features in vivo.

INTRODUCTION

Differentiated chondrocytes maintain their phenotype via synthesis of cartilage-specific extracellular matrix (ECM) molecules including collagen type II and sulfated proteoglycans, like aggrecan¹⁸⁵. Chondrocytes easily lose essential characteristics when they are removed from their natural environment and cultured in vitro or expanded for the purpose of cartilage tissue engineering^{185, 186}. Chondrocyte dedifferentiation also occurs in the presence of retinoic acid, nitric oxide, or proinflammatory cytokines like interleukin (IL)-1 β and Tumor necrosis factor (TNF)- α , as well as in osteoarthritis (OA)¹⁸⁶.

We and others have shown that both constitutive up- or down-regulation of the canonical Wnt pathway negatively influences cartilage development and maintenance resulting in OA-like features. This suggests that a tight regulation of this signaling cascade is crucial throughout the chondrocyte life cycle^{133-135, 187}. In this pathway, in the absence of a Wnt signal, a destruction complex comprising Axin (Conductin) and Adenomatous polyposis coli (APC) mediates the phosphorylation of β -catenin by glycogen synthase kinase-3 β (GSK3 β), which induces degradation of cytosolic β -catenin in the proteasome. Binding of Wnt to its transmembrane receptor Frizzled results in activation of Dishevelled. This is followed by reduction of GSK3 β activity and accumulation of cytoplasmic β -catenin. Upon its nuclear translocation, β -catenin will function as a co-factor of TCF/LEF transcription factors to induce expression of Wnt target genes¹³⁴. GSK3 β is constitutively active and, unlike many kinases that are activated following stimulus-dependent phosphorylation, it becomes inactive following phosphorylation¹⁸⁸. Studies reported so far indicate that Gsk3 β activity is required for both chondrocyte and osteoblast differentiation and thus for endochondral bone development¹⁸⁹. However, no data is available regarding the role of GSK3 β in maintenance of the chondrocytic phenotype.

To better understand the role of Gsk3 in regulation of the chondrocyte life cycle, we inactivated this kinase ex vivo and in vivo by using 3-[9-Fluoro-2-(piperidine-1-carbonyl)-1,2,3,4-tetrahydro-[1,4]diazepino[6,7,1-hi]indol-7-yl]-4-imidazo[1,2-a]pyridin-3-yl-pyrrole-2,5-dione, a selective and potent GSK3 β inhibitor, in this manuscript further referred to as GIN¹⁹⁰. Our results imply that Gsk3 β activity is crucial for maintenance of the chondrocytic phenotype and for the integrity of cartilage ECM, mainly by down-regulating the canonical Wnt signaling pathway. The cartilage phenotypic changes induced by GIN bear similarities to some of the clinical features commonly observed in OA.

MATERIALS AND METHODS

KS483 cell culture, immunofluorescence for β -catenin, transient transfection assays

Routine culture of KS483 cells, immunofluorescence for β -catenin and transient transfection assays were performed as previously described¹⁹¹.

Ex vivo experiments

The three middle metatarsals were dissected from E17.5 Swiss Albino mouse embryos. Explants isolated from different animals were randomly distributed and individually cultured in 500 μ l α -Minimum Essential Medium (MEM) (Invitrogen) medium containing 10% Fetal Calf Serum (FCS) (Invitrogen), 100 U Pen/Strep (Invitrogen) and 1% GlutaMax (Invitrogen). After an equilibration period of 48 h, metatarsals were challenged with vehicle or GIN as described in the results section. All ex vivo experiments were approved by the ethical committee of the Leiden University Medical Center and complied with national laws relating to the conduct of animal experiments.

Proliferation and apoptosis assays

Chondrocyte proliferation was assessed by immunohistochemistry (IHC) for proliferating cell nuclear antigen (PCNA) according to manufacturer's protocol (Santa Cruz Biotechnology). Chondrocyte apoptosis was determined by the Terminal deoxynucleotidyl transferase dUTP nick end labeling (TUNEL) reaction (Promega), as previously described¹⁹². For statistical analysis a number of N = 3 independent samples were used and each experiment was repeated at least once.

Histology, IHC, in situ hybridization (ISH)

Histology, IHC, and ISH were performed as previously described¹³³.

Quantification of Glycosaminoglycans (GAGs)

The GAG content in N = 3 whole metatarsals per condition was quantified related to the amount of DNA using the Blyscan Sulfated GAG Assay kit (Biocolor) according to manufacturer's protocol. Experiments were repeated at least once.

Gene expression profiling

For each condition, RNA was isolated from N = 15 whole metatarsals, checked for quality, amplified and labeled as previously described¹⁹³. Labeled cRNA was further used for the hybridization to Affymetrix GeneChip® Mouse Genome 430A 2.0 Array according to the manufacturer's protocol. The raw and normalized data are deposited on the website of the Department of Tissue Regeneration of the Twente University Institute for Biomedical Technology (<http://tr.tnw.utwente.nl>).

Microarray data analysis

To evaluate the large number of genes and to find gene expression trends and noteworthy signaling pathways that are involved in the GIN-mediated effects, we used principal component analysis¹⁹⁴. Using a cut-off value of 2 for the expression fold change, a list of 316 differentially expressed genes (225 down- and 91 up-regulated) was generated and used for subsequent analysis (Tables SI and SII).

Functional annotation of the differentially expressed genes identified by the principal component analysis (PCA) analysis was performed using the DAVID bioinformatics database and the Gene Ontology (GO) terms to describe their (extra)cellular location (GO_CC), molecular functions (GO_MF), and the biological processes (GO_BP) in which they are involved^{55, 195, 196}. Enrichment of GO functional groups was determined to be meaningful when the number of probe sets in our list that mapped to a specific GO term was greater than 2 with a P-value ≤ 0.001 .

Validation of the microarray analysis was performed by real-time quantitative polymerase chain reaction (PCR) as previously described¹⁹³.

In vivo experiments

All in vivo experiments were approved by the ethical committee of the Erasmus University Medical Center and complied with national laws relating to the conduct of animal experiments. Thirteen-week-old male Wistar rats (400-450 g) were housed under standard laboratory conditions (temperature 24°C, 12-h light-dark cycle) with food and water ad libitum. The animals were acclimatized to the laboratory environment for 3 weeks before the start of the experiments.

GIN treatment

In a dose-finding study (N = 4), the effect of an intra-articular injection of 100 μ l GIN dissolved in phosphate buffered saline (PBS) at concentrations of 3×10^{-7} M, 10^{-6} M, 3×10^{-6} M, and 10^{-5} M in the knee joint was investigated.

In a second experiment, eight rats were injected intra-articular at day 1, 3 and 5 with 100 μ l 10^{-5} M GIN. Four rats were injected with GIN in the left knee, the remaining four were injected in the right knee. Contralateral joints served as controls and were injected with vehicle. All animals were scanned using contrast-enhanced μ CT (CECT) before GIN injection (t = 0) and during follow up as previously described¹¹³. Rats were sacrificed at the times indicated in the text.

Microscopical analysis and quantification

IHC for β -catenin coupled with Alcian Blue (AB) counterstaining for GAGs was carried out as

previously described¹³³. Quantification of the AB staining was performed using Image-Pro Plus software, version 7.0.

Statistical analysis

All values represent median and range for experiments when $N \leq 4$ and mean and 95% confidence interval (CI) when $N \geq 5$. The paired t-test, the univariate general linear model using simple contrasts and parameter estimates and one-way analysis of variance (ANOVA) were used to assess the data, as appropriate. P values less than 0.05 were considered significant. Statistical analysis was performed using SPSS v16.0 (SPSS).

RESULTS

Inhibition of Gsk3 β through GIN results in activation of the canonical Wnt signaling pathway *in vitro* and *ex vivo*

We first performed transient transfection experiments in mesenchymal-like KS483 cells using the Wnt-responsive BAT-Luc reporter vector^{191, 197}. As expected, GIN induced a dose-dependent increase in luciferase activity, with a maximum response at 10^{-7} M (**Figure 1A**). At higher concentrations, the luciferase activity decreased, presumably due to toxic effects (**Figure 1A** and data not shown). Furthermore, GIN was significantly more potent in inducing the Wnt reporter construct than LiCl, another established inhibitor of GSK3 β . Activation of the Wnt reporter construct by 10^{-7} M GIN was accompanied by β -catenin accumulation and nuclear translocation as confirmed by immunofluorescence (**Figure 1B**). The overall level of β -catenin was notably increased in cells treated with GIN when compared to LiCl (50 mM) or Wnt3a (50 ng/ml) (**Figure 1B**).

We next investigated the effect of GIN on fetal mouse metatarsals, which represent an established model for studying the chondrocyte life cycle *ex vivo*¹⁹⁸. After incubation for 3 days, GIN dose-dependently increased the levels of β -catenin as revealed by IHC (**Figure 1C**). Metatarsals treated with either 10^{-7} M or 10^{-6} M GIN displayed β -catenin staining mainly in the nuclei, indicating an efficient activation of the canonical Wnt signal. The latter concentration resulted in immunohistochemically detectable nuclear β -catenin expression in almost all chondrocytes. Strikingly, metatarsals treated with 10^{-6} M GIN displayed a much fainter AB counterstaining in comparison to controls, indicative for loss of GAGs. Additional morphological analysis revealed no evidence of cell death, cell shrinkage, picnotic nuclei, blebbing of the cytoplasm or necrosis. Subsequent experiments using the fetal mouse metatarsal *ex vivo* culture model were performed with 10^{-6} M GIN.

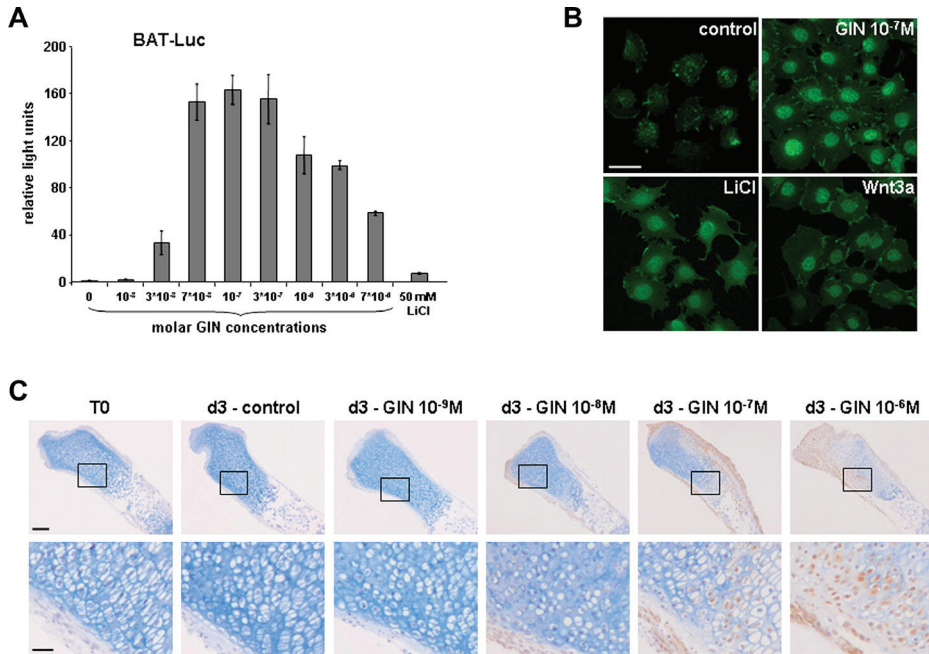


Figure 1. GIN activates the canonical Wnt signaling pathway via β -catenin. (A) GIN activated a transiently transfected Wnt reporter construct in KS483 cells dose-dependently. Values represent the mean and 95% CI (error bars) of $N = 9$ luciferase observations corrected for renilla luciferase. (B) Representative images showing the effect of GIN (10⁻⁷ M), LiCl (50 mM) and Wnt3A (50 ng/ml) on β -catenin localization in KS483 cells as revealed by immunofluorescence. Out of the three Wnt activators, GIN was most effective in stabilizing and inducing nuclear translocation of β -catenin. Scale bar = 10 μ m. (C) Representative images showing β -catenin IHC combined with AB staining on longitudinal sections of E17.5 murine metatarsals treated for 3 days with the indicated concentrations of GIN. In this experimental set-up, 10⁻⁶ M GIN induces nuclear β -catenin translocation in almost all cells without any sign of toxicity. Note the progressive decrease in the intensity of the AB staining. The boxed regions in the upper row pictures are magnified in the lower row pictures. Scale bars = 100 μ m (upper row), 25 μ m (lower row).

GIN inhibits chondrocyte proliferation and increases cartilage apoptosis

We assessed the effect of GIN on chondrocyte proliferation using IHC for PCNA. The percentage of proliferating cells was smaller in the GIN-treated group compared to controls at all time points examined (Figure 2A-E). Chondrocyte proliferation was significantly inhibited both at d1 (11.3% vs 25.9%, $P = 0.048$) and at d3 (7.6% vs 27.8%, $P = 0.014$). TUNEL staining in combination with histological evaluation was used to assess chondrocyte apoptosis. GIN did not have an effect on TUNEL positivity at 6h, d1 and d3 (Figure 2F-J). Only after prolonged GIN treatment (d7), TUNEL staining was significantly increased (22.9% vs 6.0%, $P = 0.043$). At d7, TUNEL-positive cells were predominantly identified among the hypertrophic chondrocytes in controls. In contrast, TUNEL-positive cells were also observed among the resting and proliferative

chondrocytes in the GIN-treated group. Based on histological evaluation, TUNEL-positive cells underwent apoptosis.

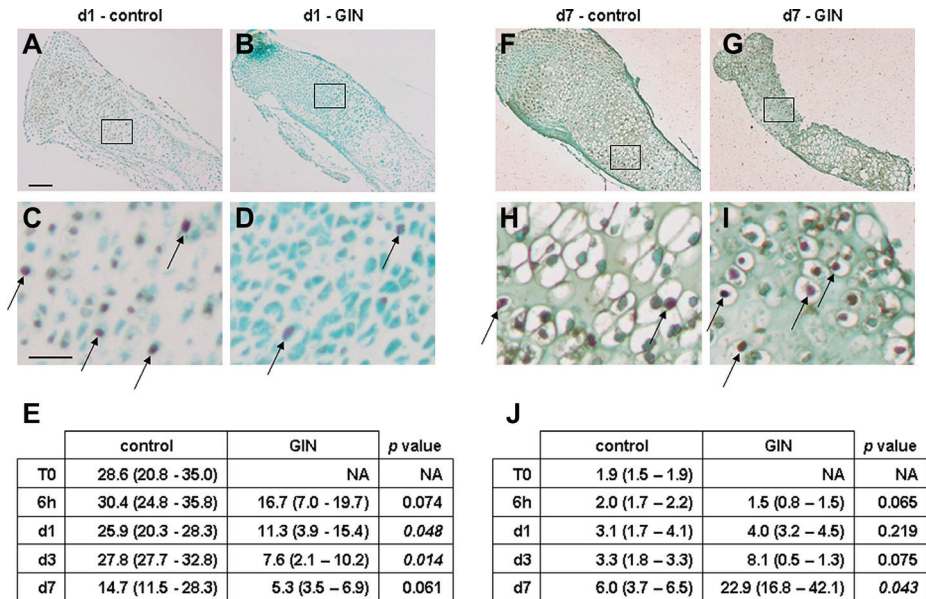


Figure 2. GIN inhibits chondrocyte proliferation and augments cartilage apoptosis. (A–D) Representative images showing PCNA IHC on metatarsals treated with vehicle (A, C) or GIN (B, D) for 1 day. Note that the number of the PCNA-positive nuclei (brown) is decreased in the GIN-treated metatarsal. (E) Quantification in $N = 3$ independent samples of the PCNA-positive nuclei (examples indicated by black arrows in C, D) indicates significant inhibition of chondrocyte proliferation upon GIN treatment at d1 and d3. PCNA-positive cells were counted on a mid sagittal tissue section. Each field contained at least 500 cells and data are expressed as median (range) % of PCNA-positive cells from total number of cells. (F–I) Representatives pictures of metatarsals cultured in control (F, H) or GIN-enriched (G, I) medium for 7 days after TUNEL staining. Note that the number of the TUNEL-positive nuclei (brown) is increased in the GIN-treated metatarsal. (J) Quantification in $N = 3$ independent samples of the TUNEL-positive nuclei (examples indicated by black arrows in H, I) indicates significantly more chondrocyte apoptosis upon prolonged GIN treatment (d7). Quantification and data expression as in (E). (C, D, H, I) High magnification pictures of the boxed regions in A, B, F, and G, respectively. Scale bars: 100 μm (A, B, F, G), 25 μm (C, D, H, I).

Inhibition of Gsk3 β induces degradation of cartilage matrix and loss of the chondrocytic phenotype ex vivo

We investigated the effect of GIN at the cellular level by IHC analysis for β -catenin, collagen type II and X, and ISH analysis for Col2a1 and Col10a1. No microscopic differences between vehicle- and GIN-treated metatarsals were observed at 6 h (data not shown). β -catenin expression at the start of the experiment and in the control metatarsals at d1, d3 and d7 was restricted to the cytoplasm of a minority of perichondrial and periosteal cells (Figure 3A, A_i, A_{iii} and A_v).

We first noticed a clear increase in the level of nuclear β -catenin after 1 day of GIN treatment (Figure 3A_{ii}). β -catenin accumulation was observed at d3 and d7 as well (Figure 3A_{iv}-A_{vi}). The level of nuclear β -catenin was inversely correlated with the intensity of the AB counterstaining (Figure 3A-A_{vi}). GIN treatment progressively decreased the GAG content in the ECM, with a near complete loss of GAGs at d7 (Figure 3F). GIN did not have an effect on mineral deposition and ossification of the metatarsals (data not shown).

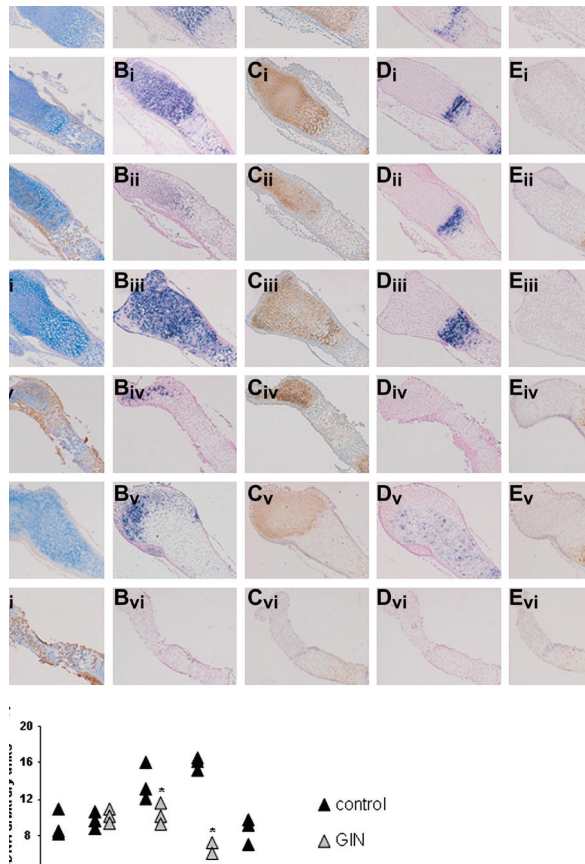


Figure 3. GIN induces loss of the chondrocytic phenotype ex vivo. Representative pictures of (A–A_{vi}) β -catenin immunostaining combined with AB staining, (B–B_{vi}) Col2a1 mRNA expression, (C–C_{vi}) Collagen type II immunostaining, (D–D_{vi}) Col10a1 mRNA expression, and (E–E_{vi}) Collagen type X immunostaining, on consecutive longitudinal sections of E17.5 mouse metatarsals (N = 3 independent samples) isolated at the indicated time points. β -catenin-positive chondrocytes lose Col2a1 expression upon GIN treatment already at d1. Chondrocyte marker expression at the mRNA level is inhibited after 3-day-long GIN treatment. Chondrocytes exposed to GIN for 7 days fail to express specific markers at both mRNA and protein level. Scale bar: 100 μ m. (F) Quantification of GAGs corrected for DNA (N = 3 independent samples) validates the microscopical findings. *P = 0.023 (d1), *P = 0.016 (d3), ***P = 0.008 (d7), all GIN vs same time point untreated. Data are expressed in arbitrary GAG/DNA units (black triangles – controls, gray triangles – GIN-treated samples).

Additional microscopic analysis revealed Col2a1 mRNA and collagen type II protein expression in the resting, proliferative and prehypertrophic chondrocytes, and their matrix, respectively, at all time points in the controls (**Figure 3B, B_i, B_{iii}, B_v, C, C_i, C_{iii} and C_v**). GIN treatment for 1 day resulted in a considerable inhibition of the mRNA expression of this chondrocyte marker, whereas its protein expression was not changed (**Figure 3B_{ii} and C_{ii}**). At d3, most of the chondrocytes in the GIN-treated metatarsals, although surrounded by a matrix rich in collagen type II, failed to express Col2a1 (**Figure 3B_{iv} and C_{iv}**). At d7, neither Col2a1 nor collagen type II expression was found in the GIN-treated metatarsals (**Figure 3B_{vi} and C_{vi}**).

Furthermore, control metatarsals displayed Col10a1 and collagen type X expression in the hypertrophic zone (**Figure 3D, D_i, D_{iii}, D_v, E, E_i, E_{iii} and E_v**). At d1, there were no differences in the expression of this mature chondrocyte marker between the control and the GIN-treated group, neither at the mRNA nor at the protein level (**Figure 3D_{iii} and E_{iii}**). At d3, GIN-treated explants displayed no Col10a1 expression, whereas collagen type X was still present in the ECM (**Figure 3D_{iv} and E_{iv}**). Ultimately, at d7, GIN induced a complete absence of both Col10a1 and collagen type X (**Figure 3D_{vi} and E_{vi}**).

Microarray analysis confirms GIN's proteolytic effects on cartilage

To further examine the effects of GIN on gene expression patterns in the fetal mouse metatarsal model, we performed cDNA microarray analysis on mRNA isolated from GIN-treated and control explants at T0, 6h, d1 and d3. We particularly designed our microarray analysis as such since GIN-treated metatarsals at d7 showed only aggravated features of the ones observed at d3. Furthermore, the increased apoptosis at d7 would have jeopardized the specificity of the results and mainly revealed differentially expressed genes related to cell death, an indirect effect of GIN treatment.

According to GO_CC terms, the vast majority of the 316 differentially expressed genes (225 down- and 91 up-regulated) encoded proteins that are active in the ECM (**Figure 4A**). Classification according to GO_MF and GO_BP terms is represented in **Figure 4B-C**, respectively. The large number of up-regulated genes and the fact that they did not categorize under any GO terms related to cell death suggested that our microarray data efficiently revealed biological effects caused by GIN treatment and not by toxicity.

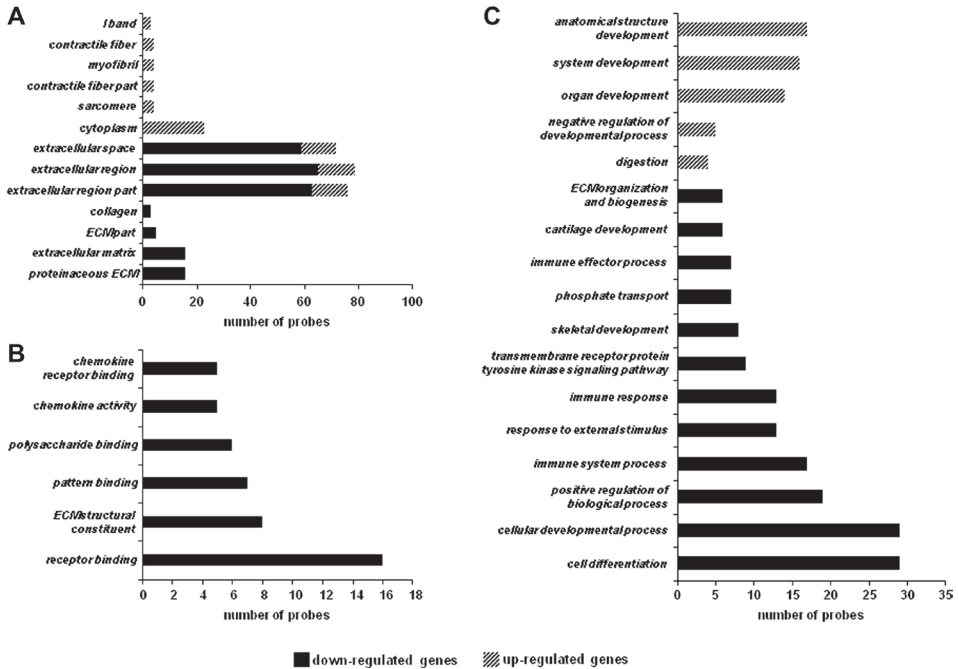


Figure 4. Functional annotation of the GIN-modulated genes according to GO terms. Functional annotation according to GO_CC (A), GO_MF (B) and GO_BP (C) terms was used to determine the enrichment of the differentially expressed transcripts indicated by PC1.

In consistence with the microscopical findings indicating significant cartilage matrix degradation, we found among the 91 up-regulated genes numerous transcripts encoding established proteinases: Matrix metalloproteinase 9 (Mmp9), Mmp10, Mmp11, and HtrA serine peptidase 1 (Htra1). Given the role of GSK3 β in canonical Wnt signaling, the microarray data showed evidence for a Wnt/ β -catenin signature as evidenced by the up-regulation of established direct targets of the β -catenin/TCF4 complex, like Axin2 and adenomatosis polyposis coli down-regulated 1 (Apcdd1). Microarray and pathway analysis did not reveal clear signatures of changes in other signaling pathways, such as Hedgehog (Hh) and Fibroblast growth factor (FGF). Furthermore, several cartilage ECM proteins were identified among the 225 down-regulated genes: unique cartilage matrix-associated protein (Ucma), matrilin 1 (Matn1), Matn3, Matn4, hyaluronan and proteoglycan link protein 1 (Hapln1), collagen, type XI, alpha 1 (Col11a1), epiphykan (Epyc), fibromodulin (Fmod), matrix Gla protein (Mgp), Col14a1, and (Col9a3). In the list of repressed genes, we also found transcripts known to encode non-cartilaginous matrix proteins like osteomodulin (Omd), osteoglycin (Ogn), microfibrillar-associated protein 4 (Mfap4), tenomodulin (Tnmd), asporin (Aspn), and fibulin7 (Fbln7), suggesting a more complex effect of the GIN treatment on the ECM.

To independently validate the results of the microarray analysis, 16 genes were selected for confirmation by quantitative real-time RT-PCR analysis. For the transcriptional analysis we therefore isolated RNA from a separate experiment that mirrored the one used to generate the microarray data. Four of these 16 genes are known to be involved in chondrocyte differentiation and cartilage maintenance (Sox9, Col2a1, Acan and Col10a1), four are members of the canonical Wnt signaling pathway (Axin1, Axin2, Gsk3b and Ctnnb1), and eight encode proteinases known to regulate maintenance and degradation of the ECM (Mmp2, Mmp3, Mmp9, Mmp13, Adamts4, Adamts5, Hyal1 and CtsK). We found a similar expression pattern of the analyzed genes, indicating that our microarray data specifically corresponded to actual gene expression patterns (Figure 5).

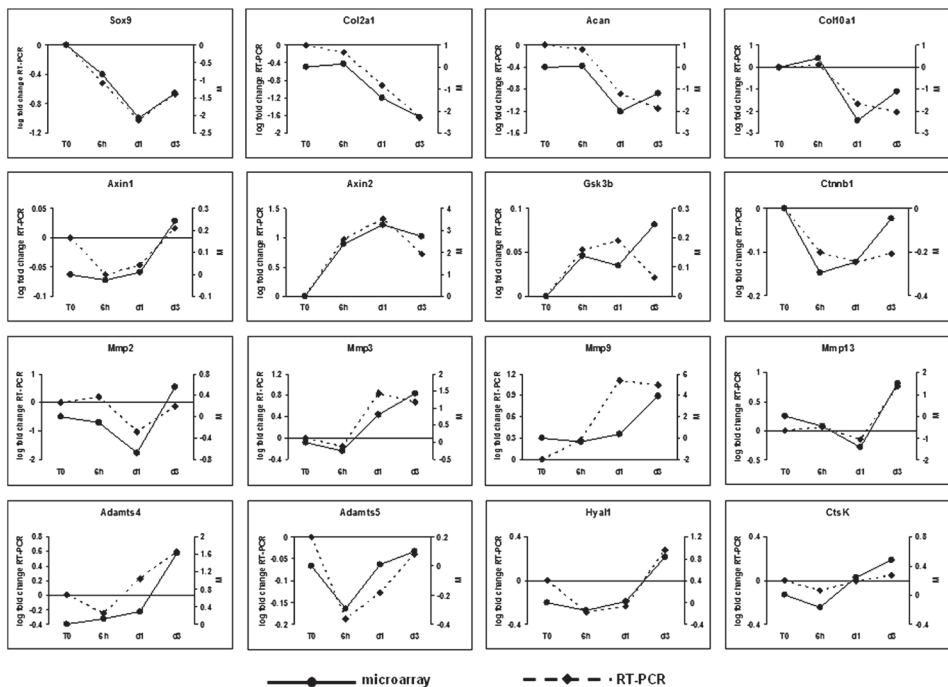


Figure 5. Quantitative Real-Time RT-PCR validates the microarray data. Correlation between qPCR and microarray results for Sox9, Col2a1, Acan, Col10a1, Axin1, Axin2, Gsk3b, Ctnnb1, Mmp2, Mmp3, Mmp9, Mmp13, Adamts4, Adamts5, Hyal1, and CtsK. The primary y-axis (left) indicates the RT-PCR results as normalized fold change on a log-scale. The secondary y-axis (right) indicates the microarray results as the log-differential expression ratios (M). Data are expressed as the mean of N = 6 metatarsals (qPCR) and N = 15 metatarsals (microarray).

We next investigated whether GIN can induce the same biological effects in an *in vivo* experimental model. In an initial experiment, we observed 72 h after GIN injection nuclear translocation of β -catenin in a dose-dependent fashion in rat knee articular chondrocytes,

whereas vehicle treatment did not induce a change in β -catenin expression in the control joints (Figure 6A, A_i, B, B_i and data not shown). Virtually all articular chondrocytes treated with the highest GIN concentration (10⁻⁵ M) showed nuclear β -catenin expression, yet they did not display any morphological changes or alterations of their ECM. We did not detect β -catenin up-regulation in other tissues such as synovium, tendons, or bone at the examined time point, nor evidence of inflammation.

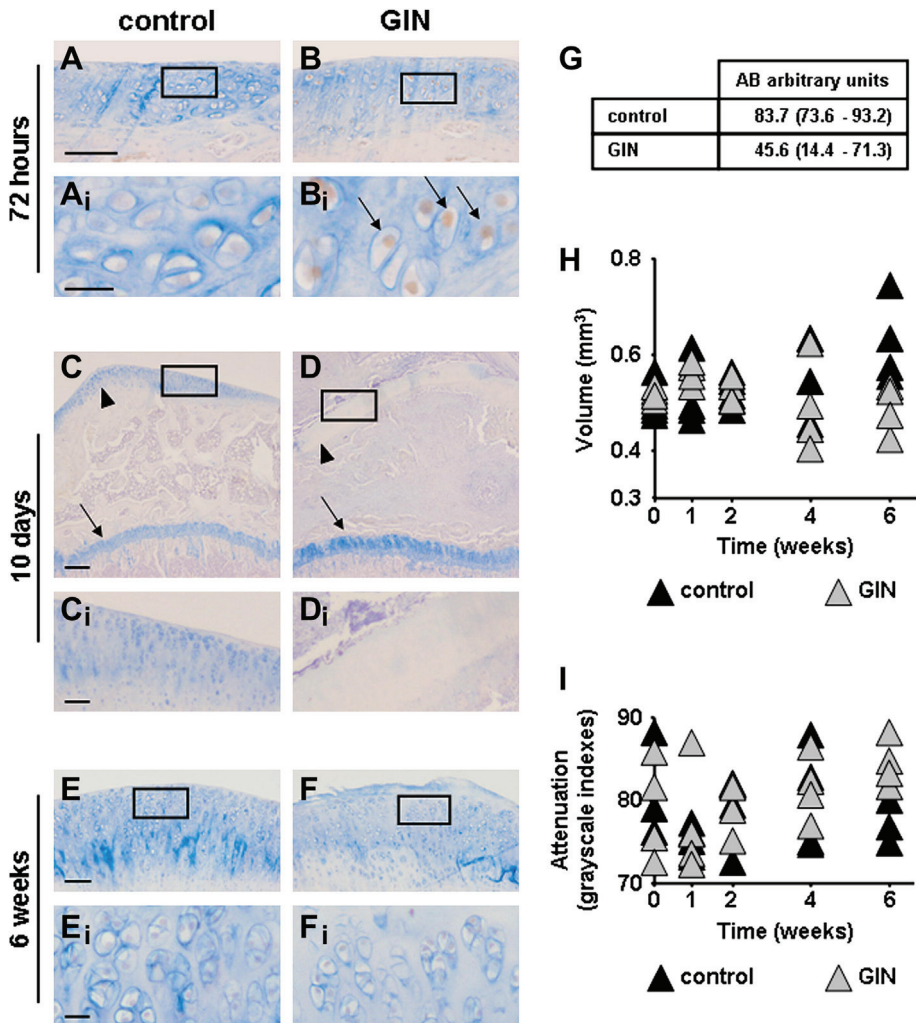


Figure 6. GIN induces OA-like effects in rat articular cartilage. (A, B) Representative pictures of β -catenin IHC combined with AB staining on longitudinal mid sagittal sections of tibial plateaus 72 h after injection with vehicle (A) or 10⁻⁵ M GIN (B). Seventy-two hours after GIN injection there is β -catenin up-regulation (arrows in B_i). (C, D) Representative pictures of AB staining on longitudinal mid-sagittal sections of proximal tibias 10 days after injection with vehicle (C) or 10⁻⁵ M GIN

(D) indicate massive ECM degradation only in the GIN-treated articular cartilage (arrowheads). GP cartilage is unaffected in both conditions (arrows). (E, F) Representative pictures of β -catenin IHC combined with AB staining on longitudinal mid-sagittal sections of tibial plateaus 6 weeks after injection with vehicle (E) or 10–5 M GIN (F). Short term GIN treatment does not lead to β -catenin up-regulation 6 weeks later, but induces OA-like morphological changes of the articular cartilage. (Ai, Bi, Ci, Di, Ei, Fi) High magnification pictures of the boxed regions in A, B, C, D, E and F, respectively. (G) Quantification of the intensity of the AB staining, at 6 weeks, in the control and GIN-treated knees (N = 4 independent samples) showing less GAGs in the treated samples. Data are expressed as median (range) AB arbitrary units, P = 0.050. (H, I) Quantification of volume and attenuation measurements from CECT-data (N = 4 independent samples) (black triangles – controls, gray triangles – GIN-treated samples). Scale bars: 200 μ m (A, B, Ci, Di, E, F), 20 μ m (Ai, Bi, Ei, Fi), 300 μ m (C, D).

In a second experiment, we injected 10–5 M GIN on day 1, 3 and 5. Four rats (“early” group) displayed signs of severe acute inflammation of the GIN-treated knee beginning at day 7 and these animals were therefore sacrificed already at day 10. No difference in β -catenin expression was observed between the GIN-treated and control knees of these animals (data not shown). In the vehicle-injected knee, the surface of the articular cartilage (AC) was smooth, the matrix was densely stained with AB and showed no signs of degeneration (**Figure 6C, C_i**). Besides displaying histological signs of inflammation (intra-articular infiltration of neutrophils and macrophages, synovocyte hyperplasia, fibrin exudation etc.), the GIN-treated knees in the “early” group displayed intensely degraded AC, containing almost no GAGs, as indicated by absence of AB staining (**Figure 6D, D_i** and data not shown) in each of the four animals.

The other four rats (“late” group) from this experiment were sacrificed after 6 weeks and again showed no difference in the β -catenin expression pattern between the GIN-treated knee and controls (**Figure 6E, E_i, F, F_i**). Whereas no morphological changes were observed in the control knees of the “late” group, GIN-treated samples from all four rats displayed superficial fibrillation of AC, focal hypocellularity of chondrocytes, and reduced AB staining. Quantification of the intensity of the AB staining revealed significantly less staining in the cartilage of GIN-treated knees in comparison to contralateral control knees (**Figure 6G, P = 0.05**).

Although not statistically significant, CECT analysis of condylar cartilage revealed a trend in reduction of cartilage volume as well as GAG-depletion (expressed by increased attenuation) in the GIN-treated knee joints in comparison to control knees (**Figure 6H-I**).

DISCUSSION

Here we show that Gsk3 β , by controlling the canonical Wnt signaling pathway, is critical for maintenance of the chondrocytic phenotype. Inhibition of Gsk3 β in chondrocytes *ex vivo* leads to loss of cartilage markers expression, induces matrix degradation by stimulating the expression of Mmps, inhibits chondrocyte proliferation and, most likely as a consequence of these effects,

induces chondrocyte apoptosis. In addition, we demonstrate that transient inhibition of Gsk3 β , following three intra-articular injections of GIN in rat knees during 1 week is associated with the appearance of OA-like features 6 weeks later. In agreement with our results, recent findings suggest that up-regulation of β -catenin through induction of proteasomal degradation of Gsk3 β in chondrocytes initiates early events of OA, while inhibition of Gsk3 β may block chondrogenesis^{199, 200}.

Besides the canonical Wnt pathway, GSK3 β also regulates signal transduction of the Hh and Fibroblast growth factor (Fgf) family of secreted proteins^{201, 202}. Given that both Hh and Fgf growth factors play important roles in the chondrocyte life cycle, we searched in our microarray results for possible target genes of these proteins among the list of transcripts differentially regulated by GIN^{203, 204}. Only PR domain containing 1, with zinc finger (ZNF) domain (Prdm1) matched this criterion, acting downstream of a sequential Wnt and Fgf signaling cascade²⁰⁵. Our microarray expression data indicated that GIN treatment up-regulated the canonical Wnt target genes Axin2 and Apcdd1, transcripts that have previously been shown to be induced only by Wnt and not by Fgf signaling²⁰⁶⁻²⁰⁸. The protein products of Axin2 and Naked cuticle homolog 2, both of which are up-regulated in the microarray, are both renowned antagonists of the canonical Wnt signal. They have been shown to participate in negative feedback regulation of β -catenin activity²⁰⁹⁻²¹¹. Taken together, these findings suggest that the intense cartilage matrix degeneration as well as the loss of the chondrocytic phenotype following GIN treatment occurred, at least in our experimental set-up, mainly due and can be explained by the activation of the Wnt/ β -catenin pathway, although we cannot exclude minor roles of other signaling pathways in which GSK3 β is known to be implicated nor of minor off-target effects of GIN.

Previously, we and others have reported that continuous exposure of chondrocytes to extensive levels of β -catenin *in vivo* induces loss of the chondrocytic phenotype as evidenced by the loss in expression of typical chondrocyte markers^{133, 134}. Microarray analysis of GIN-treated metatarsals confirmed and extended this observation. Furthermore, our microscopic analysis suggests that GIN not only induced an enhanced degradation of the ECM, but also inhibited the expression of several ECM constituents in a time-dependent manner. Noteworthy, in the metatarsal experiments the loss of expression of typical cartilage markers at the mRNA level was observed before protein degradation was noticeable. GIN treatment inhibited the expression of genes encoding collagenous (Col9a3, Col11a1, and Col14a1), and non-collagenous ECM proteins (Ucma, Matn1, Matn3, Matn4, Hapln1, Fmod, Mgp), as well as proteoglycans (Epyc). In addition, GIN stimulated the expression of proteinases Mmp9, Mmp10, Mmp11, and Htra1, which promote ECM degradation, suggesting that the loss of tissue integrity observed in the treated metatarsals is due not only to a loss of the links between the collagenous and the non-collagenous proteins in the matrix, but also to active matrix degradation.

Decreased chondrocyte proliferation, augmented apoptosis, loss of the chondrocytic phenotype and degradation of ECM together characterize the “degradative phase” of OA, the most common form of arthritis²¹². These pathological phenomena were observed after up-regulated canonical Wnt signaling by GIN treatment in our experimental set-ups *ex vivo* and *in vivo*, in agreement with recent data suggesting a link between excess signaling through the Wnt/ β -catenin pathway and OA¹³⁴. Moreover, many genes reportedly induced in OA cartilage were up-regulated by GIN treatment: *Mmp9*, *Mmp10*, *Mmp11*, *Axin2*, *Htra1*, angiopoietin-like 2 (*Angptl2*), and met proto-oncogene (*Met*)^{186, 213-217}. *Htra1*, which is increased several-fold in joint cartilage of OA patients, promotes degeneration of cartilage^{216, 218}, while *Met*, besides contributing to the altered metabolism during OA, also stimulates osteophyte development²¹⁹. *Serping1*, previously reported to be repressed in OA, and *Matn3*, whose inactivation leads to higher incidence of OA, were both down-regulated by GIN^{220, 221}. In addition, inactivation of *Frzb*, another transcript repressed by GIN treatment, renders joints more susceptible for osteoarthritic changes²²².

Our results suggest that treatment with GIN can induce cartilage degeneration of rat AC after three intra-articular injections of GIN with 2 days interval. We observed two distinct phenotypes, most likely explained by a difference in retention time of GIN in the knee joint: a severe form with acute inflammation associated with resorption already 10 days after the first injection and a milder phenotype. The potent catabolic effects of GIN on cartilage may have caused rapid and excessive cartilage degradation. These degradation products may have triggered an acute form of inflammation through the release of for example collagen type II fragments. In animals with the milder phenotype, microscopic analysis demonstrated the presence of the first signs of OA-like changes such as surface fibrillation, focal chondrocyte hypocellularity and a decrease in GAG staining in GIN-treated knees but not in the contralateral control knees 6 weeks after the last GIN injection. CECT analysis revealed a trend of less cartilage volume and more attenuation, indicative for GAG loss in the GIN-treated animals; however this observation did not reach significance. In contrast to the increased β -catenin expression in AC present 3 days after GIN injection, we did not detect increased β -catenin staining 6 weeks after GIN injection nor did we find evidence for nuclear β -catenin accumulation in the synovium, tendons or bone at each of the analyzed time points. This suggests that a transient rise in β -catenin in AC may be sufficient to trigger development of OA-like features, an observation that extends findings in conditional constitutive mice carrying a stabilized, oncogenic variant of β -catenin, which also develop OA¹³⁵. Although we did not find evidence for increased β -catenin accumulation in other joint tissues besides cartilage at the examined time points, we cannot exclude that GIN injection has resulted in a more rapid and transient rise of β -catenin in these tissues which was normalized 72 h after the injection. This may have also contributed to the observed pathology. Furthermore, we cannot exclude that the mild cartilage phenotype was due to a milder form of inflammation in the first weeks after injection. However, given the clear evidence of increased nuclear β -catenin

accumulation in AC 72 h after GIN injection and the consistency of the *in vivo* findings with the phenotypic changes and effects on gene expression of GIN in our *ex vivo* cartilage explant model, we favor the hypothesis that these first indications of cartilage degeneration were due to a transient rise in β -catenin in AC triggering cartilage catabolism and changes in the chondrocyte phenotype.

Abnormally regulated GSK3 β has been associated with many pathological conditions like Alzheimer's disease, mood disorders, diabetes and cancer¹⁸⁸. However, a direct link between GSK3 β and the pathophysiology of OA has not yet been reported. Since in our experimental set-ups the GIN-induced effects reflect some of the pathological findings normally seen in osteoarthritic chondrocytes, we speculate that Gsk3 β plays a role in the pathophysiology of this degenerative cartilage disease as well, most likely by regulating the levels of β -catenin. Whether pharmacological modulation of Gsk3 β might represent a potential novel therapeutic approach for the management of OA remains to be elucidated.

ACKNOWLEDGMENTS

This work was financially supported by an unrestricted educational grant from IPSEN FARMACEUTICA BV to RLM that we gratefully acknowledge.

CHAPTER 5

HSP90 INHIBITION PROTECT AGAINST BIOMECHANICALLY INDUCED
OSTEOARTHRITIS

*M. Siebelt, H. Jahr, H.C. Groen, M. Sandker, J.H. Waarsing, N. Kops, C. Müller,
W. van Eden, M. de Jong, H. Weinans
Arthritis Rheum. 2013Aug;65(8):2102-2112*

ABSTRACT

Introduction

Articular cartilage is evolutionary designed to facilitate joint mobilization. However, severe loading can induce chondrocyte apoptosis, which is related to osteoarthritis progression. In order to avoid apoptosis, chondrocytes synthesize heat shock proteins (Hsp). Here we report on the role of Hsp70 and Hsp90 in biomechanically induced osteoarthritis, and the possibility for Hsp90 inhibition (Hsp90i) as an intervention strategy for osteoarthritis management.

Methods

Osteoarthritis was biomechanically induced in rats through strenuous running. Disease progression was compared between running rats treated with Hsp90i and untreated running controls. From articular cartilage of both groups, Hsp70 and Hsp90 protein levels were determined using Western blots. Osteoarthritis progression was monitored with contrast-enhanced μ CT to measure cartilage degradation and subchondral bone changes, with SPECT/CT to determine synovial macrophage activation, and histology.

Results

Chronic cartilage loading led to early osteoarthritis development, characterized by degeneration of cartilage ECM. In vivo Hsp90i resulted in increased Hsp70 synthesis, which suggests that Hsp90 activity limits Hsp70 production. Hsp90i treatment improved cartilage sGAG levels to concentrations even beyond baseline and (1) protected against cartilage degradation, (2) stimulated subchondral bone thickness, and (3) suppressed macrophage activation.

Conclusion

Hsp90 plays a pivotal role in biomechanically induced chondrocyte stress responses, and intervention strategies that inhibit Hsp90 can protect or improve cartilage health and might prevent osteoarthritis development.

INTRODUCTION

Osteoarthritis (OA) is a progressive disease affecting synovium, ligaments, subchondral bone, and lead to articular cartilage degradation¹. About 30% of persons aged 65 and older are affected in either the hip or knee joint by this severely disabling disease⁴. Besides costly and invasive joint replacement surgery, treatment options are limited. Therefore, more detailed knowledge of the underlying pathogenesis of OA is essential for the development of novel disease modifying drugs.

Chondrocytes are the single cell type responsible for maintaining the extra-cellular matrix (ECM) of articular cartilage and repair of any inflicted damage. Being daily exposed to high-peak forces during physical activity, this cell type is sensitive to mechanical stimuli¹³². Acute or chronic high-intensity loads can cause cartilage damage¹⁵⁶, and chondrocytes in damaged or eroded cartilage show morphological features of apoptosis, suggesting that chondrocytes from OA patients die by active (programmed) cell death²²³. Cells can avoid apoptosis by expression of heat shock proteins (Hsp). Hsp are molecular chaperones that assist in protein folding to sustain cellular homeostasis under stressed conditions²²⁴.

Hsp70 and Hsp90 are two of the major classes of heat shock proteins involved in regulation of cell stress²²⁵. From *in vitro* experiments, it is known that HSP70 inhibits nitric oxide-induced apoptosis in chondrocytes through reduction of caspase 3 activity²²⁶. Galois et al. reported similar findings in an *in vivo* study in rats and showed that mild running (7.5km in 28days) and moderate running (15km in 28days) stimulated Hsp70 production¹⁵². These schedules protected chondrocytes from caspase 3 induced apoptosis and reduced OA progression. Other studies further support the finding that Hsp70 has the potential to prevent cartilage damage in arthritic joints^{227, 228}. Thus, Hsp70 is thought to play a protective role in early stages of chondrocyte adaptation to biomechanical joint constraints, which otherwise would lead to OA²²⁹. However, intense running (30km in 28days) reduced Hsp70 expression back to non-running control levels¹⁵² and supraphysiological loading therefore seems to exceed the intrinsic Hsp70-mediated capacity for cellular damage control, ultimately still resulting in apoptosis. This corroborates with findings, that intense or strenuous running protocols are known to induce OA^{84, 157}. It is hypothesized that with persistent stress on cartilage: (1) increased levels of Hsp70 are insufficient to protect chondrocytes²³⁰, or, (2) the co-expression of other Hsp counteract the effect of Hsp70¹⁵².

The second part of this hypothesis could be explained through Hsp90 function. Where HSP70 inhibits NF- κ B formation, Hsp90 has an antagonistic function and activates the NF- κ B pathway²²⁴. NF- κ B plays an essential role in normal physiology, but inappropriate regulation of NF- κ B is related to the pathogenesis of both OA and rheumatoid arthritis²³¹. In an *in vivo*

model for rheumatoid arthritis, Hsp90 inhibition (Hsp90i) reduced the inflammatory response, prevented cartilage damage and limited bone resorption²³². It has been shown that Hsp90 may restrict Hsp70 regulation²³³ and therefore Hsp90 upregulation in chondrocytes may counteract the beneficial Hsp70-mediated responses and facilitate OA progression. Hsp90i could positively affect the level of Hsp70 upregulation necessary and through this mechanism promote cartilage health.

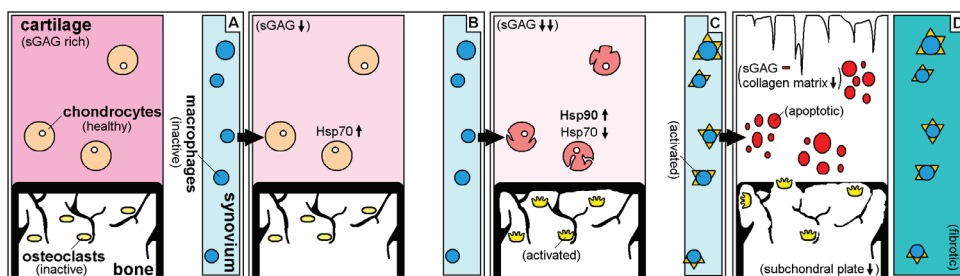


Figure 1: Hypothetical representation of Hsp70 and Hsp90 in osteoarthritis (OA). A: Healthy cartilage. Normal chondrocytes reside in a sulphated-glycosaminoglycan (sGAG) rich extra-cellular matrix (ECM). Subchondral bone is intact and supportive, inactive macrophages are present within the synovium. B: Stressed cartilage during strenuous running results in slight sGAG loss from the ECM. Due to loss of cartilage hydrostatic pressure, chondrocytes become biomechanically stressed. In order to cope, chondrocytes upregulate Hsp70. C: Persisting biomechanical stress. Diminished biosynthetic capacity of stressed chondrocytes produce less sGAG and Hsp90 is upregulated. Activated osteoclasts penetrate the subchondral plate impairing its supportive function. Macrophages produce pro-inflammatory cytokines and growth factors. D: Osteoarthritis. Eventually, a vicious circle of events as described for panel C, culminates in chondrocytes ultimately dying from apoptosis. ECM integrity becomes compromised and its biomechanical properties deteriorate. Osteoclasts tunnel their way through the subchondral bone making space for osteoblast and vascular infiltration, which will eventually lead to development of a sclerotic bone phenotype. Continuous macrophage cytokine and growth factor production has thickened the synovium and results in fibrosis, reducing the patients' range of motion and causing pain.

In summary, Hsp70 and Hsp90 related chondrocyte stress responses might play an important role in biomechanically induced cartilage stress that develops into OA (**Figure 1**). Increased physical activity in a strenuous running model for OA, exposes chondrocytes in healthy cartilage to chronic impact from joint loading (**Figure 1A**). In order to cope with this increased load, chondrocytes may upregulate Hsp70 to promote cell metabolism to sustain the ECM with sufficient sGAG (**Figure 1B**). But persisting cartilage stress through strenuous running could stimulate Hsp90 production, which counteracts the positive effects of Hsp70 and thus promotes OA development (sGAG loss, degradation of ECM, loss of subchondral bone, macrophage activation; **Figure 1C**). When cartilage ECM is damaged, OA progression will further develop and in time progress into severe joint degeneration (**Figure 1D**). In this study, we investigated the role of Hsp70 and Hsp90 in a strenuous running rat model for OA. We hypothesize that running induced loading of articular cartilage upregulates Hsp90 expression in chondrocytes

and limits Hsp70 expression, which results in a loss of Hsp70 mediated protective effect against OA progression in the knee joint. Therefore inhibition of Hsp90 might revert the degeneration effects on cartilage after strenuous running of rats.

METHODS

Study design

Thirty-eight 16-week-old male Wistar rats (Charles River Netherlands BV, Maastricht, the Netherlands) were housed with a 12-h light-dark regimen, at 21°C during the experimental period. Male rats were used in this study, since estrogen is known to influence Hsp expression 234 and OA development²³⁵. Animals received standard food pellets and water ad libitum. Five different groups were used for this study: a baseline group (n=6), two control OA groups with follow up of six weeks (n=6) and twelve weeks (n=6), and two treatment (Hsp90i via BIIB021) groups with follow up of six weeks (n=10) and twelve weeks (n=10).

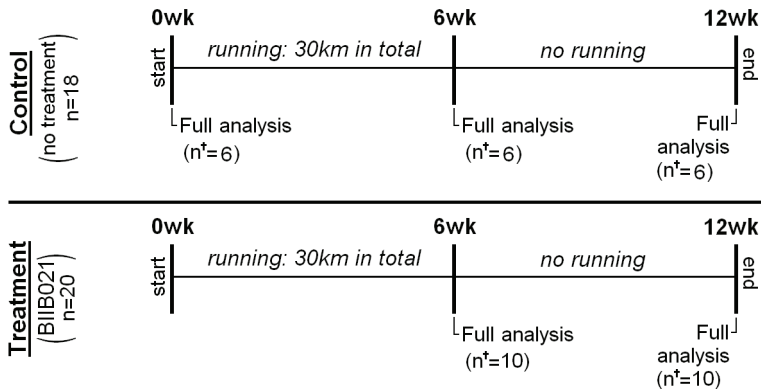


Figure 2: Experimental overview scheme indicating analytical time points and methods for each group of animals. Thirty-eight 16-week-old male Wistar rats were divided over three different groups: a baseline group (n=6), two untreated OA groups (n=12), and two Hsp90i groups (n=20). Hsp90 was inhibited through oral administration of BIIB021. All rats, with exception of the baseline group, were subjected to a six week strenuous running protocol to induce OA [13]. At the end of the experiment a full analysis sequence was done, consisting of in vivo: measurement of activated macrophages using ¹¹¹In-DTPA-folate SPECT/CT; and ex vivo: bone and cartilage analysis using EPIC-microCT, histology, Hsp70 and Hsp90 quantification using Western blotting.

All rats (except the baseline group) were forced to run on a motorized rodent treadmill (LE-8700; Panlab Harvard Apparatus, Barcelona, Spain). Strenuous running induces the development of OA through chronically mechanical loading of articular cartilage in Wistar rats⁸⁴. After an initial training week to get used to treadmill exercise, rats are forced to run one hour per day, five days per week (not on weekends). In order to warm-up rats start running at 20 cm/sec (0.72 km/h) during the first 10 minutes, followed by 50 minutes of running at 33,3

cm/sec (1.20 km/h). The pace and duration of this protocol equals approximately 50% of a total exhaustion protocol¹⁶². After completion of the six week protocol, rats have covered 30 kilometers of strenuous running and moderate OA develops in their knee joints that does not heal spontaneously¹⁵⁷. We measured HSP70 and HSP90 changes in articular cartilage to characterize chondrocyte stress responses and relate this to OA development. OA is characterized by sGAG loss from cartilage ECM, loss of cartilage ECM, bone resorption and macrophage activation. At the end of the experiment for each group, an analysis sequence of μ CT and μ SPECT/CT was performed to measure changes of these different aspects of OA. This sequence consisted of: (1) *in vivo* ^{111}In -DTPA-FA SPECT/CT to measure macrophage activation and (2) *ex vivo* EPIC- μ CT to measure bone and cartilaginous tissue changes, (3) Hsp90 and Hsp70 Western blotting from articular cartilage, and (4) histology to analyze cartilaginous tissue quality. A detailed planning scheme of all groups and conducted tests is given in Figure 2. The Animal Ethic Committee of the Erasmus Medical Centre, Rotterdam, the Netherlands, approved all conducted procedures.

HSP90 inhibition via orally administered BIIB021

All animals in both treatment groups were treated orally with the fully synthetic HSP90 inhibitor BIIB021 (Selleck Chem., Houston, Texas, USA), that competitively binds in the ATP-binding pocket of Hsp90 similar to other geldanamycin-derived Hsp90 inhibitors²³⁶. Previous work with HSP90 inhibitors have shown not to interfere with Hsp70 functioning²³⁷. BIIB021 was dissolved in DMSO and further diluted in saline to a 0.02% DMSO solution with a BIIB021 concentration 14mg/ml. During the entire study, each animal received 0.5 ml of this solution via oral probing. High doses of other types of Hsp90 inhibitors like geldanamycin derivatives, result in drug-related gastrointestinal, bone marrow or hepatic toxicities²³⁸. Therefore, per animal 7mg of BIIB021 was given three times per week, every other day (not on weekends) in order for cells in the gastrointestinal tract and bone marrow to recover from Hsp90 inhibition.

Determination of activated macrophages by SPECT/CT using ^{111}In -DTPA-FA

Activated macrophages express the folate-receptor- β allowing to monitor macrophages *in vivo* using folate radioconjugates¹³⁰. This technique was recently introduced for OA research in a rat model¹³¹. Briefly, DTPA-folate (DTPA-FA; the conjugate was kindly provided by prof. R. Schibli, Center for Radiopharmaceutical Sciences ETH-PSI-USZ, Switzerland) was incubated with $^{111}\text{InCl}_3$ (Mallinckrodt-Tyco, Petten, the Netherlands) in phosphate buffered saline (PBS, pH 6.5) for one hour at room temperature. Quality control performed by HPLC revealed a radiochemical yield of ~92% at a specific activity of >16 MBq/ μg . After addition of a solution of DTPA for complexation of traces of free $^{111}\text{In}(\text{III})$, the solution was further diluted in PBS and administered via the tail vein twenty hours prior to scanning.

SPECT/CT scans were performed with a 4-head multiplex multi-pinhole small animal SPECT/CT camera (NanoSPECT/CT™, Bioscan Inc., Washington DC, USA). Each detector head was

fitted with a tungsten-based collimator of nine 2.5mm diameter pinholes, the field of view was 24mm in width and energy peaks were set at 170keV and 240keV ($\pm 10\%$). All knee joints were scanned with both helical μ CT (acquisition time 5min) and SPECT (acquisition time 30min).

After scanning, all datasets were reconstructed at an isotropic CT voxel size of 0.2mm^3 and an isotropic SPECT voxel size 0.6mm^3 using HiSPECT software (Scivis, Göttingen, Germany). All scans were analyzed using InVivoScope processing software (Bioscan Inc.). A cylindrical region of interest (ROI) was manually determined for quantification of the radioactivity around the knee joint, all data is presented as measured activity per mm^3 .

Bone, cartilage and growth plate measurements with EPIC- μ CT

OA is characterized by loss of sGAG from the cartilage ECM, followed by cartilage degradation. Cartilage and growth plate X-ray attenuation from contrast (ioxaglate) enhanced μ CT scans (EPIC- μ CT) is inversely related to the sulfated-glycosaminoglycan (sGAG) content of cartilage¹¹³ and indicative of tissue quality¹⁵⁷. With EPIC- μ CT it is possible to accurately quantify morphometric parameters of cartilaginous tissue, as well as the subchondral bone¹⁴⁹.

Animals were euthanized directly after the SPECT/CT scan. Both knee joints were harvested and randomly designated to EPIC- μ CT or protein analysis with Western blotting. All knee joints selected for EPIC- μ CT were carefully deprived of soft tissue to a maximal extent, without harming cartilage integrity. Next, all specimens were incubated in 40% solution of ioxaglate, for 24 hours at room temperature¹³⁸. EPIC- μ CT was performed on a Skyscan 1076 in vivo μ CT scanner (Skyscan, Kontich, Belgium), using the following scan settings: isotropic voxel size of 35 μm ; a voltage of 55 kV; a current of 181 mA; field of view 68 mm; a 0.5 mm aluminum filter; over 198° with a 0.4 degree rotation step. All scans were performed using the same settings and all data were reconstructed identically. Using CT analysis software (Skyscan), these datasets were segmented using a fixed attenuation threshold between air (25) and subchondral bone (100)¹⁵⁷. In all segmented μ CT datasets, ROIs were drawn around the cartilage of the medial and lateral plateau of the tibia to calculate X-ray attenuation (arbitrary gray values), which is inversely related to sGAG content (cartilage quality), and cartilage thickness (μm). Tibia plateau cartilage was analyzed since it is predominantly affected during strenuous exercise induced osteoarthritis⁹³.

Bone was accurately segmented from all EPIC- μ CT datasets with a local threshold algorithm¹⁴¹. Cortical and trabecular bone were automatically separated using in-house software³⁵(both 3D Calculator software and separation software can be requested via email). Using the CT analysis software (Skyscan), the tibial epiphysis was selected in the segmented CT scans and analyzed for changes in cortical and trabecular bone. Both medial and lateral thickness of the subchondral plate (sub. chond. plate th.) were measured.

Histopathological examination of the knee joint

After EPIC- μ CT, the separated parts of the knee joints were fixed in paraformaldehyde, decalcified with formic acid and embedded in paraffin. Saggital sections were made at 300 μ m intervals and stained with Safranin-O to image the amount and distribution of the GAGs. All sections were stained in parallel, to minimize staining bias between different samples. The mid-section of both medial and lateral tibial plateau were digitalized with the NanoZoomer Digital Pathology program (Hamamatsu Photonics, Ammersee, Germany). From these digital images, the cartilage was isolated in silico and the staining intensity quantified with graphical software (Adobe Photoshop, San Jose, CA, USA). Cartilage thickness was measured at seven different locations using NanoZoomer (Hamamatsu), and the mean thickness was recorded as averaged histological cartilage thickness²³⁹. Additionally, medial and lateral tibia plateau histology sections were scored according to the OARSI histopathology initiative²⁴⁰.

Protein extraction and Western blotting

From all knee joints selected for protein analysis, the articular cartilage (both medial and lateral) of the tibial plateau was harvested, rinsed in physiological saline, immediately snap-frozen in liquid nitrogen and stored at -80°C until further use. The samples were pulverized for 2min at 30Hz in a TissueLyser II (Qiagen GmbH, Hilden, Germany) using chromium steel grinding balls and custom-made polytetrafluoroethylene vials. Samples were resuspended in lysis buffer²⁴¹ and purified as previously described²⁴². Protein quantification, loading of SDS-polyacrylamide gels, blotting and signal quantification was performed as previously described²⁴³ with Hsp70 and Hsp90 antigen detection as described by Xing et al.²⁴⁴ and Hirano et al.²⁴⁵, respectively, using recommended antibody dilutions. Visualization was performed on an Odyssey infrared imaging system with IRDye 680RD and IRDye 800CW secondary antibodies (1:15,000; both LI-COR Biosciences, Lincoln, Nebraska, USA), respectively. Replicate data per animal were averaged and normalized to α -tubulin (1:1,000; Cell Signaling Technology Inc., Danvers, MA, USA) as a loading control. Signal intensities were quantified using ImageJ software (ImageJ software, National Institutes of Health, Bethesda, MD).

Geldanamycin-like inhibitors that compete for the N-terminal nucleotide-binding pocket are most potently interacting with the cytoplasmic isoforms Hsp90 α and Hsp90 β ^{246, 247}, both isoforms were measured by Western Blot. BIIB021 interferes with ATPase activity of Hsp90, this described method is not able to distinguish between activation stage of the Hsp. The presented data therefore represents total Hsp content (either inactive or active).

Statistical analysis

Differences between means of baseline animals and both groups of untreated OA controls were tested using a one-way ANOVA with Bonferroni correction (Western blot, EPIC- μ CT and quantitative histology analysis; SPSS, SPSS Inc., Chicago, USA). Differences between baseline

animals and both groups of untreated OA controls in semi-quantitative histology scores were analyzed using a Kruskal-Wallis one-way ANOVA. When comparing means of quantitative outcome measurements (Western blot, EPIC- μ CT and quantitative histology analysis) between untreated OA animals and HSP90i treated animals at six or at 12 weeks, an unpaired t-test was used. A Mann-Whitney test was used when comparing means of semi-quantitative histology scores between untreated OA controls and Hsp90i treated animals. The amount of injected radioactivity per animal can influence DTPA-folate SPECT/CT macrophage measurements. In order to correct for this possible influence when comparing differences between groups, the amount of injected activity was added as covariable in a linear regression model using SPSS. For all tests, p values < 0.05 were considered significant.

RESULTS

Hsp70 and Hsp90 regulation in OA and Hsp90i

After a six week running regime, Hsp90 protein levels increased 2.1 fold in running but not in untreated OA control rats (Figure 3A). After six weeks of subsequent rest Hsp90 levels in untreated OA controls were still higher compared to baseline animals (~1.7 fold increase, Figure 3A). However, both effects were not significant ($p=0.12$). Hsp70 levels did not change at six weeks and twelve weeks compared to baseline values ($p=0.55$) (Figure 3B).

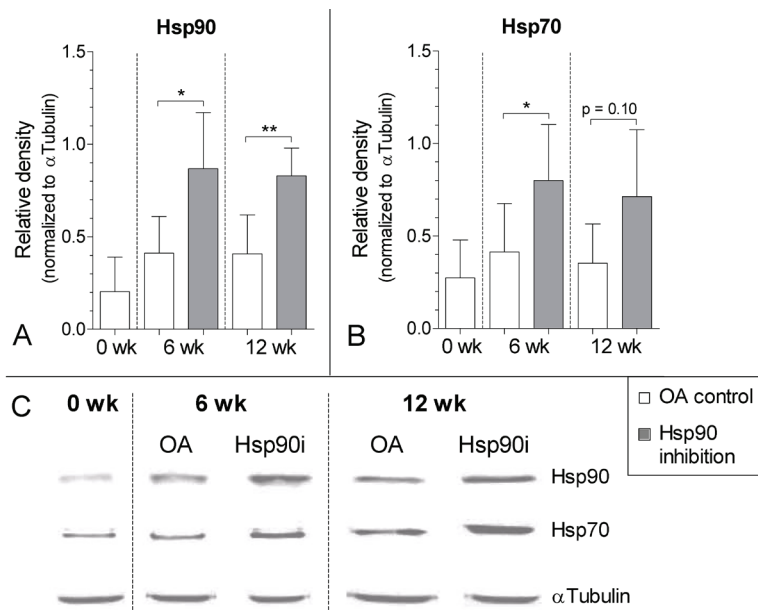


Figure 3: Changes in heat shock protein (Hsp) abundance during chronic loading and after Hsp90 inhibition in articular chondrocytes of knee cartilage. A: Hsp90 B: Hsp70 C: representative Western blots of Hsp90 and Hsp70, α -tubulin served as loading control. *: $p<0.05$, **: $p<0.01$.

Chondrocytes of HSP90i treated animals showed a different Hsp response to biomechanical stress exposure via running. Compared to untreated OA controls, Hsp90i animals produced higher amounts of Hsp90 at the end of the running protocol (~1.9 fold increase; $p=0.02$), which remained increased after the subsequent six weeks of rest (~2.2 fold increase; $p=0.001$, **Figure 3A**). The increased levels of Hsp90 are in line with a functional inactivation of Hsp90 by BIIB021, as earlier studies demonstrated a positive feedback regulation of this Hsp²³⁶. Further supportive evidence in favour of a functional Hsp90 inactivation can be derived from the subsequent Hsp70 induction^{233, 236, 248}, as observed in articular cartilage after running ($p=0.04$, **Figure 3B**). At week twelve, Hsp70 protein levels were still increased ~2.2 fold compared to non-running baseline animals ($p=0.04$), but this was not significantly different compared to untreated OA controls ($p=0.10$, **Figure 3B**). Representative images from the Western blots are shown in **Figure 3C**.

Adaptation of cartilaginous tissue

OA is characterized by a loss of sGAG from the cartilage ECM, followed by cartilage degradation. Strenuous running in untreated OA controls did not induce clear changes in articular cartilage of the medial tibia plateau (**Figure 4A-B**), while at the lateral side, cartilage did show a reduction in ECM thickness ($p=0.02$) (**Figure 4D**). Hsp90i treated animals had lower attenuation values of both medial ($p=0.04$) and lateral ($p=.002$) plateau cartilage (**Figure 4A**). This indicates that HSP90i treated rats had higher levels of sGAG to sustain the cartilage during running. Not only was the sGAG content in both medial and lateral compartments higher compared to the untreated OA controls, Hsp90i treated animals had even higher amounts of sGAG compared to healthy baseline animals. After six weeks of rest, medial cartilage still had higher sGAG levels ($p=0.04$), while lateral cartilage showed no difference in sGAG content ($p=0.88$). However, whereas the lateral cartilage of untreated OA controls was degraded, Hsp90i treated animals did not show any sign of decreased cartilage thickness and was thicker compared to the OA controls ($p=0.009$) (**Figure 4D**). In order to further validate these findings, we quantitatively evaluated the sGAG content of cartilage and cartilage thickness in histological sections. These measurements showed similar patterns between untreated OA controls and Hsp90i treated animals and confirmed our EPIC- μ CT results (**Figure 4F-I**). Additional semi-quantitative scores according to the OARSI histopathology initiative showed increased medial ($p = 0.002$) and lateral ($p = 0.012$) cartilage degeneration in untreated OA controls. In contrast, Hsp90i treated animals showed less cartilage degeneration in both anatomical regions (**Figure 4L-M**). Representative histology images from cartilage are shown in **Figure 4K**.

The growth plate is a cartilaginous tissue in which bone is formed via endochondral ossification. In rats the growth plate never closes and remains highly chondral throughout their lifespan. Increased activity through treadmill running showed that the growth plate is sensitive to high impact from joint loading. EPIC- μ CT and histology revealed that after strenuous running,

the growth plate was severely depleted from sGAG (Figure 4E,J). However, Hsp90i was able to prevent this sGAG loss. Representative histology images of the growth plate are shown in Figure 4K.

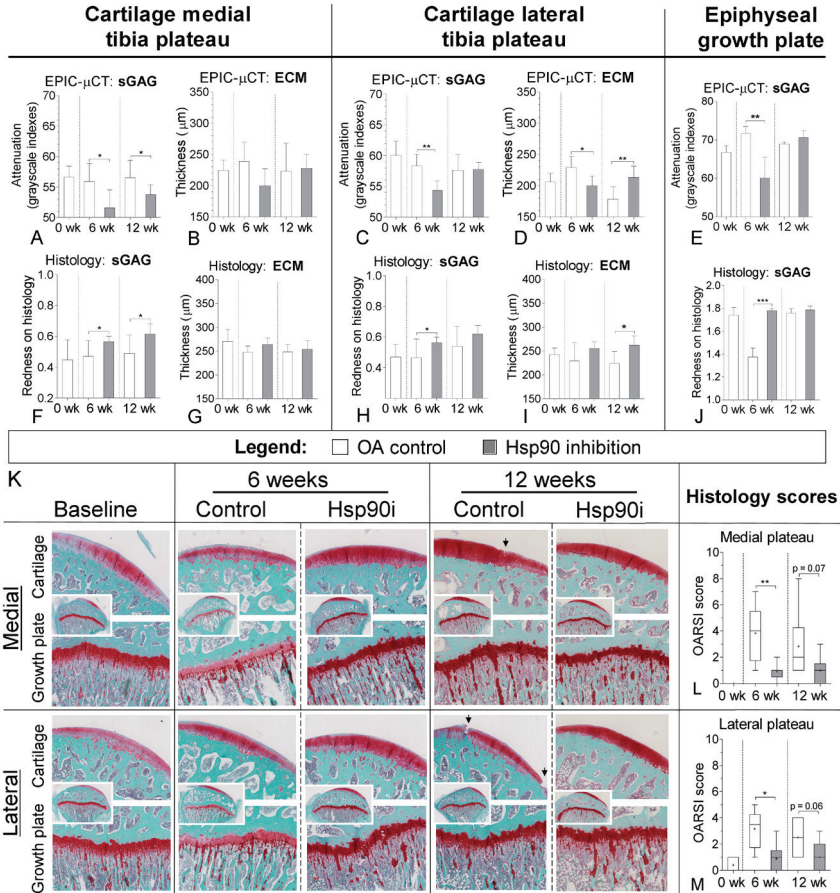


Figure 4: Differences in cartilaginous tissue between untreated OA controls and animals receiving a Hsp90-inhibitor. Cartilage and the epiphyseal growth plate were analyzed with equilibrium partitioning of an ionic contrast agent using (EPIC-) μ CT (A-E) and histology (F-J). With both techniques the amount of sulphated-glycosaminoglycans (sGAG; A,C,E,F,H,J) and cartilage extra-cellular matrix thickness (ECM; B,D,G,I) was measured. Attenuation values from EPIC- μ CT scans are inversely related to the sGAG content. *: $p < 0.05$, **: $p < 0.01$, ***: $p < 0.001$. Representative images of safranin-O stained histology sections are shown of medial and lateral tibial plateau cartilage and the medial and lateral growth plate on baseline, after six weeks of running and after an extra six weeks of rest (K). Cartilage and growth plate showed loss of sulphated-glycosaminoglycans at six weeks in untreated animals. In contrast, increased sGAG content was observed in Hsp90i treated animals. At twelve weeks, cartilage damage becomes evident in untreated animals (matrix damage is indicated with a black arrow), this damage was less in Hsp90i treated animals (L-M). During the six weeks of rest, untreated animals were able to restore the sGAG content of their growth plates.

Subchondral bone changes

OA is also characterized by periarticular bone changes which we evaluated with EPIC- μ CT scans. In untreated OA rats the medial subchondral plate thickness slowly increased during the study (~10% increase after 12 weeks, $p=0.007$). Hsp90i treated animals showed a faster response. Their subchondral bone was already thicker than that of untreated OA controls at six weeks ($p=0.04$) (Figure 5A). This increase did not progress in time and Hsp90i treated animals had a similar subchondral bone thickness compared to untreated OA controls at twelve weeks. At this time point, the lateral subchondral bone of untreated OA controls showed a different response and was ~7% thinner compared to Hsp90i treated animals ($p=0.04$, Figure 5B).

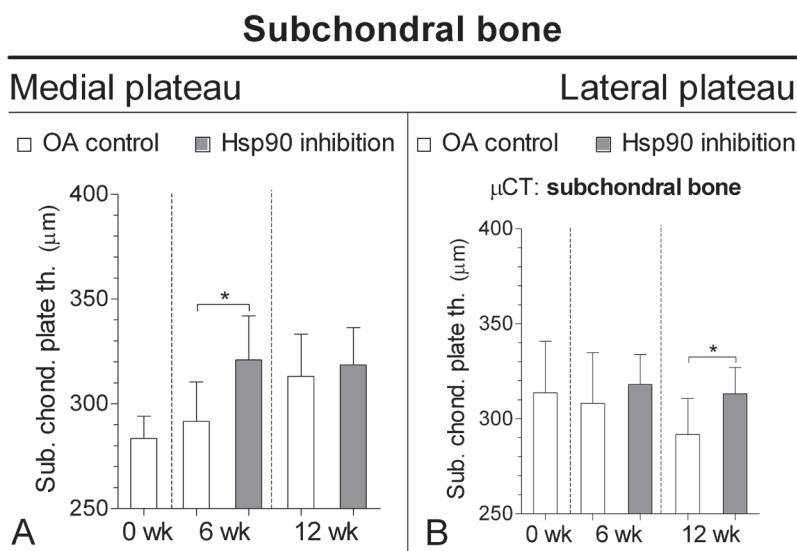


Figure 5: Subchondral bone thickness (Sub. Chond. Plate Th.) measured on μ CT of the medial (A) and lateral (B) plate.

*: $p < 0.05$

Macrophage activation

Osteoarthritis related macrophage activation was measured *in vivo* with ^{111}In -DTPA-folate (^{111}In -DTPA-FA) SPECT/CT. Animals in all groups received 82 ± 5 MBq of ^{111}In -DTPA-FA. There was a only slight trend in macrophage activation in untreated OA control animals after six weeks of running, relative to baseline animals ($p=0.1$). The amount of activated macrophages present in Hsp90i treated animals after six weeks of strenuous running was significantly lower compared to untreated OA controls ($p=0.008$, Figure 6). In Hsp90i animals, macrophage activation levels clearly increased from six to twelve weeks ($p < 0.0001$).

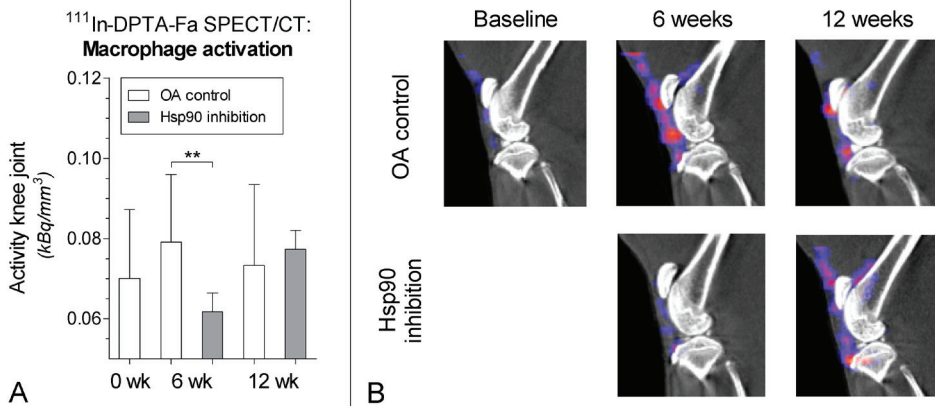


Figure 6: Macrophage activation determined after injection of ¹¹¹In-DTPA-folate using SPECT/CT. A: Quantitative outcome of measured radioactivity in the knee joint. Measurements were corrected for analyzed volume (mm³). A high radioactivity is related to more macrophage activation. B: Representative sagittal SPECT/CT images of knee joints from representative animals of each experimental group. CT images shown in black and white were used for anatomical reference, the SPECT images are shown in color. **: p<0.01

DISCUSSION

Hsps evolved to protect cells against physiological stress, but this system may become overwhelmed under high-end stresses and then tissue homeostasis is lost²⁴⁹. In the present study, we used strenuous running as an established method¹⁵⁷ to induce a mild OA phenotype (Figure 4). Running caused a trend towards Hsp90 accumulation in the articular cartilage, while Hsp70 levels were unaltered (Figure 3). In contrast to previous reports of increased Hsp70 levels after 28 days of exercise¹⁵², we only measured Hsp70 and Hsp90 after 42 and 84 days. Possibly more pronounced differences in chondrocyte Hsp expression can be found at earlier time points. We used BIIB021 treatment in this model to evaluate potential OA modifying aspects of pharmacological Hsp90 inhibition. Systemically introduced Hsp90i may be toxic²³⁸. However, our treatment regime did not result in weight or hair loss in our treated animals that could have suggested Hsp90i related toxicity.

Hsp90i resulted in elevated Hsp90 protein levels as well as higher Hsp70 levels. Previous work with BIIB021 and other Hsp90 inhibitors clearly illustrated a concentration-dependent relation of Hsp90i on both the induction of Hsp90 and Hsp70. Although elevated Hsp90 levels seem to be a counterintuitive result of Hsp90i, it is a well known response from different Hsp90 inhibitors, such as geldanamycin, 17-allylamino-17-demethoxygeldanamycin (17-AAG) and BIIB021. Through binding in the ATP-binding pocket of Hsp90 they prevent activation of Hsp90, which results in reduced Hsp90 activity with degradation downstream client proteins like HER-2, AKT and Raf-1^{236, 250}. A functional inactivation of Hsp90 by BIIB021 also induces

Hsp70 which can be explained through heat shock factor-1 (HSF-1). HSF-1 plays an established role in regulation of Hsp70 levels, it is kept in a latent state by a stress-protein complex and is activated upon proteotoxic insults (over loading) in order to activate Hsp70 gene expression²⁵¹. Hsp90 is a major repressor of HSF-1 gene expression and retains HSF-1 in an inactive nontrimeric state²⁵². When mechanical loading goes up, Hsp90 production is increased which reduces HSF-1 activity and Hsp70 upregulation is prevented. This inversed regulation of Hsp70 and Hsp90 through HSF-1 may explain why Hsp70 is known to be less responsive to increased loads²⁵³ and why the protective effect of Hsp70 for maintaining ECM homeostasis and cartilage protection is compromised in our running model. Hsp90i treated animals in our study showed increased Hsp70 protein levels. As one can expect, Hsp90i strongly induces HSF-1 in human chondrocytes²⁵⁴. This explains why diminished Hsp90 activity shifts the balance in favor of Hsp70 synthesis^{233, 236, 248} and stimulates the Hsp70 protective effect on cartilage. It is due this feedback loop that Hsp70 is used as a standard pharmacodynamic biomarker for analysis of Hsp90 inhibitors functioning in both preclinical and clinical studies²⁵⁵. But Hsp90i can also directly influence cellular processes that reduce OA progression. Hsp90i on in vitro cultured human articular chondrocytes selectively inhibit interleukine-1 β (IL-1 β) induced extracellular signal-regulated kinase (ERK) activation and resulted in reduced matrix metalloproteinase-13 (MMP-13) production²⁵⁶. Since excessive MMP-13 activity results in articular cartilage degradation, reduced MMP-13 production might prevent OA²⁵⁷. Our study results do not distinguish between whether Hsp90i reduced OA progression directly or indirectly via increased Hsp70. However, the final outcome HSP90i shows markedly reduced cartilage degradation, decreased subchondral bone remodeling conserving the subchondral plate, and reduced synovial macrophage activation.

Articular cartilage of Hsp90i treated animals in our study had higher amounts of sGAG (**Figure 4**), which likely gives cartilage the necessary hydrostatic stiffness to absorb impact during running and protect chondrocytes from increased mechanical stress. Hsp90i treatment also resulted in a prompter increase of medial subchondral bone thickness compared to untreated OA controls, and Hsp90i prevented subchondral bone plate thinning in the lateral compartment (**Figure 5**). Biomechanically stressed chondrocytes are known to upregulate their vascular endothelial growth factor (VEGF) synthesis, which may then act as an autocrine factor to trigger osteoclast activity and subchondral bone destruction in OA⁴². In addition, Hsp90i can reduce VEGF signaling through reduced activation of HIF-1 α ²⁵⁸ which may explain why the integrity of the bone-cartilage interface was protected in our study. Strenuous running did not induce macrophage activation in untreated animals. However, Hsp90i animals did show reduced levels of macrophage activation after six weeks of running (**Figure 6**). This effect may be attributed to a diminished cytokine production in macrophages and other cell types as a result of Hsp90i²⁵⁹. Furthermore, Hsp90i mediated Hsp70 upregulation can have general anti-inflammatory effects too²⁶⁰. However, despite continuous Hsp90i treatment, macrophage activation increased again during the subsequent six weeks of rest (**Figure 6**) and may suggest that Hsp90i did not directly modulate macrophage responses.

A direct translation of our results towards a clinical treatment for OA patients may not be possible. BIIB021 and other geldanamycin-derived Hsp90 inhibitors are currently already used in cancer trials. Treatment of life-threatening diseases might justify higher risks of Hsp90 associated dose-limiting toxicities²³⁸, but they can never be accepted in OA patients. Therefore, a more detailed knowledge of the downstream targets that are modulated by Hsp90i is needed. Perhaps, specific induction of HSF-1 may result in effects similar to Hsp90i-mediated OA prevention in biomechanical strained cartilage. Another way to reduce systemic side-effects would be to investigate whether a local treatment via intra-articular injections with Hsp90i is feasible and beneficial.

Hyaline articular cartilage evolved to absorb forces that develop during joint mobilization. From this perspective, it is obvious to suspect a balance between biomechanical loads and chondrocyte functioning and an imbalance is likely to result in cartilage failure and OA development. When stress on cartilage is increased either via increased loading or due to changed joint biomechanics (e.g. as a result of ligament tears)¹⁵², chondrocytes upregulate Hsps, which suggests a pivotal role in OA onset. Yet, only few studies report Hsp production by chondrocytes as possible regulators of cartilage homeostasis under stressed conditions. More research on this topic will lead to a more accurate explanatory model for pathological joint loading induced OA. This will enable physicians to provide patients with better instructions or life-style advices concerning OA development. Ambivalent effects of training on cartilage are well known in clinical patient care¹⁸³. Possibly, a combined approach of regulated physical exercise and therapeutic intervention on Hsp production could stimulate chondrocytes in OA patients in the right direction, and slow down OA progression or perhaps even restore cartilage quality.

Conclusion

The results of our *in vivo* study strongly suggest that chondrocyte stress induced Hsp90 synthesis plays an important role in the onset of OA. Strenuous running induced biomechanical stress tended to increase Hsp90 protein levels in rat articular cartilage. Hsp90 inhibition and subsequently increased Hsp70 levels enabled chondrocytes to maintain cartilage homeostasis by increasing sGAG amounts above baseline in order to protect the ECM from increasing biomechanical impacts during physical activity. Hsp90 inhibition further improved subchondral bone thickness and reduced synovial macrophage activation. Specific modulation of chondrocyte Hsp90 activity could be an attractive novel therapeutic intervention therapy to prevent osteoarthritis.

ACKNOWLEDGEMENTS

We acknowledge the Dutch Arthritis Association and the BMM/TerM P2.02 Program of the Netherlands Ministry of Economic Affairs and the Netherlands Ministry of Education, culture and Science for their financial support.

CHAPTER 6

FK506 PROTECTS AGAINST ARTICULAR CARTILAGE EXTRA-CELLULAR
MATRIX DEGRADATION

*M. Siebelt, A.E. van der Windt, H.C. Groen, M. Sandker, J.H. Waarsing,
M. de Jong, H. Jahr, H. Weinans
Osteoarthritis Cartilage. 2014April;22(4):591-600*

ABSTRACT

Introduction

Osteoarthritis (OA) is a non-rheumatologic joint disease characterized by progressive degeneration of the cartilage extra-cellular matrix (ECM), enhanced subchondral bone remodeling, activation of synovial macrophages and osteophyte growth. Inhibition of calcineurin activity through tacrolimus (FK506) in *in vitro* monolayer chondrocytes exerts positive effects on ECM marker expression. This study therefore investigated the effects of FK506 on anabolic and catabolic markers of osteoarthritic chondrocytes in 2D and 3D *in vitro* cultures, and its therapeutic effects in an *in vivo* rat model of osteoarthritis.

Methods

Effects of high and low doses of FK506 on anabolic (QPCR/histochemistry) and catabolic (QPCR) markers were evaluated *in vitro* on isolated (2D) and ECM-embedded chondrocytes (explants, 3D pellets). Severe cartilage damage was induced unilaterally in rat knees using papain injections in combination with a moderate running protocol. Twenty rats were treated with FK506 orally and compared to twenty untreated controls. Subchondral cortical and trabecular bone changes (longitudinal microCT) and macrophage activation (SPECT/CT) were measured. Articular cartilage was analyzed *ex vivo* using contrast enhanced microCT and histology.

Results

FK506 treatment of osteoarthritic chondrocytes *in vitro* induced anabolic (mainly collagens) and reduced catabolic ECM marker expression. In line with this, FK506 treatment clearly protected ECM integrity *in vivo* by markedly decreasing subchondral sclerosis, less development of subchondral pores, depletion of synovial macrophage activation and lower osteophyte growth.

Conclusion

FK506 protected cartilage matrix integrity *in vitro* and *in vivo*. Additionally, FK506 treatment *in vivo* reduced osteoarthritis-like responses in different articular joint tissues and thereby makes calcineurin an interesting target for therapeutic intervention of osteoarthritis.

INTRODUCTION

FK506 (Tacrolimus, Prograf) is an immunosuppressive drug discovered by Kino et al. in the 1980s²⁶¹. Since then, it has been used clinically for an increasing number of immunological disorders. FK506 exerts its therapeutic effects by suppression of T-cell activation, without markedly affecting bone marrow cell differentiation and proliferation²⁶². Through binding to FK506-binding proteins (FKBPs), FK506 inhibits the activity of ubiquitously expressed calcium/calmodulin dependent calcineurin (Cn). As a consequence, the calcineurin mediated dephosphorylation of transcription factors of the nuclear factor of activated T-cells (NFATs) family (NFAT1-4) is inhibited.

Besides their role in T-cell activation, Cn and NFATs are now also known to play a role in physiological processes in many other cell and tissue types and pathological conditions like cancer, degenerative brain diseases and cardiac hypertrophy²⁶³. FK506 has proven to be useful in reducing inflammation and alleviating symptoms in patients with inflammatory (rheumatoid) arthritis^{264, 265}. Interestingly, the Cn/NFAT signalling cascade is also reported to play a role in bone remodeling²⁶⁶ and chondrogenesis²⁶⁷. FK506 has been shown to induce chondrogenic differentiation of murine chondroprogenitor cells²⁶⁸. This suggests that patients with non-inflammatory joint diseases, like osteoarthritis (OA), also might benefit from a treatment with Cn inhibitors.

OA is a complex progressive disease and a disturbed balance between anabolic and catabolic activity of chondrocytes is an early pathophysiological event leading to matrix degradation. Progression of OA finally results in severe deterioration of articular cartilage and involves pathological changes throughout the joint, like extensive subchondral bone remodeling¹⁷ and activation of synovial macrophages²⁶⁹. We reported earlier that FK506 treatment of monolayer cultured osteoarthritic cells enhanced expression of anabolic markers like collagen type II (COL2), but suppressed relevant catabolic, hypertrophy and mineralization markers^{270, 271}. Another Cn inhibitor, cyclosporine A (CsA) showed similar effects on anabolic and catabolic activity of OA chondrocytes and reduced cartilage damage in a collagenase induced OA mouse model²⁷². However, this study only measured macroscopical and microscopical cartilage damage *ex vivo* and did not investigate possible effects of Cn inhibition on other tissues of the joint, like bone and synovium.

Recently, we established a novel rat OA model using a combination of papain injections with a running protocol to induce severe knee joint articular cartilage degradation together with prominent involvement of subchondral bone and synovial macrophages²⁷³. The current study aimed to elucidate the effects of systemic FK506 treatment in this OA animal model. We first characterized whether both low and high concentrations of FK506 modulate anabolic markers

in OA chondrocytes in monolayer cultures. Since chondrocytes reside in an extra-cellular matrix *in vivo*, we additionally investigated whether low dose FK506 treatment remains beneficial for extracellular matrix-embedded chondrocytes in *ex vivo* explants and pellet cultures. Finally, we tested modulating effects of FK506 in an animal model for severe cartilage degradation and analyzed articular cartilage (*ex vivo* μ CT and histology), subchondral bone (*in vivo* μ CT) and synovial macrophages activation (*in vivo* SPECT/CT) six and twelve weeks after induction of cartilage damage.

METHODS

FK506 effects on osteoarthritic chondrocytes *in vitro*

Human articular cartilage was explanted from macroscopically normal areas of femoral condyles and tibial plateaus of patients (N=9, between 55-82 years old) undergoing total knee replacement surgery for OA (MEC2004-322). Isolation of primary osteoarthritic human articular chondrocytes from cartilage tissue under standard conditions (cytokine-free Dulbecco's modified Eagle's medium (DMEM) with 4.5 g/L glucose, 10% fetal calf serum (FCS), 50 μ g/mL gentamycine and 1.5 μ g/mL fungizone; all Invitrogen, Paisley, Scotland, UK, adjusted to 380 mOsm by adding sterile sodium chloride) and monolayer experiments were performed as described earlier²⁷⁰. In short, passage 1 cells were seeded in 2D monolayer, stimulated with 0, 62 or 620 nM FK506 after 24 hours and harvested for RNA analysis (quantitative RT-PCR) six days later. Experiments were performed at least in technical duplicates from four OA donors. In addition to 2D cultures, passage 2 cells from four OA donors were cultured as 3D pellets (2x10⁵ cells/pellet) for 21 days in medium (380 mOsm) with or without addition of 62 nM FK506²⁷⁰.

To investigate the effects of FK506 on OA chondrocytes embedded in their extracellular matrix, six mm diameter full-thickness explants from femoral condyles and tibial plateaus of five OA donors were cultured as described before²⁷⁰ and cultured in medium (380 mOsm) with or without 62 nM FK506 for 7 days.

RNA and protein analysis by RT-QPCR and histology

RNA from monolayer and explant cultures was extracted, purified and quantified, and cDNA was synthesized and quantified by RT-QPCR reactions as described earlier^{271, 274}. RNA abundance was normalized to an index of the three most stable reference genes (GAPDH, HPRT1, 18sRNA or UBC) replicate values were averaged per condition per patient and gene expression was calculated as fold change of control condition (0 nM FK506)²⁷⁰. Primer sequences for COL2, ACAN, MMP1, MMP13, ADAMTS4 and ADAMTS5 were adopted from Uitterlinden et al²⁷⁴, for COL1 from Das et al²⁷⁵, and for VCAN/CSPG2 from Martin et al²⁷⁶. To quantify expression of COL9 and COL11, the following primers were tested for similar amplification efficiency and specificity²⁷⁵, and were used as respectively 20 μ l Taqman and SYBR® Green I reactions:

HsCOL9A1_F GCAGTCCATGGCAAGTTTCTCT, COL9A1_R GCTTTGCTGTGCTGGGAAAA and COL9A1_FAM TGAAGTTCAAATGGAACAGAAACTTGAGGATTATCTG; HsCOL11a1_Fw AGGAGAGTTGAGAATTGGGAATC, COL11A1_Rv TGGTGATCAGAATCAGAAGTTTCG.

The expression data are presented as $2^{-\Delta\Delta Ct}$ values based on publication by Livak & Schmittgen²⁷⁷. The cDNA abundances of each gene of interest were normalized to an index of three stable expressed reference genes to generate a normalized, so-called $2^{-\Delta Ct}$, value. Replicate values were averaged per condition, per patient, and finally expressed as fold change difference relative to the control condition (i.e. without FK506 treatment) and representing a $2^{-\Delta\Delta Ct}$ value. The Col2/Col1 ratio, like the VCAN/CSPG2 ratio, relates the expression levels of both genes to one another. Relative higher Col2 expression, as compared to Col1, is indicative of a relatively better preserved chondrocyte-specific gene expression. This also holds for VCAN/CSPG2 ratios, and was used earlier as a measure of de-differentiation of chondrocytes^{278, 279}.

(Immuno)histochemical staining for COL2 and GAG on 3D pellet cultures was performed as described before²⁸⁰. Staining intensities of pellets were quantified using ImageJ 1.42 software (<http://rsb.info.nih.gov/ij/download.html>).

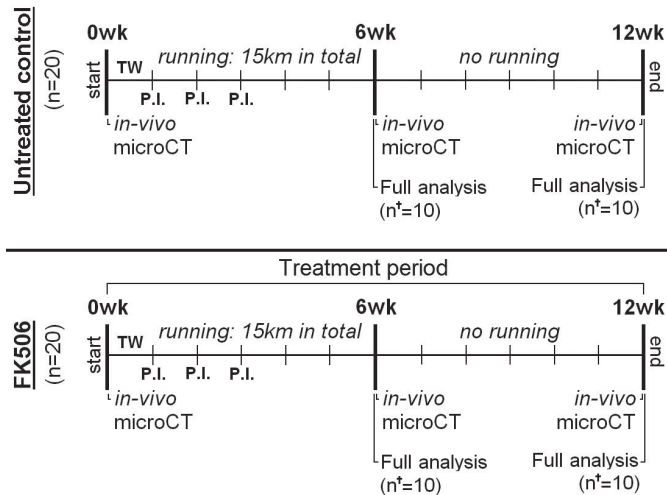


Figure 1: Experiment design indicating analytical time points and methods for each experimental group. Forty 16-week-old male Wistar rats were injected with three papain intra-articular injections (P.I.) and forced to run 15km on a motorized treadmill. Animals were divided over two different groups: an untreated osteoarthritis (OA) group (n=20) and a FK506 treated group (n=20). During the experiment three longitudinal μ CT scans were made to measure subchondral bone changes [24]. At six and twelve weeks a full analysis sequence was done in ten animals per group (n=10), consisting of: determination of activated macrophages using SPECT/CT in vivo [25]; and cartilage analysis with equilibrium partitioning of an ionic contrast agent using (EPIC-) μ CT [26] and histology ex vivo.

FK506 therapeutic effects in a rat model for severe osteoarthritis

Forty 16-week-old male Wistar rats (Charles River Netherlands BV, Maastricht, the Netherlands) were housed in the animal facility of the Erasmus Medical Centre, with a 12-h light-dark regimen, at 21°C during the experimental period, and received standard food pellets and water ad libitum. OA-like articular destruction was induced in all animals, which were then divided over two groups: twenty rats served as untreated controls and twenty rats were treated during the experiment with FK506. FK506 treated animals received FK506 suspension (1 mg/kg)²⁸¹ through oral probing, five days a week, not on weekends.

Severe cartilage damage was induced using intra-articular papain injections in the left knee joints combined with exposure to a moderate exercise protocol as described before²⁷³. In short, all animals received three intra-articular injection that consisted of 15µl 4% (w/v) papain solution (type IV, double crystallized, 15 units/mg, Sigma-Aldrich, St. Louis, MO, USA) with 15µl 0.03M L-cystein (Sigma-Aldrich)⁸¹. Their contralateral knee joint served as an internal healthy control. All rats were forced to run on a motorized rodent treadmill (LE-8700; Panlab Harvard Apparatus, Barcelona, Spain) for six weeks covering a total distance of 15km²⁷³. During the study all animals were longitudinally monitored at baseline, 6 weeks and 12 weeks with µCT to measure subchondral bone changes³⁵. At six and twelve weeks, ten rats in both groups were selected for a full analysis sequence. This sequence consisted of SPECT/CT to quantify in vivo macrophage activation¹³¹, and ex vivo EPIC-µCT and histology to measure cartilage quality¹¹³. The details of these procedures were described earlier²⁷³. The animal ethic committee of the Erasmus Medical Center, Rotterdam, the Netherlands, approved all conducted procedures. A detailed planning scheme of all groups and conducted tests is given in **Figure 1**.

Subchondral bone measurements on µCT scans

Both knees of all animals were µCT scanned under isoflurane anaesthesia, using a Skyscan 1176 in vivo µCT scanner (Skyscan, Kontich, Belgium). Ten minutes of scan time was required per knee at an isotropic voxelsize of 18µm, at a voltage of 65kV, a current of 385mA, field of view of 35mm, using a 1.0mm aluminum filter, over 1980 with a 0.5 degree rotation step, and a 270 msec exposure time. All datasets were segmented with a local threshold algorithm¹⁴¹. Cortical and trabecular bone were automatically separated using in-house software²⁸². Using Skyscan software, both subchondral plate thickness (Sb. Pl. Th. in µm) and subchondral plate porosity (Sb. Pl. Por. in mm³) of the medial and lateral compartment of the tibial plateau were measured³⁵. In the tibial epiphysis, the trabecular thickness (Tb. Th. in µm) and trabecular bone volume fraction (BV/TV), representing the ratio of trabecular bone volume (BV, in mm³) to endocortical tissue volume (TV, in mm³) were measured. Ectopic bone formation (mm³) was also quantified as a measure for osteophyte growth in these longitudinal µCT scans.

Determination of activated macrophages by SPECT/CT using 111In-EC0800

Activated macrophages express the folate receptor- β allowing monitoring macrophages in vivo using folate-based radiotracers^{130, 164}. Phosphate buffered saline (PBS, pH 6.5) DOTA-Bz-folate (EC0800, kindly provided by Endocyte Inc., West Lafayette, USA)²⁸³ was labeled with 111InCl₃ (Covendien, Petten, The Netherlands) as described previously²⁷³. Quality control was performed with ITLC-SG and revealed a radiochemical yield of ~91% at a specific activity of 50 MBq/ μ g. 111In-EC0800 (55MBq) was administered via the tail vein twenty hours prior to scanning. SPECT/CT scans were performed with a 4-head multiplex multi-pinhole small animal SPECT/CT camera (NanoSPECT/CT TM, Bioscan Inc., Washington DC, USA). All knee joints were scanned with both helical μ CT (acquisition time 5min) and SPECT (acquisition time 30min). All scans were analyzed using InVivoScope processing software (Bioscan Inc.). To reduce inter-individual variation, the absolute difference in measured radioactivity (kBq/mm³) of the OA knee joint compared to their internal control joint was calculated. This absolute difference was used when comparing means of untreated animals with FK506 treated animals.

Cartilage evaluation with contrast enhanced μ CT and histology

Equilibrium partitioning of a contrast agent using μ CT (EPIC- μ CT) has a strong correlation with cartilage sulfated-glycosaminoglycan (sGAG) content¹¹³. Animals were euthanized directly after the last SPECT/CT scan and both knee joints were harvested for EPIC- μ CT analysis. All specimens were incubated in 40% solution of ioxaglate (Hexabrix320, Mallinckrodt, Hazelwood, MO, USA) for 24 hours at room temperature¹³⁸. EPIC- μ CT was performed on the 1176 in vivo μ CT scanner (Skyscan), using the following scan settings: isotropic voxel size of 18 μ m, a voltage of 65kV, a current of 385mA, field of view 35mm, a 0.5 mm aluminum filter, 198o with a 0.5 degree rotation step, and a 235 msec exposure time. In all EPIC- μ CT datasets, X-ray attenuation (arbitrary gray values inversely related to sGAG content) and cartilage thickness (μ m) was calculated for cartilage of the medial and lateral plateau of the tibia²⁷³.

After EPIC- μ CT, the separated parts of the knee joints were fixed in 3.7% phosphate buffered formaldehyde, decalcified with formic acid and embedded in paraffin. Sagittal sections were made at 300 μ m intervals and stained with Safranin-O with a fast green counterstain to image the distribution of the GAGs. Sections were stained all at once, to minimize artifacts between different samples.

Statistical analysis

Statistical analysis of vitro studies was performed as described before²⁷⁰. Briefly, replicate raw expression data of multiple donors was tested for the effect of FK506 using Linear Mixed Model regression and 'donor' was incorporated as a random effect to correct for basal differences in expression between donors (SPSS Inc., Chicago, USA).

For the *in vivo* study, differences between means of OA induced and healthy knee joints within the same animal were tested using paired t-tests at each time point for all outcome parameters (GraphPad Software, San Diego, California, USA). When comparing differences between means of untreated animals and FK506 treated animals, an unpaired t-test was used at each time point for all outcome parameters (GraphPad Software). Longitudinal data from *in vivo* μ CT were additionally analyzed using generalized estimating equations (SPSS). For all tests, p values ≤ 0.05 were considered significant.

RESULTS

In vitro effects of FK506 on human osteoarthritic chondrocytes

Inhibition of calcineurin activity by FK506 in monolayer cultured passage 1 osteoarthritic chondrocytes increased expressions of cartilage specific collagens. Both low and high concentrations of FK506 positively stimulated COL2/COL1 ratio (62 nM FK506 by ± 2 -fold, $p = 0.067$; 620 nM by ± 3 -fold, $p = 0.001$) and COL9 expression (62 nM FK506 by ± 1.8 -fold, $p = 0.037$), while no effects were found on the ACAN/VCAN ratio or COL11 expression (Figure 2A). In cartilage explants, the osteoarthritic chondrocytes are embedded in a matrix, which might limit chondrocyte exposure to FK506. Despite the large standard deviations in the explants cultures, we found clear matrix-protective trends after FK506 treatment. A low dose of FK506 was enough to induce a similar trend of increased anabolic marker expression in explants as seen in monolayer cultured chondrocytes (Figure 2B). Moreover, the FK506 induced changes in chondrogenic marker expression seem to be even higher in the explants. In line with our previous work on monolayer chondrocytes²⁷⁰, FK506 also reduced the expression of the catabolic MMPs and important aggrecanases in the explant cultures (Figure 2B).

The FK506 induced increase in collagen expression was confirmed by immunohistology on 3D pellets cultures of osteoarthritic chondrocytes. FK506 clearly increased COL2 protein expression (to 121.4% of control, $p = 0.009$) in chondrocyte pellet cultures, while no clear effect was seen on GAG staining (Figure 2C).

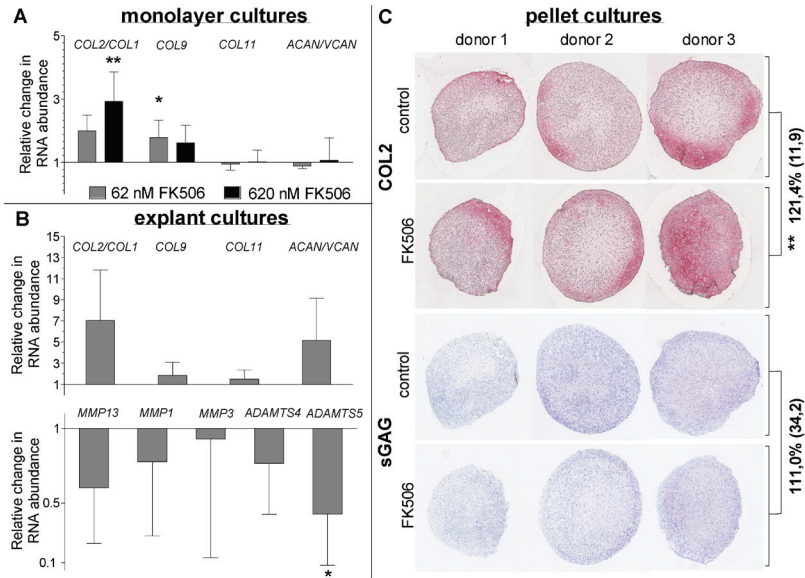


Figure 2: RNA abundance of anabolic and catabolic markers was determined in samples from human osteoarthritic monolayer (A) and explant (B) cultures. Relative changes by FK506 (grey and black bars) as compared to control (no FK506) are shown, each bar represents the fold-change compared to the control condition. Error bars indicate standard deviations. Representative images of 21-day 3D pellet cultures (C) show collagen type II immunostaining (on top, in red) and sGAG staining (thionin; on bottom, in blue) of pellets cultured with or without 62 nM FK506. Staining intensity in FK506 pellets is expressed as mean percentage (standard deviation) of that in control pellets *: $p < 0.05$, **: $p < 0.01$

In vivo effects of FK506 treatment

Bodyweight of all untreated rats at baseline was 416.4g (411.3 – 421.5g), during six weeks of treadmill running this decreased non-significantly to a mean weight of 408.3g (398.2 – 418.3g). During subsequent six weeks of rest, all rats increased in their mean bodyweight to 485.5g (473.0 – 498.0g). FK506 treated animals (mean weight at baseline was 413.6g; 409.4 – 417.8g) also did not increase in bodyweight during induction of OA-like articular destruction (mean weight after six weeks was 418.5g; 412.9 – 424.1g). After twelve weeks their mean bodyweight was 507.1g (498.8 – 515.4g), which was significantly higher compared to untreated controls ($p = 0.004$) (Figure 3). During the course of the experiment, none of the animals showed signs of FK506-induced cytotoxicity, like weight or hair loss.

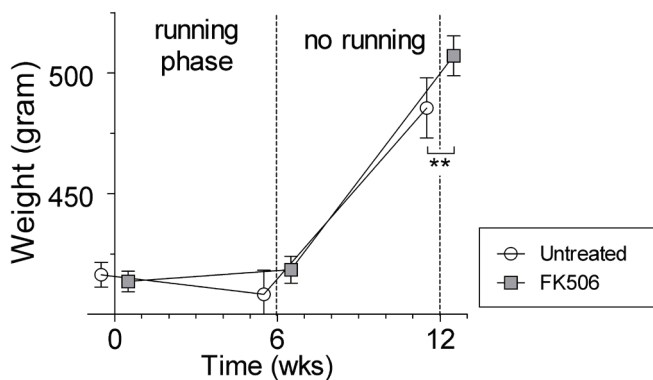


Figure 3: Increase in rat bodyweight (gram) during the experiment of OA control (white circles) and FK506 treated (gray squares) animals. **: $p < 0.01$, error bars indicate 95% confidence intervals.

Osteoarthritic changes of articular cartilage

Intra-articular papain injections combined with moderate exercise in untreated controls induced severe sGAG depletion from both medial and lateral cartilage compartments of the tibia plateau. This sGAG depleted state persisted throughout the experiment (**Figure 4A-B**). After the running protocol at six weeks, cartilage of the medial compartment was slightly reduced in thickness (**Figure 4C**). Lateral cartilage thickness was severely degraded (**Figure 3D**) and resulted in almost completely denuded subchondral bone (**Figure 3E**). During subsequent six weeks of rest medial cartilage continued to degrade, in the lateral compartment an ongoing decline in cartilage thickness was absent (**Figure 4C**). Representative medial and lateral cartilage images from safranin-O stained histology from untreated controls at six and twelve weeks are shown in **Figure 5**.

Compared to untreated controls, FK506 treated animals had similar sGAG depleted cartilage in medial and lateral compartments of the tibia plateau (**Figure 4A-B**). Lateral cartilage was reduced in thickness to similar extent as untreated controls (**Figure 4D**). However, medial cartilage showed a trend towards thicker ECM compared to untreated control at six weeks, although this was not significant ($p = 0.15$). In contrast to the progressive degradation of medial cartilage as seen in untreated controls at twelve weeks, medial cartilage thickness of FK506 treated animals remained constant and was significantly thicker at twelve weeks compared to untreated controls ($p = 0.02$) (**Figure 4C**).

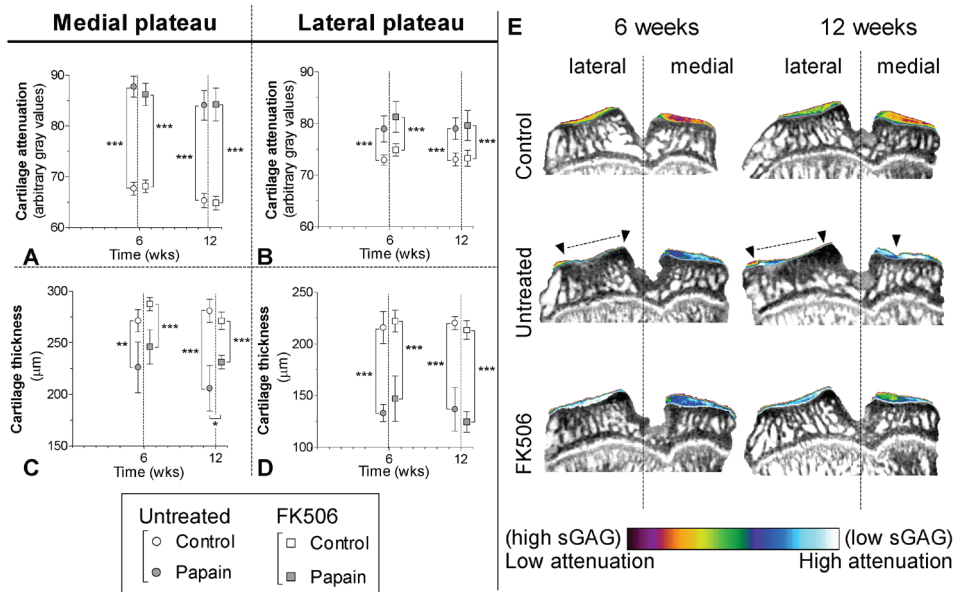


Figure 4: Cartilage quality and quantity was determined from untreated OA (circles) and FK506 treated (squares) rats with equilibrium partitioning of an ionic contrast agent using (EPIC)- μ CT (A-D). The amount of sulphated glycosaminoglycans (sGAG) (arbitrary gray values; A,B) and cartilage thickness (μm ; C,D) were measured of medial (A,C) and lateral (B,D) cartilage compartments of the tibia plateau harvested from healthy joints (blank boxes) and OA induced joints (gray boxes). Attenuation values from EPIC- μ CT scans are inversely related to the sGAG content, meaning that a high attenuation corresponds to low sGAG content. Coronal images from EPIC- μ CT scans of the tibia plateau show the amount of cartilage (erosions indicated with \blacktriangle and dashed lines) and sGAG content (displayed in color). *: $p < 0.05$, **: $p < 0.01$, ***: $p < 0.001$, error bars indicate 95% confidence intervals.

Although lateral cartilage did not differ significantly in sGAG content or thickness between untreated and FK506 treated rats, we did observe a small difference between both groups. In four FK506 treated rats, but in none of the untreated rats, there were small and focal regions of lateral tibia cartilage that showed intact but totally sGAG depleted ECM (Figure 4E). A difference that was also found on safranin-O stained histology sections as shown in Figure 5.

Subchondral bone changes

Subchondral bone plate thickness of medial tibia compartment in untreated controls and FK506 treated rats was slightly reduced after six and twelve weeks of follow up (Figure 6A), but did not differ between both groups ($p = 0.83$). Medial plate porosity did not increase in both experimental groups throughout the experiment (Figure 6B). Lateral compartment subchondral bone thickness of untreated OA joints was clearly increased compared to their healthy control joint at six weeks ($p < 0.0001$), and there was also more subchondral plate porosity ($p = 0.02$)

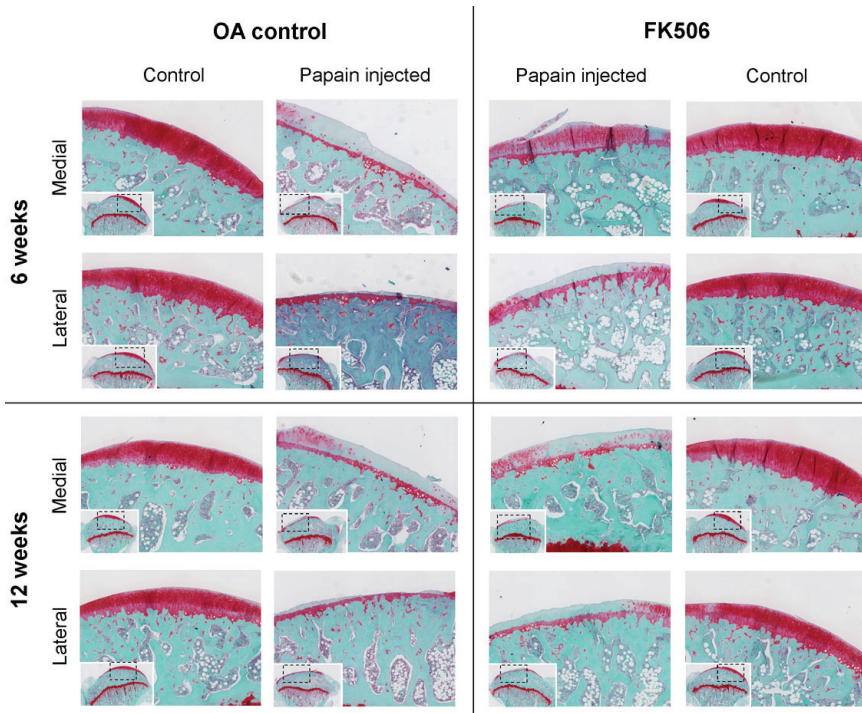


Figure 5: Safranin-O stained histology sections of medial and lateral tibial plateau cartilage after six weeks and twelve weeks of follow up. Medial cartilage of untreated OA knee joints with depleted sulphated-glycosaminoglycan at six weeks and twelve weeks, and only mildly degraded extra-cellular matrix (ECM). Lateral cartilage ECM was almost totally eroded, only the calcified cartilage layer remained present and showed ECM denudation of cartilage ECM. Much less ECM degradation occurred in FK506 treated animals. The lateral compartment cartilage was severely eroded, however 4/10 rats showed focal regions with complete sGAG depleted but partially intact ECM.

(Figure 6C,G,H). Subchondral plate thickness further increased during subsequent six weeks of rest ($p < 0.0001$). Plate porosity also seemed to increase further, but there was no significant difference compared to internal healthy control joints. FK506 treated animals also had a thicker subchondral bone plate at six ($p < 0.0001$) and twelve ($p < 0.0001$) weeks compared to their internal healthy control joints. When longitudinal subchondral bone changes in OA joints of both groups were analyzed with generalized estimating equations, FK506 treated rats had thinner lateral subchondral bone plates compared to untreated controls ($p = 0.03$) (Figure 6C,G). FK506 rats did not develop subchondral plate porosity. This was significantly lower at six weeks ($p = 0.02$), but not at twelve weeks anymore (Figure 6D,H). After six weeks of treadmill exercise-mediated trabecular bone thickness ($p = 0.05$) and BV/TV ($p = 0.03$) was lower in FK506 treated animals compared to untreated controls (Figure 6E,F). Reduced trabecular thickness normalized during subsequent six weeks of rest, while the BV/TV ratio increased compared to untreated controls ($p = 0.02$).

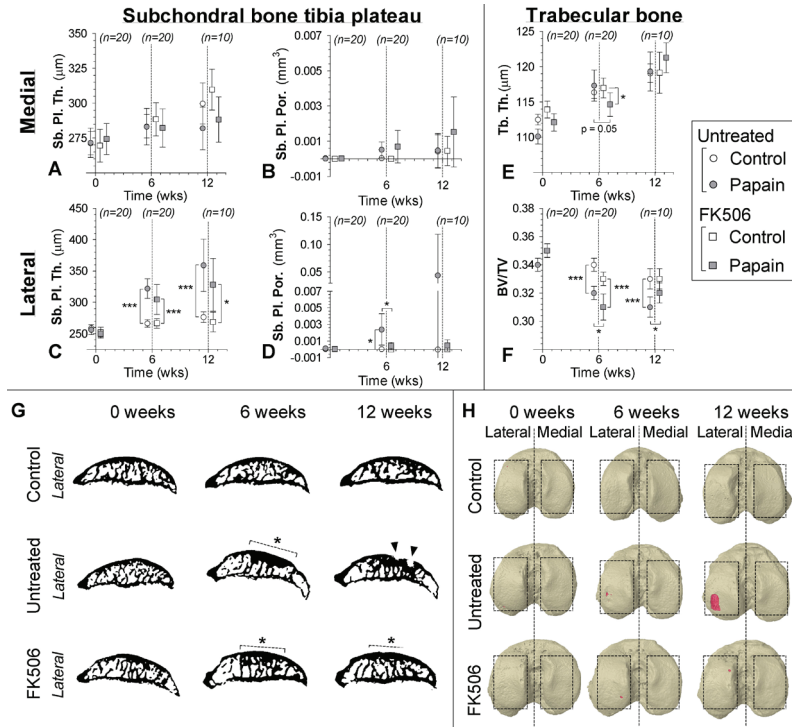


Figure 6: Subchondral bone changes analyzed with longitudinal in vivo μCT in untreated OA (circles) and FK506 treated (squares) animals. Subchondral plate thickness (Sb. Pl. Th.; A, C) and porosity (Sb. Pl. Por.; B, D) were measured in the medial (A,B) and lateral (C,D) compartment of the tibial epiphysis. Changes in trabecular thickness (Tb. Th.; E) and trabecular bone volume fraction (BV/TV; F) were measured in tibial epiphyseal bone marrow. Representative sagittal images from binary μCT scans (G) show pore development (indicated with \blacktriangle) and development of subchondral sclerosis (indicated with dashed line and $*$). Three-dimensional top views of the tibial plateau at different time points (H) show subchondral pore (red color) development. $*$: $p < 0.05$, $**$: $p < 0.01$, $***$: $p < 0.001$, error bars indicate 95% confidence intervals.

During six weeks of moderate running, FK506 treated animals formed less ectopic bone formation compared to untreated animals ($p = 0.007$) (Figure 7B,C). This difference in ectopic bone formation between FK506 treated animals and untreated controls was still measured after the subsequent six weeks of rest ($p = 0.04$) (Figure 7B,C).

Macrophage activation and osteophytes

Each animal received 54 ± 2 MBq of $^{111}\text{In-EC0800}$ under isoflurane anaesthesia. There were no significant differences of injected activity between experimental groups. After completion of the running protocol, both untreated and FK506 treated rats revealed similarly increased radioactive uptake in their papain injected knee joints compared to their internal healthy control joints (Figure 7A,C). After six subsequent weeks of rest, radioactive uptake in OA induced

joints of FK506 treated animals dropped to control levels. The absolute difference in radioactive uptake between OA induced and healthy control joints in FK506 treated animals was lower compared to the absolute differences measured in untreated controls (Figure 7A,C).

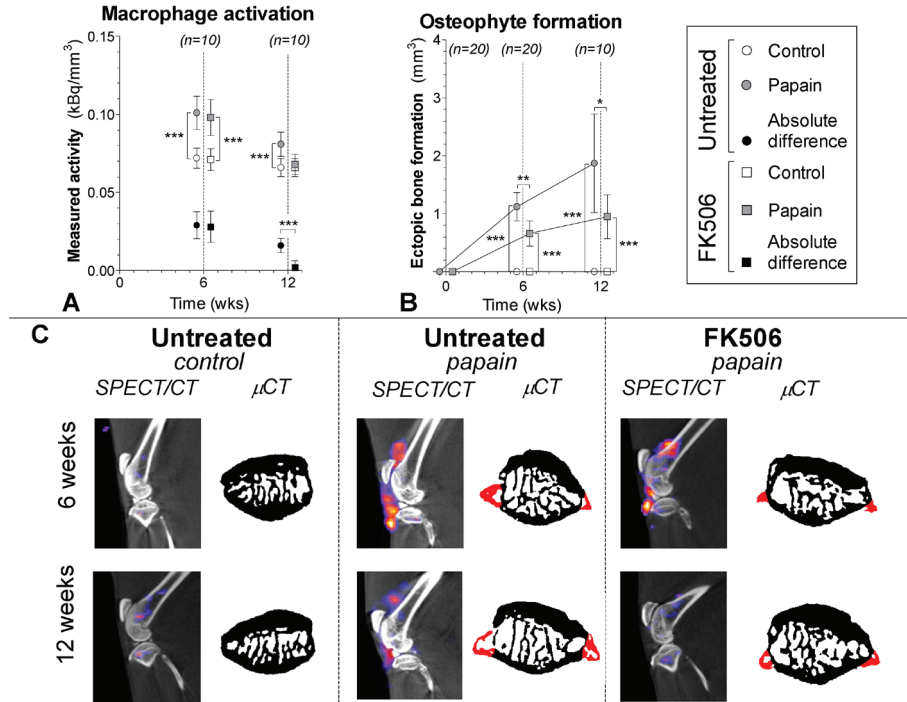


Figure 7: Macrophage activation determined in untreated OA animals (circles) and FK506 treated animals (squares) by injection of ¹¹¹In-EC0800 using SPECT/CT. A: Quantified radioactivity in healthy joints (blank boxes) and OA joints (gray boxes) normalized to the size of the analyzed cylindrical region of interest (kBq/mm³). Absolute differences per animal were calculated (kBq/mm³) to reduce inter-individual variation (black boxes). A high radioactivity is related to more macrophage activation. B: Ectopic bone formation (mm³) as a measure for osteophyte development was quantified on longitudinal bone μ CT scans. C: Sagittal SPECT/CT images of knee joints from representative animals. CT images shown in black and white were used for anatomical reference, the SPECT images are shown in color. Transaxial images from patellar bone extracted from binary μ CT images show ectopic bone formation (red color). *: $p < 0.05$, **: $p < 0.01$, ***: $p < 0.001$, error bars indicate 95% confidence intervals.

DISCUSSION

Osteoarthritis is characterized by a loss of cartilage matrix, because chondrocytes cannot maintain tissue homeostasis due to a disturbed balance between anabolic and catabolic activities. Inhibiting calcineurin activity with immunosuppressive agents like cyclosporin A²⁷² or FK506^{270, 271} increases the anabolic, while suppressing the catabolic, activity of osteoarthritic chondrocytes.

In this study, we found that both high and low concentrations of FK506 improved the COL2/COL1 ratio and COL9 expression in monolayer cultured human osteoarthritic chondrocytes (**Figure 2A**). Then, in 3D chondrocyte pellet cultures, FK506 clearly increased COL2 content, while no effect was seen on sGAG staining (**Figure 2C**). These data indicate that calcineurin inhibition through FK506 may protect the structural integrity of the ECM. Next, we studied the effects of low dose FK506 treatment in cartilage explants, in which the chondrocytes are still embedded in their native extracellular matrix. The explants were harvested from macroscopically 'healthy' cartilage areas of the degenerated side. However, on microscopic level there might be still big differences in grade of degeneration between explants of the same donor. To limit the effects of these differences, explants were first pooled before assigning them to a certain culture condition. Despite the large standard deviations, we found a clear trend towards stimulated anabolic but reduced catabolic activities after FK506 treatment (**Figure 2B**).

Finally, we evaluated whether FK506 also exerts similar favorable effects in a severe OA in vivo model with a different response in medial and lateral compartments of tibia plateau cartilage²⁷³. Six weeks of OA-like damage induction severely erodes lateral compartment cartilage and results in complete denudation of subchondral bone. Medial cartilage becomes sGAG-depleted with a slightly degraded ECM, a process that continued progressively during the course of the experiment (**Figure 4 and 5**). FK506 treatment in vivo did not increase sGAG levels nor did it protect against sGAG loss (**Figure 4A-B**). However, it did protect against structural matrix degradation (**Figure 4C**), which was in line with our in vitro results (**Figure 4**). Loss of lateral cartilage matrix could not be prevented with FK506 treatment (**Figure 4D**). Longitudinal μ CT analysis showed reduced sclerotic bone formation in the lateral compartment of FK506 treated animals (**Figure 6C**). Previous experiments with this severe OA model suggest that subchondral sclerosis might develop when cartilage is completely lost and subchondral bone is denuded²⁷³. In some FK506 treated animals we found focal regions of cartilage on the lateral tibia plateau that showed totally sGAG depleted but partially intact ECM. This suggest, that FK506 might have delayed lateral cartilage matrix degradation and thus reduced formation of subchondral sclerosis. However, calcineurin inhibition is also known to modulate bone turnover²⁸⁴ and therefore may have reduced sclerosis through direct modulation of osteoclast and osteoblast activity. CsA and FK506 have both been described to induce osteopenia through anti-anabolic effects on osteoblastic cells²⁸⁵ and to reduce bone formation through inhibition of osteoblast differentiation^{286, 287}. This could be another explanation for the reduced development of subchondral sclerosis in the lateral compartment, but has to be further investigated.

Another cell type that is modulated by FK506 are macrophages¹⁷⁸. We determined activated macrophages using ¹¹¹In-EC0800 and quantitative SPECT/CT (**Figure 7A**). During OA progression, macrophages become activated¹³¹ and their TGF β /BMP-2 production has previously been related to osteophyte development^{59, 60}. In our in vivo experiment, animals developed clear

osteophytes at the margins of the patella (**Figure 7B**). FK506 treatment reduced osteophyte development while the total amount of activated macrophages was equal after six weeks of follow up. This may suggest that FK506 treatment limits cytokine production by activated synovial macrophages and previous reports on calcineurin inhibition in macrophages showed reduced cytokine production²⁸⁸⁻²⁹⁰. FK506 may initially activate Toll-like receptors (TLR) pathways in activated macrophages, which can enhance NF κ B activity²⁹⁰ and stimulate expression of cytokines, like TNF α , IL1 α , IL1 β , IL12 and iNOS²⁸⁸. However, prolonged exposure to calcineurin inhibitors has been shown to also secondarily inactivate this TLR induced pro-inflammatory cytokine expression by negative feedback loops²⁸⁹. As such, continuous FK506 exposure may eventually suppress NF κ B pathways, but activate caspases 3 and 9 to enhance macrophage apoptosis²⁹⁰. Possibly, FK506 induced macrophage apoptosis may explain why radioactive folate uptake in our experiments was restored to levels comparable to healthy control joints (**Figure 7A**).

Osteoclasts are large multinucleated cells of the monocyte-macrophage hematopoietic lineage and are also influenced by FK506. During osteoclastogenesis macrophage colony-stimulating factor (M-CSF) and receptor activator of nuclear factor- κ B ligand (RANKL) stimulate precursor cells to acquire osteoclast characteristics²⁹¹. NFATc1 is an essential terminal differentiation factor of osteoclastogenesis and can be blocked in a dose-dependent fashion using CsA or FK506²⁹². CsA and FK506 treatment suppress RANKL stimulated osteoclastogenesis²⁹³⁻²⁹⁵, and especially inhibits late stages of the osteoclast life cycle²⁹⁶. By this mechanism Cn inhibition can diminish the activity of mature osteoclasts and reduce bone resorption²⁹⁷⁻²⁹⁹. FK506 mediated suppression of osteoclast maturation and subsequently hindered subchondral bone resorption may therefore explain why less subchondral pores were measured in FK506 animals.

Systemic FK506 treatment is known to induce toxic side effects³⁰⁰. Throughout the experiment our animals gained weight (**Figure 3**), and FK506 animals increased more in weight from 6 to 12 weeks of follow-up. However, this result could not clearly be related to side-effect of FK506, which usually results in a loss of weight. At the end of the twelve week experiment liver function (AST, ALT, alkaline phosphatase) and kidney function (creatinin and urea) were normal (**Figure 8**). Liver and kidney histology gave no indication that FK506 induced liver or kidney fibrosis (**Figure 8**). Despite these promising findings, systemic FK506 treatment cannot be translated towards clinical OA care directly. FK506 induced side effects are well described in patients after long term use and is unacceptable for a therapeutic strategy in human OA patients. To reduce long term use and is unacceptable for a therapeutic strategy in human OA patients. To reduce toxicity, local intra-articular treatment may be used, but repetitive intra-articular injections also increase the risk of iatrogenically arthritis and should be avoided. FK506-coupled biodegradable delivery systems might be able to prolong intra-articular FK506 exposure and sustain long term therapeutic action³⁰¹, hopefully without systemic adverse effects.

Laboratory tests on blood samples		Untreated OA control	FK506	p value
Liver	AST	54.13 ± 10.30	78.22 ± 61.08	p = 0.22
	ALT	86.75 ± 27.32	218.11 ± 277.30	p = 0.16
	Alkaline phosphatase	91.25 ± 14.08	87.78 ± 15.21	p = 0.71
	Albumin	35.88 ± 1.46	34.56 ± 1.94	p = 0.69
Kidney	Creatinin	16.00 ± 1.60	20.33 ± 4.18	p = 0.11
	Urea	5.69 ± 0.84	7.01 ± 0.89	p = 0.11

A

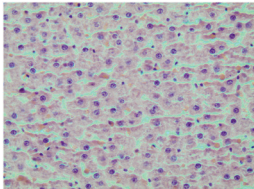
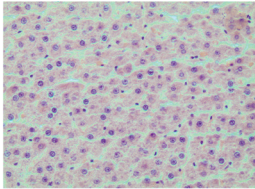
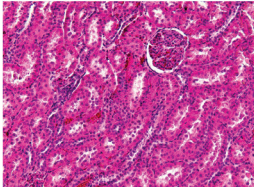
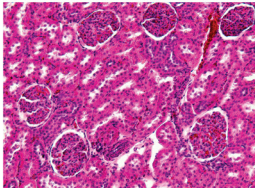
	Untreated control	FK506
B Liver		
C Kidney		

Figure 8: Toxicity analysis. Blood samples did not differ between experimental groups and gave no indication of liver or kidney toxicity (A). Liver (B) and kidney (C) histology showed no indication of FK506 induced toxicity.

Conclusion

Inhibition of calcineurin activity with FK506 stimulated anabolic activity, while reducing catabolic productivity of osteoarthritic human chondrocytes. Systemic treatment with FK506 in a rat model for severe osteoarthritis also protected against cartilage extra-cellular matrix degradation. Additionally, there was also less development of subchondral sclerosis, macrophage activation and osteophyte formation. Altogether, our data suggests that calcineurin inhibition with FK506 proves to be a promising candidate for therapeutic management of osteoarthritis.

ACKNOWLEDGEMENTS

We acknowledge the Dutch Arthritis Association and the Smart Mix Program of the Netherlands Ministry of Economic Affairs and the Netherlands Ministry of Education, culture and Science for their financial support.

CHAPTER 7

ALENDRONATE TREATMENT PROTECT AGAINST CARTILAGE MATRIX
DEGRADATION DURING SEVERE OSTEOARTHRITIS PROGRESSION

*M. Siebelt, J.H. Waarsing, H.C. Groen, C. Müller, S.J. Koelewijn, E. de Blois,
J.A.N. Verhaar, M. de Jong, H. Weinans
Bone. 2014Sep;66:163-70*

ABSTRACT

Introduction

Osteoarthritis (OA) is a non-rheumatoid joint disease characterized by progressive degeneration of extra-cellular cartilage matrix (ECM), enhanced subchondral bone remodeling, osteophyte formation and synovial thickening. Alendronate (ALN) is a potent inhibitor of osteoclastic bone resorption and results in reduced bone remodeling. This study investigated the effects of pre-emptive use of ALN on OA related osteoclastic subchondral bone resorption in an in vivo rat model for severe OA.

Methods

Using multi-modality imaging we measured effects of ALN treatment within cartilage and synovium. Severe osteoarthritis was induced in left rat knees using papain injections in combination with a moderate running protocol. Twenty rats were treated with subcutaneous ALN injections and compared to twenty untreated controls. Animals were longitudinally monitored for 12 weeks with in vivo μ CT to measure subchondral bone changes and SPECT/CT to determine synovial macrophage activation using a folate-based radiotracer. Articular cartilage was analyzed at 6 and 12 weeks with ex vivo contrast enhanced μ CT and histology to measure sulfated-glycosaminoglycan (sGAG) content and cartilage thickness.

Results

ALN treatment successfully inhibited subchondral bone remodeling. As a result we found less subchondral plate porosity and reduced osteophytosis. ALN treatment did not reduce subchondral sclerosis. However, after the OA induction phase, ALN treatment protected cartilage ECM from degradation and reduced synovial macrophage activation. Surprisingly, ALN treatment also improved sGAG content of tibia cartilage in healthy joints.

Conclusion

Our data was consistent with the hypothesis that osteoclastic bone resorption might play an important role in OA and may be a driving force for progression of the disease. However, our study suggest that this effect might not solely be effects on osteoclastic activity, since ALN treatment also influenced macrophage functioning. Additionally, ALN treatment and physical activity exercised a positive effect in healthy control joints, which increased cartilage sGAG content. More research on this topic might lead to novel insights as to improve cartilage quality.

INTRODUCTION

Osteoarthritis (OA) is characterized by articular cartilage degradation and has long been seen as primarily a cartilage disorder. However, nowadays OA is considered as a 'whole joint disease' and it is thought that pathological changes in one joint tissue might compromise structure and function of other joint tissues. Changes within the subchondral bone have been known for a long time to play a role within OA development¹⁷.

Within a healthy joint, the thin dome-like shaped subchondral plate is supported by vertical oriented trabeculae and plays an important role to evenly distribute forces from weight-bearing. Healthy subchondral bone protects cartilage from high peak stresses and possible matrix damage. Animal studies showed that during early OA there is a marked reduction in subchondral bone thickness^{26, 73} and there are increased numbers of subchondral pores^{44, 47}. On TRAP-stained histology sections, bone resorption and pore formation as a consequence of increased osteoclast activity³⁰², result in loss of integrity and plasticity at the osteochondral junction. This compromises its biomechanical function and could promote cartilage damage. Due to all the evidence that subchondral bone remodeling is involved in disease progression, bisphosphonates were suggested to be useful as an interesting intervention strategy to treat OA.

Alendronate (ALN), risedronate and zoledronate are all nitrogen-containing bisphosphonates and potent inhibitors of osteoclastic resorption used clinically for the treatment of osteoporosis³⁰³. Both alendronate and zoledronate have demonstrated positive results when used as an OA modifying agent in preclinical animal studies^{46, 304-307}. It is suggested that osteoclast-mediated resorption of mineralized cartilage at the subchondral bone-cartilage interface is an early initiating event in OA pathobiology and that only early bisphosphonates use after OA induction will result in the observed positive effect on cartilage health³⁰⁷. If in fact osteoclast activation during OA is time-dependent and reduces with ongoing OA stages, this might explain the disappointing results from large clinical trials on the role of bisphosphonates as treatment for OA. These trials included a very heterogeneous patient population, in which a large portion of patients had already severely progressed OA. Therefore, it is less likely that these patients benefit from osteoclast inhibition through bisphosphonates³⁰⁸⁻³¹³.

Late or progressive OA shows a different type of subchondral bone remodeling. Several animal studies showed that an initial thinning of the subchondral bone plate^{28, 314} is followed by a recovery phase leading to subsequent thickening of the subchondral plate due to enhanced osteoblast activity²⁷⁻²⁹. During this un-physiological high bone turnover in OA joints, there is an altered phenotypic expression of osteoblasts, which results in the production of sclerotic bone together with cyst formation and osteophyte development⁴⁴⁻⁴⁶. It has been hypothesized that as

a result of the functional coupling between osteoclasts and osteoblasts, increased osteoclastic bone resorption induces a rise in osteoblast activity leading to increased subchondral bone thickness and sclerosis³⁵. If true, bisphosphonate intervention to inhibit osteoclastic bone resorption might intervene with eventual formation of subchondral sclerosis by osteoblasts.

Recently, we established a novel rat OA model using a combination of papain injections with a running protocol which induces severe knee joint articular cartilage degradation together with activation of synovial macrophages and prominent involvement of subchondral bone²⁷³. In this particular study we found that papain injection alone induced moderate OA features, like sGAG and slight cartilage matrix loss, enhanced loss of the subchondral cortical plate. As a result of OA induction through papain injections and running, there was a complete different response and rats develop a pronounced sclerotic bone phenotype within the lateral compartment of the proximal tibia plateau combined with severe loss of cartilage matrix. In the current study, we investigated whether pre-emptive inhibition of osteoclast function through bisphosphonate treatment could prevent the development bone sclerosis, and possibly could prevent or reduce the development of OA. We used longitudinal *in vivo* microCT scans to measure effects of ALN treatment on subchondral sclerosis development and *ex vivo* microCT on cartilage samples to see if cartilage was protected against degradation. Besides marked changes of articular cartilage and subchondral bone in this model for OA, we know there is also abundant activation of synovial macrophages²⁷³. Therefore, we also measured whether ALN treatment had an effect on synovial macrophage activation using a folate-based radiotracer for *in vivo* SPECT/CT imaging³¹⁵.

METHODS

Effect of systemic alendronate treatment on severe osteoarthritis progression

Forty 16-week-old male Wistar rats (Charles River Netherlands BV, Maastricht, the Netherlands) were housed in the animal facility of the Erasmus University Medical Centre, with a 12-h light-dark regimen, at 21°C during the experimental period, and received standard food pellets and water *ad libitum*. Severe osteoarthritis was induced in all animals using intra-articular papain injections in their left knee joints combined with exposure to a moderate exercise protocol as described before²⁷³. In short, all animals received three intra-articular injections in their left knee joints with 30µl papain/L-cystein solution⁸¹. Their right knee joint served as an internal healthy control. All rats were forced to run on a motorized rodent treadmill (LE-8700; Panlab Harvard Apparatus, Barcelona, Spain) 500m/day during 5 days/week, for six weeks covering a distance of 15km in total²⁷³.

Animals were divided over two groups: twenty rats served as untreated controls and twenty rats were treated during the experiment with three times weekly subcutaneous ALN injections (2.4µg/kg) (alendronate, Sigma-Aldrich, St. Louis, MO, USA) to inhibit osteoclast bone resorption,

a dose previously reported to be comparable to the clinical dose of 10 mg/day prescribed for the treatment of postmenopausal osteoporosis³¹⁶ (Figure 1). Sterile water was used as the vehicle for dissolving ALN. Untreated animals did not receive placebo injections.

During the study all animals were longitudinally monitored with microCT to measure subchondral bone changes. At six and twelve weeks, ten rats in both groups were selected for a full analysis sequence. This sequence consisted of a SPECT/CT using a folate-based radiotracer to quantify macrophage activation *in vivo*³¹⁶, and *ex vivo* EPIC- μ CT and histology to measure cartilage quality¹¹³. For all procedures, the exact same procedures were followed as described earlier²⁷³. The animal ethic committee of the Erasmus University Medical Center, Rotterdam, the Netherlands, approved all conducted procedures. A detailed planning scheme of all groups and conducted tests is given in Figure 1.

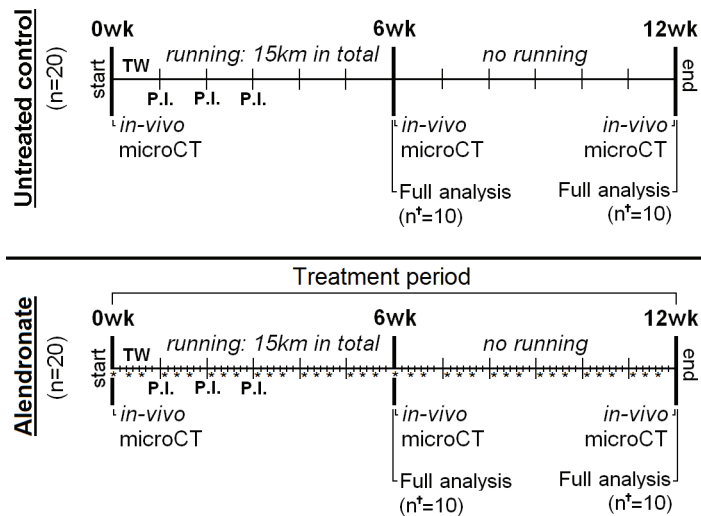


Figure 1: Experiment design indicating analytical time points and methods for each experimental group. Forty 16-week-old male Wistar rats were injected with three papain intra-articular injections (P.I.) and forced to run 15km on a motorized treadmill. Animals were divided over two different groups: an untreated group (n=20) and a group treated with alendronate (n=20). Treated animals received subcutaneous alendronate injections (2.4 μ g/kg), indicated with * in the scheme. During the experiment three longitudinal microCT scans were made to measure subchondral bone changes. At six and twelve weeks a full analysis sequence was done in ten animals per group (n†), consisting of *in vivo*: determination of activated macrophages using SPECT/CT, and *ex vivo*: cartilage analysis with equilibrium partitioning of an ionic contrast agent using (EPIC-)microCT and histology.

Subchondral bone measurements on μ CT scans

Both knees of all animals were μ CT scanned under isoflurane anesthesia, using a Skyscan 1176 *in vivo* μ CT scanner (Skyscan, Kontich, Belgium). 10 min of scan time was required per

knee at an isotropic voxel size of 18 μ m, at a voltage of 65kV, a current of 385mA, field of view of 35mm, using a 1.0mm aluminum filter, over 198 $^\circ$ with a 0.5 $^\circ$ rotation step, and a 270 msec exposure time. All datasets were segmented with a local threshold algorithm¹⁴¹. Cortical and trabecular bone were automatically separated using in-house software²⁸². Using Skyscan software, both subchondral plate thickness (Sb. Pl. Th. in μ m) and subchondral plate porosity (Sb. Pl. Por. in mm^3) of the medial and lateral compartment of the tibial plateau were measured³⁵. In the tibial epiphysis, the trabecular thickness (Tb. Th. in μ m) and trabecular bone volume fraction (BV/TV), representing the ratio of trabecular bone volume (BV, in mm^3) to endocortical tissue volume (TV, in mm^3). We additionally quantified the amount of ectopic bone formation as a measure for osteophyte growth (mm^3) on longitudinal μ CT scans.

Determination of activated macrophages by SPECT/CT using 111In-EC0800

Activated macrophages express the folate receptor- β allowing monitoring macrophages in vivo using folate-based radiotracers^{130, 163, 164}. Phosphate saline-buffered (PBS, pH 6.5) DOTA-Bz-folate (EC0800, kindly provided by Endocyte Inc., West Lafayette, USA)²⁸³ was labeled with 111InCl₃ (Covidien, Petten, The Netherlands) as described previously²⁷³. Quality control was performed with ITLC-SG and revealed a radiochemical yield of >95% at a specific activity of 50 MBq/ μ g. 111In-EC0800 (55 MBq) was administered via the tail vein 20h prior to scanning. SPECT/CT scans were performed with a 4-head multiplex multi-pinhole small-animal SPECT/CT camera (NanoSPECT/CTTM, Bioscan Inc., Washington DC, USA). All knee joints were scanned with both helical μ CT (acquisition time 5min) and SPECT (acquisition time 30min). All scans were analyzed using InVivoScope post-processing software (Bioscan Inc.). To reduce inter-individual variation, the absolute difference in measured radioactivity (kBq/ mm^3) of the OA knee joint compared to the contralateral control joint was calculated. This absolute difference was used when comparing mean values of untreated animals with ALN treated animals.

Cartilage evaluation with contrast enhanced μ CT and histology

Equilibrium partitioning of a contrast agent using microCT (EPIC- μ CT) has a strong correlation with cartilage sulfated-glycosaminoglycan (sGAG) content¹¹³. In EPIC- μ CT an equilibrium-state exists between sGAG and contrast agent after a 24 hour incubation period. Resulting cartilage X-ray attenuation in these scans is inversely related to sGAG content and thereby represent cartilage quality. This technique is suited for quantitative analysis of cartilage degradation for preclinical evaluation of OA¹¹⁷.

Animals were euthanized directly after the last SPECT/CT scan and both knee joints were harvested for EPIC- μ CT analysis. All specimens were incubated in 40% solution of ioxaglate for 24h at room temperature¹³⁸. EPIC- μ CT was performed on the same μ CT scanner, using the following scan settings: isotropic voxel size of 18 μ m, a voltage of 65kV, a current of 385mA, field of view 35mm, a 0.5 mm aluminum filter, 198 $^\circ$ with a 0.5 degree rotation step, and a

235ms exposure time. In all EPIC- μ CT datasets, X-ray attenuation (arbitrary gray values related to sGAG content) and cartilage thickness (μm) was calculated for cartilage of the medial and lateral plateau of the tibia²⁷³.

After EPIC- μ CT, the separated parts of the knee joints were fixed in paraformaldehyde, decalcified with formic acid and embedded in paraffin. Sagittal sections were made at 300 μm intervals and stained with Safranin-O to image the amount and distribution of the GAGs. Sections were stained all at once, to minimize protocol differences between different samples.

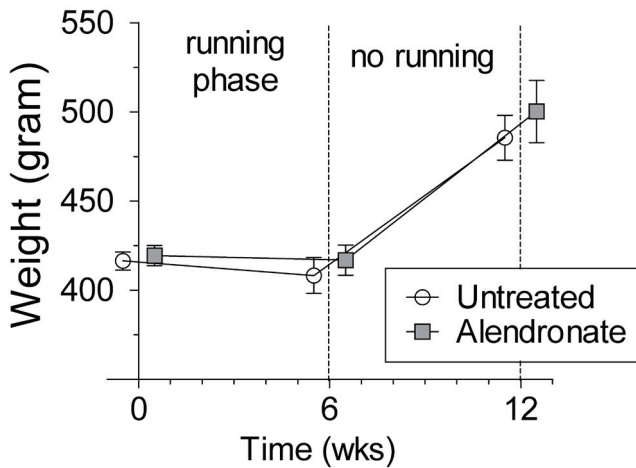


Figure 2: Increase of bodyweight (gram) of untreated control rats (white circles) and alendronate treated rats (gray squares).

Statistical analysis

All measurements were consistent with a normal distribution according to D'Agostino and Pearson omnibus normality tests. Differences between means of OA induced and healthy knee joints within the same animal were tested using paired t-tests at each time point for all outcome parameters (GraphPad Software, San Diego, California, USA). When comparing differences between means of untreated OA animals and ALN treated OA animals, an unpaired t-test was used at each time point for all outcome parameters (GraphPad Prism Software). When osteophytes and subchondral pores do not develop, this was scored as zero. Therefore, we used a one-sample t-test and tested whether the outcome of OA induced joints differed from zero (GraphPad Software). Longitudinal data from in vivo μ CT were additionally analyzed using generalized estimating equations (GEE) (SPSS Inc., Chicago, USA). For all tests, p values ≤ 0.05 were considered significant.

RESULTS

Effects of systemic alendronate treatment

All untreated (non-alendronate) rats did not increase in weight from 416.4g (411.3 – 421.5g) to 408.3g (398.2 – 418.3g) after six weeks of treadmill running. During subsequent six weeks of rest, all untreated rats increased in bodyweight to 485.5g (473.0 – 498.0g). ALN treated animals showed the same patterns, with no increase in weight during the first six weeks, from 419.4g at the start of the experiment (413.8 – 425.0g) to 416.9g (408.4 – 425.4g), and an increase in weight to 500.2g at twelve weeks (483.9 – 516.5g) (Figure 2).

Subchondral bone changes

During the experiment, healthy knee joints of untreated animals showed increased subchondral trabecular thickness ($p < 0.001$) and decreased BV/TV ($p < 0.001$) (Figure 3A-B). Due to OA induction there was a reduction in BV/TV ($p < 0.001$) compared to the contralateral healthy knee joint in untreated animals, while trabecular thickness was not different from the healthy control ($p = 0.29$). Both healthy and OA joints of ALN treated animals showed a reduced increase of trabecular thickness during the 6 weeks running and subsequent period to 12 weeks ($p < 0.001$) and higher BV/TV ($p < 0.001$) compared to untreated animals at 12 weeks but not at 6 weeks (Figure 3A-B).

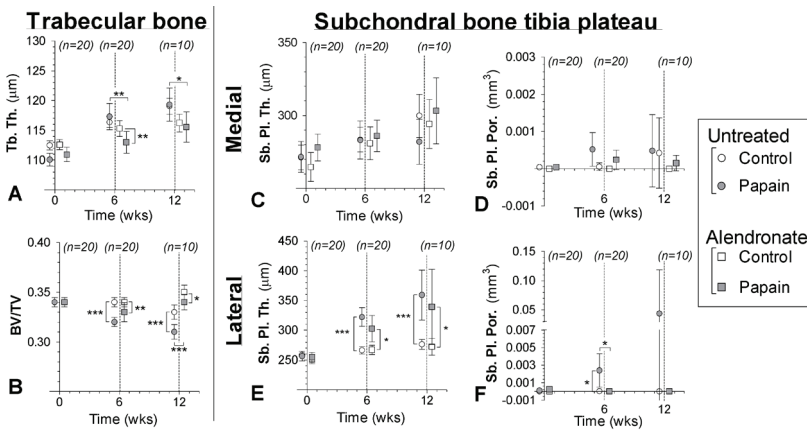


Figure 3: Subchondral bone changes analyzed with longitudinal in vivo μCT in untreated animals (circles) and alendronate treated animals (squares). Changes in trabecular thickness (Tb. Th.; A) and trabecular bone volume fraction (BV/TV; B) were measured in tibial epiphysis bone marrow. Subchondral plate thickness (Sb. Pl. Th.; C, E) and porosity (Sb. Pl. Por.; D, F) were measured in the medial (C,D) and lateral (E,F) compartment of the tibial epiphysis. *: $p < 0.05$, **: $p < 0.01$, ***: $p < 0.001$, error bars indicate 95% confidence intervals.

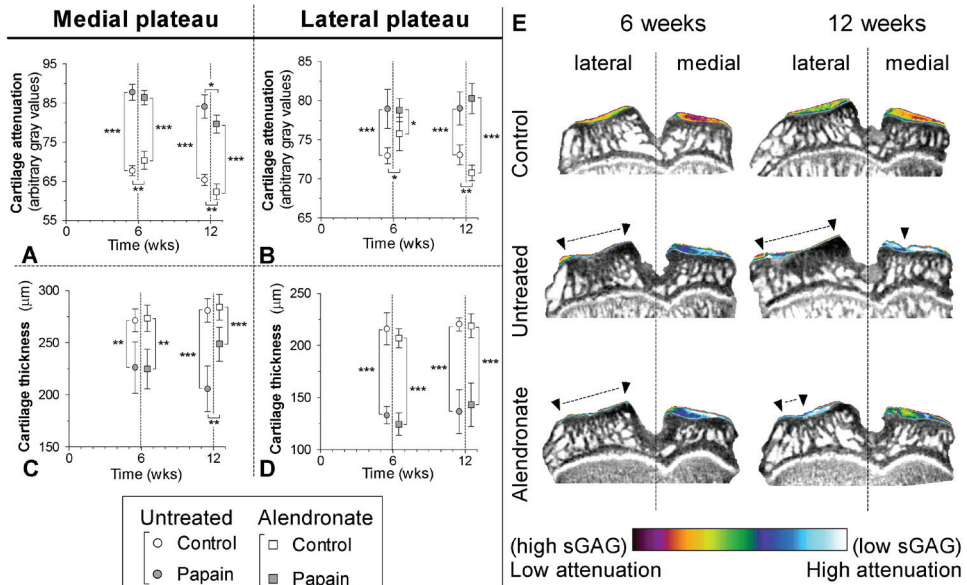


Figure 4: Cartilage quality and quantity was determined from samples of untreated (circles) and alendronate treated (squares) rats with equilibrium partitioning of a ionic contrast agent using (EPIC-) μCT (A-D). The amount of sulphated-glycosaminoglycans (sGAG) (arbitrary gray values; A,B) and cartilage thickness (μm ; C,D) were measured of medial (A,C) and lateral (B,D) cartilage compartments of the tibia plateau harvested from healthy joints (blank boxes) and OA induced joints (gray boxes). Attenuation values from EPIC- μCT scans are inversely related to the sGAG content, meaning that a high attenuation corresponds to low sGAG content. (E) Coronal images from representative EPIC- μCT scans of the tibia plateau show the amount of cartilage (erosions indicated with \blacktriangle and dashed lines) and sGAG content (displayed in color). * $p < 0.05$, ** $p < 0.01$, *** $p < 0.001$, error bars indicate 95% confidence intervals.

GEE analysis of medial subchondral plate thickness of untreated animals showed that the subchondral bone plate of OA joints increased less in thickness compared to healthy joints ($p = 0.008$), where in ALN treated animals there was no difference between healthy and OA joints ($p = 0.26$) (Figure 3C). However, there was no significant difference in medial subchondral plate thickness of OA joints between untreated and ALN treated animals ($p = 0.12$). There was also no increased porosity of the medial subchondral bone plate for untreated and ALN treated rats.

At the lateral side after six weeks of running subchondral sclerosis developed in the OA joints of untreated animals compared to its contralateral healthy knee joint ($p < 0.0001$), which persisted after six weeks of rest ($p < 0.0001$) (Figure 3E). In ALN treated animals sclerosis did also develop in OA induced joints. GEE analysis between OA joints of untreated and ALN treated animals did not find a significant difference in the development of subchondral sclerosis ($p = 0.12$) (Figure 3E).

ALN treated animals totally lacked subchondral plate porosity at 6 weeks ($p = 0.02$) (**Figure 3F**). At twelve weeks, this effect was however not significant anymore ($p = 0.24$). This was predominantly due to the rather large variation in subchondral porosity in untreated animals. This variation resulted from the reduction in number of animals at 12 weeks and some of them not showing any porosity.

Osteoarthritic changes of articular cartilage

OA induction in untreated animals induced severe sGAG depletion from both medial and lateral cartilage compartments of the tibia plateau. This sGAG depleted state persisted throughout the experiment (**Figure 4A**). Although there was significant sGAG loss in OA joints of ALN treated rats compared to their healthy joints at both six ($p < 0.0001$) and twelve weeks ($p < 0.0001$), ALN treated animals had more sGAG in cartilage of the medial plateau at twelve weeks compared to OA joints of untreated rats ($p = 0.02$) (**Figure 4A**). After the running protocol at six weeks, cartilage of the medial compartment was reduced in thickness compared to healthy knee joints in untreated rats ($p = 0.007$) and ALN treated rats ($p = 0.003$) (**Figure 4C**). Compared to healthy joints this matrix degradation persisted during the following six weeks of rest in untreated rats ($p = 0.0005$). However, medial cartilage thickness of OA joints in ALN treated animals was thicker compared to OA joints of untreated animals ($p = 0.003$) (**Figure 4C**). Lateral cartilage thickness was degraded (**Figure 4D**) and resulted in almost completely denuded subchondral bone (**Figure 4E**) in both untreated and ALN treated animals. Representative medial and lateral cartilage images from safranin-O stained histology from untreated OA controls at six and twelve weeks are shown in **Figure 5**.

Interestingly, after the six week running phase in both medial ($p = 0.03$) and lateral ($p = 0.01$) cartilage of healthy joints in ALN treated animals, there was a reduced sGAG content compared to healthy cartilage of untreated animals (**Figure 4A-B**). During the next six weeks of rest, untreated animals showed a ~3% improvement in sGAG content of medial tibia cartilage and 0.1% of the lateral tibia cartilage. Interestingly, after these six weeks of rest, the medial tibia cartilage improved ~13% and the lateral tibia cartilage ~7% in ALN treated animals and was significantly higher in both the medial ($p = 0.01$) and lateral cartilages ($p = 0.005$) compared to untreated animals (**Figure 4A-B**).

In **Figure 4E** representative images from EPIC- μ CT scans are depicted. These Figures clearly show the loss of sGAG from the articular cartilage due to the OA induction, as well as the loss of cartilage matrix on the lateral tibia plateau. At twelve weeks, ALN treated animals show less irregularity of medial tibia plateau cartilage matrix, which is also thicker compared to untreated animals.

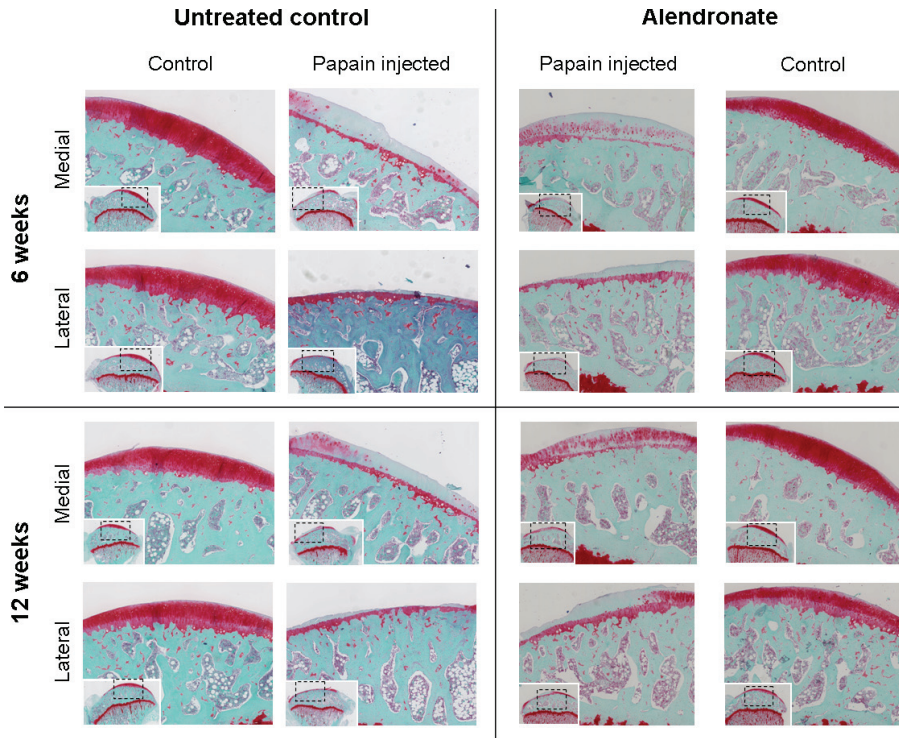


Figure 5: Safranin-O stained histology sections of medial and lateral tibial plateau cartilage after six weeks and twelve weeks of follow up. Untreated animals show severely sulphated-glycosaminoglycan (sGAG) depleted medial tibia cartilage at six and twelve weeks. Cartilage extra-cellular matrix (ECM) was slightly degraded at six weeks, but progressive loss of cartilage ECM was found at twelve weeks. ALN treated animals showed a similar loss of sGAG and loss of ECM at six weeks, however, after twelve weeks more sGAG was present and the ECM was less degraded compared to untreated animals. In both untreated and ALN treated animals, lateral cartilage ECM was almost totally eroded with only the calcified cartilage layer that remained.

Effect of systemic alendronate treatment on synovial macrophage activation

At both 6 weeks and 12 weeks each animal received 55 ± 5 MBq of $^{111}\text{In-EC0800}$ with no significant differences of injected activity between experimental groups. At six weeks, untreated rats (~40%) and ALN treated rats (~28%) had increased radioactive uptake in their OA-induced knee joints compared to their contralateral healthy control joints (Figure 6A,C). However, a comparison between both groups showed no significant difference in radioactive uptake. During this period of moderate running, ALN treated animals formed less mineralized osteophyte formation compared to untreated animals, but this effect was not significantly different ($p = 0.07$) (Figure 6B,C).

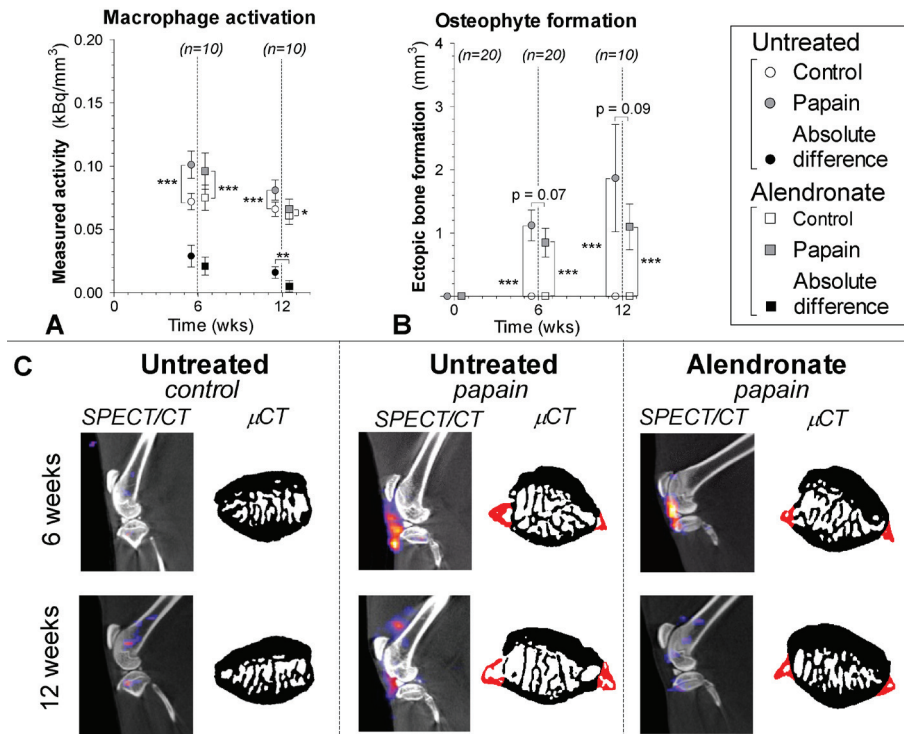


Figure 6: Macrophage activation determined in untreated animals (circles) and alendronate treated animals (squares) after injection of ¹¹¹In-EC0800 using SPECT/CT. A: Quantitative outcome of measured radioactivity in the healthy joints (blank boxes) and OA joints (gray boxes) normalized to the size of the analyzed cylindrical region of interest (kBq/mm³). Absolute differences per animal were calculated (kBq/mm³) to correct for differences in biodistribution of ¹¹¹In-EC0800 (black boxes). A high radioactivity is related to more macrophage activation. B: Ectopic bone formation (mm³) as a measure for osteophyte development was quantified on longitudinal bone μ CT scans. C: Sagittal SPECT/CT images of knee joints from representative animals. CT images shown in black and white were used for anatomical reference, the SPECT images are shown in color. Micro-SPECT images show radioactivity accumulation, one fixed threshold used for all images. Transaxial images from patellar bone extracted from binary μ CT images show ectopic bone formation (red color). *: $p < 0.05$, **: $p < 0.01$, ***: $p < 0.001$, error bars indicate 95% confidence intervals.

After six subsequent weeks of rest untreated animals still had ~23% increased radioactivity uptake in their OA-induced knee joints. In ALN treated animals this amount dropped to an ~8% increase, however it was still significantly more compared to their healthy control joint ($p = 0.02$). The absolute difference in radioactive uptake between OA induced and healthy control joints in ALN treated animals was lower compared to the absolute differences measured in untreated controls ($p = 0.003$) (Figure 6A,C). At twelve weeks there was again a tendency of reduced osteophyte formation in ALN treated animals as compared to untreated controls, but again these data were not significantly different ($p = 0.09$) (Figure 6B,C). However, GEE

analysis showed that during the entire experiment, ALN treated animals developed significantly less ectopic bone formation compared to untreated controls ($p = 0.008$).

DISCUSSION

Inhibiting osteoclastic bone resorption through bisphosphonate treatment has shown beneficial effects in pre-clinical animal OA studies, but these reporting studies made use of OA models that are relatively mild in nature^{46, 306, 307}. Osteoclast activation is suggested to be time-dependent and reduces with ongoing OA stages, and might explain the disappointing results from large clinical trials on the role of bisphosphonates as treatment for OA³⁰⁸⁻³¹³. In this study we investigated whether a preemptive start of alendronate could reduce the severe OA progression known to develop after papain injections combined with moderate running exercise²⁷³.

This study demonstrates that healthy knee joints of untreated (but running) animals showed ~5% subchondral bone loss while trabecular thickness increased ~5%. This has previously been described to occur during normal bone remodeling as a consequence of aging and increased physical activity³¹⁷. OA induced knee joints of untreated animals showed an enhanced loss of BV/TV, which can be related to increased trabecular bone remodeling in OA joints of rodents²⁹. In contrast to untreated animals, our results show that ALN treatment resulted in functional impaired bone remodeling in both healthy and OA knee joints, which can be related to inhibited osteoclast bone resorption³¹⁶. It has been suggested that a functional coupling between osteoclasts and osteoblasts eventually induces subchondral sclerosis³⁵, but ALN treatment in our study did not reduce subchondral sclerosis formation (**Figure 3**). This suggests that a direct influence of osteoclastic function on the formation of subchondral sclerosis is rather unlikely.

This sclerotic bone phenotype only developed at sites where there was a total loss of articular cartilage. Due to this loss of cartilage, force dissipation through the subchondral bone must have changed severely. We hypothesize that subsequent increased mechanical stimuli within the underlying subchondral bone, might have triggered the mechanosensory response of osteocytes³¹⁸ and subsequently induced sclerosis. In OA patients osteocytes become more elongated³¹⁹ and produce less sclerostin³²⁰. Sclerostin is known for its anti-anabolic effect on osteoblasts through an antagonist function on the Wnt signaling pathway. Normally, Wnt signaling induces osteoblast maturation and prevents osteoblast apoptosis, which subsequently stimulates bone formation³²¹. When sclerostin production by osteocytes is reduced, Wnt is promoted and osteoblasts are stimulated to form bone, which in this case, might result in increased or sclerotic bone formation. No direct evidence for this specific relation was found in this study, and validation of such a theory would require more research.

ALN treatment did not prevent the deleterious erosion of lateral tibia cartilage. However, medial compartment cartilage was protected from further degradation of cartilage extra-cellular matrix due to ALN treatment. This suggests that in this model, osteoclastic activity somehow fuels an ongoing process of cartilage degradation. Besides this protective effect on cartilage matrix in OA induced joints, ALN treatment improved sGAG content in healthy joints of treated animals. Our results do not explain why ALN has this effect on cartilage. However, one hypothesis could be that through inhibition of osteoclast bone resorption by ALN, the supportive function of subchondral bone is not reduced and remains stiff during running exercise. As a consequence, chondrocytes are exposed to increased mechanical stress and produce less sGAG⁸⁴. However when stress levels are relieved in the period between 6 and 12 weeks, chondrocytes recover and increase sGAG production. Possibly due to the stiffer subchondral cortical bone plate and higher stress levels, chondrocytes in ALN treated animals produced more sGAG to further enhance cartilage quality. The effects of training on cartilage are already well known in clinical patient care¹⁸³, possibly this effect might be enhanced with pre-emptive ALN treatment. However, more research is necessary to establish a relationship between osteoclast activity, chondrocyte sGAG production, and the role of biomechanical impact due to physical exercise.

Analysis of macrophage activation using folate receptor targeted SPECT/CT also showed interesting results. After six weeks of OA induction both groups showed no difference in macrophage activation, however, after 12 weeks macrophage activation was significantly reduced in ALN treated animals compared to untreated animals. Recently, bisphosphonates have been reported to significantly reduce pain in patients with clinical and radiographic knee osteoarthritis³²². Synovitis and activation of synovial macrophages are related to patient complaints, like joint dysfunction and pain¹⁵⁹, and has been related to the progression of cartilage erosion^{323, 324}. Possibly, a loss of macrophage activation in ALN treated animals reflected the reduced amount of articular cartilage degradation. But, bisphosphonates are known to influence macrophage responses as well²⁵ and ALN treatment could directly have reduced macrophage activation. Then again, the finding that pre-emptive use of ALN did not reduce macrophage activation after six weeks does not support this explanation.

Although we found some promising results in this study, it is important to point out that using animal models for OA research does not allow for direct translation towards clinical care. There are simply too many factors related to the study design that might have a distinct influence on experimental outcome (for example, species, strain, age). Additionally, this study has two major limitations. First, we did not use a saline injection as a control in untreated animals. Hypothetically, handling of animals during subcutaneous injections might have caused some form of stress that might have caused a bias in our study. And second, we lacked a pure control without exercise and without OA induction, this may cause a bias in our study. From a biological point of view, it is known that skeletal growth in rats is related to changing cartilage

matrix biology and phenotypic characteristics of chondrocytes^{180, 181}. And from a biomechanical point of view, the way rats run can never be compared to the way humans do. In light of biomechanics, pain is also an important aspect that is likely to have influenced our outcome. Rats that suffer pain from OA induction are known to change their weight-bearing behavior⁷⁷. Unfortunately, we were not able to record their discomfort using an incapacitance test or pain measurement. Therefore, we are unable to discuss to what extent pain might have influenced our outcome.

Conclusion

Reduced subchondral bone loss and reduced osteophyte formation was found after OA induction in ALN treated compared to non-ALN treated rats. ALN treatment also reduced cartilage degradation and suggests that osteoclastic activity is a driving force behind ongoing OA articular cartilage degradation. However, this effect might not be solely due to osteoclastic activity, since the results of our study showed clear interaction of ALN treatment in macrophage activation. Furthermore, ALN treatment during moderate exercise influenced sGAG production in healthy cartilage and after a period of rest, resulted in increased cartilage sGAG content. More studies on the mechanisms of ALN treatment in healthy joints together with physical exercise training could provide more insight and potentially lead to new treatment strategies that can improve cartilage quality.

ROLE OF FUNDING SOURCE

Sources of funding are Dutch Arthritis Association (LLP 11) and the Smart Mix Program of the Netherlands Ministry of Economic Affairs and the Netherlands Ministry of Education, culture and Science. The funding sources had no role in the study design, collection, analysis or interpretation of data; in the writing of the manuscript or in the decision to submit the manuscript for publication.

CHAPTER 8

TRIAMCINOLONE ACETONIDE ACTIVATES AN ANTI-INFLAMMATORY
AND FOLATE RECEPTOR POSITIVE MACROPHAGE THAT PREVENTS
OSTEOPHYTOSIS IN VIVO

*M. Siebelt, N.M. Korthagen, W. Wei, H.C. Groen, Y.M. Bastiaansen-Jenniskens,
C. Müller, J.H. Waarsing, M. de Jong, H. Weinans.*

Submitted

ABSTRACT

Introduction

Triamcinolone acetonide (TA) is commonly used in osteoarthritis management to reduce pain. Possibly, TA limits cartilage degradation and osteophyte formation. Interestingly, macrophage activation is strongly associated with osteophyte formation during osteoarthritis progression. This study investigated the effect of TA injections on *in vivo* macrophage activation, which was related to osteophyte development and joint degeneration. The mechanism through which TA exerts this effect could be explained from *in vitro* macrophage differentiation experiments.

Methods

Osteoarthritis was induced in rat knees using papain injections and a running protocol. Untreated and TA treated animals were longitudinally monitored for 12 weeks with *in vivo* μ CT to measure subchondral bone changes. Synovial macrophage activation was measured *in vivo* using folate receptor β (FR β) targeted SPECT/CT. Articular cartilage was analysed at 6 and 12 weeks with *ex vivo* contrast enhanced μ CT and histology. Effects of TA on macrophages were also studied *in vitro* through fluorescence-activated cell sorting for CD163 and FR β expression, and mRNA expression of IL10.

Results

In contrast to untreated control animals, intra-articular injections with TA strongly enhanced FR β + macrophage activation and fully prevented osteophyte formation. There were no beneficial effects of TA against cartilage degradation or subchondral bone sclerosis. In *in vitro* cultures, TA strongly induced monocytes differentiation CD163+ and FR β + macrophages. Addition of TA to M-CSF stimulated M2 macrophages showed enhanced IL10 expression on mRNA level.

Conclusion

TA injections potently induce a CD163+ and FR β + subtype of activated macrophage with anti-inflammatory characteristics, like reduced IL10 production *in vitro* and lack of osteophytosis *in vivo*.

INTRODUCTION

Osteoarthritis (OA) is characterized by deterioration of articular cartilage and extensive subchondral bone remodeling^{326, 327}, but there is also an inflammation within the synovial lining of the osteoarthritic joint¹⁵⁹. During OA progression, synovial macrophages become activated and secrete many pro-inflammatory cytokines and growth factors. These cytokines and growth factors are thought to detrimentally change the articular joint.

First, activated synovial macrophages have been proposed to enhance transforming growth factor beta (TGF β) production. Due to TGF β , synoviocytes increase their production of bone morphogenetic protein (BMP) 2 and BMP4, as a consequence, osteophytes develop within the OA joint^{59, 60}. Secondly, it is thought that enhanced growth factors and cytokines production by activated macrophages facilitates cartilage extra-cellular matrix (ECM) degradation, contributes to synovial fibrosis³²⁸, and induces pain³²⁹. The latter is of special interest, since pain management plays a pivotal role in clinical management of OA.

Pain management for OA patients can be achieved through analgesia like paracetamol or non-steroid anti-inflammatory drugs (NSAIDs), or with intra-articular injection of corticosteroids. Intra-articular injections with corticosteroids provide excellent results against OA related pain³³⁰, and is an advocated treatment for individuals suffering knee OA³³¹. More specific, triamcinolone acetonide (TA) injections are even more effective in pain reduction compared to other corticosteroids³³².

In 1985 Williams et al reported that TA quite effectively protects against osteophyte development in a pre-clinical model for OA³³³. This finding suggests that TA somehow intervenes with synovial macrophage activation and might prevent subsequent TGF β induced osteophyte development. More recently in 2014, this finding was reproduced in a post-traumatic model of OA using intra-articular injections of dexamethasone³³⁴. These authors additionally showed that corticosteroid therapy reduced cartilage destruction. It remains unclear through which mechanisms corticosteroids exert this positive effect on macrophages and other joint tissues within the joint during OA development. This effect might result from the marked influence of corticosteroids on macrophage differentiation.

Inactive macrophages are able to differentiate into different active subtypes. First, the classically (or M1) activated macrophages are activated through a cell-mediated immune response. Especially interferon- γ (IFN γ), lipopolysaccharides (LPS), or tumour-necrosis factor (TNF) are known inducers of M1 macrophages^{335, 336}. Alternatively (or M2) activated are macrophages related to humoral immunity tissue repair³³⁷. Interleukin (IL) 4 is known to induce a wound healing M2 activated macrophage whose activity is related to tissue repair³³⁸. Interestingly, in

response to corticosteroids yet another activated macrophage subtype develops, known as regulatory macrophages³³⁹. Regulatory macrophages are considered anti-inflammatory and produce large amounts of IL10³⁴⁰. Possibly, intra-articular injection of TA polarizes macrophage activations towards this M2b phenotype with subsequent beneficial effects on osteophyte formation and cartilage degradation.

Recently, we established an *in vivo* model for severe OA that shows severe degradation of articular cartilage, enhanced subchondral bone sclerosis formation, and pronounced osteophyte formation²⁷³. Using folate receptor (FR) β targeted single photon emission computed tomography (SPECT/CT) to quantitatively measure macrophage activation^{130, 164}, we also found abundant activation of synovial macrophages within knee joints of this rat model for OA²⁷³. In this rat model for severe OA, we investigated the *in vivo* effect of intra-articular TA injections on macrophage activation using FR β targeted SPECT/CT. We hypothesized that intra-articular treatment with TA reduces the amount of macrophage activation, and therefore diminishes osteophyte formation as described by Williams et al³³³. Furthermore, using longitudinally applied μ CT for *in vivo* bone analysis and *ex vivo* equilibrium partitioning of a contrast agent using μ CT (EPIC- μ CT), we also analyzed whether intra-articular TA injections might have a beneficial effect on OA related subchondral sclerosis and cartilage degradation as well. In order to explain our *in vivo* results, we performed several *in vitro* experiments. In these experiments, we characterized M1 and M2 differentiated macrophages by their cell-surface receptor expression. We analyzed whether the addition of TA was able to polarize macrophages towards a certain subtype, and whether TA influenced FR β expression.

METHODS

Effects of intra-articular injections of triamcinolone on severe osteoarthritis progression

Forty 16-week-old male Wistar rats (Charles River Netherlands BV, Maastricht, the Netherlands) were housed in the animal facility of the Erasmus Medical Centre, with a 12-h light-dark regimen, at 21°C during the experimental period, and received standard food pellets and water *ad libitum*. Animals were divided over two groups: twenty rats served as untreated OA controls and twenty rats were treated during the experiment with weakly intra-articular injections of TA. TA (Kenacort, Bristol-Myers Squibb, Woerden, the Netherlands) was diluted with saline to a concentration of 1.43 mg/ml. Animals were injected weekly with 70 μ l of this solution (100 μ g TA) in their OA induced knee joint using a 27G needle (Sherwood-Davis & Geck, Gosport, UK). TA was chosen due its superior function on pain reduction in human patients compared to another corticosteroid³³⁰.

In all animals from both experimental groups, severe osteoarthritis was induced using intra-articular papain injections in their left knee joints combined with exposure to a moderate exercise protocol as described before²⁷³. In short, all animals received three intra-articular injection that consisted of 15µl 4% (w/v) papain solution (type IV, double crystallized, 15 units/mg, Sigma-Aldrich, St. Louis, MO, USA) with 15µl 0.03M L-cystein (Sigma-Aldrich)⁸¹. Their contralateral knee joint served as an internal healthy control. All rats were forced to run on a motorized rodent treadmill (LE-8700; Panlab Harvard Apparatus, Barcelona, Spain) for six weeks covering a distance of 15km (500meter/day, 5 days a week)²⁷³. During the study all animals were longitudinally monitored with µCT to measure subchondral bone changes. At six and twelve weeks, ten rats in both groups were selected for a full analysis sequence. This sequence consisted of SPECT/CT to quantify in vivo macrophage activation³⁴¹, and ex vivo EPIC-µCT and histology to measure cartilage quality¹¹³. For all procedures, the exact same procedures were followed as described earlier²⁷³. The animal ethic committee of the Erasmus Medical Center, Rotterdam, the Netherlands, approved all conducted procedures. A detailed planning scheme of all groups and conducted tests is given in Figure 1.

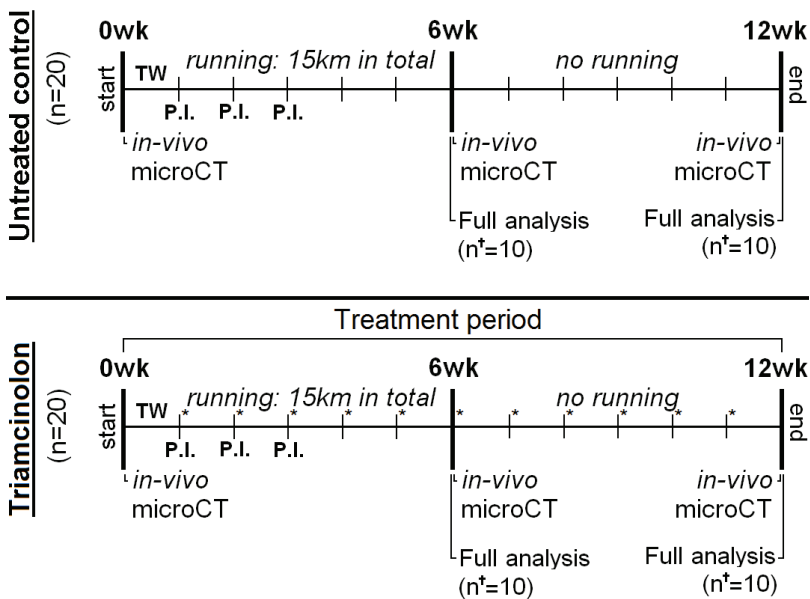


Figure 1: Experiment design indicating analytical time points and methods for each experimental group. Forty 16-week-old male Wistar rats were injected with three papain intra-articular injections (P.I.) and forced to run 15km on a motorized treadmill. Animals were divided over two different groups: an untreated osteoarthritis (OA) group (n=20) and a group treated with intra-articular triamcinolone injections (n=20). Triamcinolone animals were treated with weakly intra-articular triamcinolone injections (100µg/injection), indicated with * in the scheme. During the experiment three longitudinal µCT scans were made to measure subchondral bone changes. At six and twelve weeks a full analysis sequence was done in ten animals per group (n=10), consisting of in vivo: determination of activated macrophages using SPECT/CT; and ex vivo: cartilage analysis with equilibrium partitioning of an ionic contrast agent using (EPIC-)µCT and histology.

Subchondral bone measurements on μ CT scans

Both knees of all animals were μ CT scanned under isoflurane anaesthesia, using a Skyscan 1176 in vivo μ CT scanner (Skyscan, Kontich, Belgium). Ten minutes of scan time was required per knee at an isotropic voxelsize of $18\mu\text{m}$, at a voltage of 65kV, a current of 385mA, field of view of 35mm, using a 1.0mm aluminium filter, over 1980 with a 0.5 degree rotation step, and a 270 msec exposure time. All datasets were segmented with a local threshold algorithm¹⁴¹. Cortical and trabecular bone were automatically separated using in-house software²⁸². Using Skyscan software, both subchondral plate thickness (Sb. Pl. Th. in μm) and subchondral plate porosity (Sb. Pl. Por. in mm^3) of the medial and lateral compartment of the tibial plateau were measured³⁵. In the tibial epiphysis, the trabecular thickness (Tb. Th. in μm) and trabecular bone volume fraction (BV/TV), representing the ratio of trabecular bone volume (BV, in mm^3) to endocortical tissue volume (TV, in mm^3). We additionally quantified the amount of ectopic bone formation as a measure for osteophyte growth (mm^3) on longitudinal μ CT scans.

Determination of activated macrophages by SPECT/CT using ^{111}In -EC0800

Activated macrophages express the folate receptor- β allowing monitoring macrophages in vivo using folate-based radiotracers^{130, 163, 164}. Phosphate saline-buffered (PBS, pH 6.5) DOTA-Bz-folate (DOTA-Bz-Folate, EC0800, kindly provided by Endocyte Inc., West Lafayette, USA)^{269, 326} was labelled with $^{111}\text{InCl}_3$ (Covendien, Petten, The Netherlands) as described previously²⁷³. Quality control was performed with ITLC-SG and revealed a radiochemical yield of $\sim 91\%$ at a specific activity of 50 MBq/ μg . ^{111}In -EC0800 (55MBq) was administered via the tail vein twenty hours prior to scanning. SPECT/CT scans were performed with a 4-head multiplex multi-pinhole small animal SPECT/CT camera (NanoSPECT/CT TM, Bioscan Inc., Washington DC, USA). All knee joints were scanned with both helical μ CT (acquisition time 5min) and SPECT (acquisition time 30min). All scans were analyzed using InVivoScope processing software (Bioscan Inc.). To reduce inter-individual variation, the absolute difference in measured radioactivity (kBq/ mm^3) of the OA knee joint compared to their internal control joint was calculated. This absolute difference was used when comparing means of untreated animals with TA treated animals.

Cartilage evaluation with contrast enhanced μ CT and histology

Equilibrium partitioning of a contrast agent using μ CT (EPIC- μ CT) has a strong correlation with cartilage sulphated-glycosaminoglycan (sGAG) content¹¹³. Animals were euthanized directly after the last SPECT/CT scan and both knee joints were harvested for EPIC- μ CT analysis. All specimens were incubated in 40% solution of ioxaglate, for 24 hours at room temperature¹³⁸. EPIC- μ CT was performed on the same μ CT scanner, using the following scan settings: isotropic voxel size of $18\mu\text{m}$, a voltage of 65kV, a current of 385mA, field of view 35mm, a 0.5 mm aluminium filter, 1980 with a 0.5 degree rotation step, and a 235 msec exposure time. In all EPIC- μ CT datasets, X-ray attenuation (arbitrary gray values related to sGAG content) and cartilage thickness (in μm) was calculated separately for cartilage of the medial and lateral plateau of the tibia²⁷³.

After EPIC- μ CT, the separated parts of the knee joints were fixed in paraformaldehyde, decalcified with formic acid and embedded in paraffin. Sagittal sections were made at 300 μ m intervals and stained with Safranin-O to image the amount and distribution of the GAGs. Sections were stained all at once, to minimize artefacts in between different samples.

Surface receptor expression on monocyte-derived macrophages in vitro

Monocytes were isolated from peripheral blood of healthy human donors using sequential Ficoll-Hypaque and Percoll density gradients (GE Healthcare, Uppsala, Sweden) and cultured in RPMI/glutamax (Gibco BRL, Life Technologies, Belgium) with additional penicillin (100 U/ml), streptomycin (100 μ g/ml), and 10% fetal calf serum (FCS, Gibco BRL). Monocyte-derived macrophages were generated by culturing monocytes for 7 days in the presence of 800 U/ml human recombinant granulocyte-macrophage colony-stimulating factor (GM-CSF; for M1 subtype differentiation) or 25ng/ml human recombinant macrophage colony-stimulating factor (M-CSF; for M2 subtype differentiation) (GM-CSF and M-CSF were both acquired from R&D Systems, Minneapolis). To study the influence of TA on macrophage differentiation 100nM TA (Kenacort, Bristol-Myers Squibb, Woerden, the Netherlands) was added to the culture medium during these 7 days. The culture medium was refreshed after 3-4 days.

Flow cytometry

The expression of membrane receptors was evaluated by incubating the cells with specific fluorescent antibodies. First, the cells were incubated with a rabbit anti-human FOLR2 antibody (Thermo Fisher Scientific, Rockford, USA) at 4°C for 30 minutes in the presence of rabbit serum. This was followed by incubation with a fluorescein (FITC) labelled goat anti-rabbit antibody (Thermo Fisher Scientific), CD80-PE (Clone L307.4, BD Biosciences, San Jose, USA), CD163-PERCP-CY5.5 (clone GHI/61, Biolegend, San Diego, USA), CD14 APC-AF750 (clone RMO52, Beckman Coulter, Brea, USA), CD206-PC-7 (clone 3.29B1.10, Beckman Coulter) and CD16-APC (clone 3G8, Life technologies, Frederick, USA). Flow cytometry was performed on a FACS Canto II cytometer (Becton Dickinson) according to the manufacturer's protocols. Fluorescence minus one controls were used to identify gating boundaries. Values were expressed as mean fluorescent intensity (MFI) ratio compared to an unstained control (fold change).

Detection of IL10 mRNA levels by real-time quantitative (RQ)-PCR

Messenger RNA was isolated using RNeasy Mini Kit (Qiagen, Venlo, the Netherlands) After on-column DNase-I treatment (QiagenRNAse-free DNase kit), RNA was quantified using Nanodrop ND-1000 (Isogen Life Science, De Meern, theNetherlands)and reverse transcribed into cDNA using the iScript cDNA Synthesis Kit (Biorad, Veenendaal, theNetherlands.).Gene expression was analysed using the CFX384 Real-Time PCR Detection System (Biorad). The qPCR reactions were performed in duplicate in 384-well plates in a final volume of 10 μ l, using IQ SYBR Green Supermix (Biorad).IL10 mRNA levels were normalised to those of the reference genes TBPandHPRT. Primers used were: IL10 forward

5'-GACTTTAAGGGTTACCTGGGTTG-3', reverse 5'-TCACATGCGCCTTGATGTCTG-3', TBP forward 5'-TGCACAGGAGCCAAGAGTGAA-3', reverse 5'-CACATCACAGCTCCCCACCA-3'. HPRT forward 5'-TATTGTAATGACCAGTCAACAG-3', reverse 5'-GGTCCTTTCCACCAGCAAG-3'.

Statistical analysis

For the in vivo study, differences between means of OA induced and healthy knee joints within the same animal were tested using paired t-tests at each time point for all outcome parameters (GraphPad Software, San Diego, California, USA). When comparing differences between means of untreated OA animals and TA treated animals an unpaired t-test was used at each time point for all outcome parameters (GraphPad Software). Statistical significance among the different cell treatments was assessed using one-way ANOVA with Bonferroni's correction (SPSS Inc., Chicago, USA). Longitudinal data from in vivo μ CT were additionally analyzed using generalized estimating equations (SPSS Inc., Chicago, USA). For all tests, p values ≤ 0.05 were considered significant.

RESULTS

Effects of intra-articular triamcinolone treatment

Bodyweight of all untreated rats at baseline was 416.4g (411.3 – 421.5g), during six weeks of treadmill running this did not increase (mean weight 408.3g; 398.2 – 418.3g). During subsequent six weeks of rest, all rats increased in bodyweight (mean weight 485.5; 473.0 – 498.0g). TA treated animals (mean weight at baseline was 423.6g; 417.3 – 429.9g) lost bodyweight during OA induction (mean weight after six weeks was 391.2g; 385.1 – 397.2g) and was lower compared to untreated OA animals ($p = 0.004$). After twelve weeks their mean bodyweight increased to 434.6 (422.2 – 446.9), but was still significantly lower compared to untreated OA controls ($p < 0.0001$) (Figure 2).

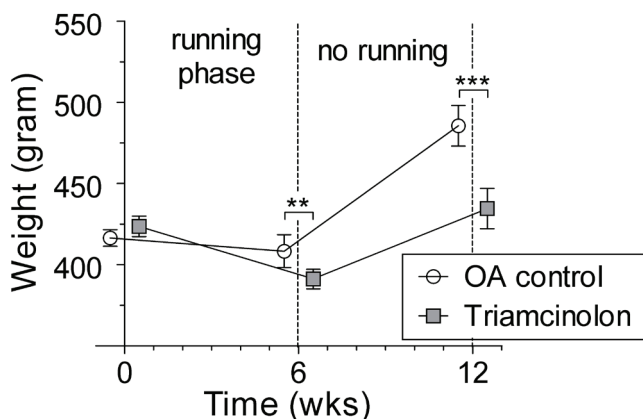


Figure 2: Increase of bodyweight (gram) of untreated control rats (white circles) and triamcinolone treated rats (gray squares).

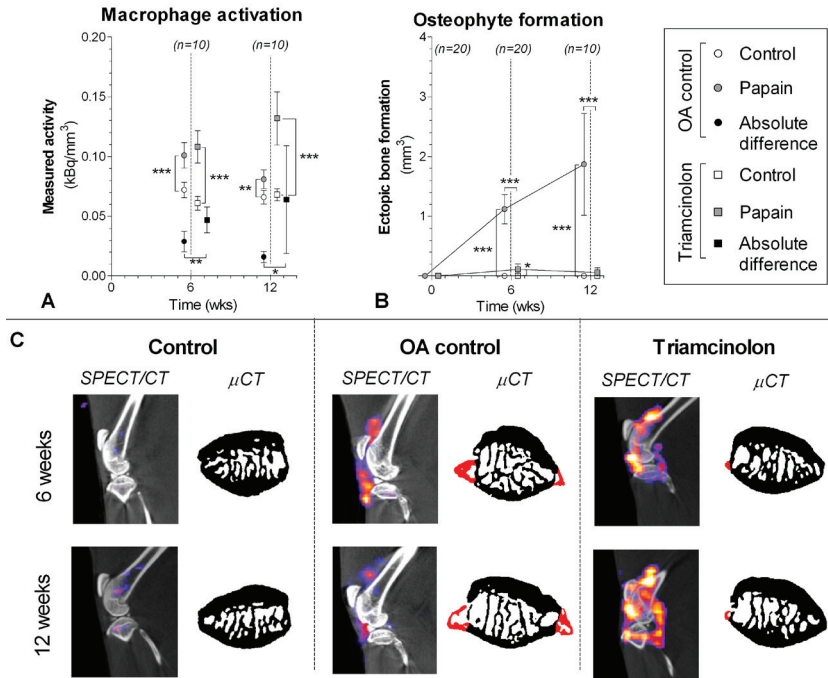


Figure 3: Macrophage activation determined in untreated OA animals (circles) and triamcinolone treated animals (squares) after injection of ¹¹¹In-EC0800 using SPECT/CT. A: Quantitative outcome of measured radioactivity in the healthy joints (blank boxes) and OA joints (gray boxes) normalized to the size of the analyzed cylindrical region of interest (kBq/mm³). Absolute differences per animal were calculated (kBq/mm³) to correct for differences in biodistribution of ¹¹¹In-EC0800 (black boxes). A high radioactivity is related to more macrophage activation. B: Ectopic bone formation (mm³) as a measure for osteophyte development was quantified on longitudinal bone μ CT scans. C: Sagittal SPECT/CT images of knee joints from representative animals. CT images shown in black and white were used for anatomical reference, the SPECT images are shown in color. Transaxial images from patellar bone extracted from binary μ CT images show ectopic bone formation (red color). *: $p < 0.05$, **: $p < 0.01$, ***: $p < 0.001$, error bars indicate 95% confidence intervals.

Effect of intra-articular triamcinolone treatment on synovial macrophage activation

Each animal received 54 ± 2 MBq of ¹¹¹In-EC0800 under isoflurane anesthesia, there were no significant differences of injected activity between experimental groups. Untreated OA control animals showed more macrophage activation in their OA induced joints at six ($p < 0.0001$) and twelve weeks ($p < 0.0001$). TA injected knee joints also showed more macrophage activation compared to their non-injected healthy knee joint ($p < 0.0001$ at six and twelve weeks). In order to correct for differences in biodistribution, we calculated paired absolute differences between healthy control joints and OA induced joints for all untreated rats and TA treated animals. Both at six ($p = 0.008$) and twelve weeks ($p = 0.04$) this analysis suggest more macrophage activation

in TA injected joints (Figure 3A,C). In line with macrophage activation in untreated animals, OA induced knee joints showed evident ectopic bone formation in untreated animals compared to their healthy control joints at six ($p < 0.0001$) and twelve weeks ($p < 0.0001$). TA injected joints showed only minimal or no osteophyte formation compared to their healthy control joints ($p = 0.02$ at six weeks, $p = 0.11$ at twelve weeks) and compared to untreated OA joints ($p < 0.0001$ at six and twelve weeks) (Figure 3B,C).

Effect of intra-articular saline injections on macrophage activation

In order to test whether the amount of macrophage activation in TA did not result from the intra articular injection, we tested in a small experiment whether saline injections also induced macrophage activation. Therefore, we injected five Wistar rats with a saline injection into a healthy knee joint. Subsequently, we SPECT/CT scanned these animals using $^{111}\text{In-EC0800}$ as described before. In these animals, we found that there was no difference in measured radioactivity between non-injected and saline-injected knee joints (Figure 4). This suggests that an intra-articular injection does not induce macrophage activation that explains the additional measured activity in the TA treated animals in the first experiment.

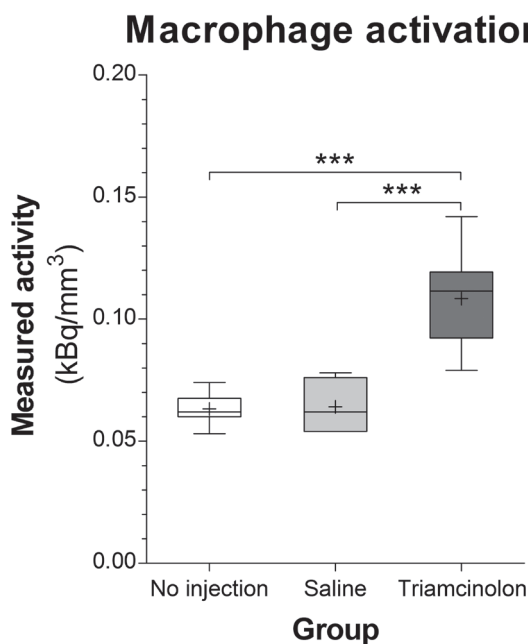


Figure 4: Effect of intra-articular injection on macrophage activation determined with $^{111}\text{In-EC0800}$ SPECT/CT. There was no difference between knee joints without intra-articular injection (white column) and knee joints injected with saline (light gray column) one day before SPECT/CT scanning. Knees injected with triamcinolone injected one day before SPECT/CT showed clearly increased radioactive uptake, which means increased macrophage activation.

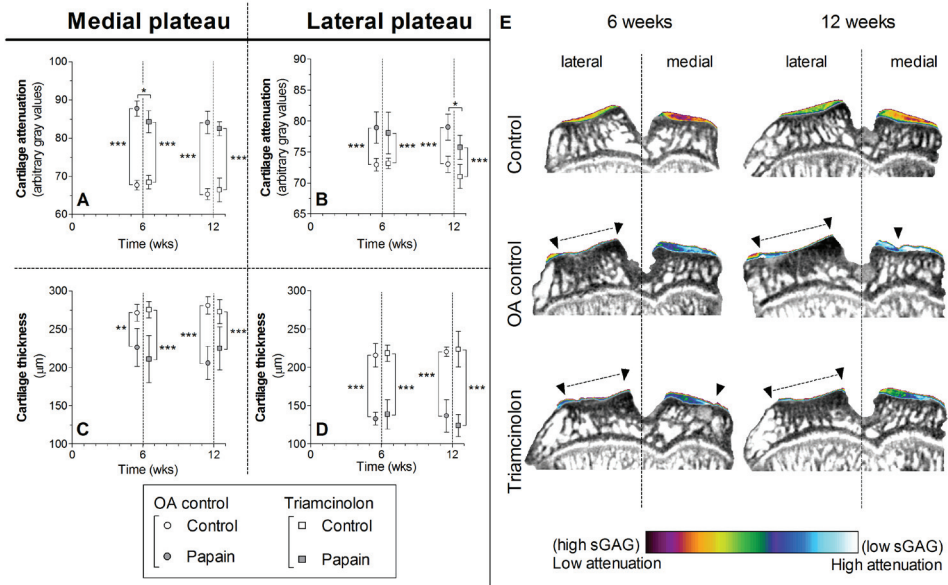


Figure 5: Cartilage quality and quantity was determined from samples of untreated (circles) and triamcinolone treated (squares) rats with equilibrium partitioning of a ionic contrast agent using (EPIC-)μCT (A-D). The amount of sulphated-glycosaminoglycans (sGAG) (arbitrary gray values; A,B) and cartilage thickness (μm; C,D) were measured of medial (A,C) and lateral (B,D) cartilage compartments of the tibia plateau harvested from healthy joints (blank boxes) and OA induced joints (gray boxes). Attenuation values from EPIC-μCT scans are inversely related to the sGAG content, meaning that a high attenuation corresponds to low sGAG content. Coronal images from representative EPIC-μCT scans of the tibia plateau show the amount of cartilage (erosions indicated with ▲ and dashed lines) and sGAG content (displayed in color). *: $p < 0.05$, **: $p < 0.01$, ***: $p < 0.001$, error bars indicate 95% confidence intervals.

Osteoarthritic changes of articular cartilage

Both medial and lateral cartilage compartments of the tibia plateau were severely sGAG depleted in untreated controls at six and twelve weeks (Figure 5A). After the running protocol at six weeks, cartilage of the medial compartment was slightly reduced in thickness (Figure 5C). Lateral cartilage thickness was severely degraded (Figure 5D) and resulted in almost completely denuded subchondral bone (Figure 5E). During subsequent six weeks of rest medial cartilage continued to degrade, in the lateral compartment an ongoing decline in cartilage thickness was not seen (Figure 5C-E). sGAG loss and cartilage degradation in triamcinolone treated animals followed the same pattern as in untreated animals. Only at six weeks medial cartilage showed slightly decreased attenuation values ($p = 0.04$), and at twelve weeks we measured lower attenuation values in lateral cartilage ($p = 0.02$). Representative medial and lateral cartilage images from safranin-O stained histology from untreated controls and triamcinolone treated animals at six and twelve weeks are shown in Figure 6.

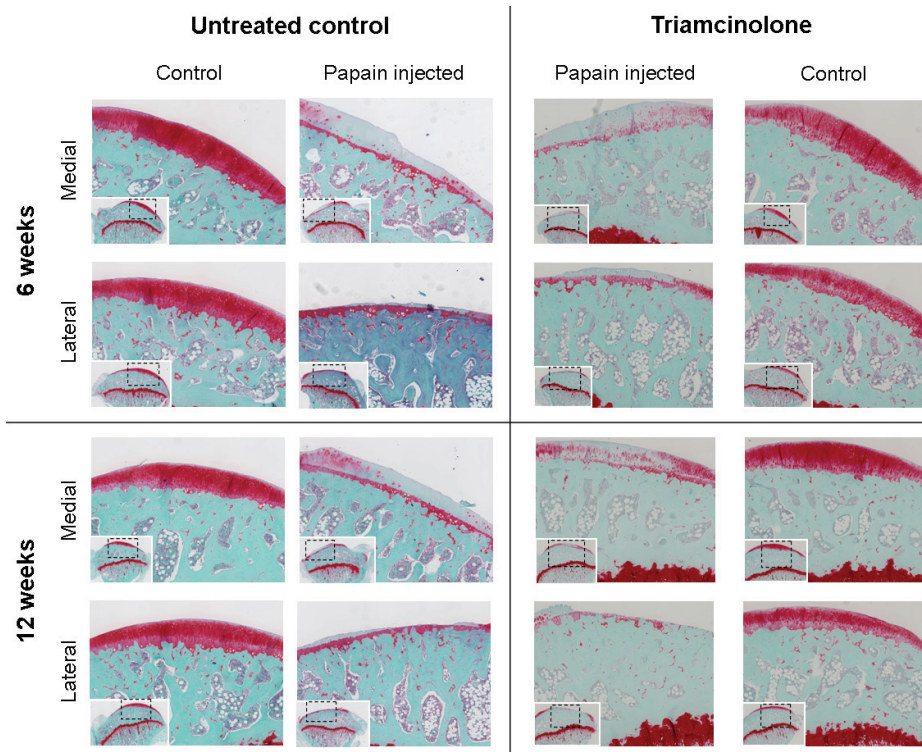


Figure 6: Safranin-O stained histology sections showing representative images of medial and lateral tibial plateau cartilage after six weeks and twelve weeks of follow up of untreated and triamcinolone treated animals.

Subchondral bone changes

Compared to their healthy control joints, medial subchondral plates in OA induced joints of untreated controls tended to decrease in thickness from six to twelve weeks, but was not significantly different ($p = 0.16$). Medial subchondral plate thickness in triamcinolone treated rats followed the same pattern as its healthy control joint (Figure 7A), but compared to untreated controls their subchondral plate was slightly thicker at twelve weeks ($p = 0.01$). Generalized estimating equations showed that medial subchondral bone plates of triamcinolone treated animals were thicker during the experiment compared to untreated controls ($p = 0.02$). Sagittal μ CT images show that this increase in subchondral plate thickness was not homogeneously distributed like in healthy controls knees, but more focal and indicative of a sclerotic phenotype (Figure 7G). Medial plate porosity did not increase in both experimental groups throughout the experiment (Figure 7B). Lateral compartment subchondral bone thickness of untreated OA joints was clearly increased compared to their healthy control joint at six weeks ($p < 0.0001$) and twelve weeks ($p < 0.0001$) (Figure 7C,H). Longitudinal measured subchondral bone thickness analyzed using generalized estimating equations showed that triamcinolone treated animals

developed more lateral subchondral sclerosis in their OA induced joints during the experiment compared to untreated controls ($p < 0.0001$). Although untreated animals developed minimal subchondral plate porosity at six weeks, no differences were found compared to triamcinolone treated animals (Figure 7D,H). Trabecular thickness did not differ between both experimental groups during the experiment (Figure 7E). BV/TV ratios were lower in OA induced joints of both groups compared to their healthy knee joints (Figure 7F), no differences were found between OA joints of untreated controls or triamcinolone treated animals. However, healthy control joints of triamcinolone treated animals had higher BV/TV ratios compared to healthy control joints of untreated animals ($p = 0.003$).

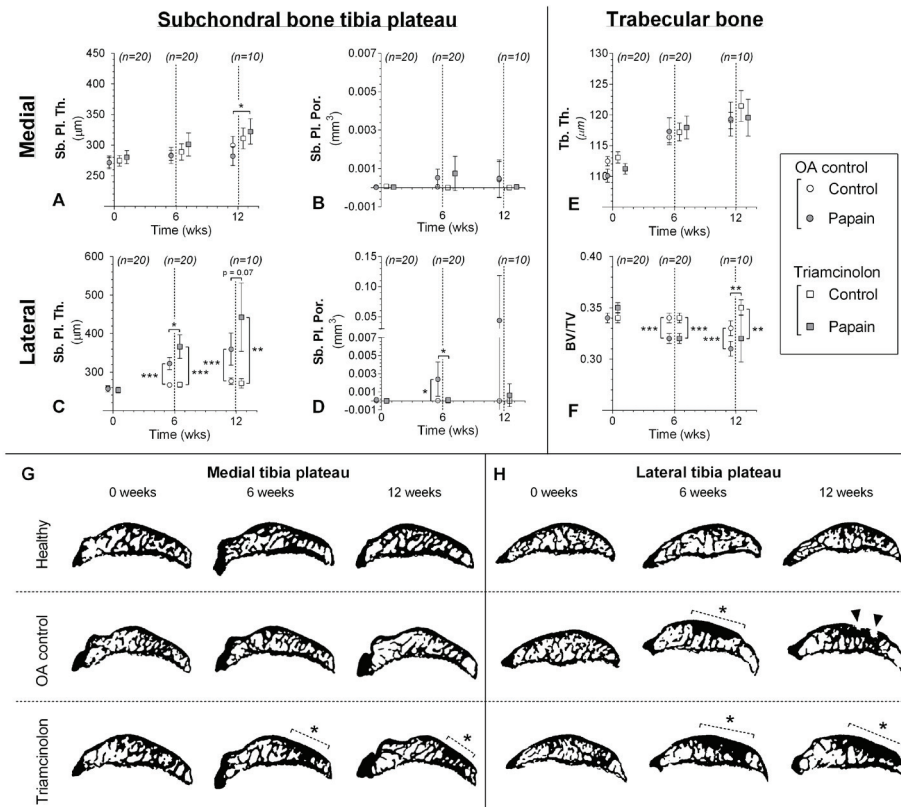


Figure 7: Subchondral bone changes analyzed with longitudinal in vivo μCT in untreated animals (circles) and triamcinolone treated animals (squares). Subchondral plate thickness (Sb. Pl. Th.; A, C) and porosity (Sb. Pl. Por.; B, D) were measured in the medial (A,B) and lateral (C,D) compartment of the tibial epiphysis. Changes in trabecular thickness (Tb. Th.; E) and trabecular bone volume fraction (BV/TV; F) were measured in tibial epiphysis bone marrow. Representative sagittal images from binary μCT scans show pore development (indicated with \blacktriangle) and development of subchondral sclerosis (indicated with dashed line and *) in the medial (G) and lateral (H) compartment of the tibial epiphysis. *: $p < 0.05$, **: $p < 0.01$, ***: $p < 0.001$, error bars indicate 95% confidence intervals.

Effects of TA treatment on in vitro cultured M1 and M2 macrophages

Monocyte-derived macrophages differentiated in the presence of GM-CSF showed enhanced expression of CD80, while CD163 expression was absent (Figure 8A-B). When monocytes were exposed to TA in addition to GM-CSF, both CD163 receptor and FR β expression increased significantly (Figure 8C). Interestingly, TA strongly decreased survival in GM-CSF stimulated monocytes, but not in M-CSF stimulated monocytes. Monocyte-derived macrophages cultured in the presence of M-CSF showed enhanced expression of CD163 and CD16, but absence of CD80 (Figure 8A-B). FR β expression in these cells was increased compared to untreated GM-CSF cells, but was not enhanced through the addition of TA (Figure 8C). Representative images from FACS experiments are shown in Figure 8D. Additionally, TA treated M-CSF macrophages showed significantly increased levels of IL10 mRNA expression (Figure 8E).

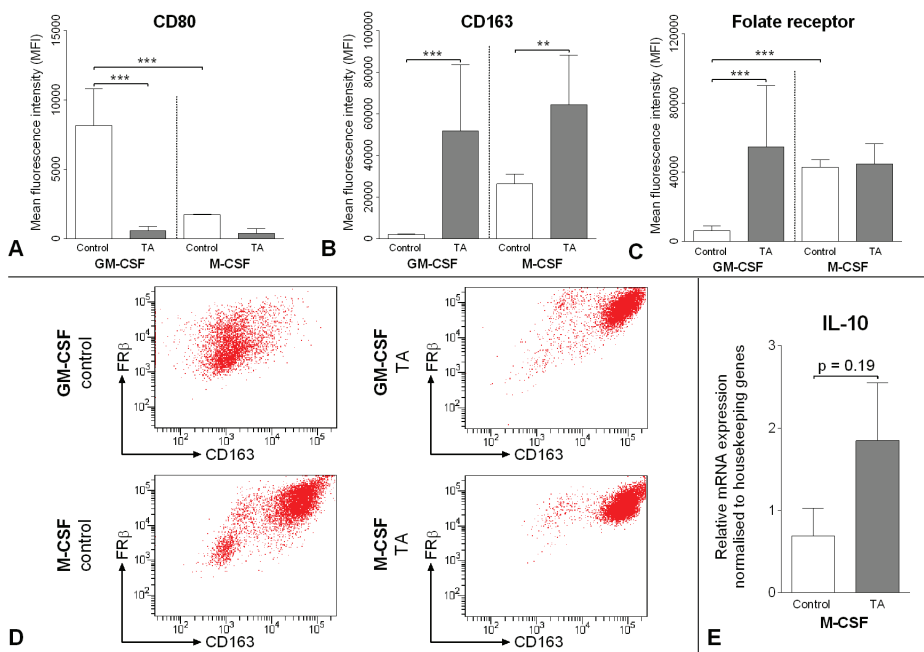


Figure 8: Expression of CD80, CD163 and folate receptor analyzed using FACS in monocyte-derived macrophages with or without triamcinolon. Data shown are representative of three independent experiments. (A-C). Representative flow cytometry plots are shown in D. Relative IL10 mRNA expression in monocyte-derived M2 macrophages with or without triamcinolon (E). Data represent two independent experiments. *: $p < 0.05$, **: $p < 0.01$, ***: $p < 0.001$, error bars indicate SEM. Discussion

DISCUSSION

In this study we investigated the effects of TA injections on in vivo macrophage activation during OA progression. In untreated animals, there was a marked increase of activated macrophages measured with in vivo FR β targeted SPECT/CT imaging (**Figure 3**). It is thought that activated macrophages in OA produce TGF β which induces BMP production in synoviocytes, which subsequently triggers osteophyte development^{59, 60}. Therefore, it was expected to see progressive growth of patellar osteophytes in untreated animals. In treated animals, however, intra-articular TA injections completely prevented osteophyte development. Interestingly, TA injections severely induced macrophage activation (**Figure 3**). Since saline injections did not reproduce this enhanced SPECT/CT signal, we can exclude the injection itself to be the cause for macrophage activation (**Figure 4**). We hypothesized that this combination of enhanced macrophage activation and prevented osteophytosis might be explained through different subtypes into which macrophages can differentiate.

Therefore, we performed in vitro experiments using GM-CSF and M-CSF cultured monocytes. GM-CSF cultured monocytes were CD80+ and CD163- typical for classical (M1) activated macrophages³⁴². Whereas M-CSF cultured monocytes were CD163+ and lacked CD80, which is typical for alternatively (M2) activated macrophages^{343, 344}. It is known that FR β is predominantly co-expressed in CD163+ macrophages³⁴⁵. Our experiments confirm this finding, since FR β was especially elevated in M-CSF cultured M2 macrophages (**Figure 8C**). However, adding TA during GM-CSF driven macrophage differentiation, these M1 activated macrophages start to co-express FR β . Interestingly, these cells stop CD80 expression and increase CD163 expression, suggesting that TA stimulates macrophages towards an activated M2 phenotype. Although this TA induced FR β + M2 activated phenotype explains the increased SPECT/CT signal in TA treated animals, this does not explain why TA treated animals lacked osteophyte formation.

Glucocorticoids are known inducers of a specific macrophage subtype, known as regulatory macrophages. These are a specific form of M2 activated macrophage which is considered anti-inflammatory. Through interaction with transcription factors, glucocorticoids regulate macrophage gene expression levels³⁴⁶. By induction of I κ B, glucocorticoids inhibit NF κ B³⁴⁷ that results in decreased production of pro-inflammatory cytokines (such as IL1, IL6 and TNF)³⁴⁸. Furthermore, the regulatory macrophage can be characterized by enhanced IL10 production¹⁷⁸. Therefore, we analyzed our in vitro cultured M2 macrophages for mRNA expression of IL10, and found that TA strongly increased IL10 expression levels in M-CSF cultured monocytes (**Figure 8E**). We believe that this underlines that TA strongly polarizes macrophage activation towards a specific anti-inflammatory macrophage subtype that does not promote osteophyte growth in our in vivo model for OA.

Besides the effects of TA on macrophages, we also investigated whether TA could be beneficial for either articular cartilage or subchondral bone. In a previous reported study using a preclinical animal model for traumatic OA, intra-articular injections with dexamethasone led to less cartilage damage³³⁴. This study could not reproduce this result. Our cartilage results showed no protection against cartilage erosion of the lateral tibia plateau, or against loss of cartilage matrix of the medial plateau (**Figure 4-5**). There were also no beneficial effects of TA against pathological changes within the subchondral bone. In fact, GEE analysis of the medial subchondral plate showed that more subchondral sclerosis developed in TA treated animals. From repeated intra-articular injections of TA, it is known that cartilage matrix metabolism is changed as measured by biomarkers within synovial fluid³⁴⁹. Furthermore, corticosteroid treatment is known to induce chondrocyte apoptosis in chondrocyte cultures and *in vivo*³⁵⁰. These data suggests that TA treatment could very well have induced direct toxic effect for chondrocytes. Subsequently, more chondrocytes death could have enhanced cartilage damage, and therefore more subchondral sclerosis developed.

More studies using SPECT/CT imaging techniques are needed to gain more knowledge related to macrophage activation and their manipulation through therapeutic strategies in all kinds of disease. Other studies already showed the possibility to image (M1) polarization of microglia (a group of macrophages within the brain) in animal models for psychiatric disorders³⁵¹. Different tracers enable us to differentiate between M1 and M2 activated macrophages³⁵², hopefully in the near future it will be possible to also use tracers in order to differentiate between different subtypes (e.g. wound-healing and regulatory) of M2 macrophages. These techniques would allow monitoring of specific *in vivo* activated macrophage subtypes in pre-symptomatic stages of OA and measure effects of pre-emptive intervention strategies dedicated to interfere with macrophage polarization. Eventually, these studies will answer questions how macrophages and related immune cells might be manipulated more specifically in order to prevent or delay disease progression.

Conclusion

Pre-emptive treatment with intra-articular TA injections showed enhanced FR β related macrophage activation in an *in vivo* model for OA, and fully prevented osteophyte development. TA strongly induced monocyte differentiation towards an M2 and anti-inflammatory macrophage phenotype. TA leads to increased IL10 mRNA levels *in vitro* and reduced osteophytosis *in vivo*, which indicates that TA potently induced an CD163+ and FR β + regulatory macrophage. Unfortunately, FR β cannot be used to differentiate between wound-healing and regulatory M2 subtypes. Future studies should aim to identify specific surface markers for each of these subtypes, in order to enable *in vivo* identification using imaging techniques like SPECT/CT. Future fine tuning of their anti-inflammatory and anti-pain capabilities, might prove beneficial against disease progression and reduce patient complaints.

ROLE OF FUNDING SOURCE

Sources of funding are Dutch Arthritis Association (LLP 22) and the TerM P2.02 Program of the Netherlands Ministry of Economic Affairs and the Netherlands Ministry of Education, culture and Science. The funding sources had no role in the study design, collection, analysis or interpretation of data; in the writing of the manuscript or in the decision to submit the manuscript for publication.

CHAPTER 9

MESENCHYMAL STEM CELLS REDUCE PAIN BUT NOT DEGENERATIVE
CHANGES IN A MONO-iodoacetate RAT MODEL OF
OSTEOARTHRITIS

G.M. van Buul, M. Siebelt, M. Leijts, P.K. Bos, J.H. Waarsing, N. Kops, H. Weinans, J.A.N.

Verhaar, M.R. Bernsen, G.J.V.M. van Osch

J Orthop Res. 2014Sep;32(9):1167-74

ABSTRACT

Introduction

Mesenchymal stem cells (MSCs) are promising candidates for osteoarthritis (OA) therapies. Evaluation and optimization of the effects of these therapies on multiple outcome measures is required before translation into clinical application. The purpose was to study the effects of intra-articular injected bone marrow derived MSCs, as well as freshly isolated bone marrow mononuclear cells (BMMNCs), on pain, cartilage damage, bone changes and inflammation in a rat OA model *in vivo*.

Methods

OA was induced unilaterally by injection of mono-iodoacetate (MIA). After three weeks, the 24 animals were randomly divided into three groups: 1. saline control, 2. MSCs, 3. BMMNCs. Four weeks after treatment, pain was assessed with an incapitance tester, subchondral bone alterations were measured with μ CT and cartilage quality and joint inflammation were analyzed with histology.

Results

Both therapies were well tolerated by the animals. Animals treated with MSCs distributed significantly more weight to the affected limb after treatment than before treatment, which was not observed in the other groups. MIA injected knees displayed significant cartilage damage, subchondral bone alterations and synovial inflammation compared to contralateral knees. No statistically significant differences between treatment groups regarding any of these outcome measures were observed.

Conclusion

In our OA model, injected MSCs were able to reduce MIA induced pain, as measured by an increased weight distribution to the affected limb. No statistically significant effects of the cellular therapies on structural damage and synovial inflammation were found. This is the first study evaluating the effect of cell therapy on pain, as well as structural changes and synovial inflammation in a small animal OA model. Pain is the most relevant clinical outcome measure; thereby the results of our study underline the potential of MSCs as an OA therapy. Additional studies should focus on more pain aspects as well as the relation with structural damage to further optimize cellular therapies for OA treatment.

INTRODUCTION

Osteoarthritis (OA) is a degenerative joint disease characterized by inflammation and catabolic processes, leading to progressive cartilage degeneration. Cartilage has limited intrinsic repair capacity and so far no drugs are available to structurally modify OA processes³⁵³. Mesenchymal stem cells (MSCs) are promising candidates for cartilage regeneration and OA therapies since they have chondrogenic potential and the ability to form extracellular matrix³⁵⁴. Additionally, MSCs have immunomodulatory and trophic capacities by secreting anti-inflammatory factors and growth factors³⁵⁵, which could possibly encounter inflammatory and catabolic aspects of OA. Therefore, MSCs have been injected intra-articular in pre-clinical and some initial clinical studies as a treatment for cartilage damage and OA, showing promising results³⁵⁶⁻³⁶⁴. Animal studies using cell tracking after cell injection showed only limited cartilage formation by chondrogenic differentiation of these MSCs^{356, 359, 360, 362-364}. Instead, injected cells were mostly found in other parts of the joint, such as the synovium. Furthermore, decreased levels of inflammatory cytokines in synovial fluid were found in MSC-treated OA joints³⁶⁵. These findings underline the potential dual role of MSCs as an OA modifying drug, not only able to regenerate damaged cartilage but also positively contributing to joint homeostasis.

The effects of MSC therapy on pain or other clinical outcome measures are difficult to assess in animal studies, and therefore they are not extensively documented. Nevertheless, pain is the main reason to proceed to joint replacement in OA patients³⁶⁶. As structural joint damage and pain in patients are not well correlated^{366, 367}, separate evaluation of these outcome measures is essential to assess the efficacy of cell therapies. The mono-iodoacetate (MIA) model has been extensively studied as a pain model for OA in animals³⁶⁸⁻³⁷⁰.

Although MSCs appear promising for OA therapy, several practical issues hinder broad clinical translation. Extensive culture procedures are necessary to obtain MSCs, a costly and time consuming procedure requiring special facilities. Bone marrow mononuclear cells (BMMNCs) on the other hand, can be harvested in a one-step procedure. These cells contain various progenitors³⁷¹ which could also attenuate degenerative OA processes. In order to evaluate multiple aspects of OA pathology and to explore potential options to enhance clinical translatability, we studied the effects of intra-articular injected cultured rat MSCs, as well as rat BMMNCs, on pain, cartilage damage, bone changes and inflammation in a MIA rat OA model *in vivo*.

METHODS

Ethical approval

All animal experiments were performed after approval of the animal ethical committee (protocol # EMC116-10-07 and EMC 116-11-03).

Preparation and colony forming capacity of bone marrow derived cells

Rat MSCs were isolated by flushing morselized femurs and tibiae from four week old male Wistar rats. The harvested cells were cultured in MSC culture medium, consisting of DMEM containing 10% fetal calf serum (FCS, Lonza, Verviers, Belgium), 50 µg/ml gentamicin, 1.5 µg/ml fungizone (both Invitrogen, Carlsbad, CA, USA), 1 ng/ml fibroblast growth factor-2 (Instruchemie B.V., Delfzijl, The Netherlands), and (0.1 mM l-ascorbic acid 2-phosphate Sigma, St. Louis, MO, USA). All media were renewed twice a week. Passage 2-3 cells were used for intra-articular injection.

Rat bone marrow mononuclear cells (BMMNCs) were obtained by cell separation of the harvested bone marrow using a Ficoll gradient (Ficoll-Paque™ PLUS, $d = 1,077$, GE Healthcare, Vienna, Austria) at 1,000 G. BMMNCs were removed from the gradient interface, washed in physiological saline and subsequently injected. To assess the presence of MSCs in BMMNCs, aliquots of these cells were seeded at a density of 12×10^4 cells/cm² and cultured in MSC culture medium. After 10 days, colonies consisting of more than 50 cells were counted to determine the percentage of colony forming cells. It was demonstrated that these isolated BMMNCs had an average of one colony forming cell per $84,000 \pm 20,000$ mononuclear cells, confirming previous studies describing one cell in 10,000 - 250,000 BMMNCs to have MSC characteristics^{372, 373}.

Induction and treatment of osteoarthritis

Osteoarthritis was induced unilaterally in 24 male Wistar rats (Harlan Netherlands BV, Horst, the Netherlands) of 16 weeks old. OA induction was performed by an intra-articular injection of 300 µg mono-iodoacetate (MIA). Contralateral control knees were not injected with any substance. Rats were randomly divided into three treatment groups: 1. Control; 2. MSCs and 3. BMMNCs. Saline was used as a control and as vehicle for all other injections; all injections were applied under isoflurane anesthesia in a volume of 50 µl using a 27G needle (Sherwood-Davis & Geck, Gosport, UK). Treatments were given three weeks after OA induction to allow the initial inflammatory phase after MIA injection to cease and structural damage to occur. MSCs were given at a dose of 1×10^6 cells per joint, BMMNCs were given at a dose of 10×10^6 cells per joint. Viability of all cells was assessed before injection and after injection, on the remainder of the cells in the syringe, by means of trypan blue exclusion tests. Overall cell viability for both cell types was $96.0 \pm 3.9\%$ before injection and $95.4 \pm 1.1\%$ (mean \pm SD) for the remainder of the cells after injection. Rats were euthanized four weeks after treatment, knee joints were harvested for further analyses.

Hind limb weight distribution measurements

Hind limb weight distribution was measured using an incapitance tester (Linton Instrumentation, Norfolk, UK) as an index of joint discomfort as described previously³⁶⁸. Animals were habituated to the apparatus starting two weeks prior to experiments. Rats were positioned

on the incapitance tester with each hind limb resting on a separate force plate. The force exerted by each hind limb was measured in grams and averaged over a 3 second period. Each rat was measured for 5 subsequent times per day on 2 consecutive days by an observer blinded to the given treatment. The average of 10 obtained readings was used to calculate the weight on the affected limb as a percentage of total weight distributed by both hind limbs. Rats were measured before inducing OA, three weeks after inducing OA (before treatment) and two and four weeks after treatment.

μCT procedure and analysis

To evaluate cartilage damage before cell treatment a μCT arthrography (μCTa) was performed as described previously¹¹⁵. Briefly, rat knees were injected with 50 μl non-diluted ioxaglate 320 (Hexabrix, Hazelwood, MO), mixed with epinephrine 10 μg/ml (Centrafarm, Etten-Leur, the Netherlands) to induce vasoconstriction and to prevent loss of intra-articular ioxaglate. A μCTa was made using the Skyscan 1076 μCT scanner (Skyscan, Kontich, Belgium). Scan time was fifteen minutes at anisotropic voxel size of 35 μm, voltage of 55 kV, current of 181 mA, field of view 35 mm and a 0.5 mm aluminum filter, over 198° with a 1° rotation step. All scans were reconstructed identically. Patellar cartilage volume was measured in 3D using data analysis software (CT Analyzer, Skyscan)¹⁵⁷.

For subchondral bone analysis, fixated knee joints were scanned four weeks after treatment ex vivo. Scan time was 30 minutes at an isotropic voxel size of 18 μm, voltage of 60 kV, current of 167 mA, field of view 35 mm and a 0.5mm filter over 198° with a 0.4° rotation step. Ex vivo μCT scans were segmented into binary datasets using an automated thresholding algorithm¹⁴¹. The subchondral bone part of the distal femur epiphysis was separated from other bone structures using in-house software. Subchondral plate thickness, plate volume and total pore volume was measured in the cortical bone of the femoral trochlea³⁵. Subchondral plate porosity was expressed as a percentage of the subchondral plate volume.

All MIA injected knees and two contralateral control knees per treatment group were used for analyses, leading to a total of 8 knees per group.

Tissue harvest and histologic evaluations

After euthanasia, all rat knees were excised and fixed in formalin 4% (v/v) for one week. After μCT scanning, joints were decalcified with formic acid 10%(v/v) for 3 weeks and embedded in paraffin. Coronal sections were stained with Safranin O to evaluate structural cartilage damage and Thionin to visualize the amount and distribution of GAG. Thionin was used to evaluate GAG distribution due to a low sensitivity of Safranin O in the case of severe GAG loss³⁷⁴. Cartilage quality was evaluated with a score ranging from 0-6 for structure using previously described stages by Pritzker et al.¹⁴³, and a score ranging from 0-4 for GAG staining intensity. GAG

staining intensity and structure grading were multiplied with a previously described staging score: 1. 0–25%; 2. 25–50%; 3. 50–75%; 4. 75–100% of cartilage surface affected¹⁵⁷. This way, a maximum score of 16 for GAG staining intensity and 24 for structural damage could be obtained for each cartilage structure, where a high score represents severe GAG loss or structural damage. Scoring was performed on the patella, trochlea, tibial plateau and femoral condyles at three different positions. An average score for GAG and structure was calculated for each joint compartment.

Synovial inflammation was assessed using a hematoxylin eosine staining. Synovial thickness was measured from the bone margin to the capsule in the parapatellar recesses at the location where the synovium folds from the capsule over the femoral bone, based on a previously described method³⁷⁵. Synovial thickness was determined at the medial and the lateral side at three positions and averaged to obtain a single value per knee. Measurements were performed using the NanoZoomer Digital Pathology program (Hamamatsu Photonics, Ammersee, Germany). Synovial inflammation was assessed by ranking the knees in an order from minimum to maximum (score 1 - 40) based on synovial fibrillation and cellular infiltration in the subsynovial tissue.

All MIA injected knees and two contralateral control knees per treatment group were used for analysis by an observer blinded to the given treatment, leading to a total of 8 knees per group.

Cell tracking experiments

To evaluate adequate injection of cells in the joint and to assess longitudinal cell viability, we performed a cell tracking experiment using bioluminescence imaging (BLI) and magnetic resonance imaging (MRI).

A self-inactivating luciferase lentivirus was prepared by transient transfection of HEK293T cells as mentioned before³⁷⁶. {Guenoun, 2013 #49} Rat mesenchymal stem cells (Millipore, Billerica, MA, USA) were grown to 50% confluency in a 24 well plate in DMEM/F10, 10% Fetal Calf Serum (FCS), penicillin/streptomycin (P/S) and infected with 50 μ l lenti-viral stock, resulting in luciferase-expressing MSCs.

One day prior to injection, Fluc-MSCs were labelled using superparamagnetic iron oxides. SPIO labelling was performed using ferumoxides (Endorem®, Guerbet S.A., Paris, France) complexed to protamine sulfate (LEO Pharma N.V., Wilrijk, Belgium) as described earlier³⁷⁷. For removal of extracellular iron, cells were washed with PBS containing heparin 10 U/ml (LEO Pharma B.V., Breda, the Netherlands).

One million cells were injected, suspended in 50 μ l saline, bilaterally in the knees of 3 male

Wistar rats. These rats had OA induced unilaterally, identical to the procedure previously described, to study whether there would be a difference in cell survival dependent on the damaged joint environment. MR imaging was performed once, immediately after cell injection, to confirm intra-articular localisation of the cells. Scanning was performed on a preclinical 7.0T MR 901 Discovery MRI scanner (General Electric Healthcare, Milwaukee, Wisconsin) equipped with a 150mm bodycoil for transmission, and a 4 channel cardiac coil (Rapid Biomed GmbH, Rimpar, Germany) for signal reception. A 3D FSPGR sequence was used to scan rat knees injected with SPIO-Fluc-MSCs (TE/TR=10.0/30.0 ms, NEX=2, FOV=6.00 x 4.50 cm², acquisition matrix 512 x 512, Slice thickness = 0.50 mm, Bandwidth = 31.25 kHz, Flip angle = 16°).

To evaluate the presence of living cells over time, luciferase activity of injected SPIO-Fluc-MSCs was measured using the Xenogen IVIS Spectrum (Caliper LS, Hopkington, MA, USA) 5 min after the intra-peritoneal injection of D-luciferine (Promega). Animals were scanned repeatedly until the signal became below detection limit, resulting in data at days 1, 3, 7, 14 and 21. Optical intensity is reported as arbitrary units. Data were analyzed using the software Living Image version 3.2 (Caliper LS).

Statistical analysis

The effect of treatment on the difference between weight distribution on the hind limbs before and after MIA and between the cellular treatments were analyzed using a repeated measures ANOVA test for all groups, followed by a paired t-test for the treatment groups separately. Quantitative μ CT and histology data was analyzed by means of unpaired t-tests to evaluate MIA induced effects and one-way ANOVA tests for treatment effects. Semi-quantitative histology scores were compared using non-parametric Mann-Whitney tests to assess MIA induced effects and Kruskal Wallis-tests for treatment effects (SPSS, SPSS Inc, Chicago, USA). For all tests, P values < 0.05 were considered statistically significant.

RESULTS

All cell injections were well tolerated by the animals without any macroscopic sign of inflammation.

Hind limb weight distribution

To evaluate pain, we determined weight distribution over the hind limbs (Figure 1, top row). Rats loaded both hind limbs equally at the start of the experiments: the limbs that later received MIA bore 50.6 ± 1.6 % of the weight and the contralateral limbs 49.4 ± 1.6 % (mean \pm SD). Three weeks after MIA injection, weight distributed to the affected leg was significantly reduced compared to baseline (45.9 ± 6.1 % vs 50.6 ± 1.8 %, $P=0.002$, mean \pm SD) (Figure 1A), indicating pain sensation. No differences were observed between the treatment groups at this

timepoint ($P = 0.937$), pointing towards a random distribution of MIA induced pain. Two weeks after treatment, no significant differences in weight distribution were observed in any of the treatment groups (data not shown). Four weeks after treatment, the group treated with MSCs was the only group that had significantly more weight distributed to the affected limb after treatment than pre-treatment ($51.2 \pm 5.0\%$ vs $46.5 \pm 4.1\%$, $P = 0.003$, mean \pm SD) (Figure 1B-D).

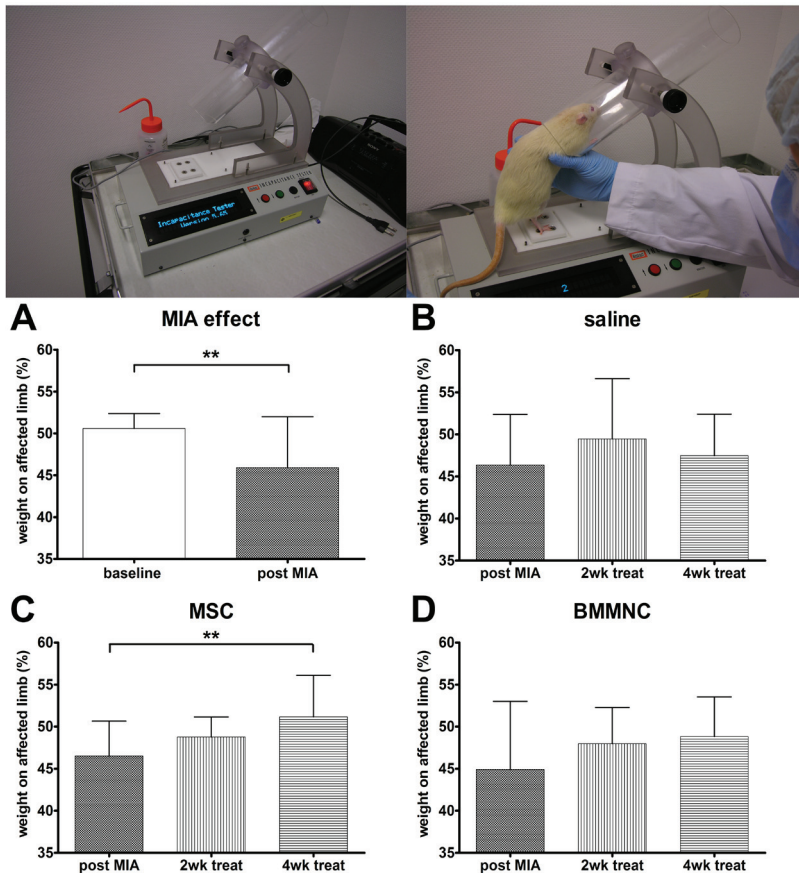


Figure 1: Assessment of hind limb weight distribution. Hind limb weight distribution was determined as an index of joint discomfort (upper row). MIA caused a reduction of weight distributed to the affected limb (A). Rat MSC injection was the only treatment that caused a significant increase in weight distributed on the OA limb (B-D), $*** P < 0.001$.

Structural integrity: cartilage quality, subchondral bone alterations and synovial inflammation

μ CT arthrography was used to assess loss of cartilage volume elicited by the MIA injection as a measure of cartilage quality before cell therapy. MIA injected knees displayed a smaller

cartilage volume than control knees ($0.48 \pm 0.15 \text{ mm}^3$ vs $0.82 \pm 0.17 \text{ mm}^3$, $P < 0.001$, mean \pm SD, data not shown). This volume depletion as measured by μ CT arthrography is a combination of cartilage matrix loss as well as GAG depletion, thereby representing both these aspects of cartilage damage¹⁵⁷. Cartilage volume did not differ between the MIA injected knees of the different treatment groups ($P = 0.929$), indicating a random distribution of cartilage damage before application of the treatment.

Cartilage damage at the end of the experiments was measured on histology with a semiquantitative score for GAG loss and structural damage. Cartilage damage was most pronounced in the patellofemoral region and all presented data reflect this compartment. For this compartment the scores of the patella and the trochlea were summed up, leading to a score range for GAG loss from 0 to a maximum loss of 32 and a score range for structural damage from 0 to a maximum damage of 48. MIA injected knees showed more GAG loss than non-MIA injected knees ($24.0 (0.0 - 32.0)$ vs $1.5(0.0 - 2.0)$, $P < 0.001$, range (95 % CI)) (**Figure 2A-B**, top row). No significant differences were observed between the treatment groups ($P = 0.393$). Structural cartilage damage was significantly present in MIA injected knees versus control knees ($4.4 (0.0 - 8.5)$ vs $1.3 (0.0 - 2.2)$, $P < 0.001$, range (95 % CI)) (**Figure 2C**). Between the different treatment groups, no statistically significant differences were found ($P = 0.959$).

Ex vivo μ CT was used to evaluate trochlear subchondral bone porosity and thickness after treatment. Overall, MIA injected knees had a significantly more porous ($6.3 \pm 6.2 \%$ vs $2.0 \pm 0.8 \%$, $P < 0.001$, mean \pm SD) and thinner ($221.1 \pm 29.4 \mu\text{m}$ vs $253.8 \pm 19.1 \mu\text{m}$, $P = 0.005$, mean \pm SD) subchondral plate than control knees (**Figure 2D-F**, middle row), which is in concordance with previously reported early OA related changes^{29, 35, 378}. No statistically significant differences between treatment groups were observed regarding porosity ($P = 0.208$) or subchondral plate thickness ($P = 0.607$).

Synovial inflammation was evaluated by measuring synovial thickness at the parapatellar recesses and ranking the samples based on synovial fibrillation and cellular infiltration (Fig 2G-I (lower row)). MIA injected knees had a thicker synovium ($730.4 \pm 94.8 \mu\text{m}$ vs $601.6 \pm 32.6 \mu\text{m}$, $P < 0.001$, mean \pm SD) and inflammation was ranked higher ($24.5 (5.0 - 40.0)$ vs $5.0 (1.0 - 12.0)$, $P < 0.001$, range (95 % CI)) than control knees without MIA. No significant differences were observed between treatment groups for synovial thickness ($P = 0.115$) or inflammation ranking ($P = 0.111$).

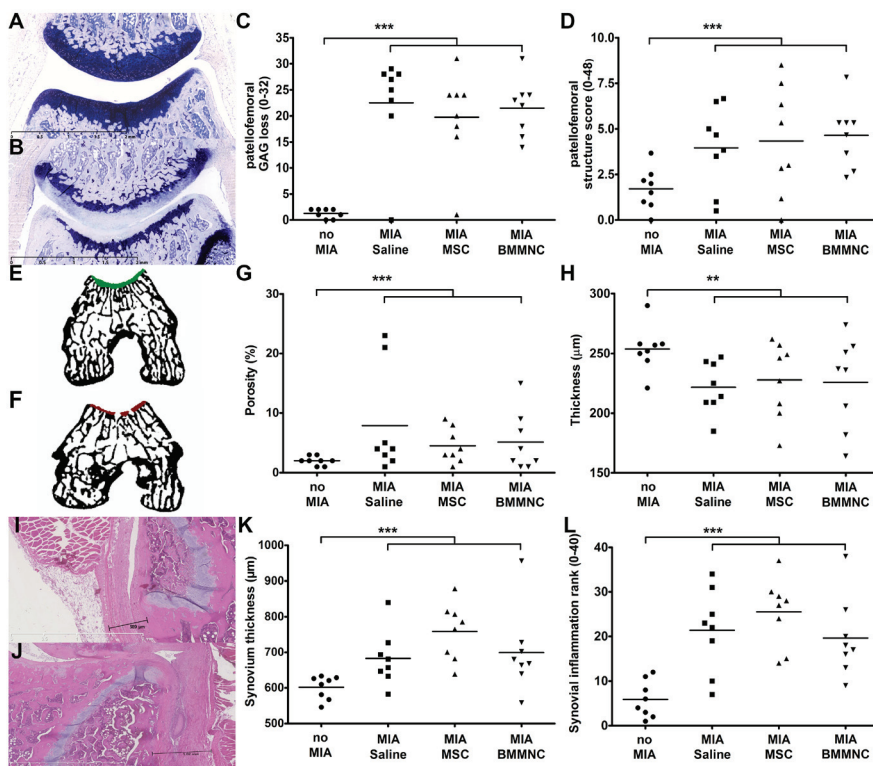


Figure 2: Structural integrity: cartilage quality, subchondral bone alterations and synovial inflammation. Thionin staining demonstrated evident GAG loss and mild structural cartilage damage in MIA injected knees compared to contralateral control knees (A-C, upper row). No significant differences between treatment groups were found. μ CT analyses displayed increased porosity and thinning of trochlear subchondral bone plates in MIA injected animals compared to contralateral control knees (D-F, middle row). Between the treatment groups, no significant differences were observed. Hematoxylin eosine staining illustrating increased synovial thickness, fibrillation and subsynovial cellular infiltration in MIA injected knees compared to contralateral control knees (G-I, lower row). No significant differences between treatment groups were found. *** $P < 0.001$. Magnification A and G upper row 25 x, magnification G lower row 100x, ** $P < 0.005$, *** $P < 0.001$.

Cell tracking experiments

MR images confirmed intra-articular localisation of injected SPIO-Fluc MSCs by the presence of signal voids in the joint space (Figure 3A). BLI signal of injected MSCs could be clearly observed in the knee joints (Figure 3B), and increased up to three days to a 5.3-fold increase in OA knees and a 5.7 fold increase in healthy knees (Figure 3C). From day 3 onwards, a gradual decrease of the BLI signal occurred and after three weeks the signal became undetectable in three of the six knees and was near detection limit in the other three knees. None of the time-points displayed a clear difference in OA and healthy joints.

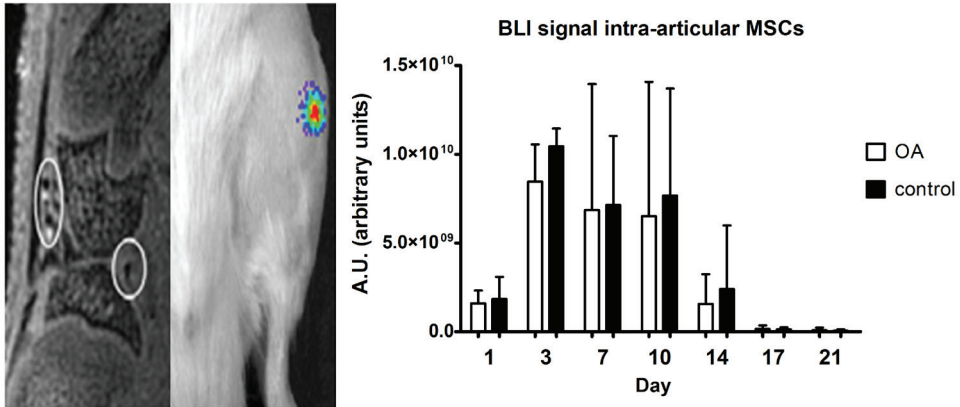


Figure 3: Cell tracking experiments. Injected SPIO-Fluc MSCs were found in the joint space by MRI (A). BLI signal of injected MSCs showed the presence of viable cells in the knee joints (B). This signal increased up to three days and thereafter gradually decreased till the end of the study period (C). None of the time-points indicated a clear difference in OA and healthy joints.

DISCUSSION

MSCs are promising candidates for OA treatment since they have chondrogenic potential, as well as a function in immunomodulation and tissue regeneration by the secretion of soluble factors³⁷⁹. We compared the effects of intra-articular injected cultured rat MSCs and BMMNCs on pain, in addition to inflammation and structural damage in a rat OA model *in vivo*. The MSC treated group, but not the BMMNC or the saline treated group, significantly increased loading of the affected limb after treatment, indicating a decrease in pain sensation. Nevertheless, no significant difference between the different treatment groups on any of the structural outcome measures were found.

The effects of MSC therapy on pain or other clinical outcome measures are difficult to assess in animal OA studies, and therefore they are not extensively documented. To date, two studies describe the influence of MSCs on pain and range of motion in large animal OA models, with conflicting results. Black et al. reported an improvement in lameness, pain on manipulation and range of motion in dogs treated with adipose derived MSCs compared to placebo for naturally developed hip³⁸⁰. Frisbie et al. on the other hand, found no improvement in pain and range of motion after bone marrow derived MSC treatment in a horse OA model of the middle carpal joint³⁶⁵. These different findings could be due to many causes, including differences in used cell types, cell culture protocols or OA models. Additionally, pain is a complicated phenomenon because of the existence of different pain phenotypes and their different mechanisms, including inflammatory and neuropathic pain³⁸¹. In animal studies, pain can be evaluated indirectly, using for instance weight bearing or gait analyses, or directly by assessing for instance paw

withdrawal threshold in response to mechanical or thermal stimuli³⁸². Our findings show a significant decrease in pain, as measured by an increased weight bearing of the affected limb, after intra-articular application of MSCs. Further evaluation on multiple pain aspects is needed to assess the efficacy of MSC as a therapy to alleviate pain in clinical OA.

One of the goals of our study was to compare the efficacy of cultured MSCs and freshly isolated BMMNCs in their OA modifying capacity. No severe adverse effects were observed in our study after intra-articular application of allogeneic rat MSCs or allogeneic rat BMMNCs. Albeit MSCs have been previously described to be immune privileged^{379, 383}, more recent reports show that MSCs maintain a degree of immunogenicity that may limit their longevity and attenuate their advantageous effects³⁸⁴⁻³⁸⁶. This could also explain the limited cell survival we observed three weeks after injection in our BLI experiments. We found no macroscopic signs of inflammatory responses in the (sub)acute phase after cell injections, indicating that they did not induce a substantial immune response. Nevertheless, we cannot rule out that the MSCs used in this study elicited a mild immunological reaction given their non-autologous origin. This might counteract possible favorable effects of these cells, resulting in mild overall treatment effects or the fact that the pain reduction was only observed at the four week time point.

We used a mild OA model since we hypothesized that a fully degenerated joint would be beyond the repair capacity of cellular therapies. A disadvantage of this approach is that at the moment of cell injections, not all animals had developed evident OA-like characteristics on μ CTa. After excluding animals without MIA-induced cartilage damage at the moment of treatment (four animals in total), the possible beneficial effects of MSC compared to saline became more pronounced for all outcome measures, albeit they still did not reach statistical significance, possibly due to the reduced power (data not shown).

Previous studies have shown positive effects of intra-articular injected MSCs on cartilage quality in various animal models^{356, 363, 387}. These studies used surgical OA models with a joint instability component. Two of these reports used cell tracking and showed homing of the cells mainly to the damaged structure and the synovium^{356, 363}. This indicates an indirect protective effect of the MSCs and does not point towards actual regeneration of cartilage. The fact that there was no joint instability component in our model which could have been attenuated by MSCs, could explain the modest effects on joint structures of our cellular treatments. This is in accordance with Frisbie et al., who found no effect of MSCs on cartilage quality in a horse osteochondral defect OA model³⁶⁵. In addition, Matsumoto et al. found just a trend towards improved cartilage quality after injection of muscle-derived stem cells (MDSCs) in a rat MIA OA model³⁶². The effects of MDSCs became only clear after they were transduced with bone morphogenetic protein 4 and sFlt-1, a vascular endothelial growth factor antagonist. We used an OA model affecting the entire joint without mechanical instability, in that way resembling the

majority of clinical OA patients. The fact that in such models repeatedly modest effects of stem cell therapies on joint structures are reported and that the effects are increased after genetic cell manipulation indicates that further optimization is required before large scale clinical application can be considered.

Another factor influencing the effect of MSCs could be the time of injection. We injected our cell preparations three weeks after induction of OA, after the inflammatory phase of the MIA model had ceased. Although MSCs are known to have immunosuppressive capacities³⁷⁹, MSCs need stimulation in order to exert their immunosuppressive role^{388, 389}. Possibly, the amount of inflammation in our model did not elicit an immunomodulatory MSC function, thereby minimizing potential beneficial effects.

The capacity of intra-articular injected MSCs to regenerate cartilage in defects or to limit cartilage damage in surgical OA models with a joint instability component has been demonstrated by others^{356, 359-361, 363, 364, 387, 390, 391}, indicating the potential of this strategy for joint diseases. In the current study, animals treated with MSCs significantly increased loading of their affected limb 4 weeks after cell injections, indicating a reduced pain sensation. The fact that we did not observe clear effects on the other outcome measures in our study could have many causes including the use of a mild OA model, the absence of apparent inflammation upon time of injection or the fact that we used non-autologous cells. Further optimization could make use of selection or pre-treatment of MSCs³⁹² to generate subpopulations which are most suitable for modifying OA processes. Since OA is a multifactorial disease consisting of many simultaneous processes, assessment of the effect of cellular therapies on various pain aspects, as well as structural joint aspects and joint inflammation in multiple OA models is essential in reaching these goals.

ACKNOWLEDGEMENTS

We acknowledge Anne-Marie Zuurmond, Angela Koudijs and Koen van der Mark (TNO, Leiden, the Netherlands) for providing the incapitance tester and their help in ascertaining its use; Erik Lubberts (Erasmus MC, Rotterdam, the Netherlands) for his recommendations in assessing synovial inflammation; Jamal Guenoun and Alessandro Ruggiero for their help with BLI experiments; and Sylvia van Buul for critically reviewing the manuscript. Furthermore, the authors gratefully acknowledge the support of the Smart Mix Program of the Netherlands Ministry of Economic Affairs and the Netherlands Ministry of Education, Culture and Science (SSM06004).

CHAPTER 10

CLINICALLY APPLIED CT ARTHROGRAPHY TO MEASURE THE
SULFATED GLYCOSAMINOGLYCAN CONTENT OF CARTILAGE

*M. Siebelt, J. van Tiel, J.H. Waarsing, T.M. Pijpers, M. van Straten, R. Booijs,
M.L. Dijkshoorn, G.J. Kleinrensink, J.A.N. Verhaar, G.P. Krestin, H. Weinans, E.H. Oei*
Osteoarthritis Cartilage. 2011Oct;19(10):1183-9

ABSTRACT

Objective

Similar to delayed gadolinium enhanced MRI of cartilage, it might be possible to image cartilage quality using CT arthrography (CTa). This study assessed the potential of CT arthrography as a clinically applicable tool to evaluate cartilage quality in terms of sulfated glycosaminoglycan content (sGAG) and structural composition of the extra-cellular matrix (ECM).

Methods

Eleven human cadaveric knee joints were scanned on a clinical CT scanner. Of each knee joint, a regular non-contrast CT (ncCT) and a ioxaglate injected CTa scan were performed. Mean X-ray attenuation of both scans were compared to identify contrast influx in seven anatomical regions of interest (ROI). All ROIs were rescanned with contrast-enhanced μ CT, which served as the reference standard for sGAG content. Mean X-ray attenuation from both ncCT and CTa were correlated with μ CT results and analyzed with linear regression. Additionally, residual values from the linear fit between ncCT and μ CT were used as a covariate measure to identify the influence of structural composition of cartilage ECM on contrast diffusion into cartilage in CTa scans.

Results

CTa resulted in higher X-ray attenuation in cartilage compared to ncCT scans for all anatomical regions. Furthermore, CTa correlated excellent with reference μ CT values (sGAG) ($R=0.86$; $R^2=0.73$; $p<0.0001$). When corrected for structural composition of cartilage ECM, this correlation improved substantially ($R=0.95$; $R^2=0.90$; $p<0.0001$).

Conclusions

Contrast diffusion into articular cartilage detected with CTa correlates with sulfated glycosaminoglycan content and to a lesser extent with structural composition of cartilage ECM. CTa may be clinically applicable to quantitatively measure the quality of articular cartilage.

INTRODUCTION

The current reference standard for osteoarthritis (OA) staging is the Kellgren and Lawrence score based on knee radiography⁹⁴. However, this technique is not sensitive enough to detect OA at an early stage. Sulfated glycosaminoglycan (sGAG) is a key molecule in articular cartilage and its content is an indicator of cartilage health¹⁰³. Loss of sGAG from the articular cartilage is a hallmark of early OA and occurs well before OA is detected radiographically^{182, 393}.

Micro computed tomography (μ CT) used together with a negatively charged contrast agent (ioxaglate) is a well established technique to image sGAG-distribution in cartilage^{113, 116, 394}. The technique is comparable to delayed gadolinium enhanced magnetic resonance imaging of cartilage (dGEMRIC)⁹⁸⁻¹⁰¹. Previous *in vitro* work has shown that there is a clear inverse relationship between the amount of ioxaglate in the cartilage measured with μ CT and the negatively charged sGAG content of the cartilage measured with biochemical essays ($R^2 = 91-94\%$)^{113, 394}, and histology ($R^2 = 77\%$)¹¹⁴. *In vivo* research in small animals has also demonstrated that μ CT arthrography is able to accurately measure changes in cartilage quality^{115, 157}.

In humans, CT arthrography (CTa) using intra-articular injected contrast agent is an established clinical technique for imaging of knee abnormalities^{395, 396}. However, it is solely used for detection of morphologic derangements rather than assessment of cartilage sGAG content. In this cadaver study we determined whether it is possible to quantitatively measure the sGAG content of human articular cartilage with a clinical CT system, after intra-articular injection of a contrast agent. We also investigated to what extent the contrast influx into cartilage is influenced by the structural composition of the extra-cellular matrix (ECM).

METHODS

Cadaver specimens

Thirteen cadaveric lower extremities from eleven individuals who had donated their bodies to science (seven female, four male; mean age at death 74 years, age range at death 30 - 96 years) were available. All extremities were freshly frozen at -20°C until start of the experiment. Prior to first imaging, all specimens were slowly defrosted in a cooled environment (7°C) for 5 days. All extremities were at room temperature during imaging.

Acquisition and post-processing of non-contrast CT and CT arthrography data

Non-contrast CT (ncCT) was performed of all knee joints using a second generation dual source multidetector spiral CT scanner (SOMATOM Definition Flash, Siemens Healthcare AG, Erlangen, Germany) with a tube voltage of 80kV and an effective mAs-value of 3140. Scan time per ncCT was approximately 30 seconds per scan. All specimens were scanned in the standard

anatomic axial plane. All scans were reconstructed with an effective slice thickness of 0.75 mm and a sharp reconstruction kernel (B75s). Multiplanar reconstruction was performed (image pixel size 0.265mm) (Figure 1A-C).

Immediately after ncCT, 20ml of 30% ioxaglate solution (diluted in saline) (Hexabrix 320, Mallinckrodt, Hazelwood, MO, USA)³⁹⁶ was injected intra-articularly using a 18 gauge needle. All knees were flexed (~120°) and extended (~0°) for 5 minutes in order to achieve optimal distribution of the contrast agent throughout the joint. Ten minutes after contrast injection, all knees were rescanned using the same CT scanner, scanning parameters (30 seconds/scan), and reconstruction methods (Figure 1D-F).

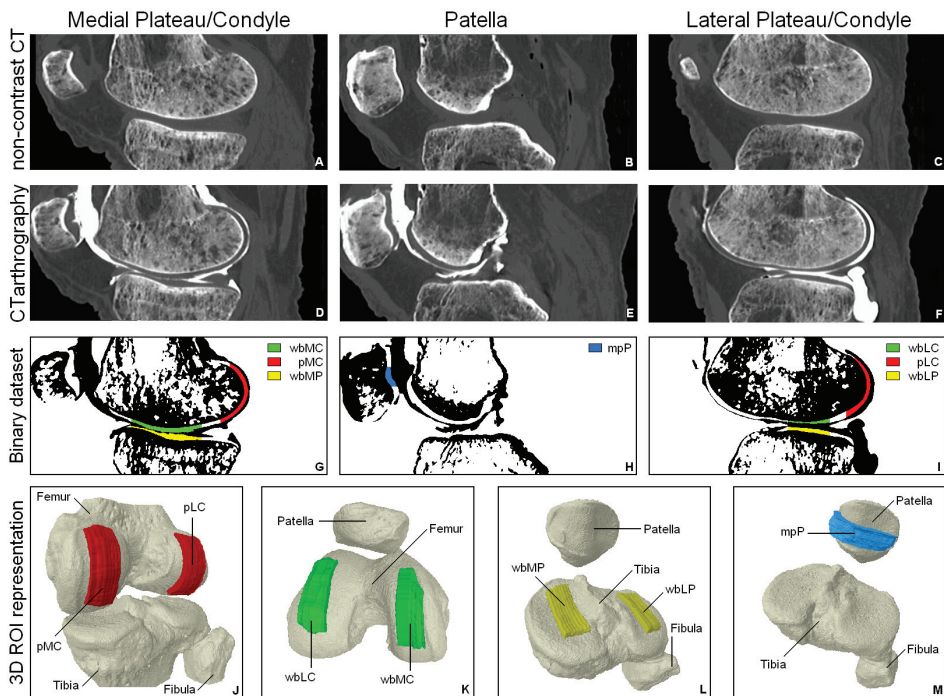


Figure 1: Representative sagittally reconstructed images of a knee joint from non-contrast CT (ncCT) (A-C) and after intra-articular contrast injection for CT arthrography (CTa) (D-F), after segmentation into a binary dataset showing the definition of the regions of interest. (G-I), and a 3D representation of all seven analyzed ROIs (J-M): weight-bearing medial and lateral condyle (wbMC/wbLC; posterior medial and lateral condyle of the femur (pMC/pLC); weight-bearing medial and lateral plateau of the tibia (wbMP/wbLP); mid portion of patellar cartilage (mpP).

All scans were converted into binary datasets using one fixed attenuation threshold (430 Hounsfield units) that was selected visually to render the best possible segmentation of cartilage in all datasets (Figure 1G-I and Figure 2)¹¹⁵. Using analysis software (Skyscan, Kontich, Belgium),

per knee seven regions of interest (ROIs) were manually defined. Each cartilage ROI extended over 40 contiguous sagittal slices. These cartilage ROIs consisted of the central weight-bearing area of both medial and lateral femoral condyles (wbMC and wbLC), the posterior non-weight bearing area of both femoral condyles (pMC and pLC), both weight-bearing medial and lateral tibial plateaus (wbMP and wbLP) and the mid-portion of patellar cartilage (mpP) (Figure 1G-M). Anterior margins of the weight-bearing femoral condyles and tibial plateaus were defined at the level of the posterior aspect of the anterior meniscal horn. The posterior margins were defined at the level of the anterior aspect of the posterior meniscal horn. The posterior non-weight bearing femoral condyle ROI extended backward from the level of the dorsal margin of the posterior meniscal horn. We calculated the mean X-ray attenuation of cartilage in these ROIs on non-contrast and contrast-enhanced clinical CT scans.

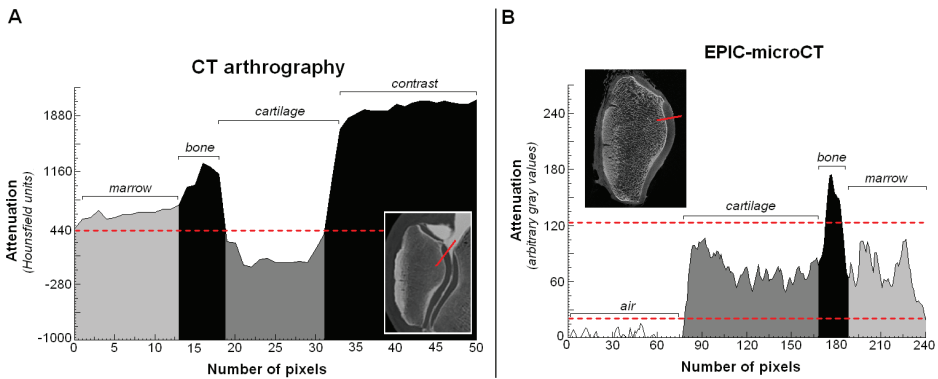


Figure 2: Profile line through different structures (red line in insert) of both CT arthrography (A) and EPIC-microCT (B). On the x-axis subsequent pixels in the profile line are represented, the y-axis indicates the attenuation values of these pixels. With the red dotted line, we have visualized the level of our selected thresholds per technique (CT arthrography <430 Hounsfield units; EPIC-microCT >25 and <125 gray values).

Equilibrium partitioning of an ionic contrast agent using (EPIC)- μ CT

Because EPIC- μ CT has shown strong correlation with cartilage sGAG content, we selected this as our reference test for sGAG content of cartilage^{113, 114, 394}. In EPIC- μ CT an equilibrium-state exists between sGAG and contrast agent after a long incubation period. Due to the equilibrium, structural composition of the cartilage ECM³⁹⁷ does not influence the interaction between contrast and sGAG content of cartilage¹¹⁴.

After CTA, the knee joints were dissected into five parts: both medial and lateral femoral condyles, both medial and lateral tibial plateaus and the patella. Soft tissue was removed to a maximal extent, without harming cartilage integrity. In order to achieve equilibrium between the contrast agent and sGAG in cartilage, all dissected specimens were incubated in an ioxaglate contrast solution for 24 hours at room temperature^{137, 138, 398}. It is advocated to use the highest

possible concentration of contrast, allowing best cartilage segmentation to achieve highest sensitivity for changes in sGAG content^{114, 116}. We used a 20% solution of ioxaglate, which resulted in the best cartilage segmentation at the air/cartilage and bone/cartilage interfaces.

EPIC- μ CT was performed on a μ CT scanner (Skyscan1076, Skyscan, Kontich, Belgium). The following scan settings were used: isotropic voxel size of 35 μ m; a voltage of 55 kV; a current of 181 mA; field of view 68 mm; a 0.5 mm aluminum filter; 198° with a 0.4 degree rotation step. Scanning time per specimen was 6 - 10 hours, depending on the size of the specimen (condyle, plateau or patella) which was scanned. A plastic foil was wrapped around the specimen to avoid dehydration. All scans were performed using the same settings and all data were reconstructed identically.

Using Skyscan analysis software, these datasets were segmented using a fixed attenuation threshold between air (25 gray value) and subchondral bone (120 gray value) that was selected visually for the best segmentation result in all datasets. In all segmented μ CT datasets, similar ROIs of the cartilage regions corresponding with ROIs of the clinical CTa were drawn and the mean X-ray attenuation was calculated again. These μ CT based mean attenuation values were used as the reference for sGAG content against which the attenuation values on ncCT and CTa were compared.

Contrast diffusion influenced by structural composition of cartilage ECM

An important difference between the μ CT and CTa scans is that with μ CT scanning, the contrast agent and sGAG are partitioned at equilibrium. However, the principle of CTa is dependent on a diffusion process before equilibrium, which is influenced by the electrostatic interaction between sGAG and ioxaglate¹⁵⁷. Therefore, measurements from *non-equilibrium* CTa are also influenced by other factors than sGAG content alone^{137, 138, 398}. In particular, so-called tissue dragging influences the interaction between contrast and sGAG^{147, 148}. A high tissue drag results from an intact collagen network and is predominantly present in the top layers of healthy cartilage where collagen is densely packed parallel to the cartilage surface and acts as a barrier membrane^{399, 400}. Consequently, contrast diffusion goes slowly in regions with high tissue drag. When collagen is structurally impaired, e.g. in OA, tissue dragging diminishes and more contrast penetrates in comparison to healthy cartilage due to a higher diffusion rate.

In non-contrast CT, X-ray attenuation of cartilage results only from initial dissimilarities in cartilage composition (e.g. collagen, sGAG and water content). Together with the information on sGAG content from μ CT, the influence of this structural composition of the cartilage on CTa outcome was further investigated using statistical models.

Statistical analysis

To assess if the influx of contrast agent into the cartilage could be detected, we compared the attenuation values per anatomical region between ncCT and CTa scans with paired student's t-tests. To evaluate to what extent the attenuation values represented sGAG content, we fitted linear regression models of the mean X-ray attenuation values of both the ncCT and CTa to the results of μ CT scans for each knee compartment, of which we report the Pearson's correlation coefficients. To test if the correlation with μ CT was different between ncCT and CTa, we compared the slopes of both models. These analyses were performed using GraphPad (Graphpad Software Inc., San Diego, USA).

In this study we used thirteen knees from eleven individuals. The use of two knees from one individual could potentially lead to an overestimation of the correlation between μ CT and CTa measurements^{401, 402}. Exclusion of either one of the knees in the two patients that were scanned bilaterally did, however, not influence the results of our study. Therefore, we did not apply a statistical correction.

Next, we investigated to what extent the influx of contrast was influenced by structural composition of cartilage ECM itself. The spatial variation in X-ray attenuation inside cartilage from ncCT scans is related to both structural composition of cartilage ECM and its sGAG content. Thus, when ncCT attenuation values are fitted to μ CT values (representing sGAG content) using linear regression, the residuals, which is that part of the ncCT values which is not explained by μ CT, contain information on structural composition independent of sGAG content. When these residuals are subsequently added as a covariable to the linear regression model that relates CTa to μ CT values, the contribution of these residuals to the model represent the extent to which the influx of the contrast is influenced by structural composition of the cartilage ECM, independent of sGAG content. These analyses were performed using SPSS (SPSS Inc., Chicago, USA). All p-values < 0.05 were considered to be statistically significant.

RESULTS

Cadaver subjects

After CT scanning, three extremities were excluded from the study due to clearly visible calcifications inside the cartilage. Thus, a total of ten cadaveric knee joints from nine individuals were included in the analysis (six female, three male; mean age at death 69 years; age range at death 30 – 94 years). Furthermore, 12 cartilage ROIs were not included in our data analysis because of (motion) artefacts during μ CT scanning and segmentation errors because of severe cartilage loss¹⁵⁷.

sGAG correlation in ncCT and CTa

Mean X-ray attenuation results showed clear differences between the anatomical cartilage locations and between ncCT and CTa outcomes. In all locations, cartilage attenuation increased significantly after injection of contrast agent (Figure 3A).

Cartilage X-ray attenuation in ncCT correlated moderately with μ CT ($n=57$, $R=0.45$; $R^2=0.20$; $p=0.0003$). The correlation between cartilage X-ray attenuation from CTa scans and μ CT was strong ($n=57$, $R=0.86$; $R^2=0.73$; $p<0.0001$) (Figure 3B). The slopes of both regression lines were significantly different ($p < 0.0001$).

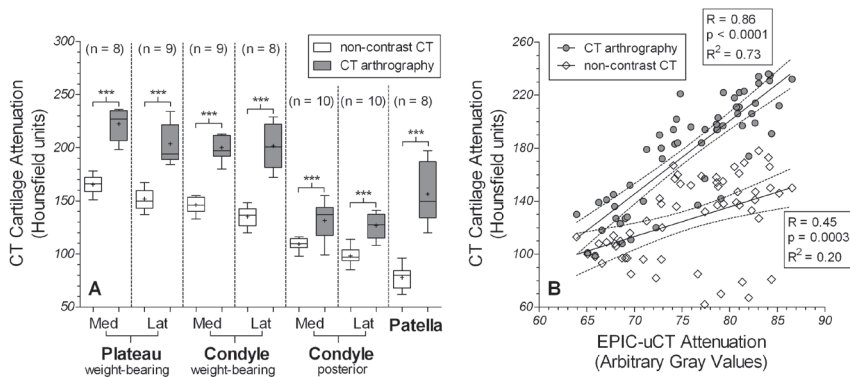


Figure 3: Contrast diffusion into cartilage. Comparison of cartilage attenuation between non-contrast CT (ncCT) and CT arthrography (CTa) scans. A: Box plot of mean attenuation in cartilage from CT and CTa scans per anatomical region. Boxes range from 25th to 75th percentile, whiskers run from min to max, the horizontal line in the box represents the median and the plus sign shows the mean. B: Correlated results of mean attenuation from EPIC- μ CT and clinical CT scans with and without injected contrast for all anatomical regions combined ($n = 57$). ***: $p < 0.0001$

sGAG content per anatomical location

The cartilage attenuation derived from CTa for all separate anatomical compartments correlated strongly with attenuation from μ CT (wbMP, wbLP: $n=17$, $R=0.89$, $R^2=0.79$, $p<0.0001$; wbMC, wbLC, pMC, pLC: $n=33$, $R=0.87$, $R^2=0.75$, $p<0.0001$; patella: $n=8$, $R=0.89$, $R^2=0.79$, $p=0.003$; Figure 4A-C). There was a clear trend for all posterior condyle regions to have lower mean attenuation values, indicating that less contrast penetrated this less weight-bearing cartilage. The patellar values were clustered in a different location than the values for the other anatomical regions. When the data was analyzed for the tibio-femoral cartilage, the correlation coefficient was 0.92 ($n=49$, $R^2=0.85$, $p<0.0001$, Figure 3D). When all regions (including mpP cartilage) were pooled, the correlation diminished slightly ($n=57$, $R=0.86$, $R^2=0.73$, $p<0.0001$, Figure 4E).

To display the spatial agreement of both techniques, Figure 5 shows representative images for cartilage attenuation for both CTa and μ CT.

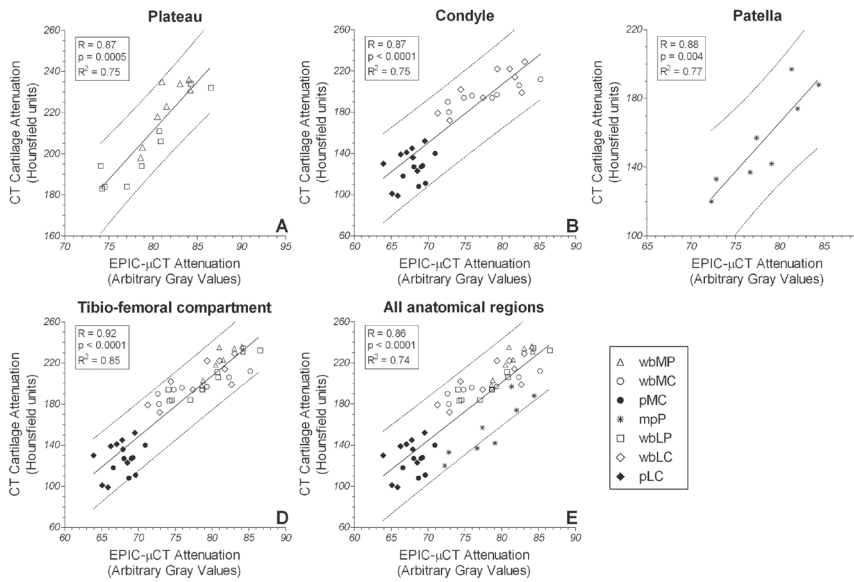


Figure 4: Correlation plots of mean attenuation from EPIC- μ CT and CT arthrography. A: weight-bearing cartilage of medial and lateral plateaus (n=17). B: weight-bearing and posterior cartilage of medial and lateral condyles (n=17). C: mid-portion of patellar cartilage (n=8). D: pooled results for both tibial and femoral compartments (n=49). E: pooled results for all regions of interest (n=57). The dashed lines indicate the 95% confidence interval of the best fit regression line. wbMP: weight-bearing medial plateau, wbMC: weight-bearing medial condyle, pMC: posterior medial condyle, mpP: mid-portion patella, wbLP: weight-bearing lateral plateau, wbLC: weight-bearing lateral condyle, pLC: posterior lateral condyle.

CTa corrected for structural composition of cartilage ECM

Figure 5 shows the results of the additional analysis into the role of structural composition of cartilage ECM for *non-equilibrium* CTa scans. When residual values from the model that fits μ CT to ncCT, which represents structural composition of the ECM independent of sGAG, were added as a covariate to the model that fits μ CT to CTa, the correlation coefficient was 0.95 (n=57, $R^2=0.90$; $p<0.0001$).

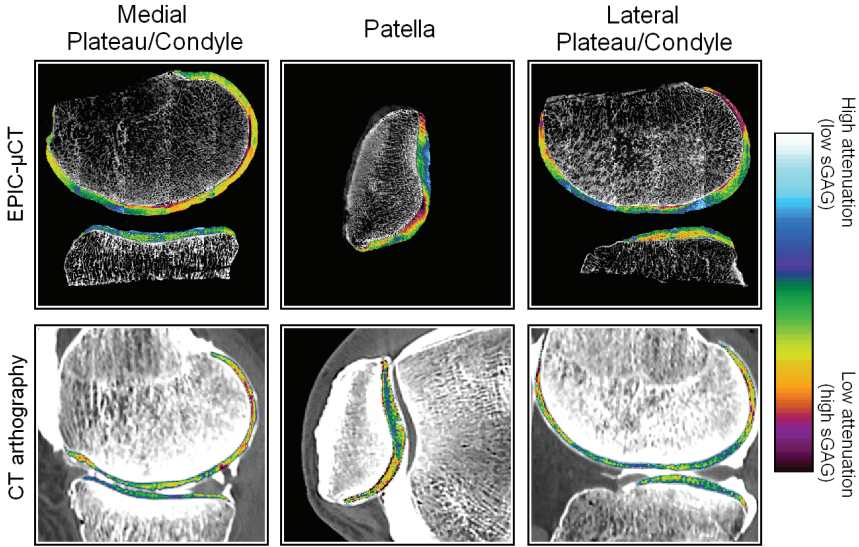


Figure 5: Images of both EPIC- μ CT and CT arthrography. The attenuation of cartilage regions is visualized in colour and representative for sGAG content. High levels of attenuation represent a low sGAG-distribution.

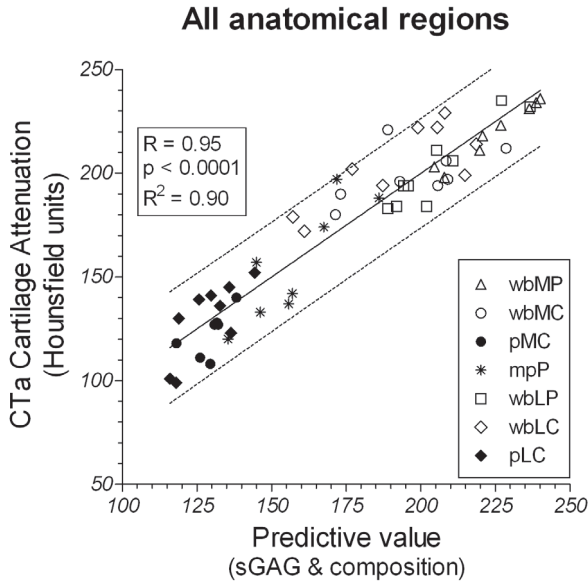


Figure 6: Predictive CT arthrography value (horizontal axis) based best fitted model from EPIC- μ CT (sGAG) and non-contrast CT residuals (cartilage ECM composition) correlated with mean attenuation of CT arthrography (vertical axis) ($n=57$). The dashed lines indicate the 95% confidence interval of the best fit regression line. wbMP: weight-bearing medial plateau, wbMC: weight-bearing medial condyle, pMC: posterior medial condyle, mpP: mid-portion patella, wbLP: weight-bearing lateral plateau, wbLC: weight-bearing lateral condyle, pLC: posterior lateral condyle.

DISCUSSION

Quantitative imaging techniques are of the utmost necessity for development and monitoring of treatment strategies targeted at early OA. Therefore, imaging techniques (e.g. like dGEMRIC) are extensively studied for their capability to measure sGAG content. This cadaver study demonstrates that cartilage attenuation from CTa is influenced by ioxaglate diffusion. And intra-articular injection of ionic ioxaglate significantly improved the correlation with the outcome of μ CT. These results are similar to previous non-clinical reports^{113, 138, 150}, supporting our hypothesis that CTa can be used as a quantitative surrogate measure of the cartilage sulfated-glycosaminoglycan content.

Patellar cartilage is known to have a different structural ECM composition^{403, 404}. In the μ CT and CTa scatter plot the patellar values were located differently than the other anatomical locations. Exclusion of patellar cartilage from our analysis improved the predictive value of CTa for sGAG content (R^2 from 73% to 85%), indicating that structural composition of cartilage ECM influences the outcome of *non-equilibrium* CTa. When residual ncCT values representing structural composition of cartilage ECM were combined with μ CT (sGAG content) as a predictive value for CTa, the R^2 values from the model fit to CTa increased from 73% to 90%. This improvement indicates to what extent contrast diffusion into cartilage is influenced by structural composition of cartilage ECM. In clinical practice, a correction for different contrast diffusion rates cannot be calculated, since a reference standard for sGAG like EPIC- μ CT is not available in clinical practice. Therefore, cartilage X-ray attenuation from CTa does not solely resemble sGAG content, but reflects a quality measure of cartilage which also concerns the structural integrity of the ECM.

Despite these encouraging results, there are limitations of CTa that need to be addressed. For example, the intra-articular injection introduces the risk of infection and also increases the risk of patient complaint of knee pain after injection. Furthermore, the high concentrations of ioxaglate used in this study, could influence cartilage electro-mechanical properties⁴⁰⁵.

CTa is best applied in early stages of OA, because with severe sGAG loss in advanced stages of OA segmentation errors will occur¹⁵⁷. Usually, early OA progression develops in relatively young patients and obviously the main concern with (repetitive) CT scans at a younger age is radiation exposure. The total dose of the scanning protocol in this study (~ 2 mSv)⁴⁰⁶ was ten times higher in comparison to previously defined radiation doses of routine knee CT scans (~ 0.2 mSv). More research is needed to determine whether the same correlation with sGAG content can be measured if radiation dose is reduced.

MRI uses no ionizing radiation and during the last years, has seen a rapid improvement with several newly developed MR-based imaging techniques to measure articular cartilage quality (e.g. dGEMRIC, Na²³ mapping, T2 mapping, and T1rho^{104, 105}). Thanks to the more widespread availability of 3.0 Tesla MR systems and the development of novel MRI sequences (e.g. Ultrashort TE¹⁰⁶, SSFP¹⁰⁷, UTE T2*¹⁰⁸, and DENSE-FSE¹⁰⁹), relatively fast MR scans can be acquired with high in plane resolution for (semi)quantitative cartilage imaging in OA research. However, these techniques still have several limitations: relative (e.g. claustrophobia) or absolute (e.g. pacemaker) contraindications for patients to undergo MRI, relatively low spatial resolution, and costs⁴⁰⁷.

Given our results in relation to previously reported outcomes of *in vivo* CT arthrography studies in small animals with an intact circulation^{115, 157}, we believe that CTa may be able to measure cartilage quality in human patients in a clinical setting. CT has a short scanning time (~30 seconds), generates images with a high isotropic resolution. Therefore, CT techniques may be a valuable alternative to MR techniques, but more research is needed for this technique to find its place in clinics and research.

In our opinion, research should first focus on optimizing the CTa protocol for clinical use. The reproducibility of CTa measurements should be evaluated in an *in vivo* environment in which all factors that influence CTa outcomes are present (intact circulation, muscle tension, joint capsule strength, etc). Future studies could also focus on the fact that recent *in vitro* studies indicate that X-ray attenuation of cartilage can predict certain biomechanical properties such as compressive stiffness¹⁵⁰. Our finding that CTa outcome is influenced by sGAG and structural composition of cartilage ECM could be used to predict the biomechanical function of articular cartilage with CT.

In conclusion, the results of this cadaver study demonstrate the proof-of-principle that CTa is able to measure cartilage quality in human knee joints. A wide implementation of this quantitative analysis of articular cartilage may detect early changes in OA patients and may contribute to the development of new treatment strategies.

ACKNOWLEDGEMENTS

We acknowledge the Dutch Arthritis Association (LLP11) and the SmartMix Program of the Netherlands Ministry of Economic Affairs and the Netherlands Ministry of Education, culture and Science for their financial support.

CHAPTER 11

CT ARTHROGRAPHY OF THE HUMAN KNEE TO MEASURE CARTILAGE
QUALITY WITH LOW RADIATION DOSE

*M. Siebelt, J. van Tiel, J.H. Waarsing, T.M. Piscaer, M. van Straten, R. Booi,
M.L. Dijkshoorn, G.J. Kleinrensink, J.A.N. Verhaar, G.P. Krestin, H. Weinans, E.H.G. Oei
Osteoarthritis Cartilage. 2012Jul;20(7):678-85*

ABSTRACT

Objective

Recently, CT arthrography (CTa) was introduced as a possible technique to quantitatively measure cartilage quality in human knees. This study investigated whether this is also possible using lower radiation dose CT protocols. Furthermore, we studied the ability of (lower radiation) CTa to distinguish between local sGAG content differences.

Design

Of ten human cadaveric knee joints, six CT scans using different radiation doses (81.33-8.13mGy) were acquired after intra-articular ioxaglate injection. The capability of CTa to measure overall cartilage quality was determined in seven anatomical regions of interest (ROIs), using EPIC- μ CT as reference standard for sGAG content. To test the capability of CTa to spatially distinguish between local differences in sGAG content, we calculated the percentage of pixels incorrectly predicted as having high or low sGAG content by the different CTa protocols.

Results

Low radiation dose CTa correlated well with EPIC- μ CT in large ROIs ($R=0.78$; $R^2=0.61$; $p<0.0001$). CTa can also distinguish between high and low sGAG content within a single slice. However, the percentage of incorrectly predicted quality pixels increases (from 35% to 41%) when less radiation is used. This makes it hard or even impossible to differentiate between spatial differences in sGAG content in the lowest radiation scans.

Conclusions

CTa acquired using low radiation exposure, comparable to a regular knee CT, is able to measure overall cartilage quality. Spatial sGAG distribution can also be determined using CTa, however for this purpose a higher radiation dose is necessary. Nevertheless, radiation dose reduction makes CTa suitable for quantitative analysis of cartilage in clinical research.

INTRODUCTION

The current reference standard for grading the severity of osteoarthritis (OA) in the knee is the radiography based Kellgren and Lawrence score⁹⁴. This technique is, however, not sensitive enough to detect or follow OA at an early stage of the disease because it only indirectly visualizes the cartilage and is not able to (semi)quantitatively measure cartilage quality⁴⁰⁸. Therefore, sophisticated magnetic resonance imaging (MRI) imaging techniques have been developed which can qualitatively measure cartilage quality in terms of the sulfated glycosaminoglycan (sGAG), collagen or sodium content of articular cartilage^{104, 182, 409}.

Recently, it has been shown that CT arthrography of the knee (CTa) is able to measure overall cartilage quality in large anatomical cartilage regions in human cadaveric knees⁴¹⁰. Similar to μ CT (μ CT) arthrography in small animals^{115, 157} and delayed gadolinium enhanced MRI of cartilage (dGEMRIC) in humans^{98, 411, 412}, this technique uses the inversed relationship between a negatively charged contrast agent (ioxaglate) and the sGAG content of cartilage.

The reported CTa protocol has a CT-Dose Index (CTDIvol) of 81.33 mGy per CTa scan, which poses a limitation on this technique⁴⁰⁶. Therefore, the radiation dose must be reduced before CTa can be used in clinical research. The use of less radiation to acquire CT scans results however, in an increase of noise in the reconstructed CT images. This increase of noise may influence the measured X-ray attenuation values and therefore interfere with the capability of measuring quality of cartilage using CTa.

Therefore, we designed a cadaver study with the purpose to investigate the effect of radiation dose reduction of CTa on its ability to measure articular cartilage quality in large cartilage regions. We also assessed the capability of CTa to distinguish between spatial high and low sGAG content of cartilage on a single slice and the influence of radiation dose reduction on this capability. The latter is of interest because it could enable the use of CTa as a tool to diagnose (focal) cartilage defects and follow the repair in these defects over time.

METHODS

Cadaveric knee joints

For this study, we used ten randomly selected cadaveric lower extremities from eight individuals who had donated their bodies to science. All extremities were frozen at -20°C directly after death. Before the start of the experiment, the specimens were defrosted slowly in a cooled environment (7°C) for five days. All extremities were at room temperature during imaging procedures.

Acquisition and post-processing of CT arthrography data

We injected 20 milliliters of 30% ioxaglate dilution (Hexabrix 320, Mallinckrodt, Hazelwood, MO, USA and saline) intra-articularly in all knee joints, using an 18 gauge needle. After the injection, we flexed ($\sim 120^\circ$) and extended ($\sim 0^\circ$) the knee joints for five minutes in order to achieve optimal distribution of the contrast agent throughout the joint cavity. Ten minutes after contrast injection, CTa scans of all knee joints were acquired using a second generation dual source multidetector spiral CT scanner (SOMATOM Definition Flash, Siemens Healthcare AG, Erlangen, Germany) with a tube voltage of 80 kV, an effective mAs value of 3140 mAs, a pitch of 0.35 and a collimation of 32×0.6 mm, resulting in a CTDIvol of 81.33 mGy⁴¹⁰. This protocol will be referred to as maximum dose in this paper. Directly after the first scan, five additional scans were acquired using the same tube voltage (80kV), but with reduced radiation exposures: 1570 mAs (50%), 1256 mAs (40%), 942 mAs (30%), 628 mAs (20%) and 314 mAs (10%) per scan. All knee joints were scanned in the axial plane with a scanning time of 30 seconds per scan. All CT datasets were reconstructed with an effective slice thickness of 0.75 mm and a sharp reconstruction kernel. Multiplanar reconstruction was performed (image pixel size 0.265mm).

Using Skyscan analysis software (Skyscan, Kontich, Belgium), we segmented all CT datasets into binary datasets using one fixed attenuation threshold of 500 Hounsfield units (HU) that was selected because it resulted in the best segmentation of the cartilage⁴¹⁰. Next, we manually defined seven anatomical cartilage regions of interest (ROIs) in all CT datasets based on the nomenclature and scheme as suggested by Eckstein *et al.*⁴¹³. Each ROI consisted of 40 consecutive slices covering the central weight bearing area of the cartilage of both the medial and lateral femoral condyles (wbMC and wbLC), the posterior non-weight bearing cartilage area of both femoral condyles (pMC and pLC), both weight bearing medial and lateral tibial plateaus (wbMP and wbLP) and the mid-portion of the patellar cartilage (mpP) (Figure 1A-C). After defining all ROIs, we calculated the mean X-ray attenuation per cartilage ROI on the CTa scans.

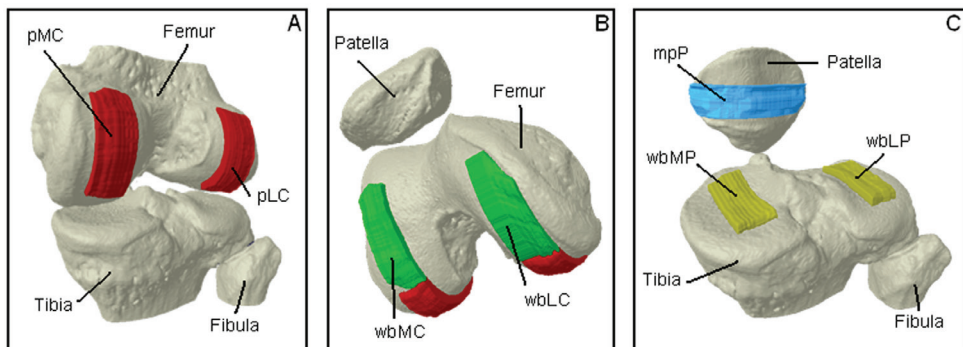


Figure 1: 3D representation of the seven analyzed large cartilage ROIs per knee joint: (A) posterior medial and lateral condyle of the femur (pMC/pLC); (B) weight-bearing medial and lateral femoral condyle (wbMC/wbLC); (C) weight-bearing medial and lateral plateau of the tibia (wbMP/wbLP) and mid portion of patellar cartilage (mpP).

Equilibrium partitioning of an ionic contrast agent using μ CT

Mean X-ray attenuation values of equilibrium partitioning of an ionic contrast agent using (EPIC)- μ CT have a good correlation with the sGAG content of articular cartilage measured with a dimethylmethylene blue essay or quantified with optical density measurements^{113, 114, 394}. Therefore, we selected the outcomes of EPIC- μ CT in mean X-ray attenuation values as our reference test of sGAG content of articular cartilage.

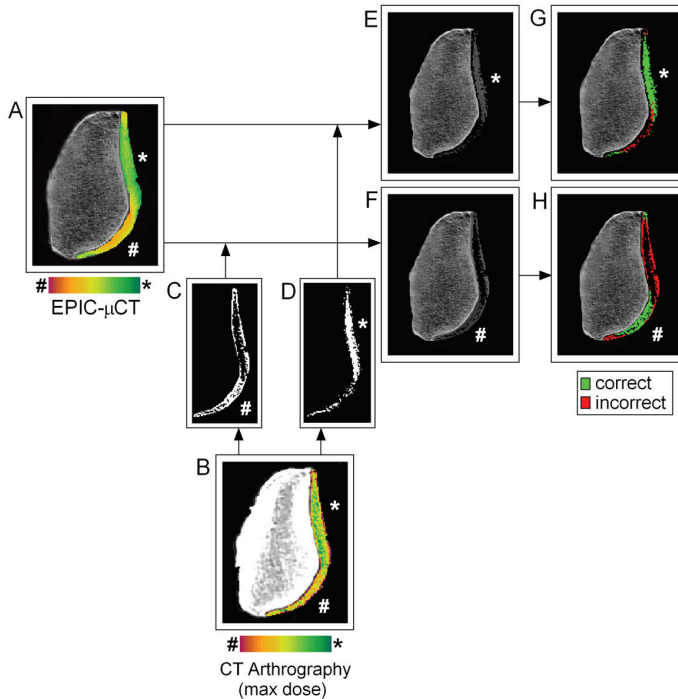


Figure 2: EPIC- μ CT datasets are used as reference for the spatial sGAG distribution of cartilage (A). Using a fixed X-ray attenuation threshold of 150 Hounsfield Units in all CTa datasets (B, only maximum radiation dose shown), a mask for high and low sGAG content was created (C-D). The masks were used as an overlay of EPIC- μ CT cartilage (E-F). Within the masked EPIC- μ CT images, the number of pixels correctly and incorrectly predicted as having a high and low sGAG content by CTa was calculated (G-H). #: high sGAG content. *: low sGAG content.

After CTa, all knee joints were dissected into five parts: the medial and lateral femoral condyles, the medial and lateral tibial plateaus and the patella. Soft tissue was removed to a maximal extent, without harming the integrity of the cartilage. In order to achieve equilibrium between the contrast agent and the sGAG content of the cartilage, all dissected specimens were incubated in an ioxaglate dilution (Hexabrix 320, Mallinckrodt, Hazelwood, MO, USA and saline) for 24 hours at room temperature^{137, 138, 398}. We used a 20% dilution of ioxaglate, which resulted in the best cartilage segmentation at the air/cartilage and bone/cartilage interfaces⁴¹⁰.

μ CT scans were performed on a Skyscan 1076 *in vivo* μ CT scanner (Skyscan, Kontich, Belgium). The following scan settings were used: isotropic voxel size of 35 μ m; a voltage of 55 kV; a current of 181 mA; field of view 68 mm; a 0.5 mm aluminum filter; 198° with a 0.4 degree rotation step⁴¹⁰. Scanning time per specimen was 6 - 10 hours, depending on the size of the specimen (patella, plateau or condyle). A plastic foil was wrapped around the specimen to avoid dehydration during scanning. All scans were performed using the same settings and all data were reconstructed identically.

Using Skyscan analysis software, we segmented the μ CT datasets using a fixed attenuation threshold between air and subchondral bone that was selected visually for the best segmentation result in all datasets⁴¹⁰. In all segmented μ CT datasets, seven anatomical ROIs of the cartilage corresponding with ROIs of the CTa were drawn manually and the mean X-ray attenuation per ROI was calculated.

Spatial analysis of cartilage quality

Using commercially available software (Matlab version 7.1, MathWorks, Natick, MA, USA and Multimodality Image Registration using Information Theory (MIRIT), Laboratory for Medical Imaging Research, Leuven, Belgium⁴¹⁴), all CTa (50%, 40%, 30%, 20% and 10%) and EPIC- μ CT datasets were registered using the dataset that was acquired at the maximum dose as reference. Registration of the datasets enabled comparison of corresponding cartilage regions (femoral condyles, tibial plateaus and patellar cartilage) in all CTa scans per knee.

To study the capability of CTa to analyze the spatial distribution of high and low sGAG content in cartilage and the influence of radiation dose reduction on this capability, we used the EPIC- μ CT as reference standard for spatial sGAG distribution in cartilage (**Figure 2A**)^{113, 114, 394}. Using Skyscan analysis software, we defined an area of high and low sGAG content in the cartilage within a central slice through the medial and lateral tibiofemoral joint and on a central slice of the mid-portion of the patellar cartilage in all CTa datasets (maximum dose, 50%, 40%, etc.) (**Figure 2B-D**). To define these areas (which we will refer to as masks from now on), we used 150 HU as cut-off point between high and low sGAG content of cartilage. We used this number based on the point where the cumulative histogram of all cartilage ROIs used in the spatial analysis of cartilage reaches 50% (**Figure 3**). Next, both masks for sGAG distribution were used as an overlay for cartilage on the registered corresponding EPIC- μ CT images (**Figure 2E-F**). Within the masked EPIC- μ CT images, we calculated the number of pixels defined as having high or low sGAG content by CTa, using a threshold of 70 gray values for EPIC- μ CT. This was again based on the cumulative histogram of all cartilage ROIs on the EPIC- μ CT images (**Figure 3**). Finally, we calculated the number of pixels which were incorrectly defined as high or low quality by CTa by adding the number of incorrectly defined pixels in both masks, dividing them by the total number of pixels in both masks together and then multiplying them by 100 to obtain the percentage of incorrectly defined pixels (**Figure 2G-H**).

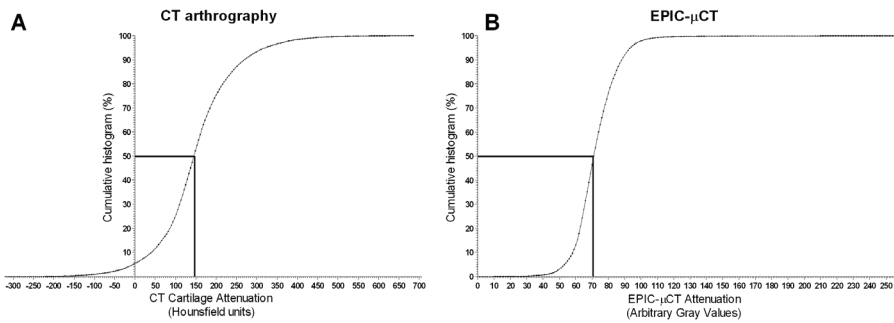


Figure 3: Cumulative histograms for clinical CTA (A) and EPIC-microCT (B).

Statistical analysis

In this study we used ten knees from eight individuals. The use of two knees from one individual could potentially lead to an overestimation of the correlation between μ CT and CTA measurements^{401, 402}. Exclusion of either one of the knees in the two patients that were scanned bilaterally did not influence the results of our study. Therefore, we decided to exclude the bilaterally scanned knees from the analysis.

The correlation between the mean X-ray attenuation values of CTA and the mean X-ray attenuation values of EPIC- μ CT was calculated per radiation dose for all cartilage ROIs pooled. Because of the fact that we analyzed seven cartilage ROIs per knee joint and the potential correlation which might already exist within all knee joints itself, we used a linear mixed model to analyze if the correlation coefficients between, CTA outcomes and EPIC- μ CT outcomes were statistically significant.

All analyses were performed using GraphPad (Graphpad Software Inc., San Diego, USA) and SPSS version 17.0 (SPSS Inc., Chicago, USA). All p-values < 0.05 were considered to be statistically significant.

RESULTS

Cadaveric knee joints

After CT scanning, four knees were excluded from the study due to clearly visible calcifications in the cartilage and due to the fact that from two individuals two knees were scanned. Thus, a total of six cadaveric knee joints from six individuals were included in the analysis (three female, three male; mean age at death 72 years; age range at death 30 – 94 years). Furthermore, 12 cartilage ROIs were not included in our data analysis because of motion artifacts during μ CT scanning and segmentation errors due to severe cartilage loss¹⁵⁷.

Correlation of CTa with sGAG content in large anatomical ROIs

Mean X-ray attenuation values of the CTa scans acquired with maximum radiation correlated strongly with the sGAG content of cartilage expressed by EPIC- μ CT attenuation values (n=33; R=0.81; R²=0.66; p<0.0001) (Figure 4A). In the analysis of the additional CTa scans with reduced radiation dose, this correlation remained strong when radiation dose was reduced; 50% of the maximum radiation dose (n=33; R=0.78; R²=0.60; p<0.0001), 40% of the maximum radiation dose (n=33; R=0.76; R²=0.58; p<0.0001), 30% of the maximum radiation dose (n=33; R=0.76; R²=0.59; p<0.0001), 20% of the maximum radiation dose (n=33; R=0.77; R²=0.59; p<0.0001), and 10% of the maximum radiation dose (n=33; R=0.78; R²=0.61; p<0.0001) radiation dose per scan was used (Figure 4B-F).

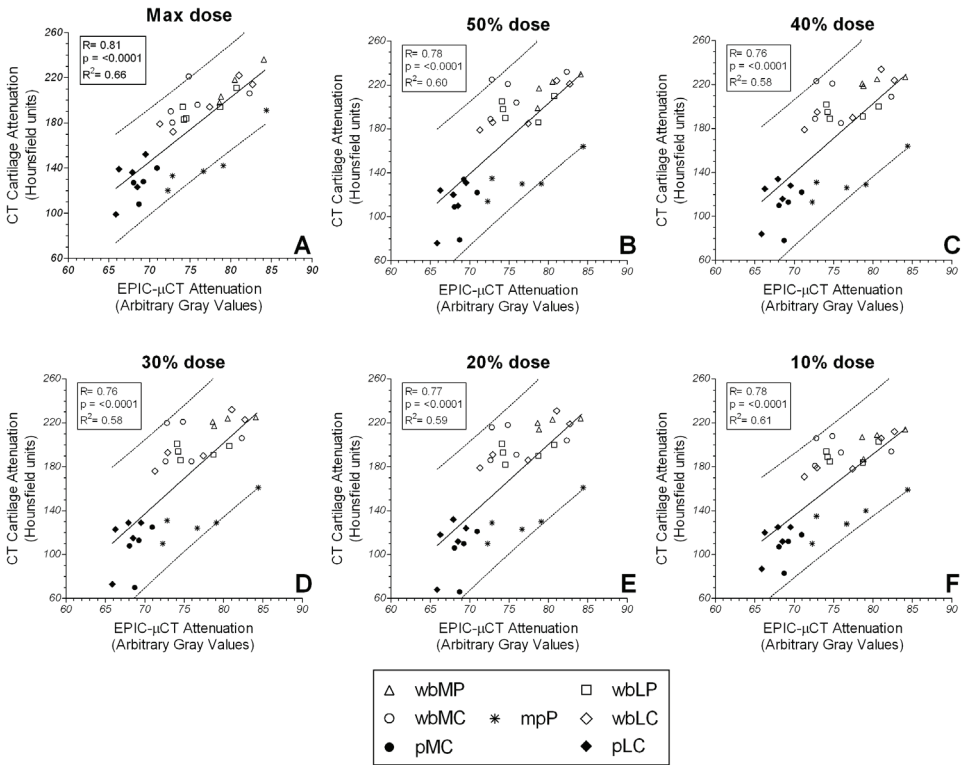


Figure 4: Correlation plots of mean attenuation from EPIC- μ CT and CT arthrography acquired using six different radiation doses. A: maximum radiation dose (n=33); B: 50% of the maximum radiation dose (n=33); C: 40% of the maximum radiation dose (n=33); D: 30% of the maximum radiation dose (n=33); E: 20% of the maximum radiation dose (n=33); F: 10% of the maximum radiation dose (n=33). The dashed lines indicate the 95% confidence interval of the best fit regression line. wbMP: weight-bearing medial plateau; wbMC: weight-bearing medial condyle; pMC: posterior medial condyle; mpP: mid-portion patella; wbLP: weight-bearing lateral plateau; wbLC: weight-bearing lateral condyle; pLC: posterior lateral condyle.

Spatial analysis of cartilage quality

The number of pixels that were incorrectly defined as having high or low sGAG content by CTa was lowest in the CTa scan acquired using the maximum radiation dose ($35\% \pm 9\%$) (Figure 5). When less radiation was used to obtain CTa, the number of pixels which were incorrectly defined as high and low quality cartilage increased (50% radiation: $37\% \pm 9\%$, 40% radiation: $38\% \pm 9\%$, 30% radiation: $38\% \pm 9\%$, 20% radiation: $39\% \pm 9\%$, 10% radiation: $40\% \pm 9\%$) (Figure 5). The effect of this increase in incorrectly defined pixels on the capability of CTa to distinguish between the spatial distribution of high and low sGAG content of cartilage within a single slice is clearly visible in Figure 6.

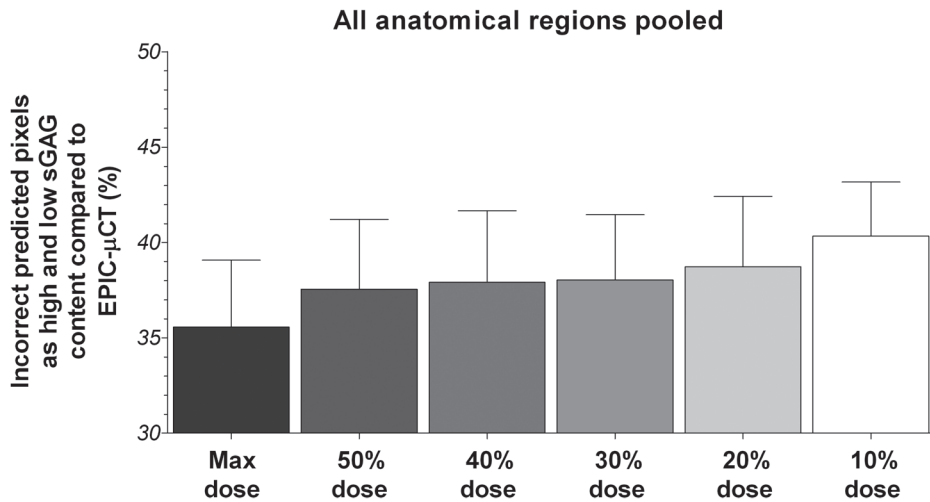


Figure 5: Bar graphs showing the percentage of pixels incorrectly predicted as high and low sGAG content by the different radiation doses (maximum, 50%, 40%, 30%, 20% and 10% of the maximum dose) used in this study. Whiskers show the 95% confidence interval of the mean.

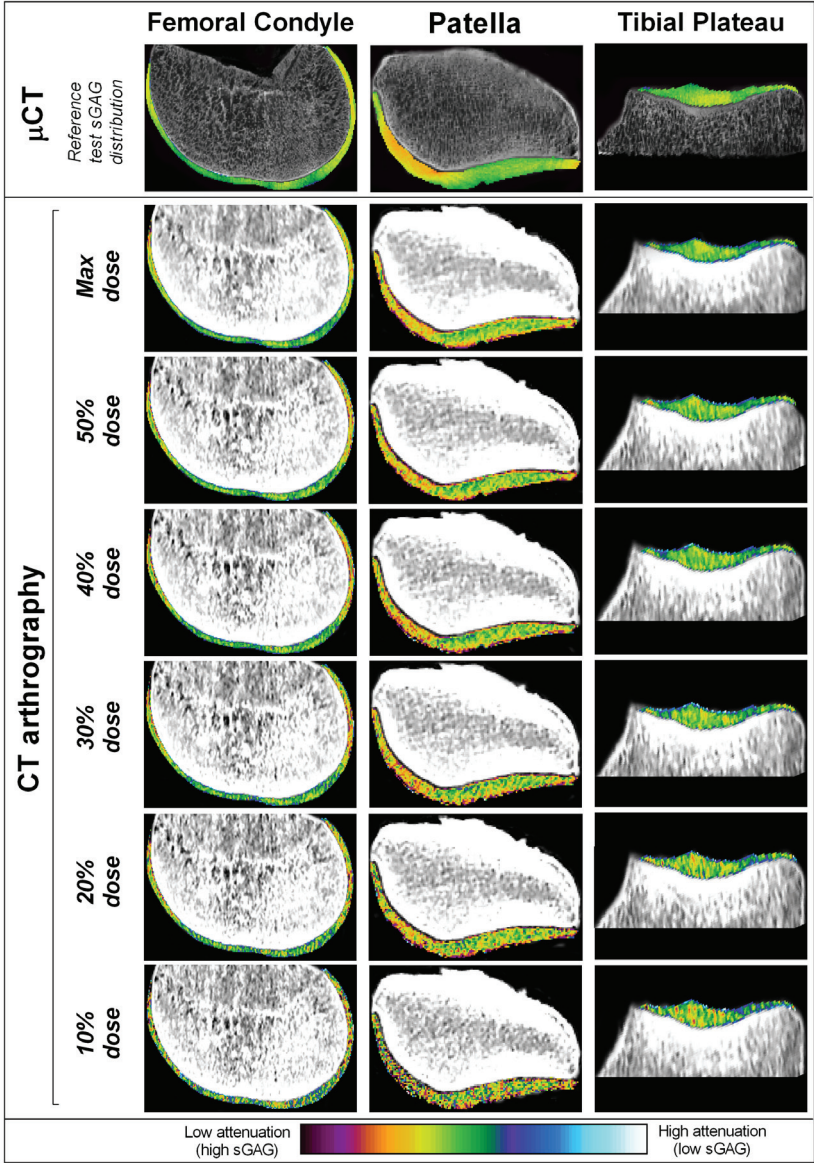


Figure 6: Registered images of both EPIC- μ CT and CT arthrography acquired using different radiation doses (maximum radiation dose, 50%, 40%, 30%, 20% and 10% of the maximum radiation dose) per scan. The attenuation of cartilage regions is visualized in color and representative for the sGAG content of the cartilage. High attenuation values represent low sGAG content and low attenuation values represent high sGAG content.

DISCUSSION

Recently, CTa was introduced as a non-destructive method to measure cartilage quality in human cadaveric knees⁴¹⁰. The main aim of the present cadaver study was to assess whether radiation dose reduction influences the ability of CTa to measure cartilage quality. Lowering the ionizing radiation dose of the acquisition protocol is necessary to make CTa suitable and acceptable for use in clinical research in humans. The results of this study demonstrate that mean attenuation values in large anatomical ROIs in CTa acquired with different radiation doses are strongly correlated with the sGAG content of articular cartilage measured with EPIC- μ CT. This correlation was similar to previous reported results in cadavers⁴¹⁰ and also similar to previously published *in vitro* results^{113, 138, 150}. When the radiation dose used to acquire CT scans was decreased, the correlation between CTa X-ray attenuation values and the sGAG content of cartilage only slightly decreased, but remained good, even if the radiation dose was reduced to approximately 10% of the original dose. The correlation between X-ray attenuation and the reference test for sGAG content remains relatively good because of the fact that the noise in the CT images averages out when calculating the mean X-ray attenuation values in relatively large cartilage ROIs.

The second aim of this study was to assess the capability of CTa to detect local differences in the sGAG content of articular cartilage and to study the effect of radiation dose reduction on this differentiation of cartilage quality within a single slice. The ability to detect local differences in cartilage sGAG content could make CTa applicable as a diagnostic tool for focal cartilage damage instead of a diagnostic arthroscopy. Additionally, it would enable the use of CTa as an imaging tool to measure the effect of cartilage repair therapies (e.g. microfracturing and autologous chondrocyte implantation^{415, 416}) similar to MRI based techniques like dGEMRIC^{417, 418}. Our results demonstrate that, using CTa acquired using the maximum radiation dose, high and low sGAG distribution can be clearly distinguished. An important remark is that the choice of the used thresholds for defining high and low sGAG content within the cartilage based on the pooled cumulative histograms has an arbitrary component. This might introduce an over or underestimation of the capability of CTa to determine local sGAG differences. The increase of noise in the CT image obtained using lowered radiation doses, however, causes an increased percentage of incorrectly defined pixels with high and low sGAG content. In the lowest radiation dose used to obtain CTa, the increased noise even makes it impossible to distinguish differences in sGAG distribution from noise in the CT images.

Based on the results of this study, we suggest using a CTa protocol with a low radiation dose if overall cartilage quality is of interest in clinical research. The lowest radiation dose we used (CTDIvol of 8.13 mGy per scan) is comparable to the dose of a regular CT scan of the knee (CTDIvol of approximately 8 mGy⁴⁰⁶). In addition to cartilage quality, morphological abnormalities

can also be diagnosed using CTa with accuracy comparable to conventional MRI sequences. This was demonstrated in previous research by De Filippo *et al.*³⁹⁵ and Vande Berg *et al.*⁴¹⁹, however, we did not investigate this in the present study. If the spatial distribution of sGAG on a single slice is of interest, we recommend using a higher radiation dose than for overall cartilage quality measurements since decrease in CNR increases the number of incorrectly predicted quality pixels and makes it hard or impossible to differentiate high from low quality cartilage at low radiation dose scans.

Despite the promising results, a limitation of CTa will remain the use of ionizing radiation, because of the risk of predisposing patients to the development of certain cancers by using (repetitive) CT scans⁴⁰⁶. Therefore, MRI based techniques which quantitatively measure cartilage quality (e.g. dGEMRIC, Na²³ mapping, T2 mapping, and T1rho^{104, 409}) remain favorable in a clinical research setting in large cohorts in humans. However, we think that by using a relatively low radiation dose protocol, subgroups of patients in which CTa is favorable of MRI can be identified (e.g. patients with contra-indications to undergo MRI). In addition, CT has also some advantages over MRI (e.g., relative short acquisition time and low costs). Therefore, we expect that low radiation dose CTa can become a complementary technique to MRI based techniques to quantitatively measure cartilage quality in clinical research. In addition to ionizing radiation, other potential limitations of CTa when applied in humans are: the risk of infection and pain due to the intra-articular injection with contrast agent, and the risk of an (allergic) reaction to the contrast agent.

Future research using CTa should focus on implementing and validating CTa in a clinical research setting in humans *in vivo* using a low radiation dose protocol. Filtering the CT data using a low-pass image processing filter will diminish the amount of noise in CT images and might enable the use of even less radiation than suggested in our study. A drawback of using such a filter is, however, the decrease in spatial resolution of the CT images. Another method to lower the radiation dose is the use of an iterative reconstruction algorithm^{420, 421} instead of the standard filtered back projection image reconstruction algorithm as used in this study. Because of the high in plane resolution of CT images acquired with multidetector CT scanners, future research could also focus on investigating the potential of CTa to detect subchondral bone changes and changes in cartilage quality simultaneously. Recently, the feasibility of contrast-enhanced peripheral quantitative CT to analyze cartilage and subchondral bone status on a single scan *in vitro* was described¹⁴⁹ and therefore it is of interest to test this as well as *in vivo* using CTa.

In conclusion, CTa acquired using a low radiation dose is able to measure overall articular cartilage quality throughout the whole human knee with a radiation dose comparable to a regular CT scan of the knee. Spatial sGAG distribution assessment is also possible using CTa,

however for this purpose a higher radiation dose is necessary. Nevertheless, due to the reduction in radiation dose, CTa might be implemented as a non-destructive tool to quantitatively measure articular cartilage in clinical research.

ACKNOWLEDGEMENTS

We acknowledge the Dutch Arthritis Association (LLP11) and the SmartMix Program of the Netherlands Ministry of Economic Affairs and the Netherlands Ministry of Education, Culture and Science for their financial support.

CHAPTER 12

GENERAL DISCUSSION

Part of this Chapter is based on the following publications:

PATHOPHYSIOLOGY OF PERI-ARTICULAR BONE CHANGES IN OSTEOARTHRITIS

H. Weinans, M. Siebelt, R. Agricola, S.M. Botter, T.M. Pijpers, J.H. Waarsing

Bone, 2012 (Aug);51(2): 190-6

THE ROLE OF IMAGING IN EARLY HIP OA

M. Siebelt, R. Agricola, H. Weinans, Y.J. Kim

Osteoarthritis Cartilage, 2014 (Oct);22(10): 1470-1480

OSTEOARTHRITIS (OA): A DISEASE CONCEPT

Articular cartilage does not repair spontaneously, cell-based strategies are far from successful clinical application⁴²², and therapeutic results from physical therapy and weight-loss are rather modest¹⁸⁴. Without disease modifying agents/therapies for OA (DMOADs) available, patients are nowadays treated with invasive and costly joint replacement surgery. Due to the increasingly ageing population, the incidence of OA is expected to rise and push (inter)national healthcare costs⁴²³. This urges the need for new and effective therapeutic strategies for OA, but so far, DMOADs have not been developed successfully yet. This may be explained by complex interactions between the biological composition of articular joints and the biomechanical demands which they are exposed to (**Figure 1**). In this section, we will discuss a hypothesis that explains the multi-cellular and multi-tissue aspects of OA development.

Physiological joint functioning and joint remodeling

All joints in the human body are formed according to a relative similar (genetic) blueprint and they all share a comparable **biological composition (BC in Figure 1A)**. The biological composition of an articular joint is composed by different tissues, and each tissue is inhabited with distinct cell types. The goal of these cells and tissues is to cope with **biomechanical demands (BD in Figure 1B)** during locomotion and physiological joint functioning (**Figure 1C**). Biomechanical demands, however, differ highly between joints. For example due to the anatomical location in the body, where some joints are weight-bearing (e.g. knee or hip), whereas others are not (e.g. shoulder or elbow). Besides its anatomical location, articular joints also experience different biomechanical demands, simply due to the fact that humans exert periods of high and low activity levels during daily life. In order to cope with these different biomechanical demands, articular joints are in need of a dynamic adaptive mechanism which allows joints to properly adjust its tissues. The existence of such a mechanism can be illustrated by two examples.

The first example involves remodeling of trabecular bone in rats. While aging, healthy Wistar rats are known to experience a loss of trabecular bone⁴²⁴⁻⁴²⁶ related to enhanced osteoblast and osteoclast activity⁴²⁷. During this process, subchondral trabecular bone is lost and thickness of remaining trabeculae increases³¹⁷. In **Chapter 3** we found a similar result in control joints of sedentary Wistar rats. These rats showed a ~5% reduction in bone trabecular fraction (BV/TV), whilst trabecular thickness increased ~5%. However, when biomechanical demands were increased through six weeks of moderate running on a motorized treadmill, control joints of running rats did not show a loss of BV/TV. This means that increased exercise levels prevents a loss of trabecular bone stock that sedentary rats lose due to ageing. However, this positive effect was lost when these running rats were given a subsequent period of six week of rest (**Chapter 3**), which suggest the necessity of a biomechanical demand to sustain a certain biological composition.

Secondly, in contrast to bone remodeling, cartilage has only recently been identified as a tissue that adapts itself to different biomechanical demands. In 2004, Tiderius et al used dGEMRIC in a cross-sectional study to evaluate sGAG content in healthy volunteers with different levels of activity. They found that human knee cartilage adapts to exercise by increasing its sGAG content⁴²⁸. In a study by van Ginckel *et al* in 2010, asymptomatic untrained human female volunteers participated in a start to running (STR) program. They compared dGEMRIC changes between sedentary and STR volunteers. As a result of increased physical exercise, the sGAG content of cartilage in these volunteers significantly increased⁴²⁹. These results imply that, next to bone, cartilage composition also changes when biomechanical demands increase.

So, cells within the joint can initiate adaptation processes that functionally improve joint tissues' ability to withstand biomechanical impact. However, it is important to realise that joint remodeling does not solely involve an upgrade in tissue quality when biomechanical demands increase. In case of a strong reduction in biomechanical demand (e.g. due to long term inactivity or loss of gravity during spaceflight or severe inactivity), cartilage⁴³⁰ and bone⁴³¹ are known to experience a severe downgrade in tissue quality as well. This suggests that articular joints strive to absorb biomechanical demands in a way that is most energy or metabolic efficient. As mentioned before, articular joints face biomechanical demands that differ highly during (daily) life. One can imagine that due to these fluctuating demands, it is almost impossible for the joint to actually achieve a perfect state of balance as depicted in **Figure 1C**. Therefore, joint tissues are likely to undergo continuous adaptation in an ongoing attempt to meet with biomechanical demands (**Figure 1D**).

This process is not limited to a response of one single cell-type within one specific tissue. Complex interaction between different compartments of the joint have been described to be enhanced during remodeling⁴³². So, cells within one tissue can interact with other cells within the same tissue (black arrows in **Figure 1A**), but they are similarly likely to interact with other cells in other joint tissues (blue arrows in **Figure 1A**). Together all cells contribute to joint remodeling as they seek a renewed balance between biological composition and biomechanical demand that allows for physiological joint functioning (**Figure 1C**). Whether these interactions occur directly through growth-factors and/or cytokine production, or indirectly through changes in force dissemination as a result of changing quality of the joint tissues, still needs to be further investigated.

Osteoarthritic remodeling of joint tissues

Several known risk factors, like age², sex⁴³³, obesity⁴³⁴ and genetics^{435, 436} are related to increased risk of OA development. These risk factors are likely to induce degenerative change in joint tissues, which results in a loss of tissue quality (**Figure 1E**). A loss of tissue quality would force cells to start joint remodeling, or normal daily activity levels may become a pathological

stressor. In **Chapter 2** we investigated different preclinical models that each represent a different etiology for OA (**Chapter 1 - Table 1**). Through intra-articular MIA injections increased chondrocyte apoptosis was induced which also can be seen in OA cartilage²²³. In the groove model, we damaged the articular cartilage ECM through surgically applied grooves²⁵ which served as a cartilage trauma model. For both models, we found an ongoing degradation of cartilage tissue progressed and development of clear OA features (**Chapter 2**). These results suggest that a loss of biological composition cannot always be compensated for through physiological remodeling, and eventually leads to OA (**Figure 1F**).

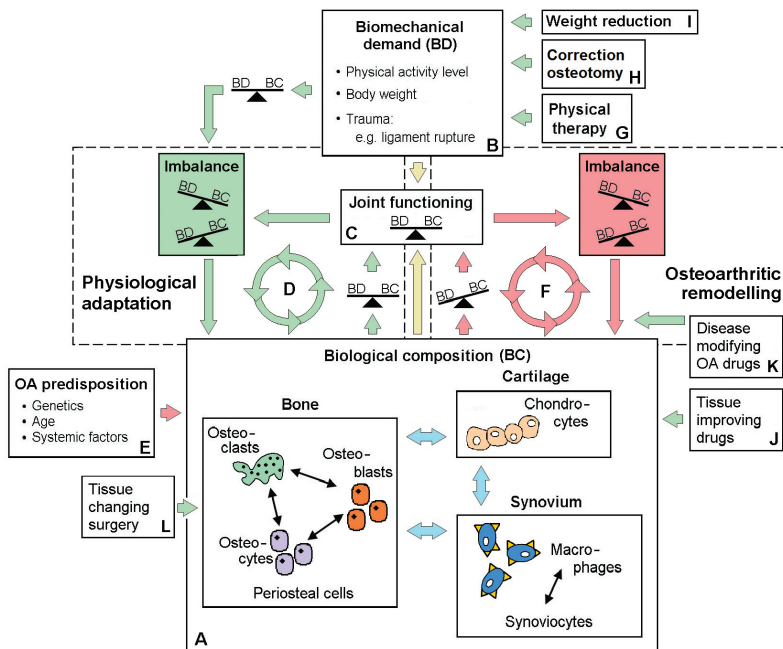


Figure 1: Schematic representation of joint functioning and joint remodeling. The biological composition of joint (A) is daily exposed to different levels of biomechanical demands (B). When both are in balance, there is a physiological form of joint functioning (C). However, it is likely this balance never exists and due to an imbalance between biological composition and biomechanical demand, joint remodeling processes are necessary to restore the balance (D). During aging of men, certain predisposition factors for OA induce changes to the biological composition of the joint (E). These changes will provoke an imbalance with the biomechanical demand and when remodeling processes do not restore the balance, vicious circles of osteoarthritic remodeling processes is initiated. Due to these continuous changes, eventually osteoarthritis will develop with cartilage degradation, subchondral sclerosis, synovitis and osteophytosis (F). OA intervention might be targeted at correcting the balance due to a change in biomechanical demand through either physical therapy (G), through surgical correction osteotomies (H), or weight reduction (I). Future studies should investigate the possibility for quality improvement of joint tissues in order to delay OA onset (J), delaying OA progression through intervention with OA related remodeling (K), or through dedicated manipulation of joint tissues (L).

If a change in biological composition is able to induce OA remodeling, according to our hypothetical scheme in **Figure 1**, a severe increase of biomechanical demand should also be able to exceed the physiological compensating mechanism and elicit OA related remodeling. From literature it is known that a change in knee biokinetics can be pathologically changed through traumatic induced joint instability. Joint instability may either result from traumatic (anterior cruciate) ligament rupture and can be reproduced through surgical transection in animal models. Both clinical studies⁴³⁷ and studies with preclinical animal models^{66, 67} have underlined that joint instability and changed knee biomechanics is related to OA progression. In order to test whether our hypothesis is also true for stable joints, we investigated the effects of strenuous exercise through treadmill running on articular cartilage of Wistar rats (**Chapter 2**). Strenuous running induced clear sGAG loss from the cartilage and when rats were not forced to run anymore, there was still an ongoing loss of sGAG from the cartilage. This suggests that increased biomechanical demand may exceed the capacity of sGAG production by chondrocytes necessary to increase cartilage hydrostatic strength, and triggers OA progression.

In order to further investigate our hypothesis that physiological joint functioning depends on a balance between biological composition and biomechanical demand, we exposed a joint with reduced biological composition to a form of exercise that is known to be non-pathological for a healthy uncompromised joint. According to our hypothesis presented in **Figure 1**, this exercise would have become a pathological stress for a joint with compromised biological composition. In **Chapter 3** we describe that, as expected, moderate exercise induced a normal physiological adaptation in healthy joints of Wistar rats. However, after sGAG depletion through intra-articular injections with papain⁸¹, moderate exercise induced severe OA progression in these cartilage quality compromised joints. Papain injected joints of moderate running rats showed more extensive sGAG loss, severe damage to the ECM with total erosion of the lateral tibia plateau cartilage (**Chapter 3**). Even after the exercise protocol, when the rats were given rest, the severity of OA features progressed. This involved marked changes throughout the joint, with development of a sclerotic bone phenotype, increased osteophyte growth, and enhanced macrophage activation within the synovium (**Chapter 3**).

The results from these experiments illustrate that joint functioning can be compromised through a change in biological composition, through supraphysiological increased biomechanical demand, and a combination of both. When either form of imbalance persists long enough or is intense enough, a threshold seems to be exceeded after which no spontaneous restoration of joint tissue quality is possible. From here on, an imbalance between biological composition and biomechanical demand will persist. As a result, an ongoing cascade of inadequate joint adaptation will start; the vicious circle of OA that eventually will impair all cells and tissues of the joint (**Figure 1F**). With involvement of all tissues in the joint, other cells like periosteal cells, osteocytes⁴³⁸, synoviocytes¹⁵⁹ and other immune cells⁴³⁹ will most likely play a role in facilitating OA progression, but the importance of their roles still need to be elucidated.

THERAPEUTIC INTERVENTIONS FOR OSTEOARTHRITIS

When discussing possible treatment options for OA in relation to our proposed disease model (Figure 1), different strategies can be considered. An obvious approach is to restore balance through a reduction of the biomechanical demand, which can be achieved in various ways. First, this might be achieved through adjustment of life style and physical therapy (Figure 1G). Physical therapy is one of the few interventions available in clinics known to be beneficial for OA patients¹⁸³. Second, biomechanical demands can be changed within through surgical correction osteotomies (e.g. of the hip⁴⁴⁰ or knee⁴⁴¹) (Figure 1H). For example, a patient with pronounced varus osteoarthritis of his/her knee can be treated with a high tibial osteotomy. Through this procedure there is a load transfer towards the unaffected compartment of the knee joint and known to relieve pain and reduce disease progression⁴⁴². And finally, also obesity is a known risk factor for osteoarthritis and this extra-weight could pose a higher biomechanical demand through increased load and changed biomechanics of weight-bearing joints⁴⁴³. A reduction in weight could therefore lead to a reduction of biomechanical loads in articular joints (Figure 1I).

Although these approaches seem straightforward, therapeutic effects on OA progression of physical therapy and weight loss are rather modest. Although results for osteotomies on pain and knee function are rather good⁴⁴⁴, they rely on specific preoperative diagnosis and cannot be applied in a generalized fashion. Targeting OA only through a reduction in biomechanical demands is likely not sufficient in managing this disease. Therefore, new therapeutic strategies are necessary to manage OA. In the next sections we will describe interventions strategies that prevent OA onset through improvement of joints tissues biological composition (Figure 1J), or attempt to reduce the effects of pathological OA remodeling (Figure 1K).

Improving quality of biological composition in joint tissues

Biomechanical induced stress responses in articular chondrocytes

Chondrocytes are responsible for maintaining the extracellular matrix (ECM) of articular cartilage and repair of any inflicted damage. Due to their location within the cartilage ECM, they are daily exposed to high-peak forces during physical activity. Chondrocytes are sensitive to mechanical stimuli and they are known to adopt a hypertrophic morphologic state when biomechanical stress levels increase¹³². If this stressed condition persists, chondrocytes may even die through apoptosis²²³. Heat shock proteins (Hsp) are proteins that help to sustain cellular homeostasis under stressed conditions and are regulators of the apoptic pathways²²⁴. Galois et al demonstrated exercise to induce upregulation of Hsp70, protecting the cartilage from instability induced OA degradation¹⁵². This protective effect from Hsp70 proved to be dependent on the degree of exercise exposure. Galois et al hypothesized that co-expression of other Hsps could limit the protective effect of Hsp70.

In **Chapter 5**, we investigated whether increased stress levels induces Hsp90 upregulation in articular chondrocytes, which might reduce the protective effect of Hsp70. Again, we found that supraphysiological joint loading induces sGAG depletion and ECM damage of articular cartilage. BIIB021 treatment successfully inhibited Hsp90 function and further stimulated Hsp70 upregulation. Interestingly, through Hsp90 inhibition chondrocytes were even able to improve cartilage sGAG content well above baseline levels, whereas untreated animals showed clear cartilage sGAG loss (**Chapter 5**). Hsp90 inhibition seemed to protect against a loss of subchondral bone and reduced synovial macrophage activation. Our results showed that Hsp90 inhibition extended chondrocytes' capability to withstand pathological stress induced by increased biomechanical demand. As a result, when stress levels were relieved, chondrocytes recuperated and adapted the cartilage through increased sGAG production without signs of OA progression. In other words, Hsp90 inhibition protected against increased cellular stress and was subsequently able to increase cartilage and subchondral bone quality (**Figure 1J**).

These results suggest that Hsp70 production in chondrocytes favors physiological joint remodeling (**Figure 1D**), whereas increased Hsp90 production could serve as a marker that indicates pathological joint functioning related to OA remodeling (**Figure 1F**). More research on Hsp production and their downstream targets as regulators of cartilage homeostasis is needed to clarify chondrocytes responses towards biomechanical loads. More data on this topic may provide us with a more accurate explanatory model for pathologic joint loading-induced OA and lead to more sensitive predictors for early OA progression. Moreover, we might be able to develop more selective drugs that intervene with chondrocyte stress regulation, with less toxicity compared to Hsp90 inhibition²³⁸. Furthermore, we found that when BIIB021 treated animals were given a six-week period of rest, cartilage sGAG content decreased again (**Chapter 5**). Again, this suggests that the biological composition of a joint is closely regulated according to the biomechanical demand it faces (**Figure 1C**). Possibly, when therapeutic management of chondrocyte stress responses becomes clinically available, beneficial effects of physical exercise might be enhanced. We would hypothesize that early protection against chondrocyte stress to protect against OA progression, would be most efficient in pre-symptomatic or early-OA patients.

Physical exercise and inhibited osteoclast functioning

Alendronate (ALN) is a nitrogen-containing bisphosphonate and a potent inhibitor of osteoclastic bone resorption used clinically for the treatment of osteoporosis³⁰³. It is suggested that osteoclast-mediated resorption of mineralized cartilage at the subchondral bone-cartilage interface is an early initiating event in OA pathobiology, and that early bisphosphonate use might result in positive effect on cartilage health³⁰⁷.

In our experiment, ALN treatment resulted in more sGAG loss from healthy articular cartilage after a six-week period of exercise. In **Chapter 7**, we discuss that through inhibited osteoclastic bone resorption by ALN the supportive function of subchondral bone is not reduced and remains stiff during running exercise. Due to this stiff subchondral bone plate, the compressive and shear forces that act upon the cartilage increase more compared to those in untreated animals. As a result, the biomechanical demand (which is non-pathological for untreated animals) becomes a pathological stressor for articular chondrocytes in treated animals. This type of biomechanical stress might induce (Hsp) stress responses in articular chondrocytes, as shown in **Chapter 5**. Consequently, chondrocytes reduce sGAG synthesis and first need to survive during this stressed condition. But when animals are given rest and do not need to run anymore, articular cartilage in ALN treated rats show a significant increase in sGAG content compared to untreated animals. This indicates that chondrocytes are able to recuperate and upregulate sGAG production. Through enhanced sGAG content energy diverting capacities of cartilage are enhanced, which allows cartilage to withstand more biomechanical demand. Therefore, we conclude that ALN inhibited osteoclast functioning contributes to enhanced cartilage adaptation in a stressed situation.

This effect might be translated towards clinical care and help to prevent or delay OA development in patients at risk for OA. In this case, a combination of preemptive ALN treatment combined with physical exercise might prove to be beneficial for clinical patient care. ALN treatment has the major advantage that it is already widely used for clinical treatment of osteoporosis, so application of ALN treatment as means to enhance the effect of physical therapy on articular cartilage could be investigated within the near future rather easily.

Therapeutic strategies targeted to reduce OA remodeling

Nowadays there are only a few treatment options for OA available, which can be summarized to analgesics, physical therapy and joint replacement arthroplasty. Within the past decade, there has been a tremendous effort within the scientific field to generate new therapeutic strategies for OA. So far, the outcome has been rather disappointing and no real advances have been made. The experiments with different therapeutic strategies in this thesis also do not provide 'a giant leap for mankind'. It is fair to say that OA is not likely treated through one single DMOAD. Our results do indicate certain specific cell-cell interactions during OA progression. These mechanisms might explain a part of OA pathology and could prove worthwhile when simultaneously targeted for treatment of OA.

Chondrocyte hypertrophy and osteoclastic recruitment

The bone-cartilage subunit has been under investigation for quite some time, and has been proposed as the key-unit for OA progression³²⁶. As stated in our introduction, chondrocytes show features of reactivation of endochondral ossification during OA progression. Normally

chondrocytes are able to endure constant deforming forces during joint movement⁴⁴⁵, and triggers them to produce anabolic factors that enhance cartilage quality⁴⁴⁶. As demonstrated in **Chapter 3**, a pathological biomechanical trigger through strenuous running induces sGAG loss and cartilage ECM damage. Interestingly, near the cartilage-bone interface, there were increased numbers of large chondrocytes on histology sections (**Figure 2**)⁴⁴⁷. This specific cellular morphology is likely for chondrocyte hypertrophy. Previous studies already showed that a pathological joint strain induces chondrocyte dedifferentiation towards a hypertrophic state¹³².

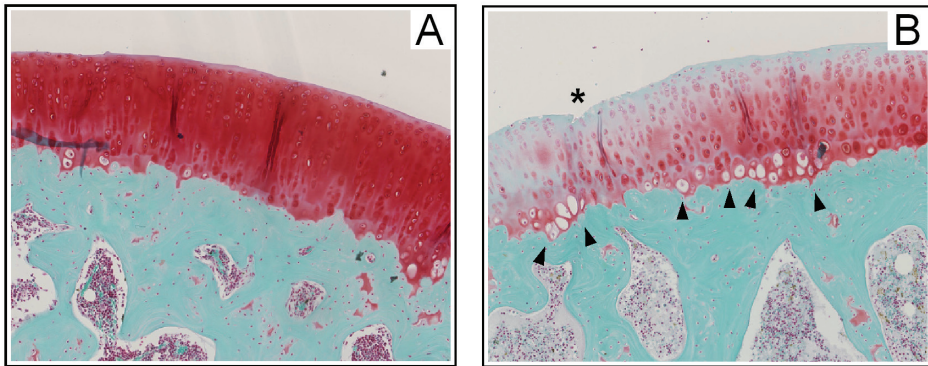


Figure 2: Rat knee joint showing the cartilage and subchondral bone of a normal (healthy) control (A) and of a rat that underwent a running protocol of 5 kilometers per week for a period of 6 weeks. A striking difference in sGAG staining in cartilage and clear hypertrophy of chondrocytes in the deep cartilage zone can be seen between both samples.

In **Chapter 4** we show that GSK3 β activity plays a critical role for preservation of a chondrogenic phenotype. Normally, the canonical Wnt/ β -catenin signaling pathway is a critical regulator of chondrocyte phenotype and cartilage homeostasis. In this pathway, GSK3 β down-regulates transduction of the canonical Wnt signal by promoting degradation of β -catenin. GSK3 β inhibition leads to accumulation of β -catenin and resulted in a loss of cartilage marker expression, matrix degradation through MMP production. It is a known feature that hypertrophic chondrocytes secrete catabolic factors and degrade cartilage quality^{448, 449}. Furthermore, GSK3 β inhibition reduced chondrocyte proliferation and induced chondrocyte apoptosis. Since the apoptotic pathways are regulated by Hsps, one can imagine that stress responses also play a role during this process (**Chapter 5**).

What is evident, is that the preservation of a chondrogenic phenotype is crucial for maintenance of healthy cartilage. A way to preserve a healthy chondrocyte phenotype might be through calcineurin (Cn) activity. Cn has been associated with dedifferentiation of cultured chondrocytes towards a hypertrophic phenotype²⁷¹. In **Chapter 6**, we inhibited Cn activity using FK506. *In vitro* cultured chondrocytes and cartilage explants with FK506 showed increased

anabolic and reduced catabolic ECM marker expression, and FK506 also protected against progressive ECM degradation *in vivo*. This suggests that FK506 was able to induce cartilage ECM favorable responses within chondrocytes. However, we also tested the effect of osteoclast inhibition through alendronate (ALN) on OA progression in the same *in vivo* model for OA (**Chapter 7**). Surprisingly, ALN treatment showed quite similar results compared to FK506 use. This raises the question whether FK506 indeed protected cartilage ECM through preservation of the chondrogenic phenotype of chondrocytes.

As during endochondral ossification, chondrocytes dedifferentiate and adopt a hypertrophic state during OA progression. *In vitro* cultured chondrocytes are known to increase VEGF production when biomechanically triggered towards hypertrophy^{40,42}. This effect was reproduced in an *in vivo* study. Chondrocytes in the deep layers of cartilage also increase VEGF production due to surgical induced knee instability⁴⁵⁰. Besides its effect on angiogenesis, VEGF has a strong chemotactic effect on osteoclasts^{41, 451, 452}.

Osteoclasts are large multinucleated cells that derive from monocyte-macrophage hematopoietic lineage. During osteoclastogenesis macrophage colony-stimulating factor (M-CSF) and receptor activator of nuclear factor- κ B ligand (RANKL) stimulate precursor cells to acquire osteoclast characteristics²⁹¹. This results in expression of tartrate-resistant acid phosphatase (TRAP) in differentiating cells and is followed by fusion into multinucleated cells capable of resorbing mineralized matrix. Interestingly, osteoclast maturation is known to be influenced by FK506. FK506 treatment influences RANKL stimulated osteoclastogenesis^{293, 294}, and especially inhibit late stages of the osteoclast life cycle through predominant induction of apoptosis in TRAP-positive multinucleated osteoclasts²⁹⁶. Through this mechanism inhibited calcineurin activity diminishes activity of mature osteoclasts and reduces bone resorption²⁹⁷⁻²⁹⁹. Since FK506 was introduced orally and its effect relied on systemic distribution, it is possible that FK506 never reached the cartilage and was not therapeutically active on chondrocytes directly. Since FK506 treatment also reduced subchondral porosity in OA induced knee joints (**Chapter 6 - Figure 5D**), the beneficial effect on cartilage could have resulted from an effect on osteoclast activity. However, this explanation remains a hypothesis and should be further investigated. But based on our results from both ALN and FK506 treatment, it is reasonable to suggest a specific interaction between biomechanically stressed (hypertrophic) chondrocytes and osteoclast activation that facilitates OA progression and poses an important target for development of future treatment.

Osteocyte and osteoblast induced subchondral sclerosis

In our model for severe OA there is also a marked development of subchondral sclerosis (Chapter 3). Botter et al hypothesized that as a result of the functional coupling between osteoclasts and osteoblasts, increased osteoclastic bone resorption induces a rise in osteoblast activity leading to increased subchondral bone thickness and sclerosis³⁵. If true, sclerotic bone formation might be prevented through inhibition of osteoclastic bone resorption. We tested this hypothesis in Chapter 7 and although ALN treatment functionally inhibited osteoclastic bone resorption, there was still a transient increase in subchondral sclerosis. This indicates that a functional coupling between osteoclasts and osteoblast is not the (main) reason for formation of this specific bone phenotype.

CT analysis of subchondral bone in our experiments of Chapter 6-8 showed that sclerotic bone especially developed at sites where there was either a complete loss of sGAG or a complete denudation of bone (Chapter 7). Interestingly, animals treated with IAI triamcinolone injections developed more sclerosis within the medial compartment of the tibia plateau (Chapter 8). As clinically observed during this experiment, animals treated with triamcinolone better endured running on the motorized treadmill. Since triamcinolone is known for its effect on pain³³⁰ and improves gait⁴⁵³, these animals might have put more weight on their OA induced knee joint. However, we did not study this, for example by using an incapacitation tester as described in Chapter 9, therefore this remains an assumption. But the observation that sGAG loss, degradation of cartilage ECM, and amount of biomechanical impact all play a role in subchondral sclerosis formation, raises the idea that a mechanical stimuli triggers subchondral sclerosis.

A cell within the (subchondral) bone that could perceive these biomechanical changes is the osteocyte⁴⁵⁴. The osteocyte resides within lacunae of bone matrix and is a mechanosensory cell, sensitive to changes of load-transfer from the overlying cartilage. Bone samples of OA patients have shown that osteocytes change their morphology and become more elongated³¹⁹. Besides this change in cellular shape, osteocytes produce less sclerostin during OA progression^{320, 321}. Increased sclerostin production by osteocytes is known to reduce bone formation through an anti-anabolic effect, which is currently under scientific attention within the field of osteoporosis research⁴⁵⁵. Normally Wnt signaling stimulates bone formation through osteoblasts, but sclerostin inhibits Wnt signaling and reduces bone formation by osteoblasts⁴⁵⁶. Through reduced sclerostin production in OA, the anti-anabolic effect of sclerostin on osteoblasts is lost and bone formation might be increased. This sclerostin-hypothesis for OA, in which increased mechanical stimuli is sensed by osteocytes and subsequently stimulates osteoblasts to deposit bone via reduced sclerostin production, might explain how sclerosis develops independently from osteoclast activity. Currently, the monoclonal antibody romosozumab is used in osteoporosis research as means to increase bone stock in these patients through binding of sclerostin⁴⁵⁷. Possibly,

therapeutic intervention in the osteocyte-osteoblast relation through stimulation of sclerostin might help to prevent against subchondral sclerosis development and preserve a physiological form of subchondral bone in OA patients.

Synovial macrophage activation induced osteophytosis, synovitis and pain

OA is characterized by an inflammatory response that induces synovial hyperplasia, stimulates macrophage infiltration, neoangiogenesis, and fibrosis¹⁵⁹. Due to the transient rise of activated macrophages within the synovium, synoviocytes produce BMPs that lead to osteophytosis within the joint^{59, 60}. Recent research efforts investigated this low-grade synovitis and related it to pain, joint dysfunction, and it might even promote rapid cartilage degradation^{333, 334}.

In our experiments we analyzed macrophage activation using FR β targeted SPECT/CT. When examining our results more closely, a pattern of macrophage activation in our different studies can be identified. When comparing the data presented in **Chapters 5-8**, most macrophage activation was found directly after completion of a running protocol. Cartilage analysis using EPIC- μ CT showed sGAG loss and ECM degradation was most severe during this phase. When animals were not forced to run anymore, the amount of macrophage activation reduced in all our studies, as was the degree of sGAG loss and ECM degradation. As discussed before, FK506 and ALN treatment protected against further ECM degradation in the non-running phase. In these two studies, the amount of macrophage declined even further equal to healthy control values (**Chapter 6-7**). This suggests that the amount of macrophage activation passively responds to the loss of sGAG and collagen fragments that are lost from articular cartilage. In order to support this finding, we studied the immunomodulatory effects of intra-articular triamcinolone injections on macrophage activation and whether this reduces sGAG loss and degradation of cartilage matrix (**Chapter 8**).

Corticosteroid therapy reduces synovitis and pain, and acts on macrophage activation. A few preclinical studies have shown that intra-articular corticosteroid injections might be beneficial for preservation of cartilage matrix^{333, 334}. These results suggest that macrophage activation actively participates in the OA continuum and contributes to cartilage degradation. In our experiment, triamcinolone treatment efficiently reduced macrophage induced osteophytosis (**Chapter 8**). This contradictory effect of increased macrophage activation in relation to a lack of osteophytosis, is likely to be explained due to a strong polarization effect towards a non-inflammatory subtype of activated macrophage¹⁷⁸. But although triamcinolone treatment was started pre-emptively and induced a polarization towards a non-inflammatory macrophage subtype well before OA induction, it did not result in a beneficial effect for cartilage in this model for OA progression. In our opinion, this further emphasizes that macrophage activation is induced by a loss of sGAG and collagen fragments from cartilage, but does not actively contribute its degradation during OA progression.

Mesenchymal stem cells (MSCs) are also known to have immunomodulatory and trophic capacities by secreting anti-inflammatory factors and growth factors³⁵⁵ and MSC-treated OA joints produce less inflammatory cytokines³⁶⁵. In **Chapter 9**, we studied the effect of intra-articular injected MSCs on pain, cartilage damage, bone changes, and inflammation in a rat OA model *in vivo*. The MIA model for OA was selected for this purpose, since this model was previously validated as a rat model for OA pain⁷⁷ and is known for a transient inflammatory response⁹¹. This study provided one interesting finding, animals treated with MSCs distributed significantly more weight on their affected limb. This suggests that MSC treatment reduced pain perception in these animals, possibly resulting from an immunomodulatory effect of MSCs on synovitis.

In conclusion, macrophages seem to be activated due to cartilage debris and elicit an inflammatory response that induces osteophytosis, synovitis and pain. Subsequently, synovitis and pain result in a limited range of motion in OA affected joints^{458, 459}. When macrophage activation and synovitis is effectively treated either through MSCs or triamcinolone, pain is reduced and weight-bearing upon the affected joint can be normalized. However, cartilage quality in these situations remained poor. According to our hypothesis depicted in **Figure 1**, less pain induces an increase in biomechanical demand upon an inferior biological composition. As stated before, the mechanosensory capabilities of the osteocytes could trigger osteoblasts increase bone deposition and form sclerosis. This hypothesis might explain why triamcinolone animals showed slightly increased subchondral sclerosis in the medial tibia compartment (**Chapter 8 – Figure 7**). Future studies should try to incorporate the possible effects of macrophage activation on synovitis, pain, weight-bearing and mobility. Besides the development of a more complete picture of OA as a whole joint disease, more knowledge could lead therapeutic manipulation of macrophage activation that does contribute to a joint's health.

CT BASED IMAGING TECHNIQUES

The term early OA is gaining much attention in the OA literature, with the idea that earlier detection might give better options for treatment. This is a very reasonable assumption, since a completely deteriorated joint would require not only cartilage regeneration, but a drastic restoration of the deformed bone as well. This drives the need for a more sensitive imaging technology that recognizes early OA. Some argue that lack of such an imaging technique is the major impediment why new DMOADs have not been developed yet. However, new imaging techniques will not solely help to identify early OA in our patients. Osteoarthritis should be considered a group of overlapping diseases⁴⁶⁰. Like CAM impingement induced hip OA, future research using modern imaging techniques will unravel more and more of these different subtypes of OA. With this identification, patients can be selected according to their subtype and allow for more specific development of new DMOADs per subtype.

Cartilage evaluation using computed tomography

Through intra-articular injection of an ionic contrast, CT arthrography (CTa) scans can accurately measure sGAG¹⁵. We performed two studies in order to translate CTa based sGAG analysis from preclinical use towards clinical applications in humans (**Chapter 10 and 11**). Both studies showed that ionic contrast influx into cartilage measured with CTa is an excellent measure of sGAG content and composition of cartilage ECM. Of course, scanning with CT based techniques poses a radiation issue for patients. In **Chapter 11** we show that using less radiation exposure increased noise within CTa scans and reduced spatial analysis of sGAG distribution. But analysis of larger volumes of cartilage from low radiation dose CTa scans still correlated well with EPIC- μ CT, which makes this technique suitable as a quantitative cartilage analysis method ready for use in clinical research.

Further ongoing improvements in CT (detector) technology and newer software will provide scans with detailed high resolution images, even using low amounts of radiation exposure. A new technique that sensitively measures changes in bone and cartilage would enable us to identify patients suffering from early OA. Consequently, this will allow for quicker and more sensitive testing of new therapeutic interventions for OA. However, nowadays there is no clear definition that indicates which sGAG content should be considered healthy or diseased. Up till now, quantitative analysis of cartilage using dGEMRIC has not provided us with a clear answer yet. It would be meaningful to generate reference data with normal ranges of such variation in a broad population. As such, we would be able to depict thresholds for a potential diseased status, or think about odds ratios for developing OA. Most important, we would learn whether or not we should put the label “early OA” to some of these cartilage changes we can pick up with our modern imaging techniques. Still, using radiation based techniques like CT to generate this type of data remains debatable.

Imaging of joint functioning

As mentioned many times before, sGAG production is dependent on mechanical loading in humans⁴²⁸. Quantitatively cartilage analysis using dGEMRIC showed that moderate exercise improved sGAG content in patients at risk for OA⁴⁶¹. These results show that OA intervention should somehow be related to physical exercise as means to improve cartilage quality. One can imagine that between individual patients, there are large differences in biological composition. Physical therapy, as it is currently applied in clinics, should be considered a rather ‘one-size-fits-all’ approach and likely to be insufficient for many OA patients. The next challenge for quantitative imaging techniques will be to provide a scientifically funded approach with regards to physical therapy. CT based scanning modalities could prove to be very suited for this type of OA research.

CT allows for simultaneous subchondral bone and cartilage analysis¹⁴⁹, providing more comprehensive data that can be translated towards biomechanical joint functioning. For example, from CT scans it is possible to generate images that allow for 3D quantification of morphological abnormalities⁴⁶². Currently, there already exist new motion simulation techniques that can evaluate joint dynamics based on CT scans. This type of motion analysis can indicate whether morphological joint changes might induce pathological joint functioning and identify whether this possibly induces OA⁴⁶³. Furthermore, using finite element models⁴⁶⁴, we are able to convert CT parameters for cartilage and bone quality towards a load-taking capacity outcome⁴⁶⁵. Using these techniques might enable us to relate the biological composition of different tissues (**Figure 1A**) to a certain level of biomechanical demand (**Figure 1B**). Applying these imaging techniques and new analysis tools might enable physicians to define a specific type of physical activity with proper intensity that meets the capabilities of the diseased OA joint in one specific human patient (**Figure 1G**). Through such an approach, unique conditions in each individual can be coupled to specific therapeutic actions, generating a more personalized medicine mindset.

SUMMARY

SUMMARY

The articular joint is a complex structure in the human body that allows movement under high mechanical loading during daily activities. Osteoarthritis (OA) is a degenerative disease of articular joints that involves pathologic changes in articular cartilage, subchondral bone, synovium, menisci, ligaments, and probably even other structures as well. In this thesis, we studied different aspect of progressing OA pathology in different animal models using multi-modality imaging techniques (like μ CT and μ SPECT/CT) dedicated for small laboratory animal research. Furthermore, we investigated several therapeutic strategies that might be beneficial for OA management.

First, we longitudinally analyzed OA progression in different OA models using μ CT-arthrography (μ CTa) scans. In **Chapter 2**, we describe a new approach to more accurately segment cartilage from μ CTa scans, enabling more detailed analysis of cartilage degradation in time. When applied for analysis of OA progression during a 24 week follow-up time in three different OA models, each model showed distinct patterns of disease progression. In particular, the strenuous running model showed a marked loss of sulphated glycosaminoglycans (sGAG) from articular cartilage during treadmill running. Unexpectedly, when rats did not run anymore, this sGAG loss progressed during follow-up. This finding suggests that increased biomechanical exposure through strenuous running initiates an ongoing cascade of OA processes that likely exceeds the ability for spontaneous cartilage repair.

In contrast to our finding in **Chapter 2**, from literature it is known that physiological joint loading through exercise can stimulate cartilage quality and enhance cartilage sGAG content in healthy joints. In **Chapter 3**, we investigated whether physical exercise exerts a similar effect on sGAG depleted cartilage. In this chapter we show that moderate exercise is harmless for healthy cartilage, but is detrimental for articular joints in rats with severely sGAG depleted cartilage. Not only cartilage degraded to a far more severe extent, there was also more formation of subchondral sclerosis, fulminant activation of macrophages, and increased osteophytosis.

Next, we performed experiments that target chondrocytes in order to intervene with OA progression. The canonical Wnt/ β -catenin signaling pathway is a critical regulator of cartilage homeostasis and development and influences cell death through apoptosis mechanisms. In this pathway, glycogen synthase kinase-3 β (GSK3 β) down-regulates transduction of the canonical Wnt signal by promoting degradation of β -catenin. In **Chapter 4**, we show that inhibition of GSK3 β leads to chondrocyte apoptosis and induces OA.

Another interesting regulator of cartilage homeostatis are heat shock proteins (Hsp). Hsp70 can be upregulated in chondrocytes through exercise, which protects chondrocytes against

apoptotic cell death. However, this effect is limited due to suspected upregulation of Hsp90, which has an antagonistic function on Hsp70. In **Chapter 5**, we tested whether Hsp90 inhibition might prevent degenerative effects from strenuous running on articular cartilage. We found that Hsp90 inhibition upregulated Hsp70 in articular chondrocytes and stimulated sGAG production, which ultimately prevented cartilage ECM damage in the rat running model.

A loss of chondrogenic phenotype due to OA induced chondrocyte hypertrophy is associated with calcineurin (Cn) activity. In **Chapter 6** we studied whether Cn inhibition through FK506 treatment improves chondrocyte phenotype *in vitro* and whether FK506 might prevent OA *in vivo*. *In vitro* monolayer and 3D pellet cultures of chondrocytes treated with FK506 showed both induced anabolic and reduced catabolic extracellular matrix (ECM) marker expression. When FK506 was applied *in vivo*, it prevented degradation of ECM, reduced subchondral sclerosis, and synovial macrophage activation. Our data suggest that FK506 induces an anabolic response in articular chondrocytes that protects cartilage ECM.

The cartilage-bone interface is long suspected to be the key-region in OA development. It has been hypothesized that a functional coupling between osteoclasts and osteoblasts exists that eventually will lead to sclerosis formation during OA progression. In **Chapter 7**, we investigated whether inhibited osteoclastic bone resorption through alendronate treatment intervened with formation of subchondral sclerosis formation and its effect on OA progression. Alendronate treatment functionally inhibited osteoclastic bone resorption, but the formation of sclerosis was not prevented. This suggests that other cells, like osteocytes, might play an important role in the formation of sclerosis. However, alendronate treatments did (somewhat) protect against ECM degradation, indicating that increased osteoclastic activity does contribute to during OA progression.

Within the synovium reside macrophages that become activated during OA progression. It is known that these activated macrophages produce transforming growth factor (TGF) β . Due to enhanced TGF β production, the synoviocytes enhance bone morphogenetic protein (BMP) production. Consequently, these BMPs stimulate development of osteophytes. It is also known, that intra-articular use of corticosteroids inhibits osteophytosis. However, the mechanisms through which this effect is generated are still unknown. In **Chapter 8** we studied what effect intra-articular injections of triamcinolone have on synovial macrophage activation. Triamcinolone was able to prevent osteophyte formation in a severe model for OA. Interestingly, triamcinolone injections severely enhanced macrophage activation. Unfortunately, we did not find an effect on cartilage quality or quantity. In fact, triamcinolone proved to enhance subchondral sclerosis in this model for OA.

Mesenchymal stem cells (MSCs) are promising candidates for cartilage regeneration. MSCs

also have immunomodulatory and trophic capacities by secreting anti-inflammatory factors and growth factors. Cell tracking experiments showed that MSCs are able to survive up to two weeks after injection into the knee joint (**Chapter 9**). Although we found that MSCs exerted a favorable effect on pain in the mono-iodoacetate (MIA) model for OA, both MSC and freshly isolated bone marrow mononuclear cells (BMMNCs) did not modify any of the MIA induced OA changes in bone, cartilage and synovium. Further evaluation on multiple pain aspects is needed to assess the efficacy of MSC as a therapy to alleviate pain in clinical OA.

Current imaging modalities used in clinical practice (e.g. radiographs, MRI), are not likely to give us the necessary knowledge about OA pathogenesis. μ CT-arthrography is a pre-clinical technique that enables us to detect early OA events before our laboratory animals develop any clinical symptoms of disease progression. Therefore, we conducted experiments in order to translate this technique towards a clinical setting. In **Chapter 10**, CT-arthrography (CTa) scans made using a clinical CT system and compared to outcomes from EPIC- μ CT scans. CTa had an excellent correlation with cartilage sGAG content. This correlation even further improved when we combined information on sGAG content with data that reflected the cartilage ECM composition. This indicates that cartilage analysis using CTa serves as an accurate measure for cartilage quality.

In order to use a radiation based technique (like CT) in clinical practice, it is necessary to investigate whether CTa scan protocols using a lower radiation dose are still able to measure cartilage quality. In **Chapter 11** we report that CTa scans made with radiation doses ranging from 8.13 mGy to 81.33mGy, were all able to measure overall cartilage quality. CTa is therefore suitable for quantitative analysis of cartilage in clinical research. However, spatial analysis of cartilage quality on a single CT slice was highly affected by lowering the radiation dose. So, for new studies that require a high spatial resolution, will need to use a higher radiation dose.

To conclude, the results of this thesis support that OA is a 'whole joint disease'. Our data suggest that there is a dedicated balance within joint tissues to cope with the daily biomechanical demands it faces. Physiological joint functioning is impaired through loss of tissue quality, increased biomechanical demands, or a combination of both. When physiological functioning is disturbed, OA is likely to develop. We have shown that targeted interventions at different cells in the joint enable preservation of tissue quality, through which OA might be prevented. New imaging techniques for quantitative cartilage analysis (e.g. CT-arthrography) and emerging techniques that visualize cellular and molecular aspects of OA (e.g. SPECT/CT) will enhance our knowledge of OA. With these techniques, we will be able to more accurately select patients all suffering from a similar etiology of OA. The fewer the variables within OA study populations, the higher the chances in developing disease modifying agents that successfully target OA can be identified.

SAMENVATTING

SAMENVATTING

Een gewricht is een complexe structuur in het menselijk lichaam dat beweging mogelijk maakt. Artrose is een ziekte van een gewricht waarbij pathologische veranderingen plaatsvinden in kraakbeen, subchondraal bot, gewrichtskapsel, menisci, ligamenten en tal van andere structuren. Het is vooralsnog onduidelijk waarom artrose in de ene patiënt snel progressief is en in anderen tientallen jaren stabiel blijft. Om meer inzicht te krijgen in de pathogenese van artrose en de effecten van therapeutische interventies hebben we in dit proefschrift diverse beschikbare diermodellen gebruikt. Monitoren van het ziekteproces vond plaats middels beeldvormende technieken zoals μ CT en μ SPECT/CT.

In **Hoofdstuk 2** beschrijven we een nieuwe analysemethode om accuraat kraakbeen uit scans van μ CT-arthrogrammen (μ CTa) te segmenteren. In de tijd hebben we drie ratmodellen voor artrose vervolgd met behulp van μ CTa. Voor elk van deze drie modellen vonden wij een eigen patroon van verergering van artrose. Bij dieren die blootgesteld werden aan hardlopen, nam de concentratie van sulfide-glycosaminoglycanen (sGAGs) in het kraakbeen sterk af, leidend tot een sterk verminderde kwaliteit. Echter, ook wanneer deze dieren niet meer hoefden te rennen, bleef het artrose proces onverminderd doorgaan. Dit wekt de suggestie, dat een toename van de biomechanische prikkel een cascade van gebeurtenissen in het kraakbeen initieert waarbij het natuurlijke herstelmechanisme overschreden wordt.

In **Hoofdstuk 3** presenteren we hoe in een ratmodel hoe een milder hardloopschema geen negatief effect heeft op de kwaliteit van het kraakbeen in gezonde knieën van ratten. Wanneer wij door middel van papaine injecties in deze knie de hoeveelheid sGAGs in het kraakbeen lieten doen afnemen, leidde dit milde hardloopschema echter tot een sterke toename van artrose met erosie van kraakbeen, sclerose in het subchondrale bot, ontsteking in het gewrichtskapsel en een forse toename van osteofyten.

Het is bekend dat tijdens progressie van artrose chondrocyten in het kraakbeen tekenen van hypertrofie aannemen en uiteindelijk sterven via een mechanisme dat apoptose heet. Het canonieke Wnt/ β -catenine systeem is een belangrijke regulator van kraakbeen homeostase en heeft daarnaast invloed op de celdood via apoptose Glycogeen synthase kinase-3 β (GSK3 β) reguleert in dit systeem transductie van het canonieke Wnt signaal door de afbraak van β -catenin te stimuleren. In **Hoofdstuk 4** laten we zien dat remming van GSK3 β leidt tot een toename van celdood van de chondrocyt door apoptose, gepaard gaande met een toename van artrose.

Een ander eiwit van invloed op apoptose is heat shock protein 70 (Hsp70), geproduceerd door chondrocyten. Een toename van Hsp70 leidt tot minder celdood en stimuleert kraakbeen kwaliteit door toename van sGAG productie. Hsp70 productie kan gestimuleerd worden door

belasting van kraakbeen middels hardlopen. Echter, dit gunstige effect blijkt gelimiteerd. Mogelijk leidt co-inductie van een ander stress eiwit, Hsp90, tot een tenietdoening van het gunstige effect van Hsp70. In **Hoofdstuk 5** hebben we getest of remming van de werking van Hsp90 in staat was artrose te voorkomen. Het bleek inderdaad dat Hsp90 remming een stimulans is voor chondrocyten om meer Hsp70 te produceren, met als gevolg meer productie van sGAG en minder schade aan het kraakbeen ten opzicht van onbehandelde dieren.

Zoals gezegd wordt artrose gekenmerkt door verandering van normaal fenotype van de chondrocyt naar een hypertrofe morfologie. Dit proces is geassocieerd met calcineurin (Cn) activiteit. In **Hoofdstuk 6** hebben we bestudeerd of remming van Cn activiteit door behandeling met FK506 het normale fenotype van chondrocyten kan beschermen en middels die wijze artrose zou kunnen voorkomen. Onze *in vitro* studies lieten zien dat door behandeling met FK506 een toename van anabolische, maar afname van catabolische activiteit door chondrocyten plaatsvond. *In vivo* experimenten lieten zien dat behandeling met FK506 leidde tot minder afbraak van kraakbeenmatrix en vermindering van progressie van artrose in andere weefsels van het gewricht.

De interface tussen kraakbeen en bot wordt al jaren onderzocht als mogelijke ontstaansplek van artrose. Tal van veranderingen in deze interface leiden uiteindelijk tot een toename van een sclerotisch botfenotype en artrose. Mogelijk ontstaat deze sclerose door een verstoorde balans tussen botresorberende osteoclasten en botmakende osteoblasten. In **Hoofdstuk 7** hebben we getest of het remmen van botresorptie door osteoclasten leidt tot een vermindering van artrose. In dit experiment gebruikten we alendronaat om botresorptie door osteoclasten te stoppen. Hoewel door alendronaat botsclerose niet voorkomen werd, bleek sprake van minder afbraak van kraakbeenmatrix. Dit kan duiden op een centrale rol van pathologisch toegenomen osteoclast activiteit in progressie van artrose.

Gedurende progressie van artrose worden macrofagen in het gewrichtskapsel geactiveerd. Van deze macrofagen is bekend dat zij transforming growth factor (TGF) β produceren. Dit groeihormoon induceert aanmaak van botgroei stimulerende eiwitten door synoviocyten in het gewrichtskapsel, leidend tot benige uitsteeksels (osteofyten) in een gewricht. Het is bekend dat intra-articulair geïnjecteerde corticosteroïden eens sterk remmend effect hebben op de vorming van deze osteofyten. In **Hoofdstuk 8** hebben we onderzocht op welke manier intra-articulaire injecties met een corticosteroïd (triamcinolon) invloed heeft op de activatie van macrofagen. Verrassend genoeg vonden wij dat triamcinolon leidt tot een forse toename van macrofaag activiteit. Deze behandeling wist wel de vorming van osteofyten volledig te voorkomen. Helaas zagen wij geen gunstige effecten op kraakbeenkwaliteit en zelfs een toename van sclerose in de behandelde dieren.

Mononucleaire beenmergcellen (BMMNCs) en mesenchymale stamcellen (MSCs) zijn cellen die anti-inflammatoire stoffen en groeifactoren kunnen uitscheiden, met allerlei immunomodulatoire en trofische eigenschappen. In **Hoofdstuk 9** hebben we onderzocht of BMMNCs en MSCs een gunstig effect op artrose kunnen hebben. Daarvoor werden MSC in artrotische knieën van ratten ingespoten. Door middel van fluorescentie hebben we de aanwezigheid van MSCs tot twee weken na injectie kunnen traceren. De MSCs hadden een minimaal gunstig effect op pijn die de ratten in hun artrotische knie ervaarden. Zowel MSCs als vers geïsoleerde mononucleaire beenmergcellen bleken echter geen therapeutisch effect te hebben op artrotische veranderingen in bot, kraakbeen en gewrichtskapsel.

Conventionele afbeeldende technieken (zoals röntgenfoto's en MRI) geven ons onvoldoende informatie om de pathologie van artrose te ontrafelen. Met nieuwe beeldvormende technieken, zoals μ CTa, kunnen we mogelijk artrose in een veel vroeger stadium diagnosticeren. Om deze dierexperimentele CT techniek naar de kliniek te transleren hebben we een tweetal experimenten uitgevoerd. In **Hoofdstuk 10** vergeleken we kraakbeen analyse van klinisch vervaardigde CT arthrogrammen (CTa) met ex vivo gemeten sGAG concentraties met EPIC- μ CTscans. Deze vertoonden een hoge correlatie, welke aanzienlijk verbeterde wanneer naast data over sGAG, ook informatie werd toegevoegd met informatie over de collageen structuur van het kraakbeen.

Omdat beeldvormende technieken zoals CT gebruik maken van röntgenstraling, is het noodzakelijk om te onderzoeken of CTa scans met een lagere stralingsdosis nog steeds kraakbeen kwaliteit kunnen meten. In **Hoofdstuk 11** beschrijven we dat 6 verschillende CTa scans met een stralingsdosis tussen de 81.33mGy en 8.13mGy betrouwbare informatie over de concentratie sGAG in kraakbeen genereerden. Deze uitkomst impliceert dat CTa laagdrempelig gebruikt kan worden bij het diagnosticeren van patiënten met artrose. Een beperking van de lagere stralingsdosis was, dat de spatiële analyse van de CTa scans minder nauwkeurig werd. Daarom is CTa met een lage stralingsdosis minder geschikt voor studies waarbij een accurate spatiële analyse noodzakelijk is.

Concluderend onderstrepen de resultaten van dit proefschrift de hypothese dat artrose een ziekte van het hele gewricht is. Meermaals laten onze uitkomsten zien dat de verschillende weefsels in gewrichten zich continue aanpassen aan wisselende biomechanische omstandigheden. Wanneer de gewrichtweefsels in kwaliteit afnemen, of wanneer de biomechanische belasting sterk toeneemt, kan het fysiologisch functioneren van het gewricht ondermijnd worden, leidend tot activatie van cascades welke artrose induceren. Door middel van verschillende (medicamenteuze) interventies is het mogelijk om afzonderlijke cellen in het gewricht te beïnvloeden, waarmee de kwaliteit van weefsels wordt beschermd en artrose voorkomen. In de toekomst zullen beeldvormende technieken voor kraakbeen (zoals het gebruik van CT

arthrogrammen) en nieuwe moleculaire technieken (zoals SPECT/CT), een prominente rol gaan spelen om de pathogenese van artrose te ontrafelen. Het gebruik van dergelijke technieken stelt ons in staat specifieke artrose patiënten te selecteren die aan eenzelfde subtype van artrose lijden. Meer homogeniteit van patiëntgroepen zal leiden tot een toename van kansen om daadwerkelijk een nieuwe behandeling voor artrose te ontwikkelen.

REFERENCES

REFERENCES

1. Mankin HJ, Dorfman H, Lippiello L, Zarins A. **Biochemical and metabolic abnormalities in articular cartilage from osteo-arthritic human hips. II. Correlation of morphology with biochemical and metabolic data.** *J Bone Joint Surg Am.* 1971;53(3):523-37.
2. Helmick CG, Felson DT, Lawrence RC, Gabriel S, Hirsch R, Kwoh CK, et al. **Estimates of the prevalence of arthritis and other rheumatic conditions in the United States. Part I.** *Arthritis Rheum.* 2008;58(1):15-25.
3. Lawrence RC, Felson DT, Helmick CG, Arnold LM, Choi H, Deyo RA, et al. **Estimates of the prevalence of arthritis and other rheumatic conditions in the United States. Part II.** *Arthritis Rheum.* 2008;58(1):26-35.
4. Odding E, Valkenburg HA, Stam HJ, Hofman A. **Determinants of locomotor disability in people aged 55 years and over: the Rotterdam Study.** *Eur J Epidemiol.* 2001;17(11):1033-41.
5. Felson DT. **Developments in the clinical understanding of osteoarthritis.** *Arthritis Res Ther.* 2009;11(1):203.
6. Hunziker EB, Quinn TM, Hauselmann HJ. **Quantitative structural organization of normal adult human articular cartilage.** *Osteoarthritis Cartilage.* 2002;10(7):564-72.
7. Hayes DW, Jr., Brower RL, John KJ. **Articular cartilage. Anatomy, injury, and repair.** *Clin Podiatr Med Surg.* 2001;18(1):35-53.
8. Adams MA. **The mechanical environment of chondrocytes in articular cartilage.** *Biorheology.* 2006;43(3-4):537-45.
9. Knecht S, Vanwanseele B, Stussi E. **A review on the mechanical quality of articular cartilage - implications for the diagnosis of osteoarthritis.** *Clin Biomech (Bristol, Avon).* 2006;21(10):999-1012.
10. Kempson GE, Muir H, Swanson SA, Freeman MA. **Correlations between stiffness and the chemical constituents of cartilage on the human femoral head.** *Biochim Biophys Acta.* 1970;215(1):70-7.
11. Jurvelin J, Saamanen AM, Arokoski J, Helminen HJ, Kiviranta I, Tammi M. **Biomechanical properties of the canine knee articular cartilage as related to matrix proteoglycans and collagen.** *Eng Med.* 1988;17(4):157-62.
12. Vicencio JM, Galluzzi L, Tajeddine N, Ortiz C, Criollo A, Tasdemir E, et al. **Senescence, apoptosis or autophagy? When a damaged cell must decide its path--a mini-review.** *Gerontology.* 2008;54(2):92-9.
13. Lotz M, Loeser RF. **Effects of aging on articular cartilage homeostasis.** *Bone.* 2012;51(2):241-8.
14. Mackie EJ, Tatarczuch L, Mirams M. **The skeleton: a multi-functional complex organ: the growth plate chondrocyte and endochondral ossification.** *J Endocrinol.* 2011;211(2):109-21.
15. Shapiro IM, Adams CS, Freeman T, Srinivas V. **Fate of the hypertrophic chondrocyte: microenvironmental perspectives on apoptosis and survival in the epiphyseal growth plate.** *Birth Defects Res C Embryo Today.* 2005;75(4):330-9.
16. Kawaguchi H. **Endochondral ossification signals in cartilage degradation during osteoarthritis progression in experimental mouse models.** *Mol Cells.* 2008;25(1):1-6.
17. Suri S, Walsh DA. **Osteochondral alterations in osteoarthritis.** *Bone.* 2012;51(2):204-11.
18. Dye SF, Vaupel GL, Dye CC. **Conscious neurosensory mapping of the internal structures of the human knee without intraarticular anesthesia.** *Am J Sports Med.* 1998;26(6):773-7.
19. Lohmander LS, Englund PM, Dahl LL, Roos EM. **The long-term consequence of anterior cruciate ligament and meniscus injuries: osteoarthritis.** *Am J Sports Med.* 2007;35(10):1756-69.

20. Englund M, Roemer FW, Hayashi D, Crema MD, Guermazi A. **Meniscus pathology, osteoarthritis and the treatment controversy.** *Nat Rev Rheumatol.* 2012;8(7):412-9.
21. Agricola R, Heijboer MP, Bierma-Zeinstra SM, Verhaar JA, Weinans H, Waarsing JH. **Cam impingement causes osteoarthritis of the hip: a nationwide prospective cohort study (CHECK).** *Ann Rheum Dis.* 2013;72(6):918-23.
22. Agricola R, Heijboer MP, Roze RH, Reijnen M, Bierma-Zeinstra SM, Verhaar JA, et al. **Pincer deformity does not lead to osteoarthritis of the hip whereas acetabular dysplasia does: acetabular coverage and development of osteoarthritis in a nationwide prospective cohort study (CHECK).** *Osteoarthritis Cartilage.* 2013;21(10):1514-21.
23. Agricola R, Reijnen M, Bierma-Zeinstra SM, Verhaar JA, Weinans H, Waarsing JH. **Total hip replacement but not clinical osteoarthritis can be predicted by the shape of the hip: a prospective cohort study (CHECK).** *Osteoarthritis Cartilage.* 2013;21(4):559-64.
24. Dedrick DK, Goldstein SA, Brandt KD, O'Connor BL, Goulet RW, Albrecht M. **A longitudinal study of subchondral plate and trabecular bone in cruciate-deficient dogs with osteoarthritis followed up for 54 months.** *Arthritis Rheum.* 1993;36(10):1460-7.
25. Marijnissen AC, van Roermund PM, TeKoppele JM, Bijlsma JW, Lafeber FP. **The canine 'groove' model, compared with the ACLT model of osteoarthritis.** *Osteoarthritis Cartilage.* 2002;10(2):145-55.
26. Mastbergen SC, Marijnissen AC, Vianen ME, van Roermund PM, Bijlsma JW, Lafeber FP. **The canine 'groove' model of osteoarthritis is more than simply the expression of surgically applied damage.** *Osteoarthritis Cartilage.* 2006;14(1):39-46.
27. Botter SM, Glasson SS, Hopkins B, Clockaerts S, Weinans H, van Leeuwen JP, et al. **ADAMTS5-/- mice have less subchondral bone changes after induction of osteoarthritis through surgical instability: implications for a link between cartilage and subchondral bone changes.** *Osteoarthritis Cartilage.* 2009;17(5):636-45.
28. Botter SM, van Osch GJ, Waarsing JH, Day JS, Verhaar JA, Pols HA, et al. **Quantification of subchondral bone changes in a murine osteoarthritis model using micro-CT.** *Biorheology.* 2006;43(3-4):379-88.
29. Botter SM, van Osch GJ, Waarsing JH, van der Linden JC, Verhaar JA, Pols HA, et al. **Cartilage damage pattern in relation to subchondral plate thickness in a collagenase-induced model of osteoarthritis.** *Osteoarthritis Cartilage.* 2008;16(4):506-14.
30. Clark JM, Huber JD. **The structure of the human subchondral plate.** *J Bone Joint Surg Br.* 1990;72(5):866-73.
31. Duncan H, Jundt J, Riddle JM, Pitchford W, Christopherson T. **The tibial subchondral plate. A scanning electron microscopic study.** *J Bone Joint Surg Am.* 1987;69(8):1212-20.
32. Li B, Marshall D, Roe M, Aspden RM. **The electron microscope appearance of the subchondral bone plate in the human femoral head in osteoarthritis and osteoporosis.** *J Anat.* 1999;195 (Pt 1):101-10.
33. Lyons TJ, McClure SF, Stoddart RW, McClure J. **The normal human chondro-osseous junctional region: evidence for contact of uncalcified cartilage with subchondral bone and marrow spaces.** *BMC Musculoskelet Disord.* 2006;7:52.
34. Sniekers YH, Intema F, Lafeber FP, van Osch GJ, van Leeuwen JP, Weinans H, et al. **A role for subchondral bone changes in the process of osteoarthritis; a micro-CT study of two canine models.** *BMC Musculoskelet Disord.* 2008;9:20.

-
35. Botter SM, van Osch GJ, Clockaerts S, Waarsing JH, Weinans H, van Leeuwen JP. Osteoarthritis induction leads to early and temporal subchondral plate porosity in the tibial plateau of mice: an in vivo micro focal computed tomography study. *Arthritis Rheum.* 2011;63(9):2690-9.
 36. Oegema TR, Jr., Carpenter RJ, Hofmeister F, Thompson RC, Jr. The interaction of the zone of calcified cartilage and subchondral bone in osteoarthritis. *Microsc Res Tech.* 1997;37(4):324-32.
 37. Bittner K, Vischer P, Bartholmes P, Bruckner P. Role of the subchondral vascular system in endochondral ossification: endothelial cells specifically derepress late differentiation in resting chondrocytes in vitro. *Exp Cell Res.* 1998;238(2):491-7.
 38. Babarina AV, Mollers U, Bittner K, Vischer P, Bruckner P. Role of the subchondral vascular system in endochondral ossification: endothelial cell-derived proteinases derepress late cartilage differentiation in vitro. *Matrix Biol.* 2001;20(3):205-13.
 39. Bromley M, Bertfield H, Evanson JM, Woolley DE. Bidirectional erosion of cartilage in the rheumatoid knee joint. *Ann Rheum Dis.* 1985;44(10):676-81.
 40. Kurz B, Lemke AK, Fay J, Pufe T, Grodzinsky AJ, Schunke M. Pathomechanisms of cartilage destruction by mechanical injury. *Ann Anat.* 2005;187(5-6):473-85.
 41. Mackie EJ, Ahmed YA, Tatarczuch L, Chen KS, Mirams M. Endochondral ossification: how cartilage is converted into bone in the developing skeleton. *Int J Biochem Cell Biol.* 2008;40(1):46-62.
 42. Pufe T, Lemke A, Kurz B, Petersen W, Tillmann B, Grodzinsky AJ, et al. Mechanical overload induces VEGF in cartilage discs via hypoxia-inducible factor. *Am J Pathol.* 2004;164(1):185-92.
 43. Harrison MH, Schajowicz F, Trueta J. Osteoarthritis of the hip: a study of the nature and evolution of the disease. *J Bone Joint Surg Br.* 1953;35-B(4):598-626.
 44. Batiste DL, Kirkley A, Laverty S, Thain LM, Spouge AR, Holdsworth DW. Ex vivo characterization of articular cartilage and bone lesions in a rabbit ACL transection model of osteoarthritis using MRI and micro-CT. *Osteoarthritis Cartilage.* 2004;12(12):986-96.
 45. Boyd SK, Muller R, Leonard T, Herzog W. Long-term periarticular bone adaptation in a feline knee injury model for post-traumatic experimental osteoarthritis. *Osteoarthritis Cartilage.* 2005;13(3):235-42.
 46. Hayami T, Pickarski M, Wesolowski GA, McLane J, Bone A, Destefano J, et al. The role of subchondral bone remodeling in osteoarthritis: reduction of cartilage degeneration and prevention of osteophyte formation by alendronate in the rat anterior cruciate ligament transection model. *Arthritis Rheum.* 2004;50(4):1193-206.
 47. Pastoureaux PC, Chomel AC, Bonnet J. Evidence of early subchondral bone changes in the meniscectomized guinea pig. A densitometric study using dual-energy X-ray absorptiometry subregional analysis. *Osteoarthritis Cartilage.* 1999;7(5):466-73.
 48. Bailey AJ, Mansell JP, Sims TJ, Banse X. Biochemical and mechanical properties of subchondral bone in osteoarthritis. *Biorheology.* 2004;41(3-4):349-58.
 49. Couchourel D, Aubry I, Delalandre A, Lavigne M, Martel-Pelletier J, Pelletier JP, et al. Altered mineralization of human osteoarthritic osteoblasts is attributable to abnormal type I collagen production. *Arthritis Rheum.* 2009;60(5):1438-50.
 50. Fazzalari NL, Parkinson IH. Fractal properties of subchondral cancellous bone in severe osteoarthritis of the

- hip. *J Bone Miner Res.* 1997;12(4):632-40.
51. Grynblas MD, Alpert B, Katz I, Lieberman I, Pritzker KP. Subchondral bone in osteoarthritis. *Calcif Tissue Int.* 1991;49(1):20-6.
 52. Pugh JW, Radin EL, Rose RM. Quantitative studies of human subchondral cancellous bone. Its relationship to the state of its overlying cartilage. *J Bone Joint Surg Am.* 1974;56(2):313-21.
 53. Radin EL, Paul IL, Lowy M. A comparison of the dynamic force transmitting properties of subchondral bone and articular cartilage. *J Bone Joint Surg Am.* 1970;52(3):444-56.
 54. Bobinac D, Spanjol J, Zoricic S, Maric I. Changes in articular cartilage and subchondral bone histomorphometry in osteoarthritic knee joints in humans. *Bone.* 2003;32(3):284-90.
 55. Dennis G, Jr., Sherman BT, Hosack DA, Yang J, Gao W, Lane HC, et al. DAVID: Database for Annotation, Visualization, and Integrated Discovery. *Genome Biol.* 2003;4(5):P3.
 56. Li B, Aspden RM. Composition and mechanical properties of cancellous bone from the femoral head of patients with osteoporosis or osteoarthritis. *J Bone Miner Res.* 1997;12(4):641-51.
 57. Li B, Aspden RM. Mechanical and material properties of the subchondral bone plate from the femoral head of patients with osteoarthritis or osteoporosis. *Ann Rheum Dis.* 1997;56(4):247-54.
 58. Day JS, Ding M, van der Linden JC, Hvid I, Sumner DR, Weinans H. A decreased subchondral trabecular bone tissue elastic modulus is associated with pre-arthritis cartilage damage. *J Orthop Res.* 2001;19(5):914-8.
 59. van Lent PL, Blom AB, van der Kraan P, Holthuysen AE, Vitters E, van Rooijen N, et al. Crucial role of synovial lining macrophages in the promotion of transforming growth factor beta-mediated osteophyte formation. *Arthritis Rheum.* 2004;50(1):103-11.
 60. Blom AB, van Lent PL, Holthuysen AE, van der Kraan PM, Roth J, van Rooijen N, et al. Synovial lining macrophages mediate osteophyte formation during experimental osteoarthritis. *Osteoarthritis Cartilage.* 2004;12(8):627-35.
 61. Knight AD, Levick JR. Morphometry of the ultrastructure of the blood-joint barrier in the rabbit knee. *Q J Exp Physiol.* 1984;69(2):271-88.
 62. Hui AY, McCarty WJ, Masuda K, Firestein GS, Sah RL. A systems biology approach to synovial joint lubrication in health, injury, and disease. *Wiley Interdiscip Rev Syst Biol Med.* 2012;4(1):15-37.
 63. Krenn V, Morawietz L, Haupl T, Neidel J, Petersen I, Konig A. Grading of chronic synovitis--a histopathological grading system for molecular and diagnostic pathology. *Pathol Res Pract.* 2002;198(5):317-25.
 64. Bendele AM, Hulman JF. Spontaneous cartilage degeneration in guinea pigs. *Arthritis Rheum.* 1988;31(4):561-5.
 65. Silverstein E, Sokoloff L. Natural history of degenerative joint disease in small laboratory animals. 5. Osteoarthritis in guinea pigs. *Arthritis Rheum.* 1958;1(1):82-6.
 66. Stoop R, Buma P, van der Kraan PM, Hollander AP, Billingham RC, Meijers TH, et al. Type II collagen degradation in articular cartilage fibrillation after anterior cruciate ligament transection in rats. *Osteoarthritis Cartilage.* 2001;9(4):308-15.
 67. Kamekura S, Hoshi K, Shimoaka T, Chung U, Chikuda H, Yamada T, et al. Osteoarthritis development in novel experimental mouse models induced by knee joint instability. *Osteoarthritis Cartilage.* 2005;13(7):632-41.
 68. Inoue A, Takahashi KA, Arai Y, Tonomura H, Sakao K, Saito M, et al. The therapeutic effects of basic fibroblast

-
- growth factor contained in gelatin hydrogel microspheres on experimental osteoarthritis in the rabbit knee. *Arthritis Rheum.* 2006;54(1):264-70.
69. DeGroot J, Verzijl N, Wenting-van Wijk MJ, Jacobs KM, Van El B, Van Roermund PM, et al. Accumulation of advanced glycation end products as a molecular mechanism for aging as a risk factor in osteoarthritis. *Arthritis Rheum.* 2004;50(4):1207-15.
70. McDevitt CA, Webber RJ. The ultrastructure and biochemistry of meniscal cartilage. *Clin Orthop Relat Res.* 1990(252):8-18.
71. Wancket LM, Baragi V, Bove S, Kilgore K, Korytko PJ, Guzman RE. Anatomical localization of cartilage degradation markers in a surgically induced rat osteoarthritis model. *Toxicol Pathol.* 2005;33(4):484-9.
72. Elder CL, Dahners LE, Weinhold PS. A cyclooxygenase-2 inhibitor impairs ligament healing in the rat. *Am J Sports Med.* 2001;29(6):801-5.
73. Marijnissen AC, van Roermund PM, Verzijl N, Tekoppele JM, Bijlsma JW, Lafeber FP. Steady progression of osteoarthritic features in the canine groove model. *Osteoarthritis Cartilage.* 2002;10(4):282-9.
74. Bentley G. Articular cartilage studies and osteoarthrosis. *Ann R Coll Surg Engl.* 1975;57(2):86-100.
75. Guzman RE, Evans MG, Bove S, Morenko B, Kilgore K. Mono-iodoacetate-induced histologic changes in subchondral bone and articular cartilage of rat femorotibial joints: an animal model of osteoarthritis. *Toxicol Pathol.* 2003;31(6):619-24.
76. Janusz MJ, Hookfin EB, Heitmeyer SA, Woessner JF, Freemont AJ, Hoyland JA, et al. Moderation of iodoacetate-induced experimental osteoarthritis in rats by matrix metalloproteinase inhibitors. *Osteoarthritis Cartilage.* 2001;9(8):751-60.
77. Pomonis JD, Boulet JM, Gottshall SL, Phillips S, Sellers R, Bunton T, et al. Development and pharmacological characterization of a rat model of osteoarthritis pain. *Pain.* 2005;114(3):339-46.
78. van der Kraan PM, Vitters EL, van de Putte LB, van den Berg WB. Development of osteoarthritic lesions in mice by "metabolic" and "mechanical" alterations in the knee joints. *Am J Pathol.* 1989;135(6):1001-14.
79. Weng LH, Wang CJ, Ko JY, Sun YC, Wang FS. Control of Dkk-1 ameliorates chondrocyte apoptosis, cartilage destruction, and subchondral bone deterioration in osteoarthritic knees. *Arthritis Rheum.* 2010;62(5):1393-402.
80. van Osch GJ, van der Kraan PM, Vitters EL, Blankevoort L, van den Berg WB. Induction of osteoarthritis by intra-articular injection of collagenase in mice. Strain and sex related differences. *Osteoarthritis Cartilage.* 1993;1(3):171-7.
81. Murat N, Karadam B, Ozkal S, Karatosun V, Gidener S. [Quantification of papain-induced rat osteoarthritis in relation to time with the Mankin score]. *Acta Orthop Traumatol Turc.* 2007;41(3):233-7.
82. Murray DG. Experimentally Induced Arthritis Using Intra-Articular Papain. *Arthritis Rheum.* 1964;7:211-9.
83. Cifuentes DJ, Rocha LG, Silva LA, Brito AC, Rueff-Barroso CR, Porto LC, et al. Decrease in oxidative stress and histological changes induced by physical exercise calibrated in rats with osteoarthritis induced by monosodium iodoacetate. *Osteoarthritis Cartilage.* 2010;18(8):1088-95.
84. Pap G, Eberhardt R, Sturmer I, Machner A, Schwarzberg H, Roessner A, et al. Development of osteoarthritis in the knee joints of Wistar rats after strenuous running exercise in a running wheel by intracranial self-stimulation. *Pathol Res Pract.* 1998;194(1):41-7.

85. Roemhildt ML, Beynon BD, Gardner-Morse M, Badger G, Grant C. **Changes induced by chronic in vivo load alteration in the tibiofemoral joint of mature rabbits.** *J Orthop Res.* 2012;30(9):1413-22.
86. Roemhildt ML, Beynon BD, Gauthier AE, Gardner-Morse M, Ertem F, Badger GJ. **Chronic in vivo load alteration induces degenerative changes in the rat tibiofemoral joint.** *Osteoarthritis Cartilage.* 2013;21(2):346-57.
87. Sokoloff L, Crittenden LB, Yamamoto RS, Jay GE, Jr. **The genetics of degenerative joint disease in mice.** *Arthritis Rheum.* 1962;5:531-46.
88. Black A, Lane MA. **Nonhuman primate models of skeletal and reproductive aging.** *Gerontology.* 2002;48(2):72-80.
89. Bendele AM. **Animal models of osteoarthritis.** *J Musculoskelet Neuronal Interact.* 2001;1(4):363-76.
90. Moore EE, Bendele AM, Thompson DL, Littau A, Waggle KS, Reardon B, et al. **Fibroblast growth factor-18 stimulates chondrogenesis and cartilage repair in a rat model of injury-induced osteoarthritis.** *Osteoarthritis Cartilage.* 2005;13(7):623-31.
91. Guingamp C, Gegout-Pottie P, Philippe L, Terlain B, Netter P, Gillet P. **Mono-iodoacetate-induced experimental osteoarthritis: a dose-response study of loss of mobility, morphology, and biochemistry.** *Arthritis Rheum.* 1997;40(9):1670-9.
92. Kotwal N, Li J, Sandy J, Plaas A, Sumner DR. **Initial application of EPIC-muCT to assess mouse articular cartilage morphology and composition: effects of aging and treadmill running.** *Osteoarthritis Cartilage.* 2012;20(8):887-95.
93. Beckett J, Jin W, Schultz M, Chen A, Tolbert D, Moed BR, et al. **Excessive running induces cartilage degeneration in knee joints and alters gait of rats.** *J Orthop Res.* 2012;30(10):1604-10.
94. Kellgren JH, Lawrence JS. **Radiological assessment of osteo-arthrosis.** *Ann Rheum Dis.* 1957;16(4):494-502.
95. Cubukcu D, Sarsan A, Alkan H. **Relationships between Pain, Function and Radiographic Findings in Osteoarthritis of the Knee: A Cross-Sectional Study.** *Arthritis.* 2012;2012:984060.
96. Finan PH, Buenaver LF, Bounds SC, Hussain S, Park RJ, Haque UJ, et al. **Discordance between pain and radiographic severity in knee osteoarthritis: findings from quantitative sensory testing of central sensitization.** *Arthritis Rheum.* 2013;65(2):363-72.
97. Guermazi A, Roemer FW, Haugen IK, Crema MD, Hayashi D. **MRI-based semiquantitative scoring of joint pathology in osteoarthritis.** *Nat Rev Rheumatol.* 2013;9(4):236-51.
98. Bashir A, Gray ML, Hartke J, Burstein D. **Nondestructive imaging of human cartilage glycosaminoglycan concentration by MRI.** *Magn Reson Med.* 1999;41(5):857-65.
99. Eckstein F, Cicuttini F, Raynauld JP, Waterton JC, Peterfy C. **Magnetic resonance imaging (MRI) of articular cartilage in knee osteoarthritis (OA): morphological assessment.** *Osteoarthritis Cartilage.* 2006;14 Suppl A:A46-75.
100. Eckstein F, Burstein D, Link TM. **Quantitative MRI of cartilage and bone: degenerative changes in osteoarthritis.** *NMR Biomed.* 2006;19(7):822-54.
101. Bashir A, Gray ML, Burstein D. **Gd-DTPA2- as a measure of cartilage degradation.** *Magn Reson Med.* 1996;36(5):665-73.
102. Bashir A, Gray ML, Boutin RD, Burstein D. **Glycosaminoglycan in articular cartilage: in vivo assessment with delayed Gd(DTPA)(2-)-enhanced MR imaging.** *Radiology.* 1997;205(2):551-8.

-
103. Grushko G, Schneiderman R, Maroudas A. Some biochemical and biophysical parameters for the study of the pathogenesis of osteoarthritis: a comparison between the processes of ageing and degeneration in human hip cartilage. *Connect Tissue Res.* 1989;19(2-4):149-76.
 104. Crema MD, Roemer FW, Marra MD, Burstein D, Gold GE, Eckstein F, et al. Articular cartilage in the knee: current MR imaging techniques and applications in clinical practice and research. *Radiographics.* 2011;31(1):37-61.
 105. Trattnig S, Domayer S, Welsch GW, Mosher T, Eckstein F. MR imaging of cartilage and its repair in the knee--a review. *Eur Radiol.* 2009;19(7):1582-94.
 106. Gatehouse PD, Thomas RW, Robson MD, Hamilton G, Herlihy AH, Bydder GM. Magnetic resonance imaging of the knee with ultrashort TE pulse sequences. *Magn Reson Imaging.* 2004;22(8):1061-7.
 107. Bieri O, Scheffler K, Welsch GH, Trattnig S, Mamisch TC, Ganter C. Quantitative mapping of T(2) using partial spoiling. *Magn Reson Med.* 2011.
 108. Williams A, Qian Y, Bear D, Chu CR. Assessing degeneration of human articular cartilage with ultra-short echo time (UTE) T2* mapping. *Osteoarthritis Cartilage.* 2010;18(4):539-46.
 109. Neu CP, Walton JH. Displacement encoding for the measurement of cartilage deformation. *Magn Reson Med.* 2008;59(1):149-55.
 110. Muller-Gerbl M. The subchondral bone plate. *Adv Anat Embryol Cell Biol.* 1998;141:III-XI, 1-134.
 111. Muller-Gerbl M, Putz R, Kenn R. Demonstration of subchondral bone density patterns by three-dimensional CT osteoabsorptiometry as a noninvasive method for in vivo assessment of individual long-term stresses in joints. *J Bone Miner Res.* 1992;7 Suppl 2:S411-8.
 112. Eckstein F, Putz R, Muller-Gerbl M, Steinlechner M, Benedetto KP. Cartilage degeneration in the human patellae and its relationship to the mineralisation of the underlying bone: a key to the understanding of chondromalacia patellae and femoropatellar arthrosis? *Surg Radiol Anat.* 1993;15(4):279-86.
 113. Palmer AW, Guldberg RE, Levenston ME. Analysis of cartilage matrix fixed charge density and three-dimensional morphology via contrast-enhanced microcomputed tomography. *Proc Natl Acad Sci U S A.* 2006;103(51):19255-60.
 114. Xie L, Lin AS, Guldberg RE, Levenston ME. Nondestructive assessment of sGAG content and distribution in normal and degraded rat articular cartilage via EPIC-muCT. *Osteoarthritis and Cartilage.* 2010;18(1):65-72.
 115. Piscaer TM, Waarsing JH, Kops N, Pavljasevic P, Verhaar JA, van Osch GJ, et al. In vivo imaging of cartilage degeneration using microCT-arthrography. *Osteoarthritis Cartilage.* 2008;16(9):1011-7.
 116. Xie L, Lin AS, Levenston ME, Guldberg RE. Quantitative assessment of articular cartilage morphology via EPIC-microCT. *Osteoarthritis Cartilage.* 2009;17(3):313-20.
 117. Thote T, Lin AS, Raji Y, Moran S, Stevens HY, Hart M, et al. Localized 3D analysis of cartilage composition and morphology in small animal models of joint degeneration. *Osteoarthritis Cartilage.* 2013;21(8):1132-41.
 118. Beekman F, van der Have F. The pinhole: gateway to ultra-high-resolution three-dimensional radionuclide imaging. *Eur J Nucl Med Mol Imaging.* 2007;34(2):151-61.
 119. Hume SP, Brown DJ, Ashworth S, Hirani E, Luthra SK, Lammertsma AA. In vivo saturation kinetics of two dopamine transporter probes measured using a small animal positron emission tomography scanner. *J Neurosci Methods.* 1997;76(1):45-51.
 120. Hart R, Konvicka M, Filan P, deCordeiro J. SPECT scan is a reliable tool for selection of patients undergoing

- unicompartmental knee arthroplasty. *Arch Orthop Trauma Surg.* 2008;128(7):679-82.
121. Kim CK, Park KW. Characteristic appearance of facet osteoarthritis of the lower lumbar spine on planar bone scintigraphy with a high negative predictive value for metastasis. *Clin Nucl Med.* 2008;33(4):251-4.
 122. Knupp M, Pagenstert GI, Barg A, Bolliger L, Easley ME, Hintermann B. SPECT-CT compared with conventional imaging modalities for the assessment of the varus and valgus malaligned hindfoot. *J Orthop Res.* 2009;27(11):1461-6.
 123. McCrae F, Shouls J, Dieppe P, Watt I. Scintigraphic assessment of osteoarthritis of the knee joint. *Ann Rheum Dis.* 1992;51(8):938-42.
 124. Cook GJ, Ryan PJ, Clarke SE, Fogelman I. SPECT bone scintigraphy of anterior cruciate ligament injury. *J Nucl Med.* 1996;37(8):1353-6.
 125. Ryan PJ, Reddy K, Fleetcroft J. A prospective comparison of clinical examination, MRI, bone SPECT, and arthroscopy to detect meniscal tears. *Clin Nucl Med.* 1998;23(12):803-6.
 126. Vellala RP, Manjure S, Ryan PJ. Single photon emission computed tomography scanning in the diagnosis of knee pathology. *J Orthop Surg (Hong Kong).* 2004;12(1):87-90.
 127. Siegel Y, Golan H, Thein R. 99mTc-methylene diphosphonate single photon emission tomography of the knees: intensity of uptake and its correlation with arthroscopic findings. *Nucl Med Commun.* 2006;27(9):689-93.
 128. Boegard T. Radiography and bone scintigraphy in osteoarthritis of the knee--comparison with MR imaging. *Acta Radiol Suppl.* 1998;418:7-37.
 129. Boegard T, Rudling O, Dahlstrom J, Dirksen H, Petersson IF, Jonsson K. Bone scintigraphy in chronic knee pain: comparison with magnetic resonance imaging. *Ann Rheum Dis.* 1999;58(1):20-6.
 130. Turk MJ, Breur GJ, Widmer WR, Paulos CM, Xu LC, Grote LA, et al. Folate-targeted imaging of activated macrophages in rats with adjuvant-induced arthritis. *Arthritis Rheum.* 2002;46(7):1947-55.
 131. Piscaer TM, Müller C, Mindt TL, Lubberts E, Verhaar JA, Krenning EP, et al. Imaging of activated macrophages in experimental osteoarthritis using folate-targeted animal single-photon-emission computed tomography/computed tomography. *Arthritis Rheum.* 2011;63(7):1898-907.
 132. Sun HB. Mechanical loading, cartilage degradation, and arthritis. *Ann N Y Acad Sci.* 2010;1211:37-50.
 133. Miclea RL, Karperien M, Bosch CA, van der Horst G, van der Valk MA, Kobayashi T, et al. Adenomatous polyposis coli-mediated control of beta-catenin is essential for both chondrogenic and osteogenic differentiation of skeletal precursors. *BMC Dev Biol.* 2009;9:26.
 134. Chun JS, Oh H, Yang S, Park M. Wnt signaling in cartilage development and degeneration. *BMB Rep.* 2008;41(7):485-94.
 135. Zhu M, Chen M, Zuscik M, Wu Q, Wang YJ, Rosier RN, et al. Inhibition of beta-catenin signaling in articular chondrocytes results in articular cartilage destruction. *Arthritis Rheum.* 2008;58(7):2053-64.
 136. Roemer FW, Mohr A, Lynch JA, Meta MD, Guermazi A, Genant HK. Micro-CT arthrography: a pilot study for the ex vivo visualization of the rat knee joint. *AJR Am J Roentgenol.* 2005;184(4):1215-9.
 137. Silvast TS, Jurvelin JS, Aula AS, Lammi MJ, Toyras J. Contrast agent-enhanced computed tomography of articular cartilage: association with tissue composition and properties. *Acta Radiol.* 2009;50(1):78-85.
 138. Silvast TS, Jurvelin JS, Lammi MJ, Toyras J. pQCT study on diffusion and equilibrium distribution of iodinated

-
- anionic contrast agent in human articular cartilage--associations to matrix composition and integrity. *Osteoarthritis Cartilage*. 2009;17(1):26-32.
139. Hangartner TN. **Thresholding technique for accurate analysis of density and geometry in QCT, pQCT and microCT images.** *J Musculoskelet Neuronal Interact*. 2007;7(1):9-16.
140. Sarzi-Puttini P, Cimmino MA, Scarpa R, Caporali R, Parazzini F, Zaninelli A, et al. **Osteoarthritis: an overview of the disease and its treatment strategies.** *Semin Arthritis Rheum*. 2005;35(1 Suppl 1):1-10.
141. Waarsing JH, Day JS, Weinans H. **An improved segmentation method for in vivo microCT imaging.** *J Bone Miner Res*. 2004;19(10):1640-50.
142. Tang T, Muneta T, Ju YJ, Nimura A, Miyazaki K, Masuda H, et al. **Serum keratan sulfate transiently increases in the early stage of osteoarthritis during strenuous running of rats: protective effect of intraarticular hyaluronan injection.** *Arthritis Res Ther*. 2008;10(1):R13.
143. Pritzker KP, Gay S, Jimenez SA, Ostergaard K, Pelletier JP, Revell PA, et al. **Osteoarthritis cartilage histopathology: grading and staging.** *Osteoarthritis Cartilage*. 2006;14(1):13-29.
144. Barve RA, Minnerly JC, Weiss DJ, Meyer DM, Aguiar DJ, Sullivan PM, et al. **Transcriptional profiling and pathway analysis of monosodium iodoacetate-induced experimental osteoarthritis in rats: relevance to human disease.** *Osteoarthritis Cartilage*. 2007;15(10):1190-8.
145. Wei T, Kulkarni NH, Zeng QQ, Helvering LM, Lin X, Lawrence F, et al. **Analysis of early changes in the articular cartilage transcriptome in the rat meniscal tear model of osteoarthritis: pathway comparisons with the rat anterior cruciate transection model and with human osteoarthritic cartilage.** *Osteoarthritis Cartilage*. 2010;18(7):992-1000.
146. Brouwers JE, van Rietbergen B, Huijkes R. **No effects of in vivo micro-CT radiation on structural parameters and bone marrow cells in proximal tibia of wistar rats detected after eight weekly scans.** *J Orthop Res*. 2007;25(10):1325-32.
147. Maroudas A. **Distribution and diffusion of solutes in articular cartilage.** *Biophys J*. 1970;10(5):365-79.
148. Perlewitz TJ, Haughton VM, Riley LH, 3rd, Nguyen-Minh C, George V. **Effect of molecular weight on the diffusion of contrast media into cartilage.** *Spine (Phila Pa 1976)*. 1997;22(23):2707-10.
149. Aula AS, Jurvelin JS, Toyras J. **Simultaneous computed tomography of articular cartilage and subchondral bone.** *Osteoarthritis Cartilage*. 2009;17(12):1583-8.
150. Bansal PN, Joshi NS, Entezari V, Grinstaff MW, Snyder BD. **Contrast enhanced computed tomography can predict the glycosaminoglycan content and biomechanical properties of articular cartilage.** *Osteoarthritis Cartilage*. 2010;18(2):184-91.
151. Otterness IG, Eskra JD, Bliven ML, Shay AK, Pelletier JP, Milici AJ. **Exercise protects against articular cartilage degeneration in the hamster.** *Arthritis Rheum*. 1998;41(11):2068-76.
152. Galois L, Etienne S, Grossin L, Watrin-Pinzano A, Cournil-Henrionnet C, Loeuille D, et al. **Dose-response relationship for exercise on severity of experimental osteoarthritis in rats: a pilot study.** *Osteoarthritis Cartilage*. 2004;12(10):779-86.
153. Kiviranta I, Tammi M, Jurvelin J, Saamanen AM, Helminen HJ. **Moderate running exercise augments glycosaminoglycans and thickness of articular cartilage in the knee joint of young beagle dogs.** *J Orthop Res*. 1988;6(2):188-95.

154. Kiviranta I, Tammi M, Jurvelin J, Arokoski J, Saamanen AM, Helminen HJ. Articular cartilage thickness and glycosaminoglycan distribution in the canine knee joint after strenuous running exercise. *Clin Orthop Relat Res.* 1992;283:302-8.
155. Little CB, Ghosh P, Rose R. The effect of strenuous versus moderate exercise on the metabolism of proteoglycans in articular cartilage from different weight-bearing regions of the equine third carpal bone. *Osteoarthritis Cartilage.* 1997;5(3):161-72.
156. Saxon L, Finch C, Bass S. Sports participation, sports injuries and osteoarthritis: implications for prevention. *Sports Med.* 1999;28(2):123-35.
157. Siebelt M, Waarsing JH, Kops N, Piscaer TM, Verhaar JA, Oei EH, et al. Quantifying osteoarthritic cartilage changes accurately using in vivo microCT arthrography in three etiologically distinct rat models. *J Orthop Res.* 2011;29(11):1788-94.
158. Galois L, Etienne S, Grosse L, Cournil C, Pinzano A, Netter P, et al. Moderate-impact exercise is associated with decreased severity of experimental osteoarthritis in rats. *Rheumatology (Oxford).* 2003;42(5):692-3; author reply 3-4.
159. Scanzello CR, Goldring SR. The role of synovitis in osteoarthritis pathogenesis. *Bone.* 2012;51(2):249-57.
160. Huang MH, Ding HJ, Chai CY, Huang YF, Yang RC. Effects of sonication on articular cartilage in experimental osteoarthritis. *J Rheumatol.* 1997;24(10):1978-84.
161. Spataro RF, Katzberg RW, Burgener FA, Fischer HW. Epinephrine enhanced knee arthrography. *Invest Radiol.* 1978;13(4):286-90.
162. Tarini VA, Carnevali LC, Jr., Arida RM, Cunha CA, Alves ES, Seeleander MC, et al. Effect of exhaustive ultra-endurance exercise in muscular glycogen and both Alpha1 and Alpha2 Ampk protein expression in trained rats. *J Physiol Biochem.* 2013;69(3):429-40.
163. Xia W, Hilgenbrink AR, Matteson EL, Lockwood MB, Cheng JX, Low PS. A functional folate receptor is induced during macrophage activation and can be used to target drugs to activated macrophages. *Blood.* 2009;113(2):438-46.
164. Low PS, Henne WA, Doorneweerd DD. Discovery and development of folic-acid-based receptor targeting for imaging and therapy of cancer and inflammatory diseases. *Acc Chem Res.* 2008;41(1):120-9.
165. Schroeder RP, De Blois E, De Ridder CM, Van Weerden WM, Breeman WA, de Jong M. Improving radiolabelled peptide pharmacokinetics by adjusting experimental conditions for bombesin receptor-targeted imaging of prostate cancer. *Q J Nucl Med Mol Imaging.* 2012;56(5):468-75.
166. Breeman WA, de Jong M, de Blois E, Bernard BF, Konijnenberg M, Krenning EP. Radiolabelling DOTA-peptides with ⁶⁸Ga. *Eur J Nucl Med Mol Imaging.* 2005;32(4):478-85.
167. Decristoforo C, Knopp R, von Guggenberg E, Rupprich M, Dreger T, Hess A, et al. A fully automated synthesis for the preparation of ⁶⁸Ga-labelled peptides. *Nucl Med Commun.* 2007;28(11):870-5.
168. Farkas T, Bihari-Varga M, Biro T. Thermoanalytical and histological study of intra-articular papain-induced degradation and repair of rabbit cartilage. II. Mature animals. *Ann Rheum Dis.* 1976;35(1):23-6.
169. Nagaoka D, Tsukise A, Meyer W. Ultracytochemistry of glycosaminoglycans in the canine knee synovium. *Ann Anat.* 2001;183(3):229-36.
170. Siebelt M, Jahr H, Groen HC, Sandker M, Waarsing JH, Kops N, et al. Hsp90 inhibition protects against

-
- biomechanically induced osteoarthritis in rats. *Arthritis Rheum.* 2013;65(8):2102-12.
171. Crockett JC, Rogers MJ, Coxon FP, Hocking LJ, Helfrich MH. **Bone remodelling at a glance.** *J Cell Sci.* 2011;124(Pt 7):991-8.
172. Turner CH. **Three rules for bone adaptation to mechanical stimuli.** *Bone.* 1998;23(5):399-407.
173. Clarke KA, Heitmeyer SA, Smith AG, Taiwo YO. **Gait analysis in a rat model of osteoarthritis.** *Physiol Behav.* 1997;62(5):951-4.
174. O'Connor BL, Visco DM, Heck DA, Myers SL, Brandt KD. **Gait alterations in dogs after transection of the anterior cruciate ligament.** *Arthritis Rheum.* 1989;32(9):1142-7.
175. Martyn-St James M, Carroll S. **Meta-analysis of walking for preservation of bone mineral density in postmenopausal women.** *Bone.* 2008;43(3):521-31.
176. Polidoulis I, Beyene J, Cheung AM. **The effect of exercise on pQCT parameters of bone structure and strength in postmenopausal women--a systematic review and meta-analysis of randomized controlled trials.** *Osteoporos Int.* 2012;23(1):39-51.
177. Bondeson J, Wainwright SD, Lauder S, Amos N, Hughes CE. **The role of synovial macrophages and macrophage-produced cytokines in driving aggrecanases, matrix metalloproteinases, and other destructive and inflammatory responses in osteoarthritis.** *Arthritis Res Ther.* 2006;8(6):R187.
178. Mosser DM, Edwards JP. **Exploring the full spectrum of macrophage activation.** *Nat Rev Immunol.* 2008;8(12):958-69.
179. Tsuneyoshi Y, Tanaka M, Nagai T, Sunahara N, Matsuda T, Sonoda T, et al. **Functional folate receptor beta-expressing macrophages in osteoarthritis synovium and their M1/M2 expression profiles.** *Scand J Rheumatol.* 2012;41(2):132-40.
180. Adams CS, Horton WE, Jr. **Chondrocyte apoptosis increases with age in the articular cartilage of adult animals.** *Anat Rec.* 1998;250(4):418-25.
181. Horton WE, Jr., Feng L, Adams C. **Chondrocyte apoptosis in development, aging and disease.** *Matrix Biol.* 1998;17(2):107-15.
182. Felson DT, Lawrence RC, Dieppe PA, Hirsch R, Helmick CG, Jordan JM, et al. **Osteoarthritis: new insights. Part 1: the disease and its risk factors.** *Ann Intern Med.* 2000;133(8):635-46.
183. Felson DT, Zhang Y. **An update on the epidemiology of knee and hip osteoarthritis with a view to prevention.** *Arthritis Rheum.* 1998;41(8):1343-55.
184. Messier SP, Loeser RF, Miller GD, Morgan TM, Rejeski WJ, Sevick MA, et al. **Exercise and dietary weight loss in overweight and obese older adults with knee osteoarthritis: the Arthritis, Diet, and Activity Promotion Trial.** *Arthritis Rheum.* 2004;50(5):1501-10.
185. Pacifici M, Koyama E, Iwamoto M. **Mechanisms of synovial joint and articular cartilage formation: recent advances, but many lingering mysteries.** *Birth Defects Res C Embryo Today.* 2005;75(3):237-48.
186. Aigner T, Zien A, Gehrsitz A, Gebhard PM, McKenna L. **Anabolic and catabolic gene expression pattern analysis in normal versus osteoarthritic cartilage using complementary DNA-array technology.** *Arthritis Rheum.* 2001;44(12):2777-89.
187. Zhu M, Tang D, Wu Q, Hao S, Chen M, Xie C, et al. **Activation of beta-catenin signaling in articular chondrocytes leads to osteoarthritis-like phenotype in adult beta-catenin conditional activation mice.** *J*

- Bone Miner Res.* 2009;24(1):12-21.
188. Doble BW, Woodgett JR. **GSK-3: tricks of the trade for a multi-tasking kinase.** *J Cell Sci.* 2003;116(Pt 7):1175-86.
189. Kapadia RM, Guntur AR, Reinhold MI, Naski MC. **Glycogen synthase kinase 3 controls endochondral bone development: contribution of fibroblast growth factor 18.** *Dev Biol.* 2005;285(2):496-507.
190. Engler TA, Henry JR, Malhotra S, Cunningham B, Furness K, Brozinick J, et al. **Substituted 3-imidazo[1,2-a]pyridin-3-yl-4-(1,2,3,4-tetrahydro-[1,4]diazepino-[6,7,1-hi]indol-7-yl)pyrrole-2,5-diones as highly selective and potent inhibitors of glycogen synthase kinase-3.** *J Med Chem.* 2004;47(16):3934-7.
191. van der Horst G, van der Werf SM, Farih-Sips H, van Bezooijen RL, Lowik CW, Karperien M. **Downregulation of Wnt signaling by increased expression of Dickkopf-1 and -2 is a prerequisite for late-stage osteoblast differentiation of KS483 cells.** *J Bone Miner Res.* 2005;20(10):1867-77.
192. Smink JJ, Buchholz IM, Hamers N, van Tilburg CM, Christis C, Sackers RJ, et al. **Short-term glucocorticoid treatment of piglets causes changes in growth plate morphology and angiogenesis.** *Osteoarthritis Cartilage.* 2003;11(12):864-71.
193. Hoogendam J, Parlevliet E, Miclea R, Lowik CW, Wit JM, Karperien M. **Novel early target genes of parathyroid hormone-related peptide in chondrocytes.** *Endocrinology.* 2006;147(6):3141-52.
194. Jonnalagadda S, Srinivasan R. **Principal components analysis based methodology to identify differentially expressed genes in time-course microarray data.** *BMC Bioinformatics.* 2008;9:267.
195. Ashburner M, Ball CA, Blake JA, Botstein D, Butler H, Cherry JM, et al. **Gene ontology: tool for the unification of biology. The Gene Ontology Consortium.** *Nat Genet.* 2000;25(1):25-9.
196. Huang da W, Sherman BT, Lempicki RA. **Systematic and integrative analysis of large gene lists using DAVID bioinformatics resources.** *Nat Protoc.* 2009;4(1):44-57.
197. Cai Y, Mohseny AB, Karperien M, Hogendoorn PC, Zhou G, Cleton-Jansen AM. **Inactive Wnt/beta-catenin pathway in conventional high-grade osteosarcoma.** *J Pathol.* 2010;220(1):24-33.
198. Mushtaq T, Bijman P, Ahmed SF, Farquharson C. **Insulin-like growth factor-I augments chondrocyte hypertrophy and reverses glucocorticoid-mediated growth retardation in fetal mice metatarsal cultures.** *Endocrinology.* 2004;145(5):2478-86.
199. Choi YA, Kang SS, Jin EJ. **BMP-2 treatment of C3H10T1/2 mesenchymal cells blocks MMP-9 activity during chondrocyte commitment.** *Cell Biol Int.* 2009;33(8):887-92.
200. Wu Q, Huang JH, Sampson ER, Kim KO, Zuscik MJ, O'Keefe RJ, et al. **Smurf2 induces degradation of GSK-3beta and upregulates beta-catenin in chondrocytes: a potential mechanism for Smurf2-induced degeneration of articular cartilage.** *Exp Cell Res.* 2009;315(14):2386-98.
201. Katoh M. **Cross-talk of WNT and FGF signaling pathways at GSK3beta to regulate beta-catenin and SNAIL signaling cascades.** *Cancer Biol Ther.* 2006;5(9):1059-64.
202. Takenaka K, Kise Y, Miki H. **GSK3beta positively regulates Hedgehog signaling through Sufu in mammalian cells.** *Biochem Biophys Res Commun.* 2007;353(2):501-8.
203. Day TF, Yang Y. **Wnt and hedgehog signaling pathways in bone development.** *J Bone Joint Surg Am.* 2008;90 Suppl 1:19-24.
204. Ornitz DM. **FGF signaling in the developing endochondral skeleton.** *Cytokine Growth Factor Rev.*

-
- 2005;16(2):205-13.
205. Mercader N, Fischer S, Neumann CJ. Prdm1 acts downstream of a sequential RA, Wnt and Fgf signaling cascade during zebrafish forelimb induction. *Development*. 2006;133(15):2805-15.
206. ten Berge D, Brugmann SA, Helms JA, Nusse R. Wnt and FGF signals interact to coordinate growth with cell fate specification during limb development. *Development*. 2008;135(19):3247-57.
207. Jukkola T, Sinjushina N, Partanen J. Drapc1 expression during mouse embryonic development. *Gene Expr Patterns*. 2004;4(6):755-62.
208. Rousset R, Mack JA, Wharton KA, Jr., Axelrod JD, Cadigan KM, Fish MP, et al. Naked cuticle targets dishevelled to antagonize Wnt signal transduction. *Genes Dev*. 2001;15(6):658-71.
209. Jho EH, Zhang T, Doman C, Joo CK, Freund JN, Costantini F. Wnt/beta-catenin/Tcf signaling induces the transcription of Axin2, a negative regulator of the signaling pathway. *Mol Cell Biol*. 2002;22(4):1172-83.
210. Moon RT, Bowerman B, Boutros M, Perrimon N. The promise and perils of Wnt signaling through beta-catenin. *Science*. 2002;296(5573):1644-6.
211. Zeng W, Wharton KA, Jr., Mack JA, Wang K, Gadabaw M, Suyama K, et al. naked cuticle encodes an inducible antagonist of Wnt signalling. *Nature*. 2000;403(6771):789-95.
212. Sandell LJ, Aigner T. Articular cartilage and changes in arthritis. An introduction: cell biology of osteoarthritis. *Arthritis Res*. 2001;3(2):107-13.
213. Meng J, Ma X, Ma D, Xu C. Microarray analysis of differential gene expression in temporomandibular joint condylar cartilage after experimentally induced osteoarthritis. *Osteoarthritis Cartilage*. 2005;13(12):1115-25.
214. Mohtai M, Smith RL, Schurman DJ, Tsuji Y, Torti FM, Hutchinson NI, et al. Expression of 92-kD type IV collagenase/gelatinase (gelatinase B) in osteoarthritic cartilage and its induction in normal human articular cartilage by interleukin 1. *J Clin Invest*. 1993;92(1):179-85.
215. Pfander D, Cramer T, Weseloh G, Pullig O, Schuppan D, Bauer M, et al. Hepatocyte growth factor in human osteoarthritic cartilage. *Osteoarthritis Cartilage*. 1999;7(6):548-59.
216. Tsuchiya A, Yano M, Tocharu J, Kojima H, Fukumoto M, Kawaichi M, et al. Expression of mouse HtrA1 serine protease in normal bone and cartilage and its upregulation in joint cartilage damaged by experimental arthritis. *Bone*. 2005;37(3):323-36.
217. Velasco J, Zarrabeitia MT, Prieto JR, Perez-Castrillon JL, Perez-Aguilar MD, Perez-Nunez MI, et al. Wnt pathway genes in osteoporosis and osteoarthritis: differential expression and genetic association study. *Osteoporos Int*. 2010;21(1):109-18.
218. Hu SI, Carozza M, Klein M, Nantermet P, Luk D, Crowl RM. Human HtrA, an evolutionarily conserved serine protease identified as a differentially expressed gene product in osteoarthritic cartilage. *J Biol Chem*. 1998;273(51):34406-12.
219. Dankbar B, Neugebauer K, Wunrau C, Tibesku CO, Skwara A, Pap T, et al. Hepatocyte growth factor induction of macrophage chemoattractant protein-1 and osteophyte-inducing factors in osteoarthritis. *J Orthop Res*. 2007;25(5):569-77.
220. Gebauer M, Saas J, Haag J, Dietz U, Takigawa M, Bartnik E, et al. Repression of anti-proliferative factor Tob1 in osteoarthritic cartilage. *Arthritis Res Ther*. 2005;7(2):R274-84.
221. van der Weyden L, Wei L, Luo J, Yang X, Birk DE, Adams DJ, et al. Functional knockout of the matrilin-3

- gene causes premature chondrocyte maturation to hypertrophy and increases bone mineral density and osteoarthritis. *Am J Pathol.* 2006;169(2):515-27.
222. Lories RJ, Peeters J, Bakker A, Tylzanowski P, Derese I, Schrooten J, et al. Articular cartilage and biomechanical properties of the long bones in Frzb-knockout mice. *Arthritis Rheum.* 2007;56(12):4095-103.
223. Blanco FJ, Guitian R, Vazquez-Martul E, de Toro FJ, Galdo F. Osteoarthritis chondrocytes die by apoptosis. A possible pathway for osteoarthritis pathology. *Arthritis Rheum.* 1998;41(2):284-9.
224. Arya R, Mallik M, Lakhotia SC. Heat shock genes - integrating cell survival and death. *J Biosci.* 2007;32(3):595-610.
225. Samali A, Orrenius S. Heat shock proteins: regulators of stress response and apoptosis. *Cell Stress Chaperones.* 1998;3(4):228-36.
226. Terauchi R, Takahashi KA, Arai Y, Ikeda T, Ohashi S, Imanishi J, et al. Hsp70 prevents nitric oxide-induced apoptosis in articular chondrocytes. *Arthritis Rheum.* 2003;48(6):1562-8.
227. Etienne S, Gaborit N, Henrionnet C, Pinzano A, Galois L, Netter P, et al. Local induction of heat shock protein 70 (Hsp70) by proteasome inhibition confers chondroprotection during surgically induced osteoarthritis in the rat knee. *Biomed Mater Eng.* 2008;18(4-5):253-60.
228. Grossin L, Etienne S, Gaborit N, Pinzano A, Cournil-Henrionnet C, Gerard C, et al. Induction of heat shock protein 70 (Hsp70) by proteasome inhibitor MG 132 protects articular chondrocytes from cellular death in vitro and in vivo. *Biorheology.* 2004;41(3-4):521-34.
229. Takahashi K, Kubo T, Goomer RS, Amiel D, Kobayashi K, Imanishi J, et al. Analysis of heat shock proteins and cytokines expressed during early stages of osteoarthritis in a mouse model. *Osteoarthritis Cartilage.* 1997;5(5):321-9.
230. Takahashi KA, Tonomura H, Arai Y, Terauchi R, Honjo K, Hiraoka N, et al. Hyperthermia for the treatment of articular cartilage with osteoarthritis. *Int J Hyperthermia.* 2009;25(8):661-7.
231. Roman-Blas JA, Jimenez SA. NF-kappaB as a potential therapeutic target in osteoarthritis and rheumatoid arthritis. *Osteoarthritis Cartilage.* 2006;14(9):839-48.
232. Rice JW, Veal JM, Fadden RP, Barabasz AF, Partridge JM, Barta TE, et al. Small molecule inhibitors of Hsp90 potentially affect inflammatory disease pathways and exhibit activity in models of rheumatoid arthritis. *Arthritis Rheum.* 2008;58(12):3765-75.
233. Clarke PA, Hostein I, Banerji U, Stefano FD, Maloney A, Walton M, et al. Gene expression profiling of human colon cancer cells following inhibition of signal transduction by 17-allylamino-17-demethoxygeldanamycin, an inhibitor of the hsp90 molecular chaperone. *Oncogene.* 2000;19(36):4125-33.
234. Hamilton KL, Gupta S, Knowlton AA. Estrogen and regulation of heat shock protein expression in female cardiomyocytes: cross-talk with NF kappa B signaling. *J Mol Cell Cardiol.* 2004;36(4):577-84.
235. Roman-Blas JA, Castaneda S, Largo R, Herrero-Beaumont G. Osteoarthritis associated with estrogen deficiency. *Arthritis Res Ther.* 2009;11(5):241.
236. Lundgren K, Zhang H, Brekken J, Huser N, Powell RE, Timple N, et al. BIIB021, an orally available, fully synthetic small-molecule inhibitor of the heat shock protein Hsp90. *Mol Cancer Ther.* 2009;8(4):921-9.
237. Yun CH, Yoon SY, Nguyen TT, Cho HY, Kim TH, Kim ST, et al. Geldanamycin inhibits TGF-beta signaling through induction of Hsp70. *Arch Biochem Biophys.* 2010;495(1):8-13.

-
238. Glaze ER, Lambert AL, Smith AC, Page JG, Johnson WD, McCormick DL, et al. Preclinical toxicity of a geldanamycin analog, 17-(dimethylaminoethylamino)-17-demethoxygeldanamycin (17-DMAG), in rats and dogs: potential clinical relevance. *Cancer Chemother Pharmacol.* 2005;56(6):637-47.
239. Pastoureau P, Leduc S, Chomel A, De Ceuninck F. Quantitative assessment of articular cartilage and subchondral bone histology in the meniscectomized guinea pig model of osteoarthritis. *Osteoarthritis Cartilage.* 2003;11(6):412-23.
240. Gerwin N, Bendele AM, Glasson S, Carlson CS. The OARSI histopathology initiative - recommendations for histological assessments of osteoarthritis in the rat. *Osteoarthritis Cartilage.* 2010;18 Suppl 3:S24-34.
241. Boehm AK, Seth M, Mayr KG, Fortier LA. Hsp90 mediates insulin-like growth factor 1 and interleukin-1beta signaling in an age-dependent manner in equine articular chondrocytes. *Arthritis Rheum.* 2007;56(7):2335-43.
242. Wilson R, Belluoccio D, Bateman JF. Proteomic analysis of cartilage proteins. *Methods.* 2008;45(1):22-31.
243. van der Windt AE, Haak E, Das RH, Kops N, Welting TJ, Caron MM, et al. Physiological tonicity improves human chondrogenic marker expression through nuclear factor of activated T-cells 5 in vitro. *Arthritis Res Ther.* 2010;12(3):R100.
244. Xing H, Mayhew CN, Cullen KE, Park-Sarge OK, Sarge KD. HSF1 modulation of Hsp70 mRNA polyadenylation via interaction with symplekin. *J Biol Chem.* 2004;279(11):10551-5.
245. Hirano M, Shibato J, Rakwal R, Kouyama N, Katayama Y, Hayashi M, et al. Transcriptomic analysis of rat brain tissue following gamma knife surgery: early and distinct bilateral effects in the un-irradiated striatum. *Mol Cells.* 2009;27(2):263-8.
246. Guo W, Siegel D, Ross D. Stability of the Hsp90 inhibitor 17AAG hydroquinone and prevention of metal-catalyzed oxidation. *J Pharm Sci.* 2008;97(12):5147-57.
247. Soroka J, Buchner J. Mechanistic aspects of the Hsp90 phosphoregulation. *Cell Cycle.* 2012;11(10):1870-1.
248. Whitesell L, Bagatell R, Falsey R. The stress response: implications for the clinical development of hsp90 inhibitors. *Curr Cancer Drug Targets.* 2003;3(5):349-58.
249. Proctor CJ, Lorimer IA. Modelling the role of the Hsp70/Hsp90 system in the maintenance of protein homeostasis. *PLoS One.* 2011;6(7):e22038.
250. Solit DB, Zheng FF, Drobnjak M, Munster PN, Higgins B, Verbel D, et al. 17-Allylamino-17-demethoxygeldanamycin induces the degradation of androgen receptor and HER-2/neu and inhibits the growth of prostate cancer xenografts. *Clin Cancer Res.* 2002;8(5):986-93.
251. Shamovsky I, Nudler E. New insights into the mechanism of heat shock response activation. *Cell Mol Life Sci.* 2008;65(6):855-61.
252. Zou J, Guo Y, Guettouche T, Smith DF, Voellmy R. Repression of heat shock transcription factor HSF1 activation by HSP90 (HSP90 complex) that forms a stress-sensitive complex with HSF1. *Cell.* 1998;94(4):471-80.
253. Kaarniranta K, Holmberg CI, Lammi MJ, Eriksson JE, Sistonen L, Helminen HJ. Primary chondrocytes resist hydrostatic pressure-induced stress while primary synovial cells and fibroblasts show modified Hsp70 response. *Osteoarthritis Cartilage.* 2001;9(1):7-13.
254. Kimura H, Yukitake H, Tajima Y, Suzuki H, Chikatsu T, Morimoto S, et al. ITZ-1, a client-selective Hsp90 inhibitor, efficiently induces heat shock factor 1 activation. *Chem Biol.* 2010;17(1):18-27.

255. Dakappagari N, Neely L, Tangri S, Lundgren K, Hipolito L, Estrellado A, et al. An investigation into the potential use of serum Hsp70 as a novel tumour biomarker for Hsp90 inhibitors. *Biomarkers*. 2010;15(1):31-8.
256. Kimura H, Yukitake H, Suzuki H, Tajima Y, Gomaibashi K, Morimoto S, et al. The chondroprotective agent ITZ-1 inhibits interleukin-1beta-induced matrix metalloproteinase-13 production and suppresses nitric oxide-induced chondrocyte death. *J Pharmacol Sci*. 2009;110(2):201-11.
257. Neuhold LA, Killar L, Zhao W, Sung ML, Warner L, Kulik J, et al. Postnatal expression in hyaline cartilage of constitutively active human collagenase-3 (MMP-13) induces osteoarthritis in mice. *J Clin Invest*. 2001;107(1):35-44.
258. Minet E, Mottet D, Michel G, Roland I, Raes M, Remacle J, et al. Hypoxia-induced activation of HIF-1: role of HIF-1alpha-Hsp90 interaction. *FEBS Lett*. 1999;460(2):251-6.
259. Wax S, Piecyk M, Maritim B, Anderson P. Geldanamycin inhibits the production of inflammatory cytokines in activated macrophages by reducing the stability and translation of cytokine transcripts. *Arthritis Rheum*. 2003;48(2):541-50.
260. van Eden W, van der Zee R, Prakken B. Heat-shock proteins induce T-cell regulation of chronic inflammation. *Nat Rev Immunol*. 2005;5(4):318-30.
261. Kino T, Hatanaka H, Miyata S, Inamura N, Nishiyama M, Yajima T, et al. FK-506, a novel immunosuppressant isolated from a Streptomyces. II. Immunosuppressive effect of FK-506 in vitro. *J Antibiot (Tokyo)*. 1987;40(9):1256-65.
262. Sakuma S, Kato Y, Nishigaki F, Sasakawa T, Magari K, Miyata S, et al. FK506 potently inhibits T cell activation induced TNF-alpha and IL-1beta production in vitro by human peripheral blood mononuclear cells. *Br J Pharmacol*. 2000;130(7):1655-63.
263. Musson RE, Cobbaert CM, Smit NP. Molecular diagnostics of calcineurin-related pathologies. *Clin Chem*. 2012;58(3):511-22.
264. Furst DE, Saag K, Fleischmann MR, Sherrer Y, Block JA, Schnitzer T, et al. Efficacy of tacrolimus in rheumatoid arthritis patients who have been treated unsuccessfully with methotrexate: a six-month, double-blind, randomized, dose-ranging study. *Arthritis Rheum*. 2002;46(8):2020-8.
265. Yocum DE, Furst DE, Kaine JL, Baldassare AR, Stevenson JT, Borton MA, et al. Efficacy and safety of tacrolimus in patients with rheumatoid arthritis: a double-blind trial. *Arthritis Rheum*. 2003;48(12):3328-37.
266. Kang KY, Ju JH, Song YW, Yoo DH, Kim HY, Park SH. Tacrolimus treatment increases bone formation in patients with rheumatoid arthritis. *Rheumatol Int*. 2012.
267. Ranger AM, Gerstenfeld LC, Wang J, Kon T, Bae H, Gravallesse EM, et al. The nuclear factor of activated T cells (NFAT) transcription factor NFATp (NFATc2) is a repressor of chondrogenesis. *J Exp Med*. 2000;191(1):9-22.
268. Nakamura Y, Takarada T, Kodama A, Hinoi E, Yoneda Y. Predominant promotion by tacrolimus of chondrogenic differentiation to proliferating chondrocytes. *J Pharmacol Sci*. 2009;109(3):413-23.
269. Benito MJ, Veale DJ, FitzGerald O, van den Berg WB, Bresnihan B. Synovial tissue inflammation in early and late osteoarthritis. *Ann Rheum Dis*. 2005;64(9):1263-7.
270. van der Windt AE, Haak E, Kops N, Verhaar JA, Weinans H, Jahr H. Inhibiting calcineurin activity under physiologic tonicity elevates anabolic but suppresses catabolic chondrocyte markers. *Arthritis Rheum*. 2012;64(6):1929-39.

-
271. van der Windt AE, Jahr H, Farrell E, Verhaar JA, Weinans H, van Osch GJ. Calcineurin inhibitors promote chondrogenic marker expression of dedifferentiated human adult chondrocytes via stimulation of endogenous TGFbeta1 production. *Tissue Eng Part A*. 2010;16(1):1-10.
272. Yoo SA, Park BH, Yoon HJ, Lee JY, Song JH, Kim HA, et al. Calcineurin modulates the catabolic and anabolic activity of chondrocytes and participates in the progression of experimental osteoarthritis. *Arthritis Rheum*. 2007;56(7):2299-311.
273. Siebelt M, Groen HC, Koelewijn SJ, de Blois E, Sandker M, Waarsing JH, et al. Increased physical activity severely induces osteoarthritic changes in knee joints with papain induced sulphate-glycosaminoglycan depleted cartilage. *Arthritis Res Ther*. 2014;16(1):R32.
274. Uitterlinden EJ, Jahr H, Koevoet JL, Jenniskens YM, Bierma-Zeinstra SM, Degroot J, et al. Glucosamine decreases expression of anabolic and catabolic genes in human osteoarthritic cartilage explants. *Osteoarthritis Cartilage*. 2006;14(3):250-7.
275. Das RH, Jahr H, Verhaar JA, van der Linden JC, van Osch GJ, Weinans H. In vitro expansion affects the response of chondrocytes to mechanical stimulation. *Osteoarthritis Cartilage*. 2008;16(3):385-91.
276. Martin I, Jakob M, Schafer D, Dick W, Spagnoli G, Heberer M. Quantitative analysis of gene expression in human articular cartilage from normal and osteoarthritic joints. *Osteoarthritis Cartilage*. 2001;9(2):112-8.
277. Livak KJ, Schmittgen TD. Analysis of relative gene expression data using real-time quantitative PCR and the 2(-Delta Delta C(T)) Method. *Methods*. 2001;25(4):402-8.
278. Barlic A, Drobnic M, Malicev E, Kregar-Velikonja N. Quantitative analysis of gene expression in human articular chondrocytes assigned for autologous implantation. *J Orthop Res*. 2008;26(6):847-53.
279. Mandl EW, Jahr H, Koevoet JL, van Leeuwen JP, Weinans H, Verhaar JA, et al. Fibroblast growth factor-2 in serum-free medium is a potent mitogen and reduces dedifferentiation of human ear chondrocytes in monolayer culture. *Matrix Biol*. 2004;23(4):231-41.
280. Hellingman CA, Verwiel ET, Slagt I, Koevoet W, Poublon RM, Nolst-Trenite GJ, et al. Differences in cartilage-forming capacity of expanded human chondrocytes from ear and nose and their gene expression profiles. *Cell Transplant*. 2011;20(6):925-40.
281. Magari K, Nishigaki F, Sasakawa T, Ogawa T, Miyata S, Ohkubo Y, et al. Anti-arthritic properties of FK506 on collagen-induced arthritis in rats. *Inflamm Res*. 2003;52(12):524-9.
282. van der Jagt OP, van der Linden JC, Schaden W, van Schie HT, Piscaer TM, Verhaar JA, et al. Unfocused extracorporeal shock wave therapy as potential treatment for osteoporosis. *J Orthop Res*. 2009;27(11):1528-33.
283. Müller C, Vlahov IR, Santhapuram HK, Leamon CP, Schibli R. Tumor targeting using 67Ga-DOTA-Bz-folate-- investigations of methods to improve the tissue distribution of radiofolates. *Nucl Med Biol*. 2011;38(5):715-23.
284. Thiebaud D, Krieg MA, Gillard-Berguer D, Jacquet AF, Goy JJ, Burckhardt P. Cyclosporine induces high bone turnover and may contribute to bone loss after heart transplantation. *Eur J Clin Invest*. 1996;26(7):549-55.
285. McCauley LK, Rosol TJ, Capen CC. Effects of cyclosporin A on rat osteoblasts (ROS 17/2.8 cells) in vitro. *Calcif Tissue Int*. 1992;51(4):291-7.
286. Sun L, Blair HC, Peng Y, Zaidi N, Adebajo OA, Wu XB, et al. Calcineurin regulates bone formation by the osteoblast. *Proc Natl Acad Sci U S A*. 2005;102(47):17130-5.

287. Winslow MM, Pan M, Starbuck M, Gallo EM, Deng L, Karsenty G, et al. Calcineurin/NFAT signaling in osteoblasts regulates bone mass. *Dev Cell*. 2006;10(6):771-82.
288. Conboy IM, Manoli D, Mhaiskar V, Jones PP. Calcineurin and vacuolar-type H⁺-ATPase modulate macrophage effector functions. *Proc Natl Acad Sci U S A*. 1999;96(11):6324-9.
289. Jennings C, Kusler B, Jones PP. Calcineurin inactivation leads to decreased responsiveness to LPS in macrophages and dendritic cells and protects against LPS-induced toxicity in vivo. *Innate Immun*. 2009;15(2):109-20.
290. Yoshino T, Nakase H, Honzawa Y, Matsumura K, Yamamoto S, Takeda Y, et al. Immunosuppressive effects of tacrolimus on macrophages ameliorate experimental colitis. *Inflamm Bowel Dis*. 2010;16(12):2022-33.
291. Cappellen D, Luong-Nguyen NH, Bongiovanni S, Grenet O, Wanke C, Susa M. Transcriptional program of mouse osteoclast differentiation governed by the macrophage colony-stimulating factor and the ligand for the receptor activator of NFkappa B. *J Biol Chem*. 2002;277(24):21971-82.
292. Yamanaka Y, Abu-Amer W, Foglia D, Otero J, Clohisy JC, Abu-Amer Y. NFAT2 is an essential mediator of orthopedic particle-induced osteoclastogenesis. *J Orthop Res*. 2008;26(12):1577-84.
293. Ishida N, Hayashi K, Hoshijima M, Ogawa T, Koga S, Miyatake Y, et al. Large scale gene expression analysis of osteoclastogenesis in vitro and elucidation of NFAT2 as a key regulator. *J Biol Chem*. 2002;277(43):41147-56.
294. Shui C, Riggs BL, Khosla S. The immunosuppressant rapamycin, alone or with transforming growth factor-beta, enhances osteoclast differentiation of RAW264.7 monocyte-macrophage cells in the presence of RANK-ligand. *Calcif Tissue Int*. 2002;71(5):437-46.
295. Asagiri M, Sato K, Usami T, Ochi S, Nishina H, Yoshida H, et al. Autoamplification of NFATc1 expression determines its essential role in bone homeostasis. *J Exp Med*. 2005;202(9):1261-9.
296. Igarashi K, Hirotsani H, Woo JT, Stern PH. Cyclosporine A and FK506 induce osteoclast apoptosis in mouse bone marrow cell cultures. *Bone*. 2004;35(1):47-56.
297. Awumey EM, Moonga BS, Sodam BR, Koval AP, Adebajo OA, Kumegawa M, et al. Molecular and functional evidence for calcineurin-A alpha and beta isoforms in the osteoclast: novel insights into cyclosporin A action on bone resorption. *Biochem Biophys Res Commun*. 1999;254(1):248-52.
298. Chowdhury MH, Shen V, Dempster DW. Effects of cyclosporine A on chick osteoclasts in vitro. *Calcif Tissue Int*. 1991;49(4):275-9.
299. Orcel P, Denne MA, de Vernejoul MC. Cyclosporin-A in vitro decreases bone resorption, osteoclast formation, and the fusion of cells of the monocyte-macrophage lineage. *Endocrinology*. 1991;128(3):1638-46.
300. Dumont FJ. FK506, an immunosuppressant targeting calcineurin function. *Curr Med Chem*. 2000;7(7):731-48.
301. Sandker MJ, Petit A, Redout EM, Siebel M, Muller B, Bruin P, et al. In situ forming acyl-capped PCL-PEG-PCL triblock copolymer based hydrogels. *Biomaterials*. 2013;34(32):8002-11.
302. Westacott CI, Webb GR, Warnock MG, Sims JV, Elson CJ. Alteration of cartilage metabolism by cells from osteoarthritic bone. *Arthritis Rheum*. 1997;40(7):1282-91.
303. Saag KG, Emkey R, Schnitzer TJ, Brown JP, Hawkins F, Goemaere S, et al. Alendronate for the prevention and treatment of glucocorticoid-induced osteoporosis. Glucocorticoid-Induced Osteoporosis Intervention

-
- Study Group. *N Engl J Med.* 1998;339(5):292-9.
304. Muehleman C, Green J, Williams JM, Kuettner KE, Thonar EJ, Sumner DR. **The effect of bone remodeling inhibition by zoledronic acid in an animal model of cartilage matrix damage.** *Osteoarthritis Cartilage.* 2002;10(3):226-33.
305. Agnello KA, Trumble TN, Chambers JN, Seewald W, Budsberg SC. **Effects of zoledronate on markers of bone metabolism and subchondral bone mineral density in dogs with experimentally induced cruciate-deficient osteoarthritis.** *Am J Vet Res.* 2005;66(9):1487-95.
306. Sniekers YH, Weinans H, van Osch GJ, van Leeuwen JP. **Oestrogen is important for maintenance of cartilage and subchondral bone in a murine model of knee osteoarthritis.** *Arthritis Res Ther.* 2010;12(5):R182.
307. Strassle BW, Mark L, Leventhal L, Piesla MJ, Jian Li X, Kennedy JD, et al. **Inhibition of osteoclasts prevents cartilage loss and pain in a rat model of degenerative joint disease.** *Osteoarthritis Cartilage.* 2010;18(10):1319-28.
308. Bingham CO, 3rd, Buckland-Wright JC, Garnero P, Cohen SB, Dougados M, Adami S, et al. **Risedronate decreases biochemical markers of cartilage degradation but does not decrease symptoms or slow radiographic progression in patients with medial compartment osteoarthritis of the knee: results of the two-year multinational knee osteoarthritis structural arthritis study.** *Arthritis Rheum.* 2006;54(11):3494-507.
309. Buckland-Wright JC, Messent EA, Bingham CO, 3rd, Ward RJ, Tonkin C. **A 2 yr longitudinal radiographic study examining the effect of a bisphosphonate (risedronate) upon subchondral bone loss in osteoarthritic knee patients.** *Rheumatology (Oxford).* 2007;46(2):257-64.
310. Saag KG. **Bisphosphonates for osteoarthritis prevention: "Holy Grail" or not?** *Ann Rheum Dis.* 2008;67(10):1358-9.
311. Spector TD, Conaghan PG, Buckland-Wright JC, Garnero P, Cline GA, Beary JF, et al. **Effect of risedronate on joint structure and symptoms of knee osteoarthritis: results of the BRISK randomized, controlled trial [ISRCTN01928173].** *Arthritis Res Ther.* 2005;7(3):R625-33.
312. Carbone LD, Nevitt MC, Wildy K, Barrow KD, Harris F, Felson D, et al. **The relationship of antiresorptive drug use to structural findings and symptoms of knee osteoarthritis.** *Arthritis Rheum.* 2004;50(11):3516-25.
313. Lohmander S. **Can treatment with risedronate benefit patients with knee osteoarthritis?** *Nat Clin Pract Rheumatol.* 2007;3(4):198-9.
314. Wachsmuth L, Engelke K. **High-resolution imaging of osteoarthritis using microcomputed tomography.** *Methods Mol Med.* 2004;101:231-48.
315. Piscaer TM, Sandker M, van der Jagt OP, Verhaar JA, de Jong M, Weinans H. **Real-time assessment of bone metabolism in small animal models for osteoarthritis using multi pinhole-SPECT/CT.** *Osteoarthritis Cartilage.* 2013;21(6):882-8.
316. Fuchs RK, Phipps RJ, Burr DB. **Recovery of trabecular and cortical bone turnover after discontinuation of risedronate and alendronate therapy in ovariectomized rats.** *J Bone Miner Res.* 2008;23(10):1689-97.
317. Waarsing JH, Day JS, Verhaar JA, Ederveen AG, Weinans H. **Bone loss dynamics result in trabecular alignment in aging and ovariectomized rats.** *J Orthop Res.* 2006;24(5):926-35.
318. Klein-Nulend J, Bacabac RG, Bakker AD. **Mechanical loading and how it affects bone cells: the role of the osteocyte cytoskeleton in maintaining our skeleton.** *Eur Cell Mater.* 2012;24:278-91.
319. van Hove RP, Nolte PA, Vatsa A, Semeins CM, Salmon PL, Smit TH, et al. **Osteocyte morphology in human tibiae**

- of different bone pathologies with different bone mineral density--is there a role for mechanosensing? *Bone*. 2009;45(2):321-9.
320. Power J, Poole KE, van Bezooijen R, Doube M, Caballero-Alias AM, Lowik C, et al. **Sclerostin and the regulation of bone formation: Effects in hip osteoarthritis and femoral neck fracture.** *J Bone Miner Res*. 2010;25(8):1867-76.
321. Chan BY, Fuller ES, Russell AK, Smith SM, Smith MM, Jackson MT, et al. **Increased chondrocyte sclerostin may protect against cartilage degradation in osteoarthritis.** *Osteoarthritis Cartilage*. 2011;19(7):874-85.
322. Laslett LL, Kingsbury SR, Hensor EM, Bowes MA, Conaghan PG. **Effect of bisphosphonate use in patients with symptomatic and radiographic knee osteoarthritis: data from the Osteoarthritis Initiative.** *Ann Rheum Dis*. 2014;73(5):824-30.
323. Ayral X, Pickering EH, Woodworth TG, Mackillop N, Dougados M. **Synovitis: a potential predictive factor of structural progression of medial tibiofemoral knee osteoarthritis -- results of a 1 year longitudinal arthroscopic study in 422 patients.** *Osteoarthritis Cartilage*. 2005;13(5):361-7.
324. Roemer FW, Guermazi A, Felson DT, Niu J, Nevitt MC, Crema MD, et al. **Presence of MRI-detected joint effusion and synovitis increases the risk of cartilage loss in knees without osteoarthritis at 30-month follow-up: the MOST study.** *Ann Rheum Dis*. 2011;70(10):1804-9.
325. Roelofs AJ, Thompson K, Ebetino FH, Rogers MJ, Coxon FP. **Bisphosphonates: molecular mechanisms of action and effects on bone cells, monocytes and macrophages.** *Curr Pharm Des*. 2010;16(27):2950-60.
326. Suri S, Walsh DA. **Osteochondral alterations in osteoarthritis.** *Bone*. 2011.
327. Weinans H, Siebelt M, Agricola R, Botter SM, Piscoer TM, Waarsing JH. **Pathophysiology of peri-articular bone changes in osteoarthritis.** *Bone*. 2012.
328. Bondeson J, Blom AB, Wainwright S, Hughes C, Caterson B, van den Berg WB. **The role of synovial macrophages and macrophage-produced mediators in driving inflammatory and destructive responses in osteoarthritis.** *Arthritis Rheum*. 2010;62(3):647-57.
329. deLange-Brokaar BJ, Ioan-Facsinay A, Yusuf E, Visser AW, Kroon HM, vanOsch GJ, et al. **Pain in knee osteoarthritis patients associates with distinct pattern of synovitis.** *Arthritis Rheumatol*. 2014.
330. Bellamy N, Campbell J, Robinson V, Gee T, Bourne R, Wells G. **Intraarticular corticosteroid for treatment of osteoarthritis of the knee.** *Cochrane Database Syst Rev*. 2006(2):CD005328.
331. McAlindon TE, Bannuru RR, Sullivan MC, Arden NK, Berenbaum F, Bierma-Zeinstra SM, et al. **OARSI guidelines for the non-surgical management of knee osteoarthritis.** *Osteoarthritis Cartilage*. 2014;22(3):363-88.
332. Hepper CT, Halvorson JJ, Duncan ST, Gregory AJ, Dunn WR, Spindler KP. **The efficacy and duration of intra-articular corticosteroid injection for knee osteoarthritis: a systematic review of level I studies.** *J Am Acad Orthop Surg*. 2009;17(10):638-46.
333. Williams JM, Brandt KD. **Triamcinolone hexacetonide protects against fibrillation and osteophyte formation following chemically induced articular cartilage damage.** *Arthritis Rheum*. 1985;28(11):1267-74.
334. Huebner KD, Shrive NG, Frank CB. **Dexamethasone inhibits inflammation and cartilage damage in a new model of post-traumatic osteoarthritis.** *J Orthop Res*. 2014;32(4):566-72.
335. Mackness GB. **Cellular immunity and the parasite.** *Adv Exp Med Biol*. 1977;93:65-73.
336. O'Shea JJ, Murray PJ. **Cytokine signaling modules in inflammatory responses.** *Immunity*. 2008;28(4):477-87.

-
337. Gordon S. **Alternative activation of macrophages.** *Nat Rev Immunol.* 2003;3(1):23-35.
338. Loke P, Gallagher I, Nair MG, Zang X, Brombacher F, Mohrs M, et al. **Alternative activation is an innate response to injury that requires CD4+ T cells to be sustained during chronic infection.** *J Immunol.* 2007;179(6):3926-36.
339. Zizzo G, Hilliard BA, Monestier M, Cohen PL. **Efficient clearance of early apoptotic cells by human macrophages requires M2c polarization and MerTK induction.** *J Immunol.* 2012;189(7):3508-20.
340. Martinez FO, Sica A, Mantovani A, Locati M. **Macrophage activation and polarization.** *Front Biosci.* 2008;13:453-61.
341. Piscaer TM, Muller C, Mindt TL, Lubberts E, Verhaar JA, Krenning EP, et al. **Imaging of activated macrophages in experimental osteoarthritis using folate-targeted animal single-photon-emission computed tomography/computed tomography.** *Arthritis Rheum.* 2011;63(7):1898-907.
342. Ambarus CA, Krausz S, van Eijk M, Hamann J, Radstake TR, Reedquist KA, et al. **Systematic validation of specific phenotypic markers for in vitro polarized human macrophages.** *J Immunol Methods.* 2012;375(1-2):196-206.
343. Philippidis P, Mason JC, Evans BJ, Nadra I, Taylor KM, Haskard DO, et al. **Hemoglobin scavenger receptor CD163 mediates interleukin-10 release and heme oxygenase-1 synthesis: antiinflammatory monocyte-macrophage responses in vitro, in resolving skin blisters in vivo, and after cardiopulmonary bypass surgery.** *Circ Res.* 2004;94(1):119-26.
344. Verreck FA, de Boer T, Langenberg DM, van der Zanden L, Ottenhoff TH. **Phenotypic and functional profiling of human proinflammatory type-1 and anti-inflammatory type-2 macrophages in response to microbial antigens and IFN-gamma- and CD40L-mediated costimulation.** *J Leukoc Biol.* 2006;79(2):285-93.
345. Nakashima-Matsushita N, Homma T, Yu S, Matsuda T, Sunahara N, Nakamura T, et al. **Selective expression of folate receptor beta and its possible role in methotrexate transport in synovial macrophages from patients with rheumatoid arthritis.** *Arthritis Rheum.* 1999;42(8):1609-16.
346. Ogawa S, Lozach J, Benner C, Pascual G, Tangirala RK, Westin S, et al. **Molecular determinants of crosstalk between nuclear receptors and toll-like receptors.** *Cell.* 2005;122(5):707-21.
347. Ghosh S, May MJ, Kopp EB. **NF-kappa B and Rel proteins: evolutionarily conserved mediators of immune responses.** *Annu Rev Immunol.* 1998;16:225-60.
348. Scheinman RI, Gualberto A, Jewell CM, Cidlowski JA, Baldwin AS, Jr. **Characterization of mechanisms involved in transrepression of NF-kappa B by activated glucocorticoid receptors.** *Mol Cell Biol.* 1995;15(2):943-53.
349. Celeste C, Ionescu M, Robin Poole A, Laverty S. **Repeated intraarticular injections of triamcinolone acetonide alter cartilage matrix metabolism measured by biomarkers in synovial fluid.** *J Orthop Res.* 2005;23(3):602-10.
350. Nakazawa F, Matsuno H, Yudoh K, Watanabe Y, Katayama R, Kimura T. **Corticosteroid treatment induces chondrocyte apoptosis in an experimental arthritis model and in chondrocyte cultures.** *Clin Exp Rheumatol.* 2002;20(6):773-81.
351. Doorduyn J, Klein HC, Dierckx RA, James M, Kassiou M, de Vries EF. **[11C]-DPA-713 and [18F]-DPA-714 as new PET tracers for TSPO: a comparison with [11C]-(R)-PK11195 in a rat model of herpes encephalitis.** *Mol Imaging Biol.* 2009;11(6):386-98.
352. Van De Wiele C, Sathekge M, Maes A. **Targeting monocytes and macrophages by means of SPECT and PET.**

- Q J Nucl Med Mol Imaging*. 2014;58(3):269-75.
353. Harvey WF, Hunter DJ. **The role of analgesics and intra-articular injections in disease management.** *Rheum Dis Clin North Am*. 2008;34(3):777-88.
354. Pittenger MF, Mackay AM, Beck SC, Jaiswal RK, Douglas R, Mosca JD, et al. **Multilineage potential of adult human mesenchymal stem cells.** *Science*. 1999;284(5411):143-7.
355. Chen L, Tredget EE, Wu PY, Wu Y. **Paracrine factors of mesenchymal stem cells recruit macrophages and endothelial lineage cells and enhance wound healing.** *PLoS One*. 2008;3(4):e1886.
356. Agung M, Ochi M, Yanada S, Adachi N, Izuta Y, Yamasaki T, et al. **Mobilization of bone marrow-derived mesenchymal stem cells into the injured tissues after intraarticular injection and their contribution to tissue regeneration.** *Knee Surg Sports Traumatol Arthrosc*. 2006;14(12):1307-14.
357. Centeno CJ, Schultz JR, Cheever M, Robinson B, Freeman M, Marasco W. **Safety and complications reporting on the re-implantation of culture-expanded mesenchymal stem cells using autologous platelet lysate technique.** *Curr Stem Cell Res Ther*. 2010;5(1):81-93.
358. Davatchi F, Abdollahi BS, Mohyeddin M, Shahram F, Nikbin B. **Mesenchymal stem cell therapy for knee osteoarthritis. Preliminary report of four patients.** *Int J Rheum Dis*. 2011;14(2):211-5.
359. Horie M, Sekiya I, Muneta T, Ichinose S, Matsumoto K, Saito H, et al. **Intra-articular Injected synovial stem cells differentiate into meniscal cells directly and promote meniscal regeneration without mobilization to distant organs in rat massive meniscal defect.** *Stem Cells*. 2009;27(4):878-87.
360. Jing XH, Yang L, Duan XJ, Xie B, Chen W, Li Z, et al. **In vivo MR imaging tracking of magnetic iron oxide nanoparticle labeled, engineered, autologous bone marrow mesenchymal stem cells following intra-articular injection.** *Joint Bone Spine*. 2008;75(4):432-8.
361. Lee KB, Hui JH, Song IC, Ardany L, Lee EH. **Injectable mesenchymal stem cell therapy for large cartilage defects--a porcine model.** *Stem Cells*. 2007;25(11):2964-71.
362. Matsumoto T, Cooper GM, Gharaibeh B, Meszaros LB, Li G, Usas A, et al. **Cartilage repair in a rat model of osteoarthritis through intraarticular transplantation of muscle-derived stem cells expressing bone morphogenetic protein 4 and soluble Flt-1.** *Arthritis Rheum*. 2009;60(5):1390-405.
363. Murphy JM, Fink DJ, Hunziker EB, Barry FP. **Stem cell therapy in a caprine model of osteoarthritis.** *Arthritis Rheum*. 2003;48(12):3464-74.
364. Nishimori M, Deie M, Kanaya A, Exham H, Adachi N, Ochi M. **Repair of chronic osteochondral defects in the rat. A bone marrow-stimulating procedure enhanced by cultured allogenic bone marrow mesenchymal stromal cells.** *J Bone Joint Surg Br*. 2006;88(9):1236-44.
365. Frisbie DD, Kisiday JD, Kawcak CE, Werpy NM, Mcllwraith CW. **Evaluation of adipose-derived stromal vascular fraction or bone marrow-derived mesenchymal stem cells for treatment of osteoarthritis.** *J Orthop Res*. 2009;27(12):1675-80.
366. Nguyen US, Zhang Y, Zhu Y, Niu J, Zhang B, Felson DT. **Increasing prevalence of knee pain and symptomatic knee osteoarthritis: survey and cohort data.** *Ann Intern Med*. 2011;155(11):725-32.
367. Guermazi A, Roemer FW, Hayashi D. **Imaging of osteoarthritis: update from a radiological perspective.** *Curr Opin Rheumatol*. 2011;23(5):484-91.
368. Bove SE, Calcaterra SL, Brooker RM, Huber CM, Guzman RE, Juneau PL, et al. **Weight bearing as a measure**

-
- of disease progression and efficacy of anti-inflammatory compounds in a model of monosodium iodoacetate-induced osteoarthritis. *Osteoarthritis Cartilage*. 2003;11(11):821-30.
369. Combe R, Bramwell S, Field MJ. The monosodium iodoacetate model of osteoarthritis: a model of chronic nociceptive pain in rats? *Neurosci Lett*. 2004;370(2-3):236-40.
370. Vonsy JL, Ghandehari J, Dickenson AH. Differential analgesic effects of morphine and gabapentin on behavioural measures of pain and disability in a model of osteoarthritis pain in rats. *Eur J Pain*. 2009;13(8):786-93.
371. Kasten P, Beyen I, Egermann M, Suda AJ, Moghaddam AA, Zimmermann G, et al. Instant stem cell therapy: characterization and concentration of human mesenchymal stem cells in vitro. *Eur Cell Mater*. 2008;16:47-55.
372. Caplan AI. Why are MSCs therapeutic? New data: new insight. *J Pathol*. 2009;217(2):318-24.
373. Pittenger MF, Martin BJ. Mesenchymal stem cells and their potential as cardiac therapeutics. *Circ Res*. 2004;95(1):9-20.
374. Camplejohn KL, Allard SA. Limitations of safranin 'O' staining in proteoglycan-depleted cartilage demonstrated with monoclonal antibodies. *Histochemistry*. 1988;89(2):185-8.
375. Scharstuhl A, Vitters EL, van der Kraan PM, van den Berg WB. Reduction of osteophyte formation and synovial thickening by adenoviral overexpression of transforming growth factor beta/bone morphogenetic protein inhibitors during experimental osteoarthritis. *Arthritis Rheum*. 2003;48(12):3442-51.
376. Guenoun J, Ruggiero A, Doeswijk G, Janssens RC, Koning GA, Kotek G, et al. In vivo quantitative assessment of cell viability of gadolinium or iron-labeled cells using MRI and bioluminescence imaging. *Contrast Media Mol Imaging*. 2013;8(2):165-74.
377. van Buul GM, Farrell E, Kops N, van Tiel ST, Bos PK, Weinans H, et al. Ferumoxides-protamine sulfate is more effective than ferucarbotran for cell labeling: implications for clinically applicable cell tracking using MRI. *Contrast Media Mol Imaging*. 2009;4(5):230-6.
378. Morenko BJ, Bove SE, Chen L, Guzman RE, Juneau P, Bocan TM, et al. In vivo micro computed tomography of subchondral bone in the rat after intra-articular administration of monosodium iodoacetate. *Contemp Top Lab Anim Sci*. 2004;43(1):39-43.
379. Singer NG, Caplan AI. Mesenchymal stem cells: mechanisms of inflammation. *Annu Rev Pathol*. 2011;6:457-78.
380. Black LL, Gaynor J, Adams C, Dhupa S, Sams AE, Taylor R, et al. Effect of intraarticular injection of autologous adipose-derived mesenchymal stem and regenerative cells on clinical signs of chronic osteoarthritis of the elbow joint in dogs. *Vet Ther*. 2008;9(3):192-200.
381. Orita S, Ishikawa T, Miyagi M, Ochiai N, Inoue G, Eguchi Y, et al. Pain-related sensory innervation in monoiodoacetate-induced osteoarthritis in rat knees that gradually develops neuronal injury in addition to inflammatory pain. *BMC Musculoskelet Disord*. 2011;12:134.
382. Neugebauer V, Han JS, Adwanikar H, Fu Y, Ji G. Techniques for assessing knee joint pain in arthritis. *Mol Pain*. 2007;3:8.
383. Le Blanc K, Tammik C, Rosendahl K, Zetterberg E, Ringden O. HLA expression and immunologic properties of differentiated and undifferentiated mesenchymal stem cells. *Exp Hematol*. 2003;31(10):890-6.

384. Griffin MD, Ritter T, Mahon BP. Immunological aspects of allogeneic mesenchymal stem cell therapies. *Hum Gene Ther.* 2010;21(12):1641-55.
385. Hoogduijn MJ, Roemeling-van Rhijn M, Korevaar SS, Engela AU, Weimar W, Baan CC. Immunological aspects of allogeneic and autologous mesenchymal stem cell therapies. *Hum Gene Ther.* 2011;22(12):1587-91.
386. Schu S, Nosov M, O'Flynn L, Shaw G, Treacy O, Barry F, et al. Immunogenicity of allogeneic mesenchymal stem cells. *J Cell Mol Med.* 2011.
387. Toghraie FS, Chenari N, Gholipour MA, Faghieh Z, Torabinejad S, Dehghani S, et al. Treatment of osteoarthritis with infrapatellar fat pad derived mesenchymal stem cells in Rabbit. *Knee.* 2010.
388. Crisostomo PR, Wang Y, Markel TA, Wang M, Lahm T, Meldrum DR. Human mesenchymal stem cells stimulated by TNF-alpha, LPS, or hypoxia produce growth factors by an NF kappa B- but not JNK-dependent mechanism. *Am J Physiol Cell Physiol.* 2008;294(3):C675-82.
389. Groh ME, Maitra B, Szekely E, Koc ON. Human mesenchymal stem cells require monocyte-mediated activation to suppress alloreactive T cells. *Exp Hematol.* 2005;33(8):928-34.
390. Kanaya A, Deie M, Adachi N, Nishimori M, Yanada S, Ochi M. Intra-articular injection of mesenchymal stromal cells in partially torn anterior cruciate ligaments in a rat model. *Arthroscopy.* 2007;23(6):610-7.
391. Mcllwraith CW, Frisbie DD, Rodkey WG, Kisiday JD, Werpy NM, Kawcak CE, et al. Evaluation of intra-articular mesenchymal stem cells to augment healing of microfractured chondral defects. *Arthroscopy.* 2011;27(11):1552-61.
392. Waterman RS, Tomchuck SL, Henkle SL, Betancourt AM. A new mesenchymal stem cell (MSC) paradigm: polarization into a pro-inflammatory MSC1 or an Immunosuppressive MSC2 phenotype. *PLoS One.* 2010;5(4):e10088.
393. Buckwalter JA, Mankin HJ. Articular cartilage: degeneration and osteoarthritis, repair, regeneration, and transplantation. *Instr Course Lect.* 1998;47:487-504.
394. Kallioniemi AS, Jurvelin JS, Nieminen MT, Lammi MJ, Toyras J. Contrast agent enhanced pQCT of articular cartilage. *Phys Med Biol.* 2007;52(4):1209-19.
395. De Filippo M, Bertellini A, Pogliacomì F, Sverzellati N, Corradi D, Garlaschi G, et al. Multidetector computed tomography arthrography of the knee: diagnostic accuracy and indications. *Eur J Radiol.* 2009;70(2):342-51.
396. Subhas N, Freire M, Primak AN, Polster JM, Recht MP, Davros WJ, et al. CT arthrography: in vitro evaluation of single and dual energy for optimization of technique. *Skeletal Radiol.* 2010;39(10):1025-31.
397. Wiener E, Settles M, Weirich G, Schmidt C, Diederichs G. The Influence of Collagen Network Integrity on the Accumulation of Gadolinium-Based MR Contrast Agents in Articular Cartilage. *Fortschr Röntgenstr Online-Publikation 2010.* 2011.
398. Silvast TS, Kokkonen HT, Jurvelin JS, Quinn TM, Nieminen MT, Toyras J. Diffusion and near-equilibrium distribution of MRI and CT contrast agents in articular cartilage. *Phys Med Biol.* 2009;54(22):6823-36.
399. Bullough PG, Yawitz PS, Tafra L, Boskey AL. Topographical variations in the morphology and biochemistry of adult canine tibial plateau articular cartilage. *J Orthop Res.* 1985;3(1):1-16.
400. Weiss C, Mirow S. An ultrastructural study of osteoarthritis changes in the articular cartilage of human knees. *J Bone Joint Surg Am.* 1972;54(5):954-72.

-
401. Bryant D, Havey TC, Roberts R, Guyatt G. How many patients? How many limbs? Analysis of patients or limbs in the orthopaedic literature: a systematic review. *J Bone Joint Surg Am.* 2006;88(1):41-5.
402. Park MS, Kim SJ, Chung CY, Choi IH, Lee SH, Lee KM. Statistical consideration for bilateral cases in orthopaedic research. *J Bone Joint Surg Am.* 2010;92(8):1732-7.
403. Julkunen P, Korhonen RK, Nissi MJ, Jurvelin JS. Mechanical characterization of articular cartilage by combining magnetic resonance imaging and finite-element analysis: a potential functional imaging technique. *Phys Med Biol.* 2008;53(9):2425-38.
404. Kiviranta P, Rieppo J, Korhonen RK, Julkunen P, Toyras J, Jurvelin JS. Collagen network primarily controls Poisson's ratio of bovine articular cartilage in compression. *J Orthop Res.* 2006;24(4):690-9.
405. Urban JP, Hall AC, Gehl KA. Regulation of matrix synthesis rates by the ionic and osmotic environment of articular chondrocytes. *J Cell Physiol.* 1993;154(2):262-70.
406. Biswas D, Bible JE, Bohan M, Simpson AK, Whang PG, Grauer JN. Radiation exposure from musculoskeletal computerized tomographic scans. *J Bone Joint Surg Am.* 2009;91(8):1882-9.
407. Guermazi A, Burstein D, Conaghan P, Eckstein F, Heliö Le Graverand-Gastineau MP, Keen H, et al. Imaging in osteoarthritis. *Rheum Dis Clin North Am.* 2008;34(3):645-87.
408. Guermazi A, Roemer FW, Burstein D, Hayashi D. Why radiography should no longer be considered a surrogate outcome measure for longitudinal assessment of cartilage in knee osteoarthritis. *Arthritis Res Ther.* 2011;13(6):247.
409. Roemer FW, Crema MD, Trattnig S, Guermazi A. Advances in imaging of osteoarthritis and cartilage. *Radiology.* 2011;260(2):332-54.
410. Siebelt M, van Tiel J, Waarsing JH, Piscoer TM, van Straten M, Booij R, et al. Clinically applied CT arthrography to measure the sulphated glycosaminoglycan content of cartilage. *Osteoarthritis Cartilage.* 2011;19(10):1183-9.
411. Gray ML, Burstein D, Kim YJ, Maroudas A. 2007 Elizabeth Winston Lanier Award Winner. Magnetic resonance imaging of cartilage glycosaminoglycan: basic principles, imaging technique, and clinical applications. *J Orthop Res.* 2008;26(3):281-91.
412. Tiderius CJ, Olsson LE, Leander P, Ekberg O, Dahlberg L. Delayed gadolinium-enhanced MRI of cartilage (dGEMRIC) in early knee osteoarthritis. *Magn Reson Med.* 2003;49(3):488-92.
413. Eckstein F, Ateshian G, Burgkart R, Burstein D, Cicuttini F, Dardzinski B, et al. Proposal for a nomenclature for magnetic resonance imaging based measures of articular cartilage in osteoarthritis. *Osteoarthritis Cartilage.* 2006;14(10):974-83.
414. Maes F, Collignon A, Vandermeulen D, Marchal G, Suetens P. Multimodality image registration by maximization of mutual information. *IEEE Trans Med Imaging.* 1997;16(2):187-98.
415. Bedi A, Feeley BT, Williams RJ, 3rd. Management of articular cartilage defects of the knee. *J Bone Joint Surg Am.* 2010;92(4):994-1009.
416. Bos PK, van Melle ML, van Osch GJ. Articular cartilage repair and the evolving role of regenerative medicine. *Open Access Surgery.* 2010;3:109 - 22.
417. Trattnig S, Marlovits S, Gebetsroither S, Szomolanyi P, Welsch GH, Salomonowitz E, et al. Three-dimensional delayed gadolinium-enhanced MRI of cartilage (dGEMRIC) for in vivo evaluation of reparative cartilage after matrix-associated autologous chondrocyte transplantation at 3.0T: Preliminary results. *J Magn Reson*

- Imaging.* 2007;26(4):974-82.
418. Vasiliadis HS, Danielson B, Ljungberg M, McKeon B, Lindahl A, Peterson L. Autologous chondrocyte implantation in cartilage lesions of the knee: long-term evaluation with magnetic resonance imaging and delayed gadolinium-enhanced magnetic resonance imaging technique. *Am J Sports Med.* 2010;38(5):943-9.
 419. Vande Berg BC, Lecouvet FE, Poilvache P, Maldague B, Malghem J. Spiral CT arthrography of the knee: technique and value in the assessment of internal derangement of the knee. *Eur Radiol.* 2002;12(7):1800-10.
 420. Gervaise A, Osemont B, Lecocq S, Noel A, Micard E, Felblinger J, et al. CT image quality improvement using adaptive iterative dose reduction with wide-volume acquisition on 320-detector CT. *Eur Radiol.* 2011.
 421. Tamm EP, Rong XJ, Cody DD, Ernst RD, Fitzgerald NE, Kundra V. Quality Initiatives: CT Radiation Dose Reduction: How to Implement Change without Sacrificing Diagnostic Quality. *Radiographics.* 2011.
 422. Pastides P, Chimutengwende-Gordon M, Maffulli N, Khan W. Stem cell therapy for human cartilage defects: a systematic review. *Osteoarthritis Cartilage.* 2013;21(5):646-54.
 423. Hermans J, Koopmanschap MA, Bierma-Zeinstra SM, van Linge JH, Verhaar JA, Reijman M, et al. Productivity costs and medical costs among working patients with knee osteoarthritis. *Arthritis Care Res (Hoboken).* 2012;64(6):853-61.
 424. Baldock PA, Need AG, Moore RJ, Durbridge TC, Morris HA. Discordance between bone turnover and bone loss: effects of aging and ovariectomy in the rat. *J Bone Miner Res.* 1999;14(8):1442-8.
 425. Mawatari T, Miura H, Higaki H, Kurata K, Moro-oka T, Murakami T, et al. Quantitative analysis of three-dimensional complexity and connectivity changes in trabecular microarchitecture in relation to aging, menopause, and inflammation. *J Orthop Sci.* 1999;4(6):431-8.
 426. Wang L, Banu J, McMahan CA, Kalu DN. Male rodent model of age-related bone loss in men. *Bone.* 2001;29(2):141-8.
 427. Wronski TJ, Dann LM, Scott KS, Cintron M. Long-term effects of ovariectomy and aging on the rat skeleton. *Calcif Tissue Int.* 1989;45(6):360-6.
 428. Tiderius CJ, Svensson J, Leander P, Ola T, Dahlberg L. dGEMRIC (delayed gadolinium-enhanced MRI of cartilage) indicates adaptive capacity of human knee cartilage. *Magn Reson Med.* 2004;51(2):286-90.
 429. Van Ginckel A, Baelde N, Almqvist KF, Roosen P, McNair P, Witvrouw E. Functional adaptation of knee cartilage in asymptomatic female novice runners compared to sedentary controls. A longitudinal analysis using delayed Gadolinium Enhanced Magnetic Resonance Imaging of Cartilage (dGEMRIC). *Osteoarthritis Cartilage.* 2010;18(12):1564-9.
 430. Duke PJ, Montufar-Solis D. Exposure to altered gravity affects all stages of endochondral cartilage differentiation. *Adv Space Res.* 1999;24(6):821-7.
 431. Orwoll ES, Adler RA, Amin S, Binkley N, Lewiecki EM, Petak SM, et al. Skeletal health in long-duration astronauts: nature, assessment, and management recommendations from the NASA Bone Summit. *J Bone Miner Res.* 2013;28(6):1243-55.
 432. Pan J, Wang B, Li W, Zhou X, Scherr T, Yang Y, et al. Elevated cross-talk between subchondral bone and cartilage in osteoarthritic joints. *Bone.* 2012;51(2):212-7.
 433. Ouellette EA, Makowski AL. How men and women are affected by osteoarthritis of the hand. *Orthop Clin*

-
- North Am. 2006;37(4):541-8.
434. Vasarhelyi EM, MacDonald SJ. The influence of obesity on total joint arthroplasty. *J Bone Joint Surg Br.* 2012;94(11 Suppl A):100-2.
435. van Meurs JB, Uitterlinden AG. Osteoarthritis year 2012 in review: genetics and genomics. *Osteoarthritis Cartilage.* 2012;20(12):1470-6.
436. Reynard LN, Loughlin J. The genetics and functional analysis of primary osteoarthritis susceptibility. *Expert Rev Mol Med.* 2013;15:e2.
437. Felson DT. Osteoarthritis as a disease of mechanics. *Osteoarthritis Cartilage.* 2013;21(1):10-5.
438. Jaiprakash A, Prasadam I, Feng JQ, Liu Y, Crawford R, Xiao Y. Phenotypic characterization of osteoarthritic osteocytes from the sclerotic zones: a possible pathological role in subchondral bone sclerosis. *Int J Biol Sci.* 2012;8(3):406-17.
439. Haseeb A, Haqqi TM. Immunopathogenesis of osteoarthritis. *Clin Immunol.* 2013;146(3):185-96.
440. Hackenbroch MH. Intertrochanteric osteotomy for the treatment of coxarthrosis. *Arch Orthop Trauma Surg.* 1989;108(3):125-31.
441. Scott CE, Nutton RW, Biant LC. Lateral compartment osteoarthritis of the knee: Biomechanics and surgical management of end-stage disease. *Bone Joint J.* 2013;95-B(4):436-44.
442. Billings A, Scott DF, Camargo MP, Hofmann AA. High tibial osteotomy with a calibrated osteotomy guide, rigid internal fixation, and early motion. Long-term follow-up. *J Bone Joint Surg Am.* 2000;82(1):70-9.
443. Runhaar J, Koes BW, Clockaerts S, Bierma-Zeinstra SM. A systematic review on changed biomechanics of lower extremities in obese individuals: a possible role in development of osteoarthritis. *Obes Rev.* 2011;12(12):1071-82.
444. Brouwer RW, Huizinga MR, Duivenvoorden T, van Raaij TM, Verhagen AP, Bierma-Zeinstra SM, et al. Osteotomy for treating knee osteoarthritis. *Cochrane Database Syst Rev.* 2014;12:CD004019.
445. Guilak F, Ratcliffe A, Mow VC. Chondrocyte deformation and local tissue strain in articular cartilage: a confocal microscopy study. *J Orthop Res.* 1995;13(3):410-21.
446. Millward-Sadler SJ, Wright MO, Davies LW, Nuki G, Salter DM. Mechanotransduction via integrins and interleukin-4 results in altered aggrecan and matrix metalloproteinase 3 gene expression in normal, but not osteoarthritic, human articular chondrocytes. *Arthritis Rheum.* 2000;43(9):2091-9.
447. Weinans H, Siebelt M, Agricola R, Botter SM, Piscoer TM, Waarsing JH. Pathophysiology of peri-articular bone changes in osteoarthritis. *Bone.* 2012;51(2):190-6.
448. Loeser RF. Molecular mechanisms of cartilage destruction: mechanics, inflammatory mediators, and aging collide. *Arthritis Rheum.* 2006;54(5):1357-60.
449. Tanaka S, Hamanishi C, Kikuchi H, Fukuda K. Factors related to degradation of articular cartilage in osteoarthritis: a review. *Semin Arthritis Rheum.* 1998;27(6):392-9.
450. Pickarski M, Hayami T, Zhuo Y, Duong le T. Molecular changes in articular cartilage and subchondral bone in the rat anterior cruciate ligament transection and meniscectomized models of osteoarthritis. *BMC Musculoskelet Disord.* 2011;12:197.
451. Engsig MT, Chen QJ, Vu TH, Pedersen AC, Therkidsen B, Lund LR, et al. Matrix metalloproteinase 9 and vascular endothelial growth factor are essential for osteoclast recruitment into developing long bones. *J Cell Biol.* 2000;151(4):879-89.

452. Henriksen K, Karsdal M, Delaisse JM, Engsig MT. RANKL and vascular endothelial growth factor (VEGF) induce osteoclast chemotaxis through an ERK1/2-dependent mechanism. *J Biol Chem.* 2003;278(49):48745-53.
453. Kumar A, Bendele AM, Blanks RC, Bodick N. Sustained efficacy of a single intra-articular dose of FX006 in a rat model of repeated localized knee arthritis. *Osteoarthritis Cartilage.* 2015;23(1):151-60.
454. Compton JT, Lee FY. A review of osteocyte function and the emerging importance of sclerostin. *J Bone Joint Surg Am.* 2014;96(19):1659-68.
455. Appelman-Dijkstra NM, Papapoulos SE. Novel approaches to the treatment of osteoporosis. *Best Pract Res Clin Endocrinol Metab.* 2014;28(6):843-57.
456. Luyten FP, Tylzanowski P, Lories RJ. Wnt signaling and osteoarthritis. *Bone.* 2009;44(4):522-7.
457. McClung MR, Grauer A, Boonen S, Bolognese MA, Brown JP, Diez-Perez A, et al. Romosozumab in postmenopausal women with low bone mineral density. *N Engl J Med.* 2014;370(5):412-20.
458. Baker K, Grainger A, Niu J, Clancy M, Guermazi A, Crema M, et al. Relation of synovitis to knee pain using contrast-enhanced MRIs. *Ann Rheum Dis.* 2010;69(10):1779-83.
459. Hill CL, Hunter DJ, Niu J, Clancy M, Guermazi A, Genant H, et al. Synovitis detected on magnetic resonance imaging and its relation to pain and cartilage loss in knee osteoarthritis. *Ann Rheum Dis.* 2007;66(12):1599-603.
460. Brandt KD, Dieppe P, Radin E. Etiopathogenesis of osteoarthritis. *Med Clin North Am.* 2009;93(1):1-24, xv.
461. Roos EM, Dahlberg L. Positive effects of moderate exercise on glycosaminoglycan content in knee cartilage: a four-month, randomized, controlled trial in patients at risk of osteoarthritis. *Arthritis Rheum.* 2005;52(11):3507-14.
462. Harris MD, Datar M, Whitaker RT, Jurrus ER, Peters CL, Anderson AE. Statistical shape modeling of cam femoroacetabular impingement. *J Orthop Res.* 2013;31(10):1620-6.
463. Krekel PR, Vochteloo AJ, Bloem RM, Nelissen RG. Femoroacetabular impingement and its implications on range of motion: a case report. *J Med Case Rep.* 2011;5:143.
464. Das Neves Borges P, Forte AE, Vincent TL, Dini D, Marenzana M. Rapid, automated imaging of mouse articular cartilage by microCT for early detection of osteoarthritis and finite element modelling of joint mechanics. *Osteoarthritis Cartilage.* 2014;22(10):1419-28.
465. Zhang X, Carey R, Zheng L, Aiyangar A, Harner C. Subject-Specific Finite Element Modeling of the In Vivo Tibiofemoral Joint Based on CT, MRI and Dynamic Stereo-Radiography Data. *J Biomech Eng.* 2013.

APPENDICES

LIST OF ABBREVIATIONS

CURRICULUM VITAE

PHD PORTFOLIO

LIST OF PUBLICATIONS

DANKWOORD

LIST OF ABBREVIATIONS

(q)PCR	(quantitative) Polymerase chain reaction
μ CTa	Micro-computed tomography arthrography
AB	Alcian blue
AC	Articular cartilage
ACAN	Aggrecan
ADAMTS	A Disintegrin And Metalloproteinase with Thrombospondin Motifs
Angptl	Angiopoietin-like
Apcdd1	Adenomatosis polyposis coli down-regulated 1
Aspn	Asporin
Bq	Becquerel
CECT	Contrast enhanced (micro) computed tomography
CI	Confidence interval
Cn	Calcineurin
Col	Collagen
CT	Computed tomography
dGEMRIC	Delayed gadolinium enhanced magnetic resonance imaging of cartilage
DMOADs	Disease modifying osteoarthritic drugs
DNA	Deoxyribonucleic acid
ECM	Extra-cellular matrix
EPIC- μ CT	Equilibrium partitioning of an ionic contrast agent using micro-computed tomography
Epyc	Epiphycan
Fbln	Fibulin
FCD	Fixed charge density
FGF	Fibroblast growth factor
FKBPs	FK506-binding proteins
Fmod	Fibromodulin
FR β	Folate receptor β
GIN	3-[9-Fluoro-2-(piperidine-1-carbonyl)-1,2,3,4-tetrahydro-[1,4] diazepino[6,7,1-hi]indol-7-yl]-4-imidazo[1,2-a]pyridin-3-yl-pyrrole-2,5-dione
GO	Gene ontology
GO_BP	Gene ontology biological processes
GO_CC	Gene ontology (extra)cellular location
GO_MF	Gene ontology molecular functions
Gsk3 β	Glycogen synthase kinase-3 β

HA	Hyaluronic acid
Hh	Hedgehog
HPLC	High-performance liquid chromatography
Hsp	Heat shock proteins
Hsp90i	Hsp90 inhibition
IFN γ	Interferon γ
IHC	Immunohistochemistry
IL	Interleukin
ISH	In situ hybridization
JSN	Joint space narrowing
LMM	Linear Mixed Model
Matn	Matrilin
MEM	Minimum essential medium
Met	Met proto-oncogene
Mfap	Microfibrillar-associated protein
Mgp	Matrix Gla protein
MIA	Mono-iodoacetate
MMP	Matrix metalloproteinase
NFAT	Nuclear factor of activated T-cells
NF- κ B	Nuclear factor kappa-light-chain-enhancer of activated B cells
OA	Osteoarthritis
Ogn	Osteoglycin
Omd	Osteomodulin
PBS	Phosphate buffered saline
PCA	Principal component analysis
PCNA	Proliferating cell nuclear antigen
PET	Positron emission tomography
PG	Proteoglycans
RNA	Ribonucleic acid
ROI	Region of interest
sGAG	Sulfated-glycosaminoglycans
SPECT	Single-photon emission computed tomography
TNF α	Tumor necrosis factor α
Tnmd	Tenomodulin
TUNEL	Terminal deoxynucleotidyl transferase dUTP nick end labeling
Ucma	Unique cartilage matrix-associated protein
VCAN	Versican
VEGF	Vascular endothelial growth factor

CURRICULUM VITAE

Michiel Siebelt was born on the 20th of July 1982 in Nuenen, Noord-Brabant, the Netherlands. He is the third child of Dick Siebelt and Yvonne Siebelt-Martens, and youngest in the family next to his sister Evelien Siebelt and brother Teun Siebelt.

From 1994 to 1999 he attended the Rommert Casimir college, a school for higher general secondary education in Eindhoven. After his graduation, he attended the Lorentz Lyceum, a school in Eindhoven for pre-university education. He went on to study medicine at Leiden university from 2001 to 2008.



Supervised by prof. dr. Piet M. Rozing, he participated as a junior researcher at the department of orthopaedic surgery which first awoke his interest for basic research. While finishing his medical training at the department for orthopedic surgery at the Reinier de Graaf hospital in Delft, he wrote his first publication together with his brother Teun.

Michiel got accepted for a position as a PhD student at Erasmus University in Rotterdam. There, he worked until 2013 on the translational regenerative medicine program for cartilage regeneration, under the supervision of prof. dr. J.A.N. Verhaar, prof. dr. M. Hendriks-de Jong and prof. dr. ir. H. Weinans.

From 2013, he started his specialist training in order to become an orthopedic surgeon. From 2013 to 2014, he was employed as a registrar at the department of general surgery of Reinier de Graaf hospital in Delft (supervisor dr. M. van der Elst), after which he continued his training at the department of orthopedic surgery of Erasmus Medical Center in Rotterdam (supervisors prof. dr. J.A.N. Verhaar and dr. P.K. Bos).

Currently, he lives in Rijswijk together with his girlfriend Bregje van Schijndel and his son, Julius Siebelt.

PHD PORTFOLIO

Summary of PhD training and teaching activities

Name PhD student:	Michiel Siebelt
Erasmus MC Department:	Orthopedic surgery
PhD period:	August 20008 – December 2013
Promotors:	prof. dr. ir. H. Weinans
	prof. dr. ir. M. Hendriks-de Jong
	prof. dr. J.A.N. Verhaar

PhD training activities

General courses	Year	Workload (ECTS)
Animals science course, artikel 9	2009	3.0
'Get out of your lab!' – PhD instruction course	2009	2.0
AMIE: animal imaging workshop	2009	1.0
Stralingshygiëne 3B	2009	1.0
Biomedical English writing and communication	2012	4.0
Presentations		
Various presentations at research meetings of the department of orthopedics	2008 - 2012	4.0
Presentations (inter)national conferences		
Nederlandse Vereniging voor Orthopedie, Utrecht, the Netherlands 'Citation analysis of orthopaedic literature; 18 major orthopaedic journals compared for Impact Factor and SCImago'	2009	1.0
European Federation of National Associations of Orthopedics and Traumatology (EFORT) – Vienna, Austria 'Citation analysis of orthopaedic literature; 18 major orthopaedic journals compared for Impact Factor and SCImago'	2009	1.0
Nederlandse Vereniging voor Orthopedie, Utrecht 'Segmentation and analysis of in vivo contrast enhanced μ CT-data: a novel methodology for optimal quantification of cartilage degeneration'	2010	1.0

European Orthopedic Research Society – Davos, Switzerland <i>'Segmentation and analysis of in vivo contrast enhanced μCT-data: a novel methodology for optimal quantification of cartilage degeneration'</i>	2010	1.0
Orthopedic Research Society – Long Beach, Los Angeles, USA <i>'Accurate in vivo quantification of osteoarthritic cartilage changes using μCT-arthrography in three etiologically distinct rat models'</i>	2010	1.0
Nordic Cartilage Imaging Group – Oulu, Finland <i>'Accurate in vivo quantification of osteoarthritic cartilage changes using μCT-arthrography in three etiologically distinct rat models'</i>	2011	1.0
Annual BMM/TeRM meeting, Ermelo <i>'Clinical application of CT-arthrography as a measure of cartilage sulfated glycosaminoglycan content'</i> Oral presentation award	2011	1.0
European Orthopedic Research Society – Amsterdam, the Netherlands <i>'Heat shock proteins 70 and 90 in osteoarthritis progression'</i>	2012	1.0
Poster presentations		
Annual BMM/TeRM meeting, Ermelo <i>'Segmentation and analysis of in vivo contrast enhanced μCT-data: a novel methodology for optimal quantification of cartilage degeneration'</i>	2010	1.0
Osteoarthritis Research Society International (OARSI) – Brussels, Belgium <i>'Segmentation and analysis of in vivo contrast enhanced μCT-data: a novel methodology for optimal quantification of cartilage degeneration'</i>	2010	1.0
Osteoarthritis Research Society International (OARSI) – Brussels, Belgium <i>'Strenuous running as a model for osteoarthritis in rats: analyzed using contrast enhanced μCT'</i>	2010	1.0
Osteoarthritis Research Society International (OARSI) – San Diego, USA <i>'Clinical application of CT-arthrography as a measure of cartilage sulfated glycosaminoglycan content'</i>	2011	1.0

Osteoarthritis Research Society International (OARSI) – San Diego, USA	2011	1.0
<i>'CT arthrography of the knee to measure cartilage quality with low radiation exposure'</i>		

Teaching

Biomedical research techniques, presentation on 'Computed Tomography'	2009	1.0
AMIE workshop, presentation and practical demonstration on 'Computed Tomography'	2010	1.0
Biomedical research techniques, presentation on 'Computed Tomography'	2010	1.0
Weakly workgroups of Tutor first year medical students	2010	2.0
Tutoring first year medical students	2010	2.0
AMIE workshop, presentation and practical demonstration on 'Computed Tomography'	2011	1.0
Biomedical research techniques, presentation on 'Computed Tomography'	2011	1.0
AMIE workshop, presentation and practical demonstration on 'Computed Tomography'	2012	1.0
Supervision of medical students –writing of an systematic review	2012	2.0
Supervision of medical students – scientific internship, 3 students	2009 – 2013	9.0

Grant proposals

<i>'Sodium iodine symporter for cell tracing cell therapy' – Jan Dekker stichting en dr Ludgardine Bouwman stichting</i>	2010	1.0
<i>'Osteoarthritis: training is gaining' - Reumafonds</i>	2011	1.0
<i>'Stress in established OA: time to treat the whole joint?' - Reumafonds</i>	2012	1.0
<i>'Macrophage imaging: can we show both sides of the medal?' – Mrace, Erasmus MC grant; <u>Awarded</u></i>	2012	1.0

LIST OF PUBLICATIONS

1. M. Siebelt, T. Siebelt, P. Pilot, R.M. Bloem, M. Bhandari, R.W. Poolman. **Citation analysis of orthopaedic literature; 18 major orthopaedic journals compared for Impact Factor and SCImago.** *BMC Musculoskelet Disord.* 2010 Jan 4;11:4.
2. M. Siebelt, J.H. Waarsing, N. Kops, T.M. Piscoer, J.A.N. Verhaar, E.H.G. Oei, H. Weinans. **Quantifying osteoarthritic cartilage changes accurately using μ CT arthrography in three etiologically distinct rat models.** *J Orthop Res.* 2011 Nov;29(11):1788-94
3. M. Siebelt, J. van Tiel, J.H. Waarsing, T.M. Piscoer, M. van Straten, R. Booij, M.L. Dijkshoorn, G.J. Kleinrensink, J.A.N. Verhaar, G.P. Krestin, H. Weinans, E.H. Oei. **Clinically applied CT arthrography to measure the sulfated glycosaminoglycan content of cartilage.** *Osteoarthritis Cartilage.* 2011 Oct;19(10):1183-9
4. R.L. Miclea, M. Siebelt, L. Finos, J.J. Goeman, C.W. Löwik, W. Oostdijk, H. Weinans, J.M. Wit, E.C. Robanus-Maandag, M. Karperien. **Inhibition of Gsk3 β in cartilage induces osteoarthritic features through activation of the canonical Wnt signaling pathway.** *Osteoarthritis Cartilage.* 2011 Nov;19(11):1363-72
5. H. Weinans, M. Siebelt, R. Agricola, S.M. Botter, T.M. Piscoer, J.H. Waarsing. **Pathophysiology of peri-articular bone changes in osteoarthritis.** *Bone.* 2012 Aug;51(2): 190-6
6. M. Siebelt, J. van Tiel, J.H. Waarsing, T.M. Piscoer, M. van Straten, R. Booij, M.L. Dijkshoorn, G.J. Kleinrensink, J.A.N. Verhaar, G.P. Krestin, H. Weinans, E.H.G. Oei. **CT arthrography of the human knee to measure cartilage quality with low radiation dose.** *Osteoarthritis Cartilage.* 2012 Jul;20(7):678-85
7. M. Siebelt, H. Jahr, H.C. Groen, M. Sandker, J.H. Waarsing, N. Kops, C. Müller, W. van Eden, M. de Jong, H. Weinans. **Hsp90 inhibition protect against biomechanically induced osteoarthritis.** *Arthritis Rheum.* 2013 Aug;65(8):2102-12
8. S.F. Lau, C.F. Wolschrijn, H.A. Hazewinkel, M. Siebelt, G. Voorhout. **The early development of medial coronoid disease in growing Labrador retrievers: radiographic, computed tomography, necropsy and micro-computed tomography findings.** *Vet J.* 2013 Sep;197(3):724-30
9. S.F. Lau, H.A. Hazewinkel, G.C. Grinwis, C.F. Wolschrijn, M. Siebelt, J.C. Vernooij, G. Voorhout, M.A. Tryfonidou. **Delayed endochondral ossification in early medial coronoid disease (MCD): a morphological and immunohistochemical evaluation in growing Labrador retrievers.** *Vet J.* 2013 Sep;197(3):731-8
10. S.F. Lau, C.F. Wolschrijn, M. Siebelt, J.C. Vernooij, G. Voorhout, H.A. Hazewinkel. **Assessment of articular cartilage and subchondral bone using EPIC- μ CT in Labrador retrievers with incipient medial coronoid disease.** *Vet J.* 2013 Oct;198(1):116-21
11. J. van der Stok, H. Weinans, N. Kops, M. Siebelt, P. Patka, E.M.M. van Lieshout. **Properties of commonly used calcium phosphate cements selection in trauma and orthopedic surgery.** *Injury.* 2013 Oct;44(10):1368-74
12. M. Sandker, A. Petit, E. Redout, M. Siebelt, B. Müller, P. Bruin, R. Meyboom, T. Vermonden, W.E. Hennink, H. Weinans. **In situ forming acyl-capped PCLA-PEG-PCLA triblock copolymer based hydrogels: synthesis, biocompatibility and in vivo visualization.** *Biomaterials.* 2013 Oct;34(32):8002-11
13. A. Kok, G.J.M. Tuijthof, S. den Dunnen, J. van Tiel, M. Siebelt, V. Everts, C.N. van Dijk, G.M.M.J. Kerkhoffs. **Hole geometry of bone marrow stimulation does not influence cartilage repair in talar osteochondral defects in the goat.** *Clin Orthop Relat Res.* 2013 Nov;471(11):3653-62

14. J. van der Stok, H. Wang, S.A. Yavari, M. Siebelt, M. Sandker, J.H. Waarsing, J.A.N. Verhaar, H. Jahr, A.A. Zadpoor, S.C.G. Leeuwenburgh, H. Weinans. **Enhanced bone regeneration of cortical segmental bone defects using porous titanium scaffolds incorporated with colloidal gelatin gels for time and dose controlled delivery of dual growth factors.** *Tissue Eng Part A*. 2013 Dec;19(23-24):2605-14
15. M. Siebelt, H.C. Groen, S.J. Koelewijn, E. de Blois, M. Sandker, J.H. Waarsing, C. Müller, G.J.V.M. van Osch, M. de Jong, H. Weinans. **Increased physical activity severely induces osteoarthritic changes in knee joints with sulphate-glycosaminoglycan depleted cartilage.** *Arthritis Res Ther*. 2014 Jan;16(1):R32
16. M. Siebelt, A.E. van der Windt, H.C. Groen, M. Sandker, J.H. Waarsing, M. de Jong, H. Jahr, H. Weinans. **FK506 protects against articular cartilage extra-cellular matrix degradation.** *Osteoarthritis Cartilage*. 2014 April;22(4):591-600
17. G.M. van Buul, M. Siebelt, M. Leijts, P.K. Bos, J.H. Waarsing, N. Kops, H. Weinans, J.A.N. Verhaar, M.R. Bernsen, G.J.V.M. van Osch. **Mesenchymal stem cells reduce pain but not degenerative changes in a mono-iodoacetate model of osteoarthritis.** *J. Orthop. Res*. 2014 Sep;32(9):1167-74
18. M. Siebelt, H.C. Groen, S.J. Koelewijn, E. de Blois, J.H. Waarsing, M. de Jong, H. Weinans. **Alendronate treatment protect against cartilage matrix degradation during severe osteoarthritis progression.** *Bone*, 2014 Sep;66:163-70
19. M. Siebelt, R. Agricola, H. Weinans, Y.J. Kim. **The role of imaging in early hip OA.** *Osteoarthritis Cartilage*. 2014 Oct;22(10): 1470-1480
20. J. van Tiel, M. Siebelt, M. Reijman, P.K. Bos, E. Waarsing, J.A.N. Verhaar, G.J.V.M. van Osch, S.M.A. Bierma-Zeinstra, A.M. Zuurmond, G.P. Krestin, H. Weinans, E.H.G. Oei. **Quantitative CT arthrography of the human knee to measure biochemical composition: an in vivo validation study against ex-vivo reference standards for cartilage sulphated glycosaminoglycan and collagen content.** *Under Review - Radiology*.

DANKWOORD

Bij deze wil ik iedereen bedanken die een bijdrage heeft geleverd aan het tot stand komen van dit proefschrift. Een aantal mensen wil ik in het bijzonder noemen.

Professor H. H. Weinans, dat was volgens mij het eerste wat je me afleerde op het lab. Geen professor, gewoon Harrie. En de tweede les volgde niet lang daarna. In mijn eerste maanden had ik geen flauw benul waar of waarmee ik eigenlijk moest beginnen. En zo trof je me eens vroeg in de middag aan op weg naar huis. Je concludeerde dat het toch vooral een goed idee zou zijn als we met wekelijkse regelmaat elkaar op jouw kamer zouden treffen. En eigenlijk is het vanaf dat moment echt in gang gekomen. En wat was het gedurende vier promotiejaren ontzettend prettig om met je samen te werken. Je open houding, laagdrempelige benaderbaarheid, enthousiasme en voorliefde voor gezelligheid, die zelfs tot laat in Boudewijn kon eindigen. Als ik iets mis van mijn promotietijd, zijn het de wetenschappelijk discussies waarvan het enthousiasme zich rechtvevredig uitte met de nodige decibellen vanuit jouw kamertje. We hebben veel voor elkaar gekregen, en ik hoop dat we in toekomst nog een mooie aanvulling kunnen maken!

Beste professor M. de Jong, beste Marion, bij u stond de deur ook altijd open. In de laatste fase van mijn promotie had ik besloten nog een project op te starten waarbij ik veelvuldig van de SPECT/CT gebruik wilde maken. En na overleg met u, gaf u direct te kennen dat dit geen probleem was. Met uw goedkeuren hebben Harald, Stuart, Erik en Wout veelvuldig geholpen met het labelen van folaat en scannen van proefdieren. Zonder deze opbouwende instelling en ondersteunende bijdrage van alle collega's van de nucleaire geneeskunde was mijn promotie nooit zo'n succes geworden. Dank daarvoor!

Beste professor J.A.N. Verhaar, allereerst veel dank voor de kans om op uw afdeling aan een promotieonderzoek te mogen werken. Daarnaast heeft uw begeleiding mijn proefschrift veel goed gedaan. Keer op keer als ik mijn manuscripten voor beoordeling instuurde, wist u mij te verrassen met scherpe kanttekeningen van grote bijdrage voor mijn werk. Op dit moment heeft u in de kliniek eenzelfde positieve bijdrage aan mijn ontwikkeling tot orthopedisch chirurg.

Beste Erwin! Wat ben ik nog steeds dankbaar dat ik het plekje tegenover jouw bureau wist te bemachtigen. Absoluut de beste plek van het lab! Daar zittend ben jij een van mijn belangrijkste mentoren geworden. Ik bedenk me nog regelmatig hoe vaak jij diep hebt moeten zuchten als je weer eens iets aan mijn verstand probeerde te peuteren. Als gevolg van die gesprekken, moest ik dan toch mijn scans voor een tweede of derde keer opnieuw analyseren, waarvan ik de data dan keurig uitgeprint weer aan je voorlegde. En na al dat werk moest je soms uitleggen, dat wat ik daar deed, wetenschappelijk absoluut onjuist was. Juist onder deze begeleiding leerde ik

kritisch naar mijn data te kijken! En,.... dat data eigenlijk altijd minstens vier keer moet worden uitgewerkt, voordat je er überhaupt iets zinnigs over kan zeggen. Goed om je nog steeds regelmatig tegen te komen in het Hs-gebouw. Ik ga er stiekem van uit dat je tijdens mijn tweede stage in het EMC er nog steeds bent!

Beste Holger, ook jij bedankt voor al je hulp bij mijn promotie. Het begon met een succesvol sollicitatiegesprek met je, deels in het Duits, deels in het Engels, en volgens mij ook nog in het Nederlands. Maar het zou niet het laatste gesprek zijn wat we hebben gevoerd. Bij ieder idee van me deelde je altijd volop in enthousiasme. Vanuit je biologische achtergrond wist je altijd nog een achterliggende pathway te vinden, waarvan ik uiteraard nog nooit van gehoord had. Je bijdrage aan het Hsp-paper is van onschatbare waarde geweest. Niet alleen voerde je een eiwit-analyse uit, ook nam je direct het volledige protocol onder handen om de efficiëntie van toekomstige analyses te verbeteren. Blijf volharden in deze Deutsche Gründlichkeiten! Succes zal jouw kant vanzelf opkomen! Heel veel succes in Aken!

Beste professor G.J. Kleinrensink en dr. E.H.G. Oei, beste Edwin, ook voor jullie speciale dank. Na een middag brainstormen met Jasper van Tiel, boden jullie ons direct alle mogelijkheden om onze ideeën voor de kliniek verder uit te werken. En zie wat het resultaat is geworden! Twee artikelen geaccepteerd en onderdeel van dit boekje, en wat ik van Jasper heb gehoord, komen daar nog een aantal in zijn boekje bij.

Veel dank aan alle collega's van de 16^e, beste Sander, Olav, Tom, Robert-Jan, Yvonne Sniekers, Yvonne Bastiaansen-Jenniskens, Ruud, Johan, Marjan, Marianne, Gerjo, Anna, Gerben, Stefan, Roberto, Mieke, Nienke, Wu, Maarten, Mairead, Job, Belle, Vincent. Beste Nicole, Wendy, Esther en Sandra, zonder jullie had ik het eerste half jaar nooit overleefd!

Mijn paranimfen!

Beste Rintje! Wat mooi dat jij besloot door te gaan met een promotietraject bij ons op het lab. Het was even aanpoten, maar uiteindelijk lukte het ons om samen je eerste publicatie op PubMed te krijgen. Te gek! Wel irritant dat je daarna niet te stoppen was, en vervolgens als eerste van ons drieën je promotie afgerond had. Nooit zal ik vergeten hoe we ons in de nesten hadden gewerkt op een verlaten rots midden in de woestijn in de USA. En hoe goed het bier smaakte, toen we daar heelhuids weg zijn gekomen. Over een paar jaar werken we even samen in de kliniek, ik kijk er nu al naar uit!

Beste Jasper! Ontzettend veel succes hebben wij gehad. Na een middag koffie drinken, het plan opgepakt om klinisch CT arthrografie te gaan toepassen. Zie hier, twee hoofdstukken van mijn promotie, en bij jou zullen er nog een paar meer worden bijgevoegd. Daarnaast hebben we onwijs veel moeten lachen en lol gehad! Schitterend hoe wij in de Finse sauna in Oulu hebben gezeten, waar skinny dipping in de sneeuw best mannelijk is. Natuurlijk ook het borreltje muntwodka tijdens het diner met Harrie, Gyula en Edwin. Of hoe je besloot om bij -35°C een stukje af te snijden, waarbij je tot je middel in de sneeuw kwam te staan. Maar zo gaat het bij Jasper, als je A zegt... Zodoende liep je onverstoort lachend door. Precies zo, ga jij een fantastisch proefschrift afronden!

Jongens, je bent pas vrienden, als je tot veel te laat met elkaar in de kroeg hebt gezeten. Ik hoop daarom nog veel jaren aan onze vriendschap te blijven werken. H4L!

Lieve papa en mama, ik houd ontzettend veel van jullie allebei. Bedankt voor de onvoorwaardelijke steun die ik krijg. Bij alles wat ik doe, weet ik dat jullie er zijn. Niets is meer belangrijk dan dat.

En natuurlijk ook de rest van de familie! Peter en Mieke, bedankt voor de oprechte interesse in mijn werk. Nog meer dank voor al jullie steun en support wanneer dat meer dan nodig was. Jullie kennen mij als geen ander. Lieve zus en lieve broer! Allebei baas over jullie eigen toko, respect! Wat fijn als we samen bij elkaar komen! Samen met Rob, Annechien, Guus, Pien, Leen, Fiene en Jikke. Altijd heerlijk om iedereen te zien, helemaal nu ook wij een gezinnetje hebben. Dank voor al jullie begrip en geduld tijdens die moeilijke periode.

Lieve Bregje! Zonder jou was er geen proefschrift geweest. Zonder jou had ik mijn eerste dagen in de kliniek nooit overleefd. Wat is het soms moeilijk geweest in de jaren dat alleen wij er waren. Hoe heerlijk is het nu ons kleine ventje erbij is! Helemaal compleet met zijn grote handen en nu al eigenzinnige willetje. Wat een genot om samen met jou te glunderen bij zijn lach waarmee hij ons volledig inpakt. Samen zijn we super-trotse ouders, en het is een enorm gevoel van geluk om zijn dagelijkse flesje te geven. In zo'n ver level zijn we nog nooit geweest! Ik hou van jullie!

